FACULTES UNIVERSITAIRES
NOTRE-DAME DE LA PAIX
Namur

Faculté des Sciences
DEPARTEMENT DE CHIMIE
Laboratoire de Chimie Théorique

Design of molecular switches exhibiting second-order nonlinear optical responses: *ab initio* investigations and hyper Rayleigh scattering characterizations

- Version Finale -

Dissertation présentée par
PLAQUET Aurélie
en vue de l'obtention du grade
de Docteur en Sciences Chimiques

Composition du jury :

Prof. Davide Bonifazi (FUNDP, Namur, président du jury)
Prof. Koen Clays (KUL, Leuven)
Prof. Vincent Rodriguez (Université de Bordeaux 1)
Dr. Michel Sliwa (Université de Lille 1)
Dr. Frédéric Castet (Université de Bordeaux 1, co-promoteur)
Prof. Benoît Champagne (FUNDP, Namur, promoteur)

2011

Facultés Universitaires Notre-Dame de la Paix
FACULTE DES SCIENCES
Rue de Bruxelles, 61, B-5000 Namur

Conception d'interrupteurs moléculaires présentant des réponses optiques non-linéaires du deuxième ordre : étude théorique et caractérisation par diffusion hyper Rayleigh

par Aurélie Plaquet

Résumé: Les interrupteurs moléculaires sont des composés capables de commuter réversiblement entre deux ou plusieurs états stables en réponse à un stimulus extérieur. L'objectif de la thèse est la conception d'interrupteurs moléculaires présentant des contrastes optiques non-linéaires (ONL) et la mise évidence des paramètres structuraux et électroniques menant à d'importants contrastes de première hyperpolarisabilité (β) via une approche multidisciplinaire qui combine la synthèse de nouveaux composés, la caractérisation de leurs réponses optiques linéaires et non-linéaires par spectroscopie d'absorption UV-visible et par diffusion hyper-Rayleigh et l'utilisation des méthodes de la chimie théorique afin de prédire et d'interpréter les propriétés moléculaires. Ces phénomènes de commutations réversibles et les changements de propriétés qui les accompagnent présentent de nombreux intérêts, tant technologiques comme l'élaboration d'ordinateurs moléculaires qu'au niveau des organismes vivants où de nombreuses fonctions biologiques sont basées sur un phénomène de commutation. Les principaux résultats de nos travaux se situent au niveau de l'interprétation des réponses ONL et de leurs contrastes en fonction de la nature, de la position et du caractère donneur/accepteur des substituants présents sur le squelette des interrupteurs moléculaires.

Design of molecular switches exhibiting second-order nonlinear optical responses: ab initio investigations and hyper Rayleigh scattering characterizations

by Aurélie Plaquet

Abstract: Molecular switches are compounds presenting the ability to commute reversibly between two or more states in response to external stimuli. The goal of the work is the design of molecular switches exhibiting contrasts of their second-order nonlinear optical (NLO) properties and the highlight of the structural and electronic parameters leading to large contrasts of first hyperpolarizability (β) via a multidisciplinary approach combining the synthesis of new compounds, the characterization of their linear (by UV-Visible absorption spectroscopy) and nonlinear optical properties (by hyper Rayleigh scattering), and the theoretical simulations in order to predict and interpret molecular properties. These reversible switching processes and the resulting variations of molecular properties have many interests in technological area such as the development of molecular computers or in life sciences since many biological functions are based on commutation mechanisms. The major results of our investigations are the interpretation of the NLO responses and contrasts as a function of the nature, the positioning, and the donor/acceptor character of the substituents.

PhD thesis in Chemistry (Dissertation doctorale en Sciences Chimiques)
31th May 2011(31 mai 2011)
Laboratoire de Chimie Théorique
Advisors (Promoteurs) : Prof. Benoît Champagne and Dr. Frédéric Castet

Arrivée à la fin de ces quatre années de thèse, c'est avec beaucoup de reconnaissance que je vais remercier toutes les personnes qui ont participé à ce travail de près ou de loin.

Mes premiers remerciements vont au Prof. Benoît Champagne, promoteur de ce travail, pour le partage de ses connaissances scientifiques, sa rigueur, son appui et sa grande motivation qui m'ont porté tout au long de ce travail.

Je tiens également à remercier le Dr. Frédéric Castet, co-promoteur de cette thèse, pour son soutien, sa disponibilité et sa patience mais également le Prof. Vincent Rodriguez pour son aide et ses explications qui m'ont permis d'approfondir la spectroscopie hyper Rayleigh.

Mes remerciements s'adressent au Fond pour la Formation à la Recherche dans l'Industrie et l'Agriculture qui, par son soutien financier, m'a permis de mener cette thèse à son terme.

Je souhaite remercier tous nos collaborateurs, en particulier le Prof. Koen Clays, le Prof. Keitaro Nakatani, le Dr. Sergey Sergeyev, le Dr. Michel Sliwa, le Dr. Liudmil Antonov, le Dr. Filip Burěs ainsi que le Prof. Davide Bonifazi, membre du comité d'accompagnement.

Ce travail a pu aboutir aussi grâce à la bonne ambiance qui règne au laboratoire. Je citerai, le Dr. Joseph Frippiat pour sa disponibilité, le Dr. Edith Botek, pour sa gentillesse, le Dr. Vincent Liégeois pour sa bonne humeur à toute épreuve, mais aussi les post-doctorants, doctorants et mémorants, le Dr. Léa Rougier, Marc de Wergifosse, Raphaël Carion, Audrey Ségerie et Conrard Tetsassi qui sont devenus de véritables amis. Merci à tous pour votre sympathie et les bons moments passés ensemble.

Réalisée en co-tutelle, une partie de la thèse s'est déroulée à l'Institut des Sciences Moléculaires de l'Université de Bordeaux où j'ai rencontré également beaucoup de personnes m'ayant permis d'avancer. Merci à nos collaborateurs, le Prof. Jean-Luc Pozzo, le Dr. Laurent Ducasse et Frédéric Adamietz pour son aide lors des manips. Je citerai également Elena, Aude, Enora, Julien, Fabien, Raph, Marc, Nico, Tatiana et Florence pour les bons souvenirs que je garderai de Bordeaux.

Je n'aurais pas pu faire ce travail sans le soutien de mes amis, en particulier, Sylvia, Laurent, Julie, François, Marie, Martial, Stéphanie, Mathias, Laurence, Arnaud, Ludivine et Anaëlle mais également toute ma belle-famille.

Bien qu'ils n'aient pas toujours compris ce que je cherchais, toute ma famille m'a porté tout au long de ces années d'études et a cru en moi depuis le début jusque la fin sans relâche et pour cela, je remercie mes parents, Christophe, Bélinda, Sophie et Jacques. Sans s'en rendre compte les plus petits ont eux aussi participé à ma

motivation quotidienne et je remercie Simon, Henri, Emile et Eline pour leur insouciance et les moments de bonheur qu'ils m'apportent.

Sans son soutien à toute épreuve, quels que soient les circonstances ou le nombre de kilomètres qui nous séparaient, le soutien au quotidien a été assuré de main de maître par mon petit Phile, sans qui rien ne serait arrivé, merci…

Enfin, pour terminer, je souhaite dédier cette thèse à mon papa, parti beaucoup trop vite, mais qui m'aurait encouragé jusqu'au bout et qui serait fier en ce jour…

Contents

Introduction

1. Introduction

Since immemorial time, the Human knows that light interacts with matter. This interaction has been rationalized by Maxwell in 1873 by his four equations describing among other things the linear relationship between the macroscopic polarization of materials and the electro-magnetic field. However, in the sixties, with the development of LASER sources, which possess much larger intensities, it appears that nonlinear effects have also to be considered and included in describing the relationship between the polarization and the electro-magnetic field. The first observed nonlinear optical (NLO) phenomenon induced by an intense electromagnetic field from a laser was demonstrated by Franken *et al.* [1] in 1961 at the University of Michigan. They observed that, for a quartz sample irradiated with a 694 nm (red) wavelength laser, the transmitted beam was composed of a supplementary wave of double frequency, *i.e.* at 347nm (blue). Nonlinear optics includes these phenomena where the properties of light are modulated by matter (second-harmonic generation - SHG) or where the properties of matter are modulated by light (Pockels effect: the modification of the refractive index proportionally to the strength of the applied electric field).

During the last decades, in our information technology society, the amount of data to be stored has been continuously increasing, requiring memory elements smaller and smaller as well as more and more powerful. So, the tiny size of the molecules could be efficient and organic compounds with photochromic properties have received considerable attention because of their possible applications in this field. Molecular switches, which are compounds presenting the ability to commute between two or more forms displaying distinct physico-chemical properties in response to external stimuli (light, temperature, pH,...) [2], are of interest. More particularly, organic systems with commutable NLO responses are highly attractive due to their flexibility, tailored synthesis, low cost, and easy and environment friendly processing. Since few years, materials presenting large contrast of NLO properties are largely studied in view of potential applications in photonics, opto-electronics, data storage, and/or sensing devices and have motivated a lot of experimental and theoretical works [3-11].

In order to predict, interpret, and optimize the NLO properties of molecular switches, we have investigated known switching species in a pluridisciplinary approach that combines the synthesis of the compounds (by our collaborators) as well as their linear and nonlinear optical characterizations, experimentally and theoretically. In paragraph 1.1., we present principles of nonlinear optics while paragraph 1.2. introduces the concept of molecular switches as a function of the nature of the stimulus triggering off the commutation.

1.1. Nonlinear optical properties

1.1.1. General aspects

An electric field ($\vec{E}$), such as in an electromagnetic wave, always induces displacement of the electronic cloud. In an applied oscillatory field, the electrons will oscillate. At low field strengths, they oscillate at the applied frequency and the magnitude of the induced polarization is linearly proportional to the applied field:

$$\vec{P}\left(\vec{E}\right) = \vec{P}_0 + \vec{\vec{\chi}}^{(1)} \cdot \vec{E} \qquad (1\text{-}1)$$

where $\vec{P}$ is the polarization of the material, $\vec{P}_0$ is the permanent polarization, and $\vec{\vec{\chi}}^{(1)}$ is the linear susceptibility connected to the refractive index ($n^2 = 1 + \chi^{(1)}$). At high field strengths, the polarization is no longer linear. In this case, the expression of the polarization, Equation (1-1), is expended in a Taylor series with respect to the external field [12]:

$$\vec{P}\left(\vec{E}\right) = \vec{P}_0 + \vec{\vec{\chi}}^{(1)} \cdot \vec{E} + \vec{\vec{\vec{\chi}}}^{(2)} : \vec{E}\vec{E} + ... \qquad (1\text{-}2)$$

where $\vec{\vec{\vec{\chi}}}^{(2)}$ is the second-order nonlinear optical susceptibility characterizing the NLO responses of the medium. The nonlinearity of the polarization with respect to the electric field is represented in Figure 1-1:

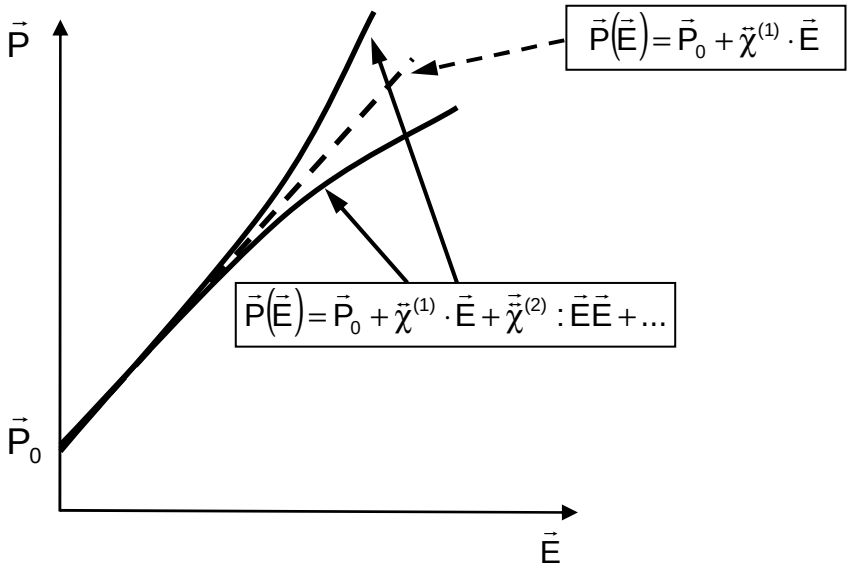

Figure 1-1: Linear and nonlinear responses of the polarization as a function of increasing the electric field amplitude.

At the molecular scale, the interaction between the electric field and the molecules is described by the dipole moment which, similarly to the polarization, can be written as:

$$\vec{\mu}(\vec{E}) = \vec{\mu}_0 + \vec{\vec{\alpha}} \cdot \vec{E} + \frac{1}{2}\vec{\vec{\beta}} : \vec{E}\vec{E} + ... \tag{1-3}$$

where $\vec{\mu}_0$ is the permanent dipole moment, $\vec{\vec{\alpha}}$ is the polarizability, and $\vec{\vec{\beta}}$ is the first hyperpolarizability tensor. Accordingly, these properties are defined as the successive derivatives of the dipole moment with respect to the electric field:

$$\alpha(E) = \left(\frac{\partial \mu(E')}{\partial E'} \right)_{E'=E} \tag{1-4}$$

$$\beta(E) = \left(\frac{\partial^2 \mu(E')}{\partial E'^2} \right)_{E'=E} = \left(\frac{\partial \alpha(E')}{\partial E'} \right)_{E'=E} \tag{1-5}$$

In this thesis, we are particularly interested by the first hyperpolarizability, β, a tensor presenting 27 components:

$$\beta = \begin{bmatrix} \beta_{xxx} & \beta_{xyy} & \beta_{xzz} & \beta_{xyz} & \beta_{xzy} & \beta_{xzx} & \beta_{xxz} & \beta_{xxy} & \beta_{yxx} \\ \beta_{yxx} & \beta_{yyy} & \beta_{yzz} & \beta_{yyz} & \beta_{yzy} & \beta_{yzx} & \beta_{yxz} & \beta_{yxy} & \beta_{yyx} \\ \beta_{zxx} & \beta_{zyy} & \beta_{zzz} & \beta_{zyz} & \beta_{zzy} & \beta_{zzx} & \beta_{zxz} & \beta_{zxy} & \beta_{zyx} \end{bmatrix} \tag{1-6}$$

As a function of the symmetry of the molecule, this tensor can be simplified. The first hyperpolarizabilities are expressed as a function of the frequency of the electromagnetic wave: $\beta(-\omega_3; \omega_1, \omega_2)$, ω_1 and ω_2 are the frequencies of the incident waves and ω_3 is the frequency of the scattered wave with $\omega_3 = \omega_1 + \omega_2$. In the case of SHG or in hyper Rayleigh scattering, $\omega_1 = \omega_2$ and the β_{ijk} and β_{ikj} components are identical so that they only remain 18 independent elements:

$$\beta = \begin{bmatrix} \beta_{xxx} & \beta_{xyy} & \beta_{xzz} & \beta_{xyz} & \beta_{xzx} & \beta_{xyx} \\ \beta_{yxx} & \beta_{yyy} & \beta_{yzz} & \beta_{yyz} & \beta_{yzx} & \beta_{yyx} \\ \beta_{zxx} & \beta_{zyy} & \beta_{zzz} & \beta_{zyz} & \beta_{zzx} & \beta_{zyx} \end{bmatrix} \tag{1-7}$$

So, in the case of the second-harmonic generation or in hyper Rayleigh scattering, the first hyperpolarizability reads $\beta(-2\omega; \omega, \omega)$, which is illustrated in Figure 1-2: $\omega_1 = \omega_2$ and the frequency of the scattered beam (blue) corresponds to the double of the incident beam (red). Finally, for the Pockels effect, the first hyperpolarizability reads $\beta(-\omega; \omega, 0)$. In the next paragraphs, the β values are expressed in atomic units (a.u.): 1.0 a.u. of $\beta = 3.6213 \times 10^{-42}$ m^4 V^{-1} = 3.206361×10^{-53} C^3 m^3 J^{-2} = 8.6392×10^{-33} esu. Note that a centrosymmetric molecule can not present a first hyperpolarizability value because:

$$\mu(-E) = -\mu(E) \quad \rightarrow \quad \beta = 0 \tag{1-8}$$

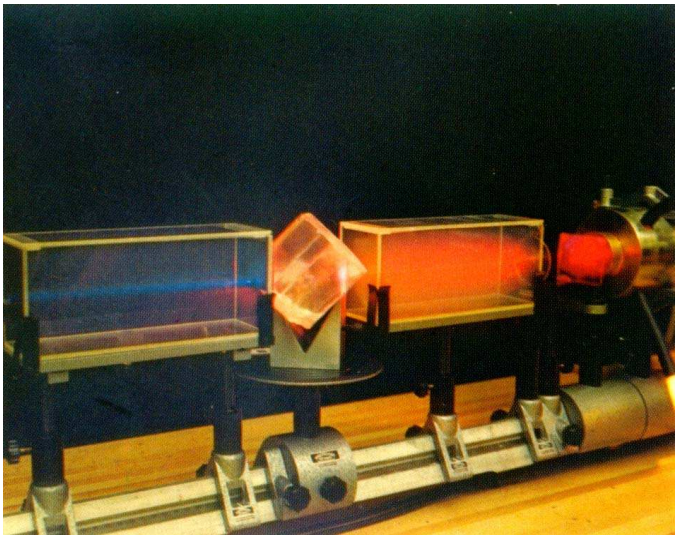

Figure 1-2: Illustration of the second-harmonic generation (From Ref. 13).

1.1.2. Second-order nonlinear optics of organic compounds

The NLO molecular properties come from donor-acceptor interactions [14]. A type of molecules exhibiting remarkable β values are the dipolar push-pull molecules that consist of strong electron-donor (D) and electron-acceptor (A) groups anchored on a π-conjugated linker (Figure 1-3). These molecules are characterized by an important charge transfer along the π-conjugated bridge and by a principal component of the first hyperpolarizability in the direction of the molecular axis. As example, *para*-nitroaniline [15] is a typical push-pull molecule (Figure 1-4). Disperse red one (DR1) [16] is another example of push-pull compound, which is widely used in nonlinear optics (Figure 1-5). This compound also undergoes a *trans* to *cis* isomerization that is induced by irradiating at 488 nm. When the irradiation is stopped, the compound comes back to the *trans* configuration.

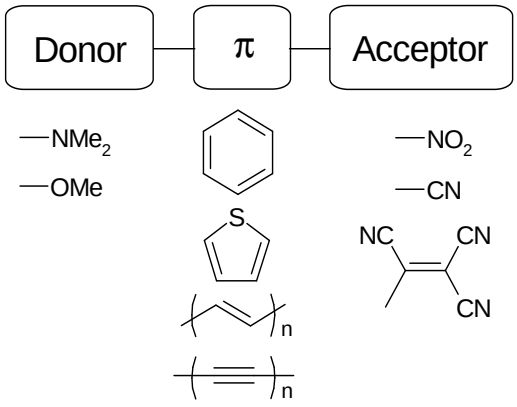

Figure 1-3: Schematic representation of a push-pull molecule composed of an electron donor group, a π-conjugated bridge, and an electron acceptor group with some examples.

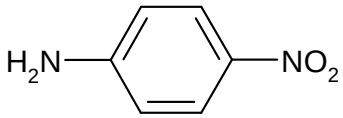

Figure 1-4: The *para*-nitroaniline molecule.

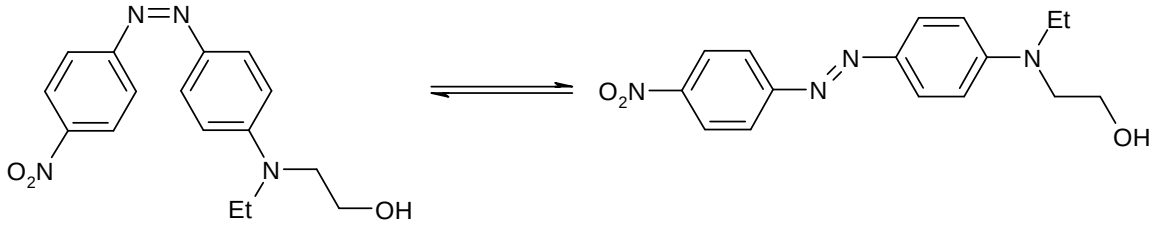

Figure 1-5: Isomerization of disperse red one (DR1).

Strong D-π-A molecules crystallize usually in a centrosymmetric arrangement, which annihilate the second-order nonlinear properties. To avoid this issue, the octupolar molecules [17] present large second-order NLO properties, such as 1,3,5-triamino-2,4,6-trinitrobenzene (TATB), an octupolar molecule with large first hyperpolarizability value (Figure 1-6).

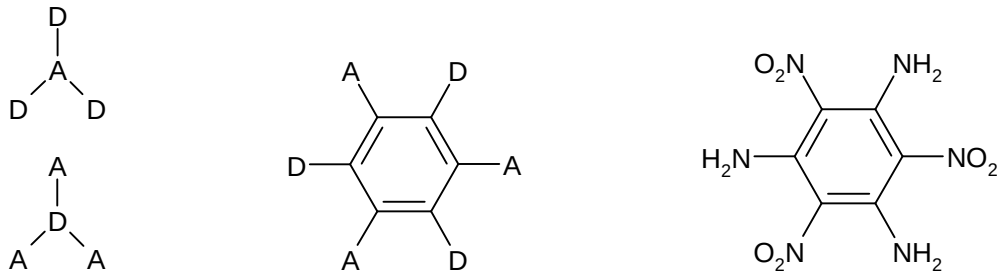

Figure 1-6: General structures of octupolar molecules and 1,3,5-triamino-2,4,6-trinitrobenzene molecule.

Other molecular geometries that generate large second-order NLO properties include V-shaped molecules [18], tetrahedral structures [19], and chiral structures [20].

The efficiency of these molecules depends on the length, the nature, and the planarity of the conjugated bridge, and on the nature and the strength of the donor and acceptor groups [21]. The search for relationships between the chemical structure and the first hyperpolarizability has shown that the charge transfer between the donor and acceptor groups is associated with a modulation of the geometry of the conjugated bridge and of the amplitude of the first hyperpolarizability [22]. To evaluate

the electron delocalization along the π-conjugated bridge, the bond length alternation (BLA) has been defined as the average difference between the single and double bond lengths of the conjugated bridge. Several studies have helped designing molecules with maximized first hyperpolarizabilities [23,24] by finding the best compromise between i) the nature and the length of the π-conjugated bridge and ii) the nature, the number, and the positioning of the substituents. Thus, it was shown that generally, the double CC bond is more efficient than a triple CC bond in the conjugated bridge, explained by the smallest value of BLA with double bonds leading to a better electron delocalization. This is illustrated in Figure 1-7 (From Ref. 25), as well as the impact of the length and the nature of the π-conjugated bridge. The β values of six D-π-A molecules are plotted as a function of the distance between the two nitrogen atoms at the chains ends. For short polyene and polyyne chains, β increases nonlinearly with the number of double or triple bonds. For a given number of units in the chain, the D-π-A molecule with doubly bonded π-conjugated linkers displays a larger β value than its triply bonded analog. Concerning the two molecules with cycles, they are less conjugated than the others. This explains why they have smaller β values. This difference of β value is explained by the difference of planarity: the more planar the molecule, the easier the electron delocalization, which leads to an increase of the β value.

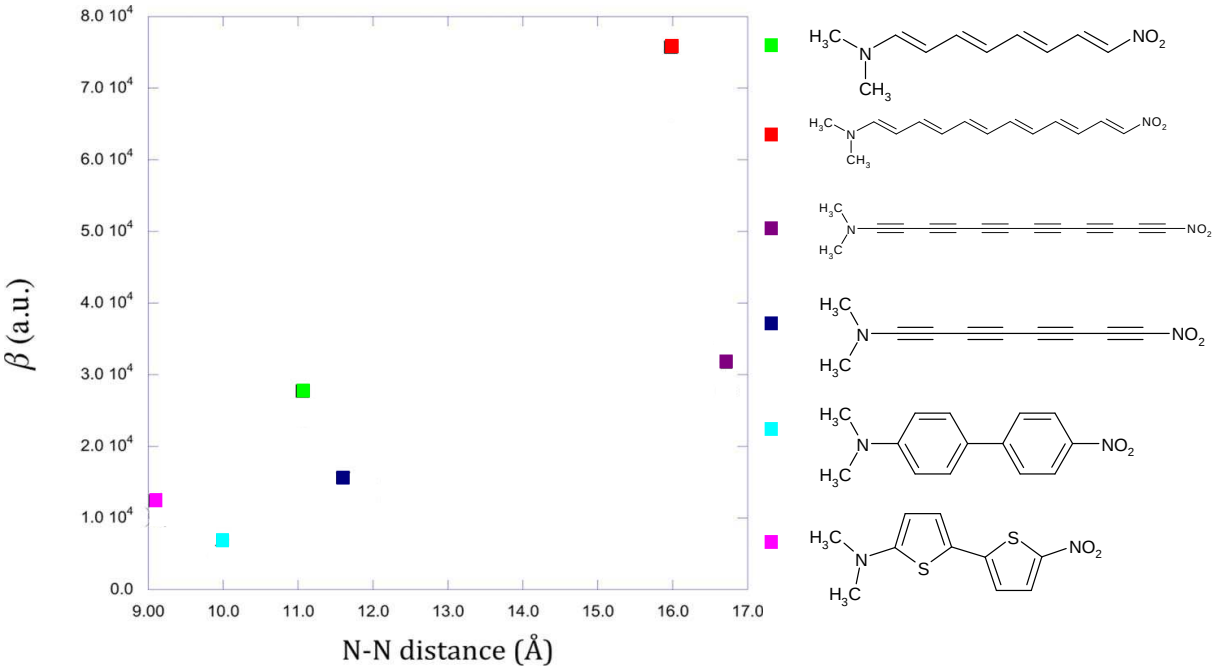

Figure 1-7: Calculated first hyperpolarizability value of six push-pull molecules as a function of the distance between the two nitrogen atoms at the chain extremities (From Ref. 25).

1.2. Molecular switches

A current challenge lies in the development of efficient switchable nonlinear optical materials. An approach to the reversible switching of NLO properties is the use of photochromic compounds. Photochromism is defined as a reversible transformation of a chemical species induced in one or both directions by absorption of electromagnetic radiation between two forms, A and B, having different absorption spectra. The thermodynamically stable form A is transformed by irradiation into form B, the back reaction can occur thermally or photochemically. The first report of photochromism was given by Fritzsche in 1867 [26], who observed the bleaching of an orange-colored solution of tetracene in the daylight and the regeneration of the color in the dark. The most spectacular evidence of photochromism is the change of colour, so the UV-visible spectra, but many other molecular properties connected to it also change along the transformation, leading to a variety of potential applications.

Since few decades, a wide range of organic NLO switches were the subject of experimental and theoretical characterizations, including azobenzene [16], anil derivatives [27], spiropyrans [28], indolino-oxazolidine [29-32], dihydroazulene [33], flavyliums [34], Ru(II)- and Fe(II)-based chromophores [5,11,35], pyridine-based octupolar chromophores [8,9], fluorescent proteins [36], etc. Some of these systems will be presented in the following paragraphs. In this area, to be useful in a device, NLO molecular switches should satisfy several conditions: i) commuting rapidly between the different forms, ii) being reversible, iii) being triggered by suitable external stimuli like electric or magnetic field, pH variation, light, redox reaction, etc, iv) displaying large NLO contrasts, and v) presenting different stable forms in solution but also in the solid state. This last point is a challenge due to the difficulty to avoid the appearance of centrosymmetry during the transition to the crystalline state.

We present in the next paragraph different switchable NLO compounds classified as a function of the stimulus used in the commutation process (irradiation, pH variation, and redox reactions).

1.2.1. pH-induced commutation

The indolino[2,1-b]oxazolidine-based derivatives [29-32] exhibit acido and photochromism (Figure 1-8). They have the ability to commute indifferently by light irradiation or pH variations between two forms, a closed colorless form and an open π-conjugated colored form, displaying very large differences in their second-order NLO responses. This system has been broadly studied through a multidisciplinary approach aiming at optimizing the β contrast between the two forms. The compound was based on an indolino-oxazolidine (X = CMe_2) moiety and the aryl group was substituted by a N,N-dimethylamino group leading to a β variation of about a factor of 31 when switching from the closed form to the open form. Then, in order to increase

the number of delocalizable electrons, the indolinic unit has been replaced by benzimidazolic unit (X = NMe) or a benzothiazolium unit (X = S). The most efficient unit turned out to be the benzothiazolium acceptor, which is 30% more effective than the indolinium one and increases the NLO response of the open form by a factor of 6, while the benzimidazolic unit has similar β values to the indolino unit. Finally, the effects of the R substituents have been rationalized by substituting the reference system (R = H) by different acceptor groups (Br, CHO, and NO_2). Calculations have predicted a global increase of β in the order: β_{HRS} (R = H) < β_{HRS} (R = Br) < β_{HRS} (R = CHO) < β_{HRS} (R = NO_2).

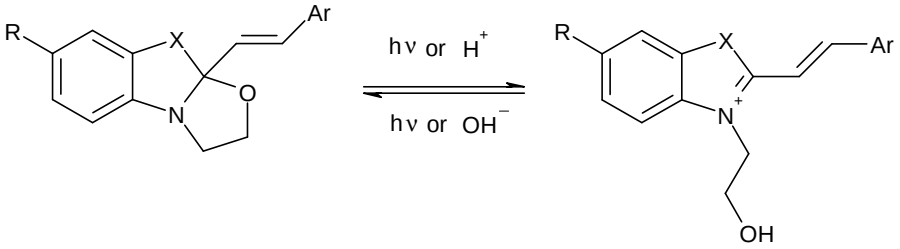

Figure 1-8: Photo and acidochromic equilibrium for switches based on the indolino-oxazolidine (X = CMe_2), benzimidazolo-oxazolidine (X = NMe), and benzothiazolo-oxazolidine (X = S) moieties.

1.2.2. Photo-induced commutation

- *Spiropyran – merocyanine equilibrium*

The transition from the spiropyran to the merocyanine forms is obtained by irradiating the spiropyran form by visible light, while the inverse reaction can be triggered by light or heat [28,37]. The transition is accompanied by a major change in the conjugation of the π electron, and thus large changes occur in the second-order NLO properties. No photochromic spiropyran or merocyanine is known to crystallize in a noncentrosymmetric crystal, so this equilibrium has been investigated in polymers and in solutions. Atassi *et al.* [38] have reported the photochemical ring opening of spiropyran in polymethylmethacrylate (PMMA) films to obtain a photo-orientation of the merocyanines by using an electric field. Chapter 4 is devoted to the optimization of the β contrast for this equilibrium initially proposed by Nakatani *et al.* [37] (Figure 1-9).

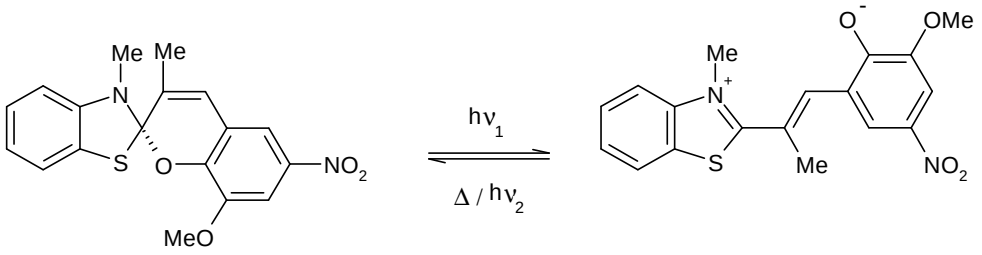

Figure 1-9: Spiropyran – merocyanine equilibrium.

- *Dinitrobenzylpyridine*

The 2-(2,4-dinitrobenzyl)pyridine (DNBP) [39,40] derivatives have also been proposed for their potential efficiency as NLO switches. The photochromic reaction implies the change from colorless **CH** or **OH** forms to a blue **NH** form (Figure 1-10). The mechanism of the process involves an intramolecular photo-induced proton transfer. The lifetime of the colored **NH** form varies between the millisecond in solution to several days in polymers. In a preliminary work, we have calculated the first hyperpolarizabilities of these three compounds. The β values increase in the order: β_{HRS} (**CH**) < β_{HRS} (**OH**) < β_{HRS} (**NH**) with contrast of about 16 between **NH** and **CH** forms. The highest values for the **NH** and **OH** forms is explained by the presence of double CC bonds in the bridge between the cycles allowing a better electron delocalization, which leads to large contrasts of first hyperpolarizabilities.

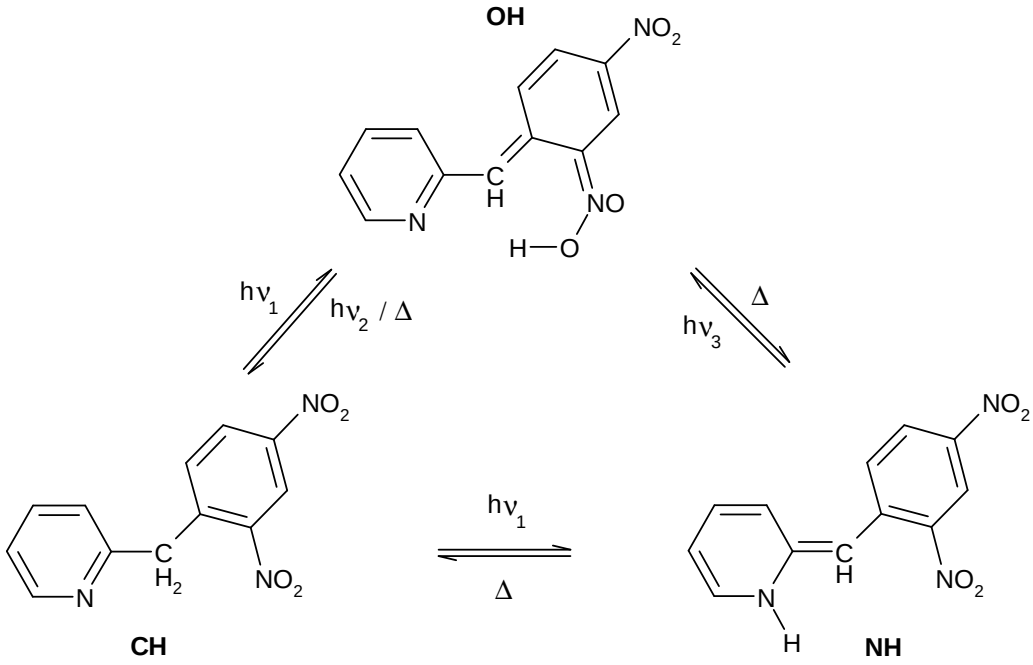

Figure 1-10: Photochemical and thermal interconversion processes of **CH**, **OH**, and **NH** tautomers in dinitrobenzylpyridine.

➢ *Anil derivatives*

Salicylideneanilines and related Schiff bases [27,41-44], usually called anils, are able to switch between an enol-imine (E) and a *cis-trans* keto-amine (enaminone) (K) forms *via* an intramolecular proton transfer reaction and a *cis-trans* isomerization, triggered only by light [44] (Figure 1-11). This tautomerization reaction can be triggered by light or by heat. Usually, the E form is the most stable and colorless or slightly yellow with an absorption band in the near UV, while the K form, metastable, is red and exhibits an additional absorption band at wavelengths larger than 400 nm. Guillaume *et al.* [45] have demonstrated that the substitution of the salicylidene ring (R) by an acceptor group or the other ring (R') by a donor group prevents the K form from being stable. The commutation between the E- and the K-form can occur both in solution and in the crystalline state but they present small β contrasts [45]. The β contrast and the solvent effects on three derivatives of this family of compounds are investigated in chapters 5 and 6.

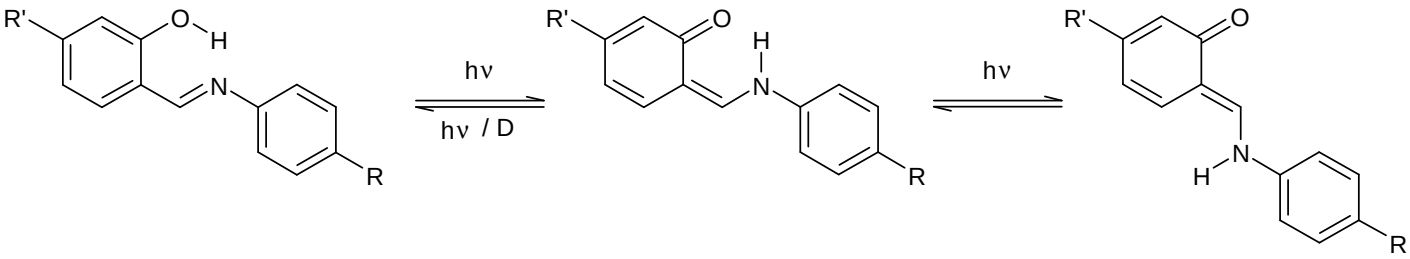

Figure 1-11: Tautomer equilibrium salicylideneaniline.

➢ *Dihydroazulene - vinylheptafulvene*

The dihydroazulene-vinylheptafulvene (DHA-VHF) systems [33,46-50] (Figure 1-12) present an interesting potential to display efficient NLO switching properties, they can commute between three forms: the DHA species that can undergo a photo-opening of the five-membered ring to form the VHF form in *cis* configuration, which can further be thermally converted into the VHF-*trans* form. When going in the opposite direction, all transformations are thermally induced. It has been noticed that the DHA to VHF transformation is usually accompanied by a change or appearance of color depending on the substituent. The impact on the β contrast of R substituents of different size is studied in chapter 7.

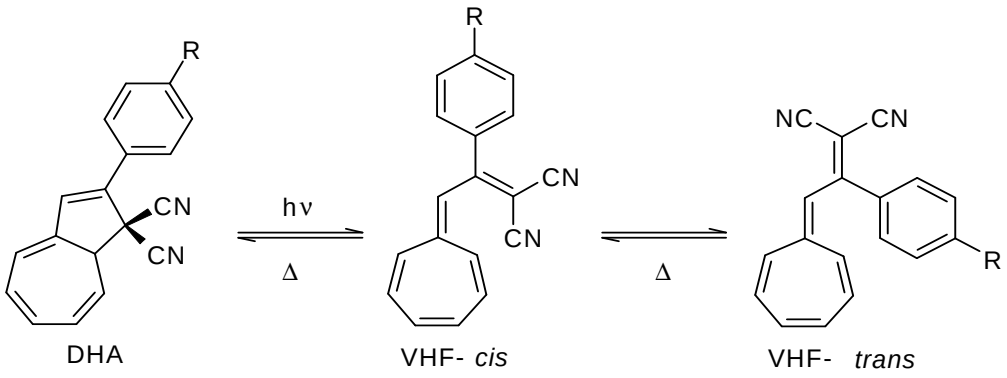

Figure 1-12: Dihydroazulene – vinylheptafulvene equilibrium.

1.2.3. Redox reactions

The redox reactions determine another class of molecular switches, in particular Ru(II)- and Fe(II)-based chromophores [5,35,51-53]. The presence of redox-active metal centers provides extensive opportunities for modulation of NLO responses. The Ru complex studied by Coe *et al.* [35] (Figure 1-13) shows very large value of first hyperpolarizability for the redox state Ru^{II}, while the Ru^{III} state is characterized by a decrease of β by a factor 1000. Indeed, the $[Ru^{III}(NH_3)_5]^{3+}$ moiety is a strong electron-attractor group as well as the pyridynium cycle, whereas the $[Ru^{II}(NH_3)_5]^{2+}$ is a electron-donor leading thereof to a push-pull molecule. This effect is completely reversed and the complex is highly stable and easily synthesized.

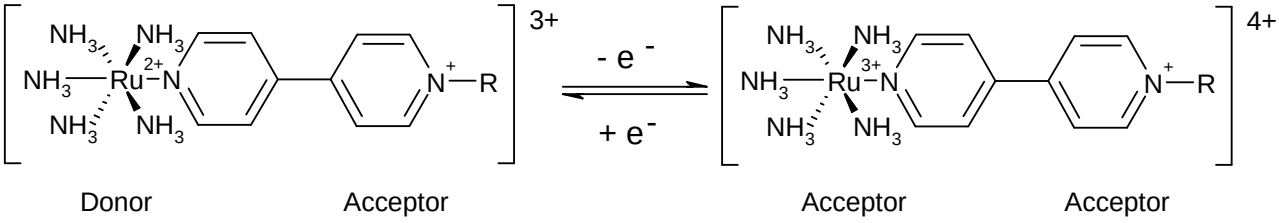

Figure 1-13: Molecular switches based on Ruthenium II complexes.

A second example of redox system involves substituted ferrocenes derivatives [51] (Figure 1-14). Radical **1** is composed of two electro-attractive units linked by a double CC bond, the polychlorinated triphenylmethyl (PTM) radical and a ferrocene group (donor), and can exist in three stable oxidation states. The reduction of **1** into its anionic form $\mathbf{1}^-$ or the oxidation into the ferrocenium radical derivative $\mathbf{1}^+$, gives rise to three different redox states. Due to their octupolar nature, substituted PTM radicals show NLO responses. The first hyperpolarizabilities of these three compounds were measured by hyper Rayleigh scattering: radical **1** displays the

highest NLO response while the β value for the anion $\mathbf{1}^-$ is divided by a factor of 18 and by 9 for $\mathbf{1}^+$.

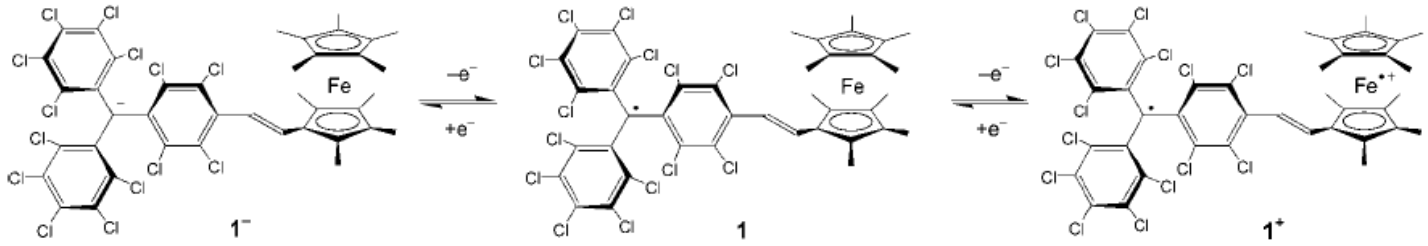

Figure 1-14: Three states of the molecular switch based on substituted ferrocene derivatives (From Ref. 51).

1.2.4. Multi-state molecular switches

➢ *Three way molecular switch based on DHA-VHF derivatives*

In a first step towards multifunctional molecular devices, Diederich *et al.* [54] have proposed a multi-state molecular switch based on the DHA-VHF equilibrium in a three-way chromophoric molecular switch controlled by pH, light, and heat (Figure 1-15) where the performed operation is dependent upon the stimulus that is chosen. These compounds display large variations in their absorption and emission spectra.

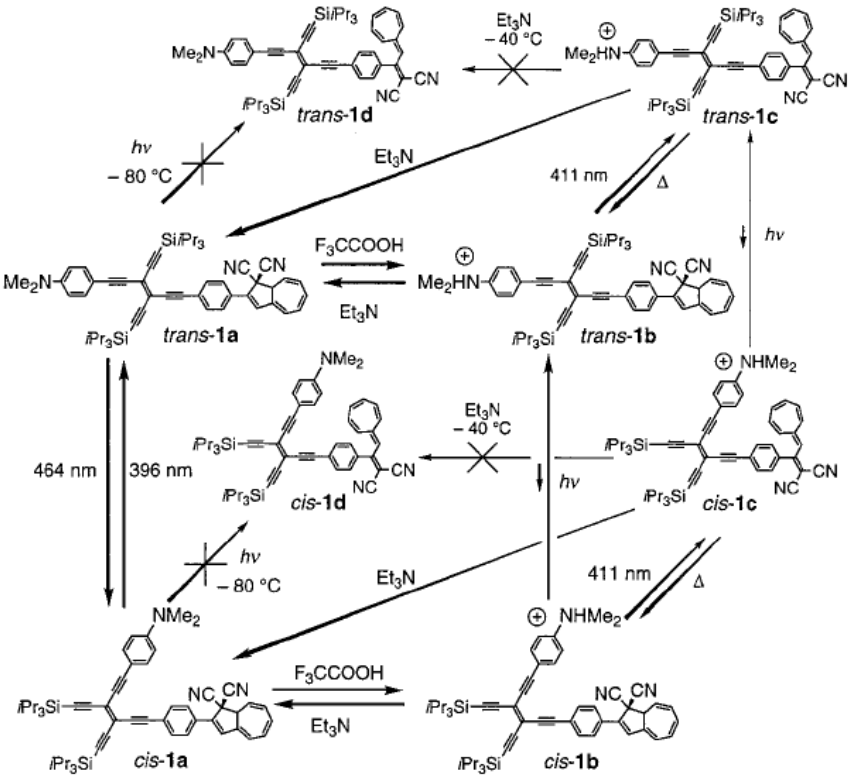

Figure 1-15: Three-way molecular switch based on DHA-VHF derivatives [54].

➢ *Biphotochromic compounds*

Recently, molecular systems composed of pairs of different photochromes, *i.e.* biphotochromes, have been synthesized and characterized [55-57]. Owing to the large number of states presenting different physico-chemical properties, they gather a real interest. As example, biphotochromes based on diarylethene and imidazo[4,5-f][1,10]phenantroline have been proposed by Xiao *et al.* [58] in 2006. These molecules are sensitive to both light and chemical stimuli. Irradiation of the initial state leads to colored solution by ring closure. The back-reaction is allowed by irradiation at visible light (620 nm). By varying the pH, the nitrogen atoms of these two forms are deprotonated (Figure 1-16).

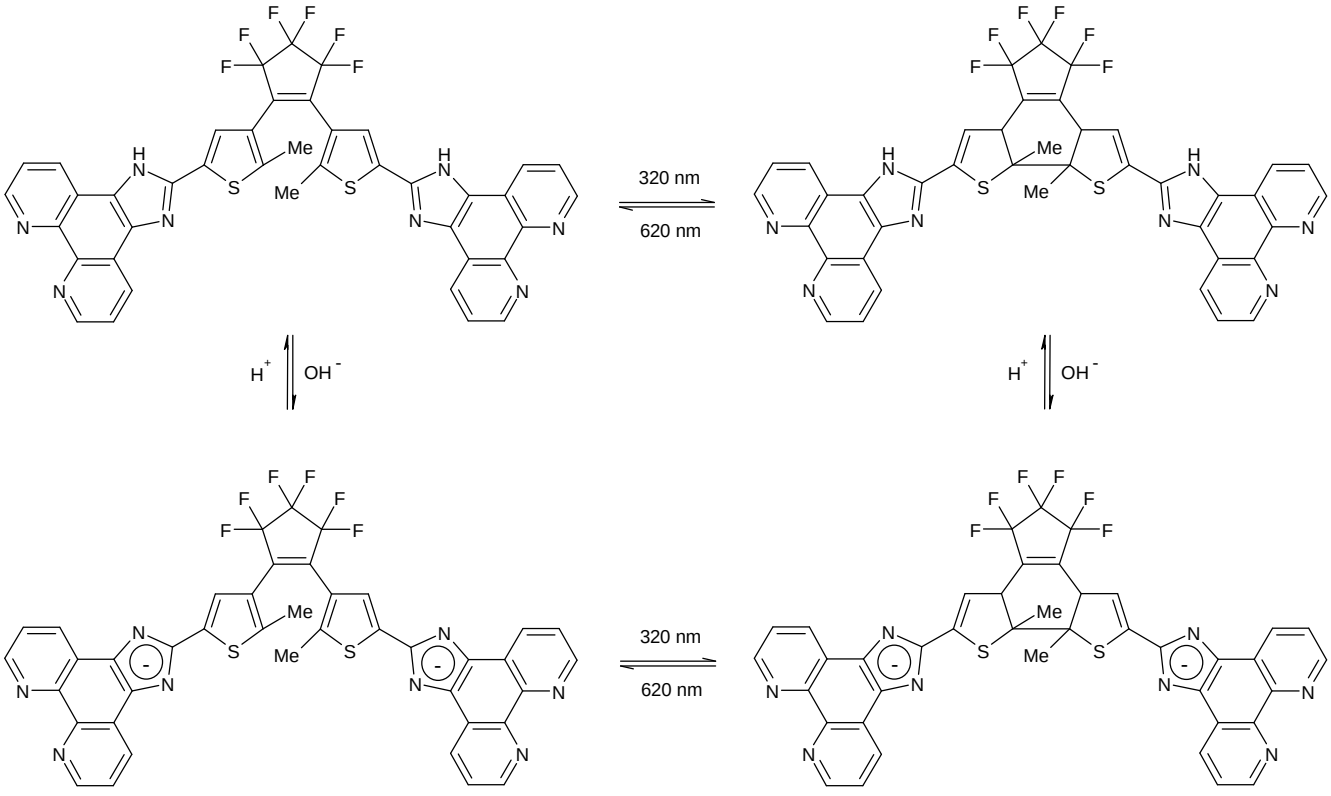

Figure 1-16: Multi-state molecular switch based on diarylethene and imidazo[4,5-f][1,10] phenantroline.

➢ *Flavylium salts*

Although until recently they have not been studied as potential NLO compounds, flavyliums salts appear highly attractive in this area [34,59-63]. As a function of the pH, different forms can be stabilized: i) the flavylium cation **AH$^+$** is stable in water in very acidic conditions, ii) by increasing the pH, the hydratation of **AH$^+$** leads to species **B**, to iii) its *cis*-chalcone **Cc** *via* ring opening, iv) these **B** and **Cc** forms are short-lived transient species, and convert into the *trans*-chalcone form, **Ct**,

owing to the isomerization of **Cc**, v) further pH increase leads to the anionic form **Ct**$^-$, while the stable *trans*-chalcone **Ct** can be converted reversibly into the **Cc** form upon light irradiation (Figure 1-17). Beyond a potential use as light-switchable pH sensors, it has been demonstrated that this complex network can be taken as a basis in view of applications for data storage, as these multistate/multifunctional systems can behave as logic devices. Indeed, it has been demonstrated that the pH and phototriggered transformations in the case of R = OH or OMe can be exploited for optical memory systems [64]. In addition, flavylium systems display photochromism after incorporation in soft materials such as micelles solution [65] or polymer [66]. Recently, the contrast of the second-order NLO response in flavylium derivatives has been investigated as a function of the nature of the substituents demonstrating that they can behave as highly efficient NLO molecular switches [67].

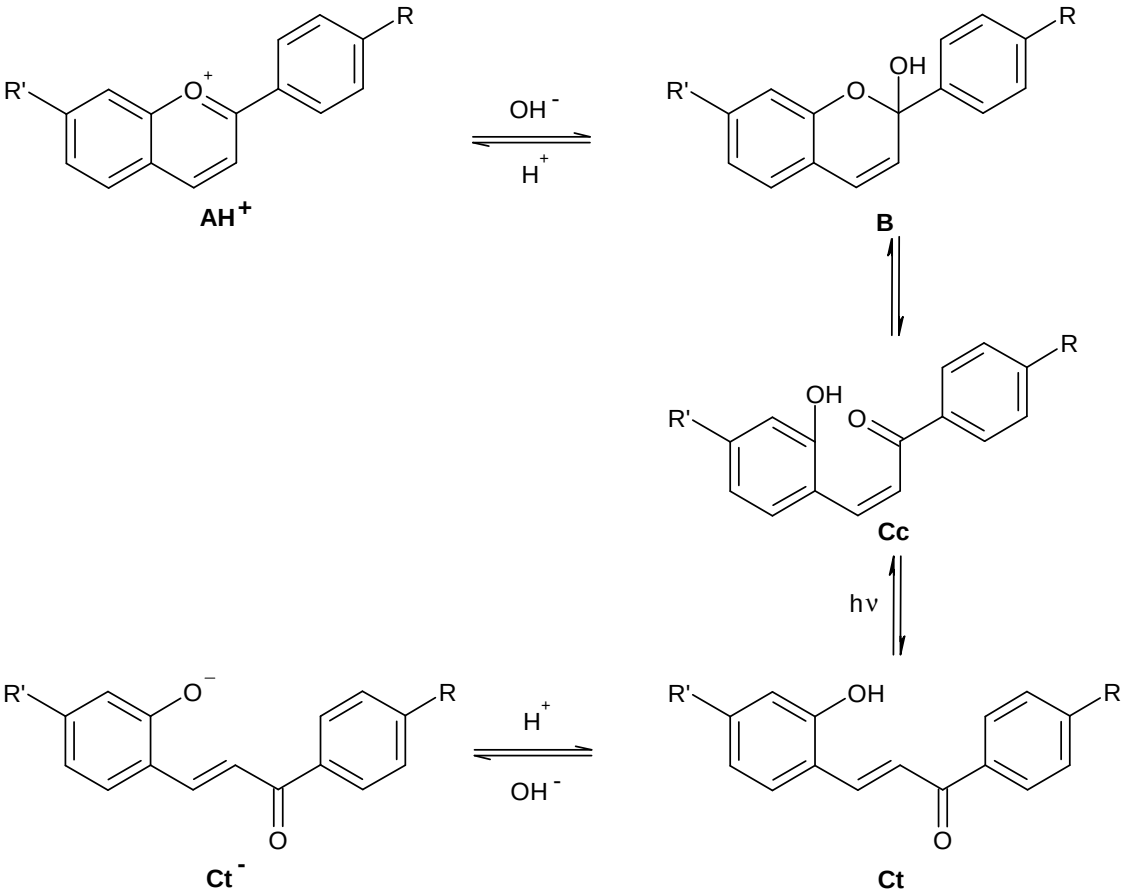

Figure 1-17: Structural transformation of flavylium compounds.

1.3. Objectives

The objective of this thesis is the design of molecular switches possessing large contrasts of second-order NLO responses by highlighting structural and electronic parameters leading to large β contrasts within a multidisciplinary approach,

which combines the synthesis of new compounds, their linear and nonlinear optical characterizations by UV-visible and hyper Rayleigh scattering spectroscopies, and theoretical simulations to predict and interpret molecular properties. This work has been carried out in co-tutelle between the FUNDP and the University of Bordeaux 1 and was focused on the experimental and theoretical characterization of several families of compounds, while the syntheses have been performed by our collaborators.

The theoretical methods used to determine the geometry as well as the linear and nonlinear optical properties of compounds of interest are presented in chapter 2, while chapter 3 presents the principles of the hyper Rayleigh scattering, the experimental method used in this thesis to determine the first hyperpolarizability.

Chapter 4 describes the derivatives of the merocyanine-spiropyran equilibrium, which commute between an open and a closed form, tuning therefore the electronic conjugation between the donor and acceptor groups. In particular, we propose efficient NLO switching compounds by selecting the best combination of substituents.

Chapters 5 and 6 address the linear and nonlinear optical properties of anil derivatives, which vary upon switching between the enol and the keto forms. Chapter 5 deals with two anil derivatives and in particular their contrast of β by comparing experimental and theoretical results. Chapter 6 concentrates on the solvent effects on the NLO responses of a third anil derivative by using different binary mixtures of solvents to displace the tautomeric equilibrium.

In chapter 7, the contrasts of second-order NLO properties in the dihydroazulene-vinylheptafulvene (DHA-VHF) equilibrium are studied as a function of the substituent R on the phenyl ring. As a preliminary step towards demonstrating switchable NLO contrast in DHA-VHF, theoretical calculations have been carried out by comparing systems with R = H, CH_3, NH_2, and NO_2.

In chapter 8 we investigate a series of six push-pull π-conjugated molecules containing the 4,5-dicyanoimidazole acceptor group, the N,N-dimethylamino donor group, and systematically enlarged π-conjugated bridges. In particular, we focus on the impact of the π-conjugated path on β. We studied how the protonation of these neutral compounds affects their first hyperpolarizabilty and their applicability as pH-triggered NLO switches.

Finally, chapter 9 deals with the characterization of symmetric and nonsymmetric chromophores based on the Tröger's base leading to the possibility of elaborating chiral molecular switches with large contrast of their first hyperpolarizability.

Conclusions and outlooks are given in chapter 10.

1.4. References

[1] P.A. Franken, A.E. Hill, C.W. Peters, and G. Weinreich, *Phys. Rev. Lett.*, **7**, 118 (1961).

[2] B. L. Feringa, *Molecular Switches*, Wiley-VCH, Weinheim (2001).

[3] B. J. Coe, *Chem. Eur. J.*, **5**, 2464 (1999).

[4] J. A. Delaire and K. Nakatani, *Chem. Rev.*, **100**, 1817 (2000).

[5] I. Asselberghs, K. Clays, A. Persoons, A.M. McDonagh, M.D. Ward, and J.A. McCleverty, *Chem. Phys. Lett.*, **368**, 408 (2003).

[6] E. Botek, M. Spassova, B. Champagne, I. Asselberghs, A. Persoons, and K. Clays, *Chem. Phys. Lett.*, **412**, 274 (2005), **417**, 282 (2006).

[7] J.F. Lamère, P.G. Lacroix, N. Farfan, J.M. Rivera, R. Santillan, and K. Nakatani, *J. Mater. Chem.*, **16**, 2913 (2006).

[8] I. Asselberghs, G. Hennrich, and K. Clays, *J. Phys. Chem. A*, **110**, 6271 (2006).

[9] M.M. Oliva, J. Casado, J.T. Lopez Navarrete, G. Hennrich, M.C. Ruiz Delgado, and J. Orduna, *J. Phys. Chem. C*, **111**, 18778 (2007).

[10] V. Aubert, V. Guerchais, E. Ishow, K. Hoang-Thi, I. Ledoux, K. Nakatani, and H. Le Bozec, *Angew. Chem. Int. Ed.*, **47**, 577 (2008).

[11] L. Boubekeur-Lecaque, B.J. Coe, K. Clays, S. Foerier, T. Verbiest, and I. Asselberghs, *J. Am. Chem. Soc.*, **130**, 3286 (2008).

[12] T. Verbiest, K. Clays, and V. Rodriguez, *Second-order nonlinear optical characterizations techniques: an introduction*, CRC Press, New York (2009).

[13] A. Yariv, *Quantum electronics*, John Wiley & Sons, New York (1975).

[14] B. L. Davydov, L. D. Derkacheva, V. V. Dunina, M. E. Zhabotinskii, V. K. Zolin, L. V. Kreneva, and M. A. Samokhina, *JEPT Lett.*, **12**, 16 (1970).

[15] K. D. Singer, J. E. Sohn, L. A. King, H. M. Gordon, H. E. Katz, and C. W. Dirk, *J. Opt. Soc. Am. B*, **6**, 1339 (1989).

[16] R. Loucif-Saïbi, K. Nakatani, J. Delaire, M. Dumont, and Z. Sekkat, *Chem. Mater.*, **5**, 229 (1993).

[17] T. Verbiest, K. Clays, C. Samyn, J. Wolff, D. Reinhoudt, and A. Persoons, *J. Am. Chem. Soc.*, **116**, 9320 (1994).

[18] C.R. Moylan, S. Ermer, S.M. Lovejoy, I.-H. McComb, D.S. Leung, R. Wortmann, P. Krdmer, and R.J. Twieg, *J. Am. Chem. Soc.*, **118**, 12950 (1996).

[19] M. Cho, S.-Y. Am, H. Lee, I. Ledoux, and J. Zyss, *J. Chem. Phys.*, **116**, 9165 (2002).

[20] T. Verbiest, S. Van Elshocht, M. Kauranen, L. Hellemans, J. Snauwaert, C. Nuckolls, T.J. Katz, and A. Persoons, *Science*, **282**, 913 (1998).

[21] D.R. Kanis, M.A. Ratner, and T.J. Marks, Chem. Rev. **94,** 195 (1994).

[22] S.R. Marder, C.B. Gorman, F. Meyers, G. Bourhill, J.L. Brédas, and B.M. Pierce, *Science*, **265**, 632 (1994).

[23] R. A. Huijts and G. L. J. Hesselhink, *Chem. Phys. Lett.*, **156**, 209 (1989).

[24] L. T. Cheng, W. Tam, S. R. Marder, A. E. Stiegman, G. Rikken, and C. W. Sprangler, *J.Phys. Chem.*, **95**, 10643 (1991).

[25] M. de Wergifosse and B. Champagne, *J. Chem. Phys.*, **134**, 074113 (2011).

[26] M. Fritzche, *Comp. Rend. Acad. Sci. Paris*, **69**, 1035 (1867).

[27] K. Nakatani and J. A. Delaire, *Chem. Mater.*, **9**, 2682 (1997).

[28] G. Berkovic, V. Krongauz, and V. Weiss, *Chem. Rev.*, **100**, 1741 (2000).

[29] L. Sanguinet, J.-L. Pozzo, V. Rodriguez, F. Adamietz, F. Castet, L. Ducasse, and B. Champagne, *J. Phys. Chem. B*, **109**, 11139 (2005).

[30] L. Sanguinet, J.-L. Pozzo, M. Guillaume, B. Champagne, F. Castet, L. Ducasse, E. Maury, J. Soulié, F. Mançois, F. Adamiez, and V. Rodriguez, *J. Phys. Chem. B*, **110**, 10672 (2006).

[31] F. Mançois, L. Sanguinet, J.-L. Pozzo, M. Guillaume, B. Champagne, V. Rodriguez, F. Adamietz, L. Ducasse, and F. Castet, *J. Phys. Chem. B*, **111**, 9795 (2007).

[32] F. Mançois, J.-L. Pozzo, F. Adamietz, V. Rodriguez, L. Ducasse, F. Castet, A. Plaquet, and B. Champagne, *Chem. Eur. J*, **15**, 2560 (2009).

[33] H. Görner, C. Fischer, S. Gierisch, and J. Daub, *J. Phys. Chem.*, **97**, 4110 (1993).

[34] R. A. McClelland and S. Gedge, *J. Am. Chem. Soc.*, **102**, 5838 (1980).

[35] B.J. Coe, S. Houbrechts, I. Asselberghs, and A. Persoons, *Angew. Chem. Int. Ed.*, **38**, 366 (1999).

[36] I. Asselberghs, C. Flors, L. Ferrighi, E. Botek, B. Champagne, H. Mizuno, R. Ando, A. Miyawaki, J. Hofkens, M. Van der Auweraer, and K. Clays, *J. Am. Chem. Soc.*, **130**, 15713 (2008).

[37] K. Nakatani, Y. Atassi, and J. A. Delaire, *Nonlinear Opt.*, **15**, 351 (1996).

[38] Y. Atassi, J. A. Delaire, and K. Nakatani, *J. Phys. Chem.*, **99**, 16320 (1995).

[39] A. Corval, K. Kuldová, Y. Eichen, Z. Pikramenou, J.M. Lehn, and H.P. Trommsdorff, *J. Phys. Chem.*, **100**, 19315 (1996).

[40] S. Houbrechts, K. Clays, A. Persoons, Z. Pikramenou, and J.-M. Lehn, *Chem. Phys. Lett.*, **258**, 485 (1996).

[41] L. Lucas, J. De Jong, J. Van Esch, R. M. Kellogg, and B. L. Feringa, *Eur. J. Org. Chem.*, **1**, 155 (2003).

[42] T. Fujiwara, J. Harada, and K. Ogawa, *J. Phys. Chem. B*, **108**, 4035 (2004).

[43] M. Sliwa, S. Létard, I. Malfant, M. Nierlich, P. G. Lacroix, T. Asahi, H. Masuhara, P. Yu, and K. Nakatani, *Chem. Mater.*, **17**, 4727 (2005).

[44] M. Sliwa, N. Mouton, C. Ruckebusch, S. Aloïse, O. Poizat, G. Buntinx, R. Métivier, K. Nakatani, H. Masuhara, and T. Asahi, *J. Phys. Chem. C*, **113**, 11959 (2009).

[45] M. Guillaume, B. Champagne, N. Markova, V. Enchev, and F. Castet, *J. Phys. Chem. A*, **111**, 9914 (2007).

[46] H. Görner, C. Fischer, and J. Daub, *J. Photochem. Photobiol. A: Chem.*, **85**, 217 (1995).

[47] T. Mrozek, H. Görner, and J. Daub, *Chem. Commun.*, 1487 (1999).

[48] J. Ern, M. Petermann, T. Mrozek, J. Daub, K. Kuldová, and C. Kryschi, *Chem. Phys.*, **259**, 331 (2000).

[49] V. De Waele, U. Schmidhammer, T. Mrozek, J. Daub, and E. Riedle, *J. Am. Chem. Soc.*, **124**, 2438 (2002).

[50] V. De Waele, M. Beutter, U. Schmidhammer, E. Riedle, and J. Daub, *Chem. Phys. Lett.*, **390**, 328 (2004).

[51] C. Sporer, I. Ratera, D. Ruiz-Molina, Y. Zhao, J. Vidal-Gancedo, K. Wurst, P. Jaitner, K. Clays, A. Persoons, C. Rivira, and J. Veciana, *Angew. Chem. Int. Ed.*, **43**, 5266 (2004).

[52] M. Malaun, R. Kowallick, A.M. McDonagh, M. Marcaccio, R.L. Paul, I. Asselberghs, K. Clays, A. Persoons, B. Bildstein, C. Fiorini, J.-M. Nunzi, MD. Ward, and J.A. McCleverty, *J. Chem. Soc., Dalton Trans.*, 3025 (2001).

[53] B. J. Coe, J. A. Harris, L. A. Jones, B. S. Brunschwig, K. Song, K. Clays, J. Garin, J. Orduna, S. J. Coles, and M. B. Hursthouse, *J. Am. Chem. Soc.*, **127**, 4845 (2005).

[54] L. Gobbi, P. Seiler, and F. Diederich, *Angew. Chem. Int. Ed.*, **38**, 674 (1999).

[55] M. Frigoli and G. H. Mehl, *Angew. Chem. Int. Ed.*, **44**, 5048 (2005).

[56] A. J. Myles, T. J. Wigglesworth, and N. R. Branda, *Adv. Mater.*, **15**, 745 (2003).

[57] G. Sevez and J.-L. Pozzo, *Dyes and Pigments*, **89**, 246 (2011).

[58] S. Xiao, T. Yi, Y. Zhou, Q. Zhao, F. Li, and C. Huang, *Tetrahedron*, **62**, 10072 (2006).

[59] R. A. McClelland and G. H. McGall, *J. Org. Chem.*, **47**, 3730 (1982).

[60] F. Pina, *J. Chem. Soc., Faraday Trans.*, **94**, 2109 (1998).

[61] F. Pina, M. J. Melo, A. J. Parola, M. Maestri, and V. Balzani, *Chem. Eur. J.*, **4**, 2001 (1998).

[62] F. Pina, J. C. Lima, A. J. Parola, and C. A. M. Afonso, *Angew. Chem. Int. Ed.*, **43**, 1525 (2004).

[63] C. A. T. Laia, A. J. Parola, F. Folgosa, and F. Pina, *Org. Biomol. Chem.*, **5**, 69 (2007).

[64] F. Pina, M. J. Melo, M. Maestri, R. Ballardini, and V. Balzani, *J. Am. Chem. Soc*, **119**, 2001 (1997).

[65] R. Gomes, A. J. Parola, C. A. T. Laia, and F. Pina, *Photochem. Photobiol. Sci.*, **6**, 1003 (2007).

[66] F. Galindo, J. C. Lima, S. V. Luis, A. J. Parola, and F. Pina, *Adv. Func. Mater.*, **15**, 541 (2005).

[67] E. Bogdan, L. Rougier, L. Ducasse, B. Champagne, and F. Castet, *J. Phys. Chem. A*, **114**, 8474 (2010).

Theoretical and computational tools

2. Theoretical and computational tools

In this chapter, the theoretical principles of the methods employed in this work are presented. The first part concerns the determination of the molecular structures. Then, the methods for determining the linear and nonlinear optical properties are presented and we finish with approaches to account for the solvent effects on these properties.

2.1. Molecular structures

All the molecular geometries were optimized at the density functional theory (DFT) level [1-3] with the B3LYP exchange-correlation functional. In this paragraph, we present the principles of DFT. Contrary to other methods, DFT method is not based on the wavefunction but on the electronic density. This theory is relied on the Hohenberg-Kohn theorems and Kohn-Sham equations.

2.1.1. From the Hohenberg-Kohn theorems to the Kohn-Sham equations

The first theorem proposed by Hohenberg and Kohn [4] states that the external potential $v(\vec{r})$ is determined, within an additive constant, by the electron density $\rho(\vec{r})$. Recalling that the external potential $v(\vec{r})$ and the number N of electrons completely determine the Hamiltonian, they also determine the wavefunction and the properties of the ground state. Therefore, the electron density that determines the number of electrons (via integration) also determines the ground state wavefunction and the other electronic properties of the system.

The second theorem, based on the variational approach, says that for a trial density, $\rho'(\vec{r})$, such that $\rho'(\vec{r}) \geq 0$ and $\int \rho'(\vec{r})\,dr = N$,

$$E_0 \leq E_v[\rho'] \tag{2-1}$$

where E_0 is the true ground state energy and $E_v[\rho'(\vec{r})]$ is the energy functional defined as :

$$\begin{aligned} E_v[\rho] &= \int \rho(\vec{r}) v(\vec{r}) d\vec{r} + T[\rho] + E_{ee}[\rho] \\ &= \int \rho(\vec{r}) v(\vec{r}) d\vec{r} + F_{HK}[\rho] \end{aligned} \tag{2-2}$$

where $T[\rho]$ is the kinetic energy of the electrons, $E_{ee}[\rho]$ is the repulsion energy between all electrons. F_{HK} is the Hohenberg-Kohn functional that includes, in addition to the kinetic energy, the classical Coulombian interaction energy, $J[\rho]$, as well as the non-classical (ncl) term:

$$F_{HK}[\rho] = T[\rho] + J[\rho] + E_{ncl}[\rho] \quad (2\text{-}3)$$

By this way, the energy is defined as a function of the electronic density. Moreover, this second theorem defines a way (and the related equations) to determine the electron-density. This approach turns out however to be difficult in practice.

To compute simply and with a good accuracy the kinetic energy, Kohn and Sham [5] invoked a non-interacting reference system, they introduced orbitals into the problem to treat electrons independently and rewrote Equation (2-3) as:

$$F[\rho] = T_s[\rho] + J[\rho] + E_{xc}[\rho] \quad (2\text{-}4)$$

E_{xc} is the exchange-correlation energy and $T_s[\rho]$ is the non-interacting kinetic energy. Therefore, E_{xc} includes i) the difference between the exact kinetic energy and $T_s[\rho]$, ii) the non-classical part of $E_{ee}[\rho]$, including iii) the self-interaction correction. Applying the variational principle, one obtains the Kohn-Sham equation comparable to Hartree-Fock (HF) equation:

$$\left[\frac{-1}{2}\nabla^2 + v_{eff}(\vec{r})\right]\psi_i(\vec{r}) = \varepsilon_i\psi_i(\vec{r}) \quad (2\text{-}5)$$

where non-interacting electrons move in an effective potential, $v_{eff}(\vec{r})$ depending on ρ(r). After introducing the linear combination of atomic orbitals, LCAO, formalism to describe the molecular orbitals:

$$FC = SCE \quad (2\text{-}6)$$

F, C, S and E are the Fock matrix, the LCAO matrix, the overlap matrix, and the energy matrix respectively. Thus, the equations are solved by starting with a trial $\rho(\vec{r})$ value (or D matrix) and by evaluating self-consistently the density and the potential until convergence.

2.1.2. Exchange-correlation functionals

The Kohn-Sham equation (Equation (2-5)) still leaves the exchange-correlation functional, E_{XC}, undefined. To obtain exact results, we have to use the exact functional. Successive approximations have been proposed:

- In the local density approximation (LDA), the exchange-correlation energy functional depends locally on the electronic density:

$$E_{XC}^{LDA}[\rho] = \int \rho(\vec{r})\ \varepsilon_{XC}^{LDA}(\vec{r}, \rho(\vec{r}))\ d\vec{r} \quad (2\text{-}7)$$

  where ε_{XC} is the exchange-correlation energy per particule of a uniform-electron gas characterized by a density ρ. The accuracy of the results is not

outstanding, in particular the overestimation of the bond energies and the underestimation of the bond lengths [6].

- The generalized gradient approximation (GGA) [6-11] takes into account the electronic density and its gradient. Thus, the exchange-correlation energy functional is expressed by:

$$E_{XC}^{GGA}[\rho] = \int \rho(\vec{r})\, \varepsilon_{XC}^{GGA}[\rho(\vec{r}); \nabla\rho(\vec{r})]\, d\vec{r} \qquad (2\text{-}8)$$

The most known GGA functional is BLYP [12-14], with Becke for the exchange part and Lee-Yang-Parr for the correlation contribution. It has been demonstrated that GGA gives excellent atomic ground-state energies, improves significantly the dissociation energies and bond lengths [15-17], describes more precisely several finite systems, and corrects the vibrational frequencies [18] of molecules built from atoms of the two first rows of the Mendeleev Table.

- The hybrid functionals, where the GGA description is improved by including a given percentage of HF exchange. Contrary to LDA or GGA, these functionals present the correct asymptotic -1/r behavior for the exchange. Several hybrid functionals [19] have been proposed like the PBE0 [20] or MPW1K [21] including 25% and 42.8% of HF exchange respectively, BHandHLYP where 50% of the exchange is described by the exact HF expression,… Actually the most popular and efficient hybrid functional is the B3LYP exchange-correlation functional developed by Stephens *et al.* [22] and containing 20% of HF exchange. This B3LYP functional is based on three semi-empirical parameters which were chosen in order to optimally reproduce the atomization and ionization energies as well as some total energies of molecules.

- The more recent LC-BLYP functional [23-27] is a long-range corrected exchange-correlation functional in which the electron repulsion operator $1/r_{12}$ is divided into short- and long-range parts by using a standard error function (erf):

$$\frac{1}{r_{12}} = \frac{1-[\alpha+\beta\,\mathrm{erf}(\mu r_{12})]}{r_{12}} + \frac{[\alpha+\beta\,\mathrm{erf}(\mu r_{12})]}{r_{12}} \qquad (2\text{-}9)$$

The first term accounts for the short range interaction and is combined with DFT exchange while the second term accounts for the long-range interaction and is combined with the HF exchange. In this expression, μ determines the balance of DFT to HF exchange at intermediate r_{12}. If μ = 0 and α = 0, it corresponds to DFT calculation. If μ = 0 and α ≠ 0, it corresponds to hybrid DFT calculation. Finally, if μ = ∞, it corresponds to standard HF calculations.

The α and β parameters satisfy the relations $0 \le \alpha + \beta \le 1$, $0 \le \alpha \le 1$, and $0 \le \beta \le 1$. The parameter α allows to incorporate the HF exchange contribution over the whole range. The parameter β allows to incorporate the DFT counterpart over the whole range by a factor of $1 - (\alpha + \beta)$. The contributions of α and β in B3LYP and LC-BLYP are represented in Figure 2-1.

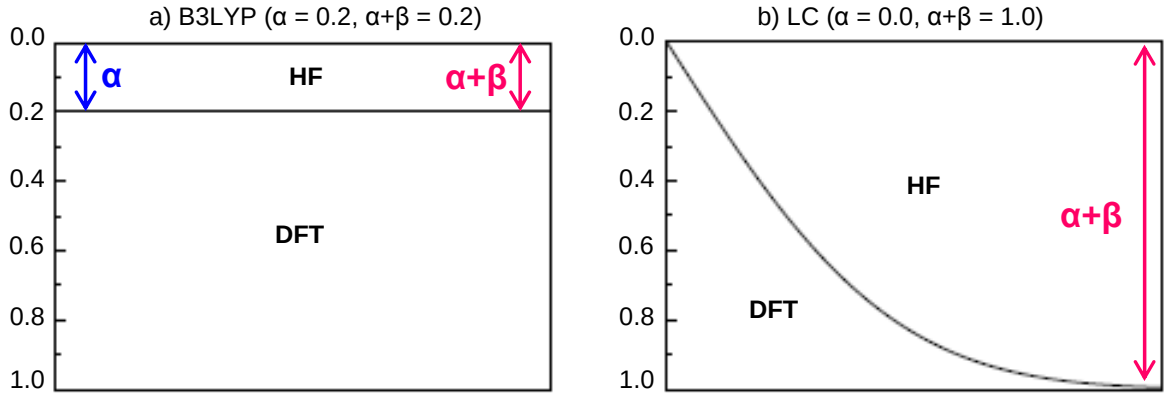

Figure 2-1: Schematic plots of the contribution to exchange from $1/r_{12}$ apportioned into DFT and HF for (a) B3LYP and (b) LC (From Ref. 26).

In this thesis, all calculations made with LC-BLYP functional are done with the parameter μ = 0.47.

2.2. Linear optical properties

In order to simulate the UV-Visible spectra and to interpret the experimental data, the excitation energies and the corresponding oscillator strengths have been evaluated at the time-dependent density functional theory (TDDFT) [28] level. Here we sketch the main equations of this time-dependent analog to DFT. So, one considers a many-electron system in the ground state, associated with the external potential $v(\vec{r})$, that is submitted to a small time-dependent perturbation $\delta v(\vec{r},t)$, leading to a change of the effective potential:

$$\delta v_{eff}(\vec{r},t) = \delta v_{pert}(t) + \delta v_{SCF}(\vec{r},t) \qquad (2\text{-}10)$$

with SCF for self-consistent field. This potential modification creates a linear response (associated with the ground state) to the density $\delta\rho(\vec{r},t)$ according to its ω-components, expressed as a function of the singly-excited determinants:

$$\delta\rho(\vec{r},\omega) = \sum_{a,i} \delta P_{ai}(\omega)\ \psi_a(\vec{r})\psi_i^*(\vec{r}) + \delta P_{ia}(\omega)\ \psi_i(\vec{r})\psi_a^*(\vec{r}) \qquad (2\text{-}11)$$

with:

$$\begin{aligned}\delta P_{ai}(\omega) &= \frac{n_a - n_i}{(\varepsilon_a - \varepsilon_i) - \omega}\delta v_{ai}^{eff} \\ &= \frac{n_a - n_i}{(\varepsilon_a - \varepsilon_i) - \omega}\left\{\delta v_{ai} + \sum_{uv} K_{ai,uv}(\omega)\delta P_{uv}(\omega)\right\}\end{aligned} \tag{2-12}$$

where n_a and n_i are the occupation numbers for the KS orbitals ψ_a and ψ_i. One can therefore express the variations in P in terms of the variations in v:

$$\left[\begin{pmatrix} A & B \\ B^* & A^* \end{pmatrix} - \omega\begin{pmatrix} 1 & 0 \\ 0 & -1 \end{pmatrix}\right]\begin{pmatrix} \delta P \\ \delta P^* \end{pmatrix} = \begin{pmatrix} -\delta v \\ -\delta v^* \end{pmatrix} \tag{2-13}$$

where,

$$A_{ai,bj} = (\varepsilon_a - \varepsilon_i)\delta_{ij}\delta_{ab} + K_{ai,bj}(\omega) \tag{2-14}$$

$$B_{ai,bj} = K_{ai,jb}(\omega) \tag{2-15}$$

The excitation energies correspond to the poles of the linear response, *i.e.* those values which make the square bracket vanishing. The A and B matrices are of dimensions $(\text{occ}\times\text{unocc})\times(\text{occ}\times\text{unocc})$. In principle, only the singly-excited state-like solutions are treated when the ω-dependence of K is removed but good performance is also often achieved for excitations having some double excitation character. K is the coupling matrix including a Coulomb-term and an exchange-correlation term:

$$\begin{aligned}K_{st\sigma,uv\tau} = &\iint \psi^*_{s\sigma}(\vec{r})\psi_{t\sigma}(\vec{r})\frac{1}{|\vec{r}-\vec{r}'|}\psi^*_{u\tau}(\vec{r}')\psi_{v\tau}(\vec{r}')d\vec{r}d\vec{r}' \\ &+ \iint \psi^*_{s\sigma}(\vec{r})\psi_{t\sigma}(\vec{r})\frac{\delta^2 E_{xc}}{\delta\rho_\sigma(\vec{r})\delta\rho_\tau(\vec{r}')}\psi^*_{v\tau}(\vec{r}')\psi_{u\tau}(\vec{r}')d\vec{r}d\vec{r}'\end{aligned} \tag{2-16}$$

σ and τ are spin functions, and $\frac{\delta^2 E_{xc}}{\delta\rho_\sigma(\vec{r})\delta\rho_\tau(\vec{r}')}$ is the exchange-correlation kernel. Evaluation of the excitation energies requires therefore the choice of an exchange-correlation potential, an exchange-correlation energy, and an exchange-correlation kernel. As in DFT method, the choice of these functionals will impact the accuracy of the results.

The linear optical properties (excitation energies and oscillator strengths) have been calculated with the B3LYP exchange-correlation functional, which generally leads to UV-Visible spectra in a good qualitative agreement with respect to experimental data for both the excitation energies and the oscillator strengths [29-33]. For example, Guillaume *et al.* [33] have demonstrated this good qualitative agreement

by determining and comparing the experimental and theoretical excitation energies of a set of merocyanine dyes. Indeed, the correlation coefficients of the linear regressions are always larger than 0.98 (Figure 2-2).

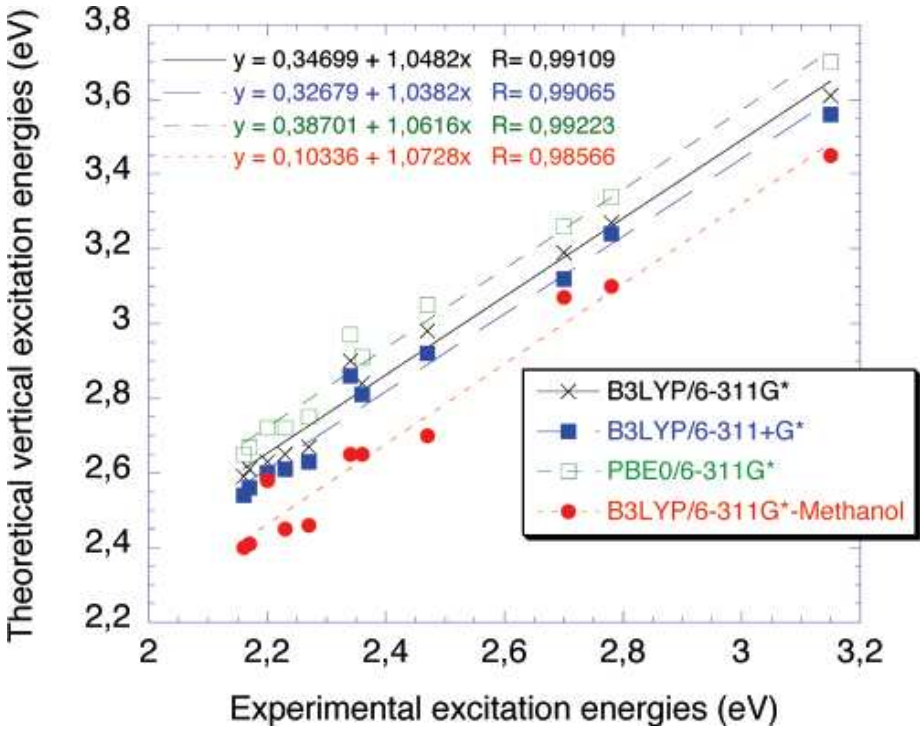

Figure 2-2: Theoretical vs experimental excitation energies of merocyanine dyes for different TDDFT levels of approximation (From Ref. 32).

2.3. Second-order nonlinear optical properties

Several methods allow the evaluation and the interpretation of the second-order nonlinear optical properties, in particular the first hyperpolarizabilities. The time-dependent Hartree-Fock (TDHF) method and the second-order Møller-Plesset (MP2) scheme are described in the next paragraphs as well as the multiplicative scheme, which combines the values obtained with TDHF and MP2 in order to take into account both the frequency dispersion and the electronic correlation effects. Finally, the DFT and TDDFT methods, which also treat the electron correlation, have been assessed.

2.3.1. The Time-Dependent Hartree-Fock method

The TDHF (Time-Dependent Hartree-Fock) [34,35] method allows to evaluate analytically the energy or dipole moment derivatives with respect to the electric field and therefore the (hyper)polarizabilities. Indeed, the expression of the dynamic first

hyperpolarizability tensor components comes from the derivatives of the LCAO dipole moment expression and is given by:

$$\beta_{abc}(-\omega_\sigma;\omega_1,\omega_2)=\left(\frac{\partial^2\mu_a}{\partial E_b(\omega_1)\partial E_c(\omega_2)}\right)_0=-2\sum_{p,q}^{K}M_{pq}^{a}D_{qp}^{bc}(\omega_1,\omega_2) \qquad (2\text{-}17)$$

where M_{pq}^{a} is the dipole moment matrix in the *a*-direction, $D_{qp}^{bc}(\omega_1,\omega_2)$ is the second-order derivative of the density matrix with respect to electric fields oriented in the *b*- and *c*-directions and of pulsations ω_1 and ω_2, and $\omega_\sigma = \omega_1 + \omega_2$. The determination of $D^{bc}(\omega_1, \omega_2)$ is based on three equations: the time-dependent Hartree-Fock equation, the normalization condition of the wavefunction, and the definition of the density matrix:

$$FC - i\frac{\partial}{\partial t}SC = SC\varepsilon \qquad (2\text{-}18)$$

$$C^{\dagger}SC = 1 \qquad (2\text{-}19)$$

$$D = CnC^{\dagger} \qquad (2\text{-}20)$$

F, C, S, D, and ε are the Fock matrix, the LCAO matrix, the overlap matrix, the density matrix, and the energy matrix, respectively while n is a diagonal matrix whose elements are equal to 2 or 0 if the molecular orbital is doubly occupied or unoccupied. Two perturbations are considered, both of E_a amplitude, but of opposite phase, ω and -ω:

$$\lambda^a(\omega)=E_a e^{i\omega t} \qquad (2\text{-}21)$$

$$\lambda^a(-\omega)=E_a e^{-i\omega t}=(\lambda^a(\omega))^* \qquad (2\text{-}22)$$

In the TDHF scheme, each matrix of Equations (2-18) to (2-20) is developed as a function of the $\lambda^a(\omega)$ and $\lambda^a(-\omega)$ perturbations. For instance for the LCAO matrix:

$$C(\omega)=C+\lambda^a(\omega)C^a(\omega)+\lambda^a(-\omega)C^a(-\omega)+\ldots \qquad (2\text{-}23)$$

$$C(\omega)^{\dagger}=C^{\dagger}+\lambda^a(-\omega)C^{a\dagger}(\omega)+\lambda^a(\omega)C^{a\dagger}(-\omega)+\ldots \qquad (2\text{-}24)$$

These expansions are introduced into Equations (2-18) to (2-20). At first order in the perturbation, one obtains:

$$F^a(\omega)C+FC^a(\omega)+\omega SC^a(\omega)=SC^a(\omega)\varepsilon+SC\varepsilon^a(\omega) \qquad (2\text{-}25)$$

$$C^{a\dagger}(-\omega)SC+C^{\dagger}SC^a(\omega)=0 \qquad (2\text{-}26)$$

$$D^a(\omega)=C^a(\omega)nC^{\dagger}+CnC^{a\dagger}(-\omega) \qquad (2\text{-}27)$$

The evaluation of D^a matrix requires the determination of the perturbed LCAO matrices $C^a(\omega)$ and $C^a(-\omega)$. To do so new unitary matrices, $U^a(\omega)$ and $U^a(-\omega)$ are defined:

$$C^a(\omega) = CU^a(\omega) \text{ and } C^a(-\omega) = CU^a(-\omega) \tag{2-28}$$

Thus, Equation (2-26) leads to:

$$U^{a\dagger}(-\omega)C^\dagger SC + C^\dagger SCU^a(\omega) = 0 \tag{2-29}$$

Or:

$$U^{a\dagger}(-\omega) + U^a(\omega) = 0 \tag{2-30}$$

Accordingly,

$$C^a(-\omega) = CU^a(-\omega) \rightarrow C^a(-\omega) = -CU^{a\dagger}(\omega) \tag{2-31}$$

It appears that only the (occ unocc) and (unocc occ) blocks of the $U^a(\omega)$ matrix are needed to determine the density matrix derivatives:

$$D^a_{rs} = \sum_{i=1}^{occ}\sum_{a=1}^{unocc} C_{ra}U^a_{ai}(\omega)C^\dagger_{is} + C_{ri}U^{a\dagger}_{ia}(-\omega)C^\dagger_{as} \tag{2-32}$$

which are evaluated from the general expression:

$$\begin{aligned} &C^\dagger F^a(\omega)C + \varepsilon U^a(\omega) + \omega U^a(\omega) = U^a(\omega)\varepsilon + \varepsilon^a(\omega) \\ \rightarrow\quad &G^a_{ia}(\omega) + \varepsilon_i U^a_{ia}(\omega) + \omega U^a_{ia}(\omega) = U^a_{ia}(\omega)\varepsilon_a \end{aligned} \tag{2-33}$$

where $G^a_{ia}(\omega) = \left(C^\dagger F^a(\omega)C\right)_{ia}$. Finally, one obtains:

$$U^a_{ia}(\omega) = \frac{G^a_{ia}(\omega)}{\varepsilon_a - \varepsilon_i - \omega} \tag{2-34}$$

In turn, $U^a(\omega)$ allows evaluating the perturbed LCAO matrix, $C^a(\omega)$, and then the first-order derivative of the density matrix. However, the $G^a(\omega)$ and $F^a(\omega)$ matrices depend upon the D^a matrix, leading to an iterative procedure. The TDHF cycle is illustrated in Figure 2-3.

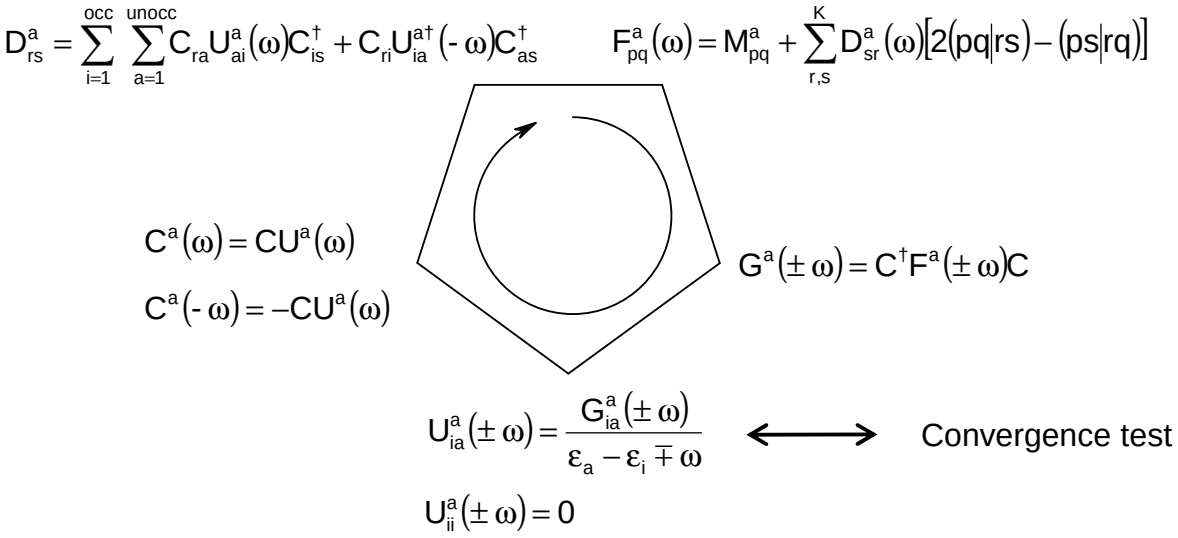

Figure 2-3: First-order TDHF cycle.

The same strategy can be applied in order to determine the second-order derivative of the density matrix, $D^{ab}(\omega_1, \omega_2)$, leading to the determination of the first hyperpolarizability. Nevertheless, it is possible to take advantage of the "2*n*+1" rule [36,37], which states that, for a variational procedure, the energies to order 2*n*+1 can be calculated from the wavefunctions to order *n* and lower. The first hyperpolarizability, which is a third-order response of the energy to external field (2*n* + 1 = 3), can be evaluated from only the first-order derivatives of the wavefunction. This rule enables to reduce considerably the computational time. In such a case Equation (2-17) can be rewritten as:

$$\begin{aligned}\beta_{abc} = &-\mathrm{Tr}\left[n\left\{U^a G^b U^c + U^c G^b U^a + U^b G^c U^a + U^a G^c U^b + U^c G^a U^b + U^b G^a U^c\right\}\right] \\ &-\mathrm{Tr}\left[n\left\{U^a U^c \varepsilon^b + U^c U^a \varepsilon^b + U^b U^a \varepsilon^c + U^a U^b \varepsilon^c + U^c U^b \varepsilon^a + U^b U^c \varepsilon^a\right\}\right]\end{aligned} \qquad (2\text{-}35)$$

where only first-order derivatives of the LCAO coefficients appear. In our calculations, the "2*n*+1" rule is employed.

Finally, it has been showed that in the static limit of the electric field, where $\omega_1 = \omega_2 = 0$, the TDHF scheme is reduced to the CPHF [38,39] (Coupled-Perturbed Hartree-Fock) equations.

2.3.2. The Møller-Plesset perturbation theory

In the TDHF scheme, the frequency dispersion is considered in the evaluation of the first hyperpolarizability. However, the electron correlation is another important parameter to take into account for evaluating β accurately. Hence, to correct the correlation error inherent to the HF method, the Møller-Plesset (MP)

perturbation theory, combined with the finite field (FF) approach, was adopted. Let us have a look at this method.

In the Hartree-Fock method, the correlation error is due to the use of the Coulomb and Pauli operators instead of the exact repulsion operator. The Møller-Plesset (MP) theory [40,41] is based on the Rayleigh-Schrödinger perturbation theory [40], which defines the second-order correction to the energy by:

$$E_i^{(2)} = \sum_{k \neq i} \frac{\left| \left\langle \Psi_k^{(0)} \middle| W \middle| \Psi_i^{(0)} \right\rangle \right|^2}{E_i^{(0)} - E_k^{(0)}} \tag{2-36}$$

where W is the operator associated to the perturbation, λW and $\Psi_k^{(0)}$ and $\Psi_i^{(0)}$ are the wavefunctions of the perturbed Hamiltonian. The evaluation of the electron correlation resulting from this perturbation, λW, corresponds to the difference between the exact repulsion operator and the approximate HF operator:

$$\lambda W = H - H_0 = \sum_{i)j} \frac{1}{r_{ij}} - \sum_i v_{HF}(i) \tag{2-37}$$

Therefore, the contributions of successive order to the energy and the wavefunction can be evaluated. The zero-order term is the sum of the occupied orbital energies:

$$E_0^{(0)} = \left\langle \Psi_0^{(0)} \middle| H_0 \middle| \Psi_0^{(0)} \right\rangle = \sum_i^N \varepsilon_i \tag{2-38}$$

The first-order correction compensates the Coulombian and exchange interactions that are counted twice in the $E_0^{(0)}$ expression:

$$E_0^{(1)} = \frac{-1}{2} \sum_i^N \sum_j^N \left\langle ij \middle\| ij \right\rangle = \frac{-1}{2} \sum_i \sum_j \left(\left\langle ij \middle| ij \right\rangle - \left\langle ij \middle| ji \right\rangle \right) \tag{2-39}$$

where i and j stand for occupied molecular orbitals. As a consequence, the HF energy is the sum of the two first terms:

$$E_0^{HF} = E_0^{(0)} + E_0^{(1)} \tag{2-40}$$

The first-order correction to the ground-state wavefunction is written:

$$\psi_0^{(1)} = \sum_{k \neq 0} \frac{\left\langle \psi_k^{(0)} \middle| W \middle| \psi_0^{(0)} \right\rangle}{E_0^{(0)} - E_k^{(0)}} \psi_k^{(0)} \tag{2-41}$$

The summation runs over all the excited states of the system. In accordance with Brillouin theorem and since the operator W only contains one- and two-electron operators, the summation over k is limited to the doubly-excited configurations:

$$\psi_0^{(1)} = \sum_{i\rangle j}\sum_{a\rangle b} \frac{\left\langle \psi_{ij}^{ab(0)} \middle| W \middle| \psi_0^{(0)} \right\rangle}{E_0^{(0)} - E_{ij}^{ab(0)}} \psi_{ij}^{ab(0)} = \sum_{i\rangle j}\sum_{a\rangle b} \frac{\langle ab \| ij \rangle}{\varepsilon_i + \varepsilon_j - \varepsilon_a - \varepsilon_b} \psi_{ij}^{ab(0)} \tag{2-42}$$

and the second-order correction is written:

$$E_0^{(2)} = \sum_{j\neq 0} \frac{\left| \left\langle \Psi_j^{(0)} \middle| W \middle| \Psi_0^{(0)} \right\rangle \right|^2}{E_0^{(0)} - E_j^0} = \sum_{i\rangle j}\sum_{a\rangle b} \frac{\left| \langle ab \| ij \rangle \right|^2}{\varepsilon_i + \varepsilon_j - \varepsilon_a - \varepsilon_b} \tag{2-43}$$

$E_0^{(2)}$ contains the major part of the electron correlation correction. The highest order corrections are generally smaller. In general, our calculations are limited to this second-order Møller-Plesset (MP2) correction.

2.3.3. The Finite Field method

The Finite Field (FF) [42] method is a numerical derivative approach, allowing the evaluation of the first hyperpolarizabilities as derivatives of the energy with respect to the electric field. Here, the nuclei are considered fixed. As mentioned previously, the first hyperpolarizability is the third-order derivative of the energy or the second-order derivative of the dipole moment with respect to the electric field (Equation (1-5)). The FF equation for the evaluation of β is:

$$\beta = -\left(\frac{\partial^3 \mathcal{E}}{\partial E^3} \right)_{E=0} = -\lim_{E\to 0} \frac{\mathcal{E}(+2E) - \mathcal{E}(-2E) - 2[\mathcal{E}(+E) - \mathcal{E}(-E)]}{2E^3} = \left(\frac{\partial^2 \mu}{\partial E^2} \right) = -\lim_{E'\to 0} \frac{\mu(+E) + \mu(-E) - 2\mu(0)}{E^2} \tag{2-44}$$

where $\mathcal{E}$ is the energy and E the amplitude of the external electric field. In this scheme, the energy is calculated for different field amplitudes and Equation (2-44) is evaluated. To remove higher-order contamination in the FF differentiation [43], the Romberg procedure is applied in combination with field amplitudes ranging from ±0.0004 to ±0.0064 a.u.. The iterative Romberg expression reads:

$$\beta_k^n = \frac{4^n \beta_k^{n-1} - \beta_{k+1}^{n-1}}{4^n - 1} \tag{2-45}$$

where n is the order of the iteration and k defines the field amplitude: $E_k = E_0\ 2^{k-1}$. Figure 2-4 and Table 2-1 sketche the Romberg's iterative scheme and illustrates it in the case of the evaluation of β_{xxx} of a 4,5-dicyanoimidazole-based molecule.

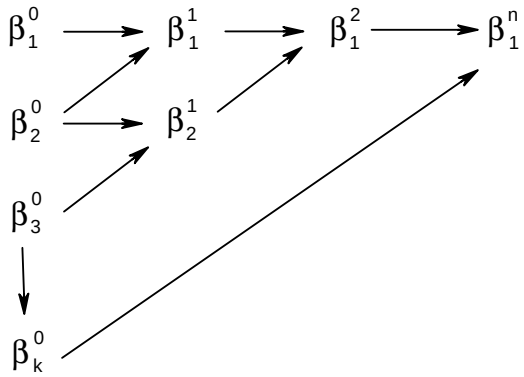

Figure 2-4: Scheme of the Romberg's procedure.

HF					**MP2**				
n / k	**1**	**2**	**3**	**4**	n / k	**1**	**2**	**3**	**4**
1	-5732.4	-5724.5	-5724.5	-5724.5	**1**	-10411.9	-10390.2	-10390.4	-10390.6
2	-5756.2	-5723.6	**-5724.8**		**2**	-10477.0	-10387.2	**-10391.2**	
3	-5853.3	-5718.2			**3**	-10746.6	-10326.6		
4	-6288.5				**4**	-12006.6			

Table 2-1: Romberg's procedure for the evaluation of β_{xxx} of a 4,5-dicyanoimidazole-based molecule at HF and MP2 levels.

It has been demonstrated [43] that the accuracy improves with the order of the Romberg iteration. The β value is determined when a convergent behavior of the values is attained, characterized by a small difference between two successive β values. As example given in Table 2-1, the selected FF/HF value is -5724.8 a.u. while the FF/MP2 one is -10391.2 a.u.. The HF value obtained from analytical differentiation using the CPHF method is -5724.8 a.u., demonstrating the accuracy of the Romberg's scheme.

2.3.4. Impact of electron correlation on the first hyperpolarizability

In this work, to take into account the electron correlation effects, most calculations were carried out by using the MP2 method in combination with the FF scheme. This method turns out to be the method of choice to predict the first hyperpolarizabilities [44] of push-pull π-conjugated systems by comparison with more accurate techniques (like CCSD(T)). Nevertheless, the validity of MP2 calculations has been verified, for instance, by including the fourth-order electron correlation effects *via* the MP4 method. The enol form of anil derivatives and three push-pull molecules (From Ref. 43) have been investigated, the results are given in Table 2-2.

	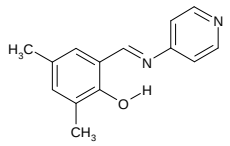	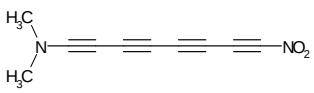	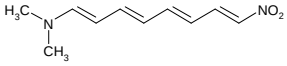	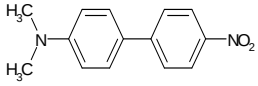
β_{HRS}^{CPHF}	360	8151	10138	3432
β_{HRS}^{MP2}	722	13255	24206	5692
β_{HRS}^{MP4}	795	13783	24943	6015
$\beta_{HRS}^{CCSD(T)}$	-	12685	21646	5550

Table 2-2: HRS static first hyperpolarizabilities (a.u.) of an anil derivative and three typical push-pull molecules (From Ref. 43) at different levels of approximation.

These results highlight the impact of the electron correlation on the evaluation of the first hyperpolarizabilities. The β values almost double for each molecule when going from CPHF to MP2. Then, the difference between MP2 and MP4 is of 10% only for the anil derivative, and less than 5% for the push-pull molecules demonstrating that MP2 method is sufficiently correlated to evaluate β while the computational cost with MP4 is largely increased compared to MP2. The validity of the chosen method is further demonstrated by considering the CCSD(T) (coupled cluster singles and doubles calculations with a perturbative estimate of triples) results. CCSD(T) is a reference method to take into account the electron correlation, more correlated than MP2 and MP4. Compared to MP2 results, the CCSD(T) values decrease by 4.3%, 10.6%, and 2.5%, respectively for molecule with triple bonds, double bonds, and cycles.

2.3.5. The multiplicative scheme

The frequency dispersion and the electronic correlation play an important role in the evaluation of the first hyperpolarizabilities and are necessary for comparison with experimental values. In this work, the TDHF and CPHF methods are respectively applied for obtaining the dynamic and static first hyperpolarizabilities, while the MP2 method is employed to account for electron correlation effects. To estimate simultaneously both effects, the multiplicative scheme [45,46] is applied. It consists in multiplying the static MP2 value by a corrective dispersion factor:

$$\beta_{MP2}(-2\omega;\omega,\omega) = \beta_{MP2}(0;0,0) \times \frac{\beta_{TDHF}(-2\omega;\omega,\omega)}{\beta_{CPHF}(0;0,0)} \quad (2\text{-}46)$$

A similar scheme was applied to the depolarization ratios:

$$DR_{MP2}(-2\omega;\omega,\omega) = DR_{MP2}(0;0,0) \times \frac{DR_{TDHF}(-2\omega;\omega,\omega)}{DR_{CPHF}(0;0,0)} \quad (2\text{-}47)$$

This multiplicative correction approximation is a very powerful tool to estimate the correlated dynamic β values [47].

2.3.6. Assessment of the DFT functionals to evaluate the first hyperpolarizability

The electron correlation impact on the first hyperpolarizabilities has been discussed in previous paragraphs. On the other hand, the DFT and TDDFT methods (presented in Chapter 2.1 and 2.3.1) are often proposed as ideal solutions to account for electron correlation because they combine low computational cost with good accuracy, including for the evaluation of the linear and nonlinear responses to electric field. Nevertheless, several studies have pointed out the drawbacks of DFT with conventional exchange-correlation functionals, *i.e.* LDA, GGA, and even hybrid functionals, when investigating the (hyper)polarizabilities of extended systems [48-53].

The performance of DFT methods is further assessed here for calculating β values and β contrasts by comparing HF and MP2 calculations to results obtained using different exchange-correlation functionals, encompassing GGA, hybrid, and LC functionals. The compounds under study are i) the acid/base or protonated/deprotonated switch of a 4,5-dicyanoimidazole-containing compound (Table 2-3), ii) three merocyanine-spiropyran systems (Table 2-4), and iii) the NO_2-substituted DHA/VHF system (Table 2-5).

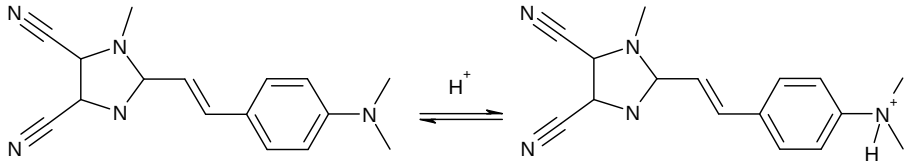

Neutral and protonated forms of the 4,5-dicyanoimidazole-containing compound **1**.

		1		**Protonated 1**		$\frac{\beta_1}{\beta_{1\text{–protonated}}}$
		β_{HRS}	DR	β_{HRS}	DR	
CPHF	$\lambda = \infty$	1915	4.97	1423	4.26	1.35
MP2		3837	5.02	2191	4.79	1.75
BLYP		4365	4.92	5574	4.83	0.78
B3LYP		3829	4.96	4156	4.75	0.92
LC-BLYP		2874	5.02	1598	4.39	1.80
TDHF	λ = 1064 nm	3086	5.09	2434	4.44	1.27
MP2 [a]		6183	5.14	3748	4.99	1.65
BLYP		25553	5.10	27201	4.97	0.94
B3LYP		10896	5.07	12050	4.90	0.90
LC-BLYP		5222	5.08	2864	4.57	1.82

Table 2-3: First hyperpolarizabilities (a.u.) and depolarization ratios of compound **1** in its neutral and protonated forms evaluated at different levels of approximation, using the 6-311+G* basis set (for the MP2 calculations, the basis set is 6-31G*).
[a] The dynamic MP2 results are obtained using Equations (2-46) and (2-47).

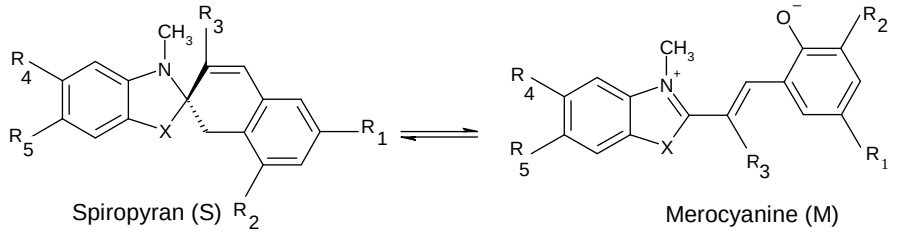

Spiropyran - merocyanine systems and their optimized substituants. **2**: $R_1 = NO_2$, $R_2 = OMe$, $R_3 = Me$, X = S, $R_4 = R_5 = H$; **3**: $R_1 = NO_2$, $R_2 = NMe_2$, $R_3 = NH_2$, X = NMe, $R_4 = H$, $R_5 = NO_2$; **4**: $R_1 = NO_2$, $R_2 = NMe_2$, $R_3 = NH_2$, X = NMe, $R_4 = H$, $R_5 = NO_2$.

		Merocyanine		**Spiropyran**		$\frac{\beta_M}{\beta_S}$
		β_{HRS}	DR	β_{HRS}	DR	
Molecule **2**						
CPHF	$\lambda = \infty$	1239	2.59	275	2.50	4.51
MP2		3091	6.07	509	3.76	6.07
BLYP		1630	2.71	1436	4.17	1.14
B3LYP		1474	2.75	945	3.87	1.56
LC-BLYP		1203	3.42	442	3.30	2.72
TDHF	λ = 1064 nm	3343	3.37	371	2.72	9.01
MP2 [a]		10293	7.90	723	4.09	14.24
BLYP		27534	4.85	6526	4.97	4.22
B3LYP		38722	4.18	2307	4.53	16.78
LC-BLYP		5199	2.36	668	3.64	7.78
Molecule **3**						
CPHF	$\lambda = \infty$	2702	3.55	305	4.44	8.86
MP2		5134	3.88	736	5.28	6.98
BLYP		7492	4.49	1776	4.96	4.22
B3LYP		5080	4.09	1144	4.98	4.44
LC-BLYP		3967	3.70	533	4.88	7.44
TDHF	λ = 1064 nm	7538	4.27	415	4.69	18.16
MP2 [a]		14774	4.67	950	5.58	15.55
BLYP		50413	2.06	50313	4.85	1.002
B3LYP		35231	4.64	3231	5.33	10.90
LC-BLYP		22528	4.72	802	5.20	28.09
Molecule **4**						
CPHF	$\lambda = \infty$	3793	3.88	544	2.49	6.97
MP2		6196	4.16	823	2.90	7.53
BLYP		45076	4.92	1487	2.59	30.31
B3LYP		16583	4.70	1157	2.53	14.33
LC-BLYP		5049	3.96	728	2.60	6.94
TDHF	λ = 1064 nm	11589	4.59	760	2.64	15.25
MP2 [a]		19585	4.92	1246	3.07	15.72
BLYP		116583	4.15	16859	4.49	6.92
B3LYP		157014	2.74	2603	2.61	60.32
LC-BLYP		37210	4.95	1112	2.72	33.46

Table 2-4: First hyperpolarizabilities (a.u.) and depolarization ratios of molecules **2**-**4** in their S and M forms evaluated at different levels of approximation, using the 6-311+G* basis set (for the MP2 calculations, the basis set is 6-31G*).
[a] The dynamic MP2 results are obtained using Equations (2-46) and (2-47).

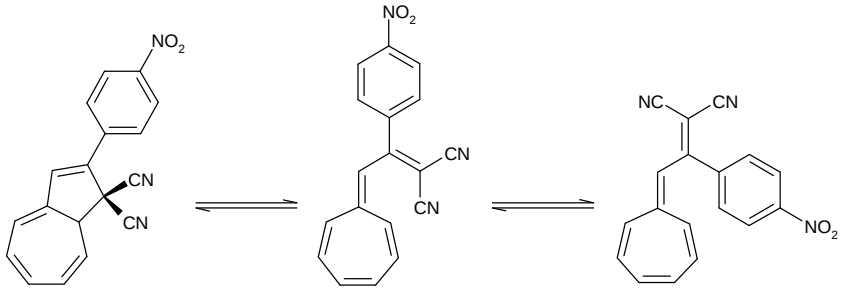

Photo and thermochromic equilibrium for a DHA-VHF system (compound **5**)

		DHA		**VHF-*cis***		**VHF-*trans***		$\frac{\beta_{VHF-cis}}{\beta_{DHA}}$	$\frac{\beta_{VHF-trans}}{\beta_{DHA}}$
		β_{HRS}	DR	β_{HRS}	DR	β_{HRS}	DR		
CPHF		997	3.83	325	2.53	979	3.05	0.33	0.98
MP2		1322	5.08	2755	5.56	3391	5.50	2.08	2.57
BLYP	$\lambda = \infty$	5244	4.77	522	4.27	631	6.22	0.10	0.12
B3LYP		3458	4.68	464	4.55	563	5.07	0.13	0.16
LC-BLYP		1148	4.31	877	4.74	1155	4.42	0.76	1.01
TDHF		2036	4.34	576	2.27	1920	2.90	0.28	0.94
MP2 [a]	$\lambda =$	2700	5.76	4883	4.99	6650	5.23	1.81	2.46
BLYP	1064	151411	5.03	752	2.94	2526	0.43	0.005	0.02
B3LYP	nm	21728	4.97	1202	6.96	6720	2.17	0.06	0.31
LC-BLYP		2495	4.67	3352	4.86	4779	4.46	1.34	1.92

Table 2-5: First hyperpolarizabilities (a.u.) and depolarization ratios of the DHA, VHF-*cis*, and VHF-*trans* forms of compound **5** evaluated at different levels of approximation, using the 6-311+G* basis set (for the MP2 calculations, the basis set is 6-31G*).
[a] The dynamic MP2 results are obtained using Equations (2-46) and (2-47).

In the case of compound **1**, adding electron correlation effects at the MP2 level leads to an increase of the β contrast by about 30% and only the LC-BLYP functional can reproduce it. Indeed, the BLYP and B3LYP β contrasts are smaller than the one determined at the HF level. In the latter case, it is also smaller than unity whereas both the HF and MP2 methods predict a larger β_{HRS} response for the base form than for the acid form, *i.e.* a β contrast larger than one. This wrong behavior is associated with a large increase of the β_{HRS} response of the protonated (charged) species. It is also interesting to note that the LC-BLYP β values are intermediate between the HF and MP2 results. In the case of compound **1**, the effects of frequency dispersion are small on the β contrast but account for an increase of β_{HRS} by about 50 to 500% for both forms. The DRs are all close to the value of 5, typical of one-dimensional π-conjugated systems, *i.e.* systems dominated by a single diagonal β tensor component.

In the case of the merocyanine/spiropyran equilibrium (Table 2-4), β_{HRS} increases upon adding electron correlation with the MP2 approach and this increase is similar for both forms. As a consequence, when going from HF to MP2, the first hyperpolarizability contrast is slightly modified: it increases for compounds **2** and **4** but decreases for compound **3**. The situation is similar for both static and dynamic (out of resonance, λ = 1064 nm) values, though the β contrasts are larger. The situation is different when considering the DFT results. In the static limit, the β contrast is systematically underestimated (the MP2 values are considered as reference) for compound **2**, whereas LC-BLYP predicts contrast in good agreement with MP2 for molecules **3** and **4**. The other XC functionals either strongly underestimate the contrast (molecule **3**) or overestimate it (molecule **4**). Turning to the dynamic quantities, the contrasts get generally much larger so that the LC-BLYP contrasts are twice larger than the MP2 ones for molecules **3** and **4**.

For the DHA-VHF system with NO_2 as substituent on the phenyl group we considered two β_{HRS} contrasts: the VHF-*trans*/DHA and VHF-*cis*/DHA contrasts. Considering the MP2 results, these contrasts are small (between 1.8 and 2.6). In general, the HF (both CPHF and TDHF) methods do not perform well because they underestimate the VHF-*trans*/DHA contrast, which is estimated to be close to unity (the limit of no contrast) whereas the VHF-*cis*/DHA contrast is estimated to be much smaller than one, assuming therefore that the largest second-order NLO response comes from the DHA form. Using DFT with the BLYP and B3LYP XC functionals provide even worse results than with HF. However, there is an improvement when using LC-BLYP, in particular for the dynamic values.

In conclusion, it appears that both the BLYP and B3LYP exchange-correlation functionals behave poorly and either strongly underestimate or overestimate the β contrasts. On the other hand, the performance of the LC-BLYP functional is better, though the improvement over HF is not systematic (see in particular some data on compounds **2, 3**, and **4**). This study highlights also the importance of the frequency dispersion on the first hyperpolarizabilities by comparing the CPHF and TDHF values for all compounds. Finally, these results justify that for evaluating the first hyperpolarizability values we adopt the TDHF, CPHF, and MP2 methods in combination with the multiplicative scheme.

2.4. Solvent effects

In order to describe the solvent effect on a solute, Tomasi and collaborators have developed the polarizable continuum model, PCM [54], and its generalized version, the integral equation formalism polarizable continuum model, IEF-PCM [55-57] that is able to treat isotropic, anisotropic, and ionic solutions. In this model, the solute is placed in a cavity surrounded by a continuous environment characterized by its

dielectric constant. This cavity is delimited by the solute van der Waals surface preventing the entry of the solvent molecules. The continuum around the cavity is polarized by the charge distribution of the solute, inducing a charge density on the surface "s" of this cavity. This density depends on the dielectric constant of the solvent and is expressed by :

$$\sigma(\vec{s}) = -\frac{\varepsilon - 1}{4\pi\varepsilon}\vec{E}_{tot} \cdot \vec{n} \qquad (2\text{-}48)$$

where ε is the dielectric constant of the continuum, $\vec{E}_{tot}$ the total electric field evaluated on the surface of the cavity, and $\vec{n}$ a unitary vector perpendicular to the surface and oriented on the outside. The total electric field can be decomposed into two terms, one concerning the charge distribution of the solute, $\gamma(\vec{r})$, and the other relative to the apparent charge distribution $\sigma(\vec{s})$ associated to the solvent, leading to:

$$\sigma(\vec{s}) = -\frac{\varepsilon - 1}{4\pi\varepsilon}\left(\vec{E}^{\gamma} + \vec{E}^{\sigma}\right) \cdot \vec{n} \qquad (2\text{-}49)$$

This expression can be rewritten as a function of the directional derivatives of the electrostatic potential:

$$\sigma(\vec{s}) = -\frac{\varepsilon - 1}{4\pi\varepsilon}\left(\vec{\nabla} V_{tot}(\vec{r})\right) \cdot \vec{n} \qquad (2\text{-}50)$$

with

$$V_{tot}(\vec{r}) = V_{\gamma}(\vec{r}) + V_{\sigma}(\vec{r}) = \int \frac{\gamma(\vec{r}')}{|\vec{r}' - \vec{r}|} d\vec{r}' + \int \frac{\sigma(\vec{s})}{|\vec{s} - \vec{r}|} d\vec{s} \qquad (2\text{-}51)$$

where $d\vec{s}$ is a surface element and $d\vec{r}'$ a volume element.

The determination of the reaction potential and of the system properties is iterative. Indeed, $\sigma(\vec{s})$ is determined by $V_{tot}(\vec{r})$, which one component also depends on $\sigma(\vec{s})$. Moreover, $V_{\sigma}(\vec{r})$ is introduced in the Hartree-Fock equation in view to include the electrostatic effects of the solvent on the wavefunction of the solute. Since the charge density does not concentrate on a single point of the surface, the electrostatic problem must be discretised. The surface is thus fractionized in finite small elements called *"tesserae"*. Each surface element, a_i, is associated to a charge q_i. The charge density on the surface is then given by :

$$\sigma(s_i) = \frac{q_i}{a_i} \qquad (2\text{-}52)$$

This allows to rewrite the potential associated with the solvent:

$$V_{\sigma}(\vec{r}) = \sum_{i=1}^{t} V_{q_i}(\vec{r}) = \sum_{i=1}^{t} q_i \int \frac{\delta(\vec{s} - \vec{s}_i)}{|\vec{r} - \vec{s}|} d\vec{s} \qquad (2\text{-}53)$$

Therefore, within each SCF cycle, a second iterative procedure is introduced to evaluate $V_\sigma(\vec{r})$ and $\sigma(\vec{s})$.

To assess the solvent impact on the molecular structures and on the first hyperpolarizabilities, an anil derivative (compound **6**) has been investigated in vacuo, in ethanol (EtOH) (ε_0 = 24.55, ε_∞ = 1.85), and in cyclohexane (C_6H_{12}) (ε_0 = 2.02, ε_∞ = 2.03). The results are listed in Tables 2-6 and 2-7. No specific solvent-molecule interactions are observed, which justifies modeling the solvent as a homogeneous field.

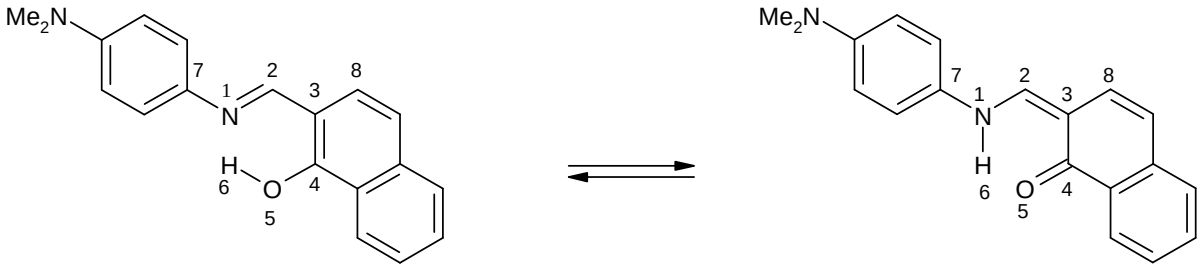

E form K form

K-form	In vacuo	In EtOH	In C_6H_{12}
C_7-N_1-C_2-C_3	177.8	178.1	177.6
C_7-N_1	1.408	1.412	1.410
N_1-C_2	1.334	1.328	1.331
C_2-C_3	1.392	1.401	1.396
C_4-O_5	1.241	1.260	1.255
N_1-H_6	1.027	1.026	1.028
O_5-H_6	1.785	1.825	1.799
BLA = $(d_{C7\text{-}N1}+d_{C2\text{-}C3}- 2d_{N1\text{-}C2})/2$	0.066	0.079	0.072

Table 2-6: Selection of dihedral angle (°), distances (Å), and BLA of compound **6** in its K form evaluated in different solvents within the IEF-PCM/B3LYP/6-311G* level.

		E-form		K-form		$\frac{\beta_{K-form}}{\beta_{E-form}}$
		β_{HRS}	DR	β_{HRS}	DR	
CPHF	In vacuo	847	5.13	700	5.39	0.83
	In EtOH	1639	5.01	1401	4.67	0.85
	In C_6H_{12}	1166	5.10	982	5.23	0.84
TDHF	In vacuo	1466	4.95	1254	4.95	0.86
	In EtOH	2179	4.93	2064	5.03	0.95
	In C_6H_{12}	2087	4.93	1824	4.81	0.87

Table 2-7: First hyperpolarizabilities (a.u.) and depolarization ratios of the E and K forms of compound **6** evaluated in different solvents using the IEF-PCM model and the 6-311+G* basis set.

Considering the geometrical parameters of the K-form, the dihedral angle is weakly modified by considering the two solvents but with a more planar structure in ethanol than in vacuo and in the cyclohexane. For the atomic distances, the most significant effect is on the C_2-C_3, C_4-O_5, and O_5-H_6 lengths. Indeed, for the C_4-O_5 length, one can notice an increase by 0.014 Å when going from vacuo to C_6H_{12} and of 0.019 Å from vacuo to EtOH. The bond-length-alternation (BLA), defined as: BLA = $(d_{C7\text{-}N1}+d_{C2\text{-}C3}-2d_{N1\text{-}C2})/2$, increases when going from vacuo to EtOH (+0.013) and to C_6H_{12} (+0.006).

For the nonlinear optical properties, one observes, for both forms, a doubling of the CPHF values by comparing vacuo and ethanol, which leads to very similar contrasts. Considering cyclohexane, the increase is of 30% for the β_{HRS} values of the two forms. For the dynamic values, there is also an increase when considering solvent effects, which is smaller than for the static values: in ethanol +50% for the E-form and +65% for the K-form, leading to contrast close to one. In cyclohexane, there is an increase of 40% for the two forms compared to the values in vacuo. On the other hand, the DR values are not affected by the solvent effects, with all DR values close to 5.

In conclusion, we have demonstrated the impact of the solvent effect and the importance to take into account this parameter in our calculations. In this thesis, the IEF-PCM method has been used to take into account the solvent effects on the geometry optimization and on the linear and nonlinear optical properties.

2.5. Computational aspects

Among the parameters to optimize for calculations, the basis sets play an important role. After a broad study of the effects of the basis set for the calculation of the first hyperpolarizabilities (presented in Chapter 4), and as presented recently by our group [44], the 6-311+G* basis set has been chosen to calculate β values with the TDHF/CPHF methods while 6-31G* basis-set is selected for MP2 calculations. These basis sets give the best compromise between computational costs and accuracy. The optimization of the molecular structures has been done with the 6-311G* basis set while the evaluation of the linear optical properties with the 6-311G* or 6-311+G* basis set.

All calculations have been carried out with the Gaussian package 2003 and 2009 [58]. The parameter "`vshift`", expressed in 10^{-3} a.u., is regularly used in the calculations. It allows shifting the level of the virtual orbitals to solve convergence problems in the scf cycles. Some results obtained for compound **3** in its merocyanine form with G03 and G09 are listed in Table 2-8.

As expected, the "vshift" value has no impact on the final β value when using G03: the values obtained are the same whatever the value given for "vshift". However, this is not the case when using G09 package with which we obtain the same values as G03 when "vshift" is not considered while with a "vshift", the values completely change: the higher the "vshift", the lower the β. Accordingly, the "vshift" parameter has not been used when using the G09 package. Nevertheless, "vshift" is sometimes necessary to allow the convergence of scf cycles, in this case G03 has been used.

G03	**no vshift**		**vshift = 50**		**vshift = 1000**		**vshift = 2000**	
	β_{HRS}	**DR**	**β_{HRS}**	**DR**	**β_{HRS}**	**DR**	**β_{HRS}**	**DR**
CPHF	2619	3.66	2619	3.66	2619	3.66	2619	3.66
MP2	5134	3.88	5134	3.88	5134	3.88	5134	3.88
G09	**no vshift**		**vshift = 50**		**vshift = 1000**		**vshift = 2000**	
	β_{HRS}	**DR**	**β_{HRS}**	**DR**	**β_{HRS}**	**DR**	**β_{HRS}**	**DR**
CPHF	2619	3.66	2619	3.66	2619	3.66	2619	3.66
MP2	5134	3.88	4903	3.87	3498	3.79	3153	3.74

Table 2-8: First hyperpolarizabilities (a.u.) and depolarization ratios of compound **3** in its merocyanine form evaluated at the MP2 level with G03 and G09 package with different values of the parameter "vshift" (10^{-3} a.u.)

2.6. References

[1] W. Kohn, *Rev*. *Mod*. *Phys*., **71**, 1253 (1999).

[2] R. G. Parr and W. Yang, in *Density-functional Theory of Atoms and Molecules*, (Oxford University Press, New York) (2005).

[3] W. Koch and M. C. Holthausen, in *A Chemist's Guide to Density Functional Theory*, (Wiley-VCH) (2001).

[4] P. Hohenberg and W. Kohn, *Phys*. *Rev*. B, **136**, 864 (1964).

[5] W. Kohn and L. J. Sham, *Phys*. *Rev*. A, **140**, 1133 (1965).

[6] C. S. Wang, B. M. Klein, and H. Krakauer, *Phys*. *Rev*. *Lett*., **54**, 1852 (1985).

[7] S. J. Vosko, L. Wilk, and M. Nusair, *Can*. *J*. *Phys*., **58**, 1200 (1980).

[8] R. O. Jones and O. Gunnarsson, *Rev*. *Mod*. *Phys*., **61**, 689 (1989).

[9] J. P. Perdew and Y. Wang, *Phys*. *Rev*. B, **45**, 13244 (1992).

[10] U. von Barth and L. Hedin, *J*. *Phys*. C, **5**, 1629 (1972).

[11] C. Filippe, X. Gonze, and C. J. Umrirgar, in *Recent Developments and Application of Density Functional Theory*, (Elsevier, Amsterdam) (1996).

[12] A. D. Becke, *Phys*. *Rev*. A, **38**, 3098 (1988).

[13] C. Lee, W. Yang, and R. G. Parr, *Phys*. *Rev*. *B*, **37**, 785 (1988).

[14] J. P. Perdew, K. Burke, and M. Ernzenhof, *Phys*. *Rev*. *Lett*., **77**, 3865 (1996).

[15] F. W. Kutzler and G. S. Painter, *Phys*. *Rev*. *B*, **45**, 3236 (1992).

[16] A. D. Becke, *J. Chem. Phys.*, **96**, 2155 (1992).

[17] A. D. Becke, *J*. *Chem*. *Phys*., **97**, 9173 (1992).

[18] J. P. Perdew, in *Electronic Stucture of Solids*, (Akademie Verlag, Berlin) (1991).

[19] W . Kohn, A. D. Becke, and R. G. Parr, *J*. *Phys*. *Chem*., **100**, 12974 (1996).

[20] C. Adamo and V. Barone, *J*. *Chem*. *Phys*., **108**, 664 (1998).

[21] B. J. Lynch, P. L. Fast, M. Harris, and D. G. Truhlar, *J. Phys. Chem. A*, **104**, 4811 (2000).

[22] P. J. Stephens, J. F. Devlin, C. F. Chabalowski, and M. J. Frisch, *J*. *Phys*. *Chem*., **98**, 11623 (1994).

[23] T. Leininger, H. Stoll, H.-J. Werner, and A. Savin, *Chem. Phys. Lett.*, **275**, 151 (1997).

[24] H. Iikura, T. Tsuneda, T. Yanai, and K. Hirao, *J. Chem. Phys.*, **115**, 3540 (2001).

[25] Y. Tawada, T. Tsuneda, S. Yanagisawa, T. Yanai, and K. Hirao, *J. Chem. Phys.*, **120**, 8425 (2004).

[26] T. Yanai, D. P. Tew, and N. C. Handy, *Chem. Phys. Lett.*, **393**, 51 (2004).

[27] M. Kamiya, H. Sekino, T. Tsuneda, and K. Hirao, *J. Chem. Phys.*, **122**, 234111 (2005).

[28] E. Runge and E. K. U. Gross, *Phys. Rev. Lett.*, **52**, 997 (1984).

[29] R. Bauernschmitt and R. Ahlrichs, *Chem. Phys. Lett.*, **256**, 454 (1996).

[30] V. Cavillot and B. Champagne, *Chem. Phys. Lett.*, **354**, 449 (2002).

[31] M. Parac and S. Grimme, *Chem. Phys.*, **292**, 11 (2003).

[32] C. Jamorski-Jödicke and H. P. Lüthi, *J. Am. Chem. Soc.*, **125**, 252 (2003).

[33] M. Guillaume, B. Champagne, and F. Zutterman, *J. Phys. Chem. A*, **110**, 13007 (2006).

[34] H. Sekino and R. J. Bartlett, *J. Chem. Phys.*, **85**, 976 (1986).

[35] S. P. Karna and M. Dupuis, *J. Comp. Chem.*, **12**, 487 (1991).

[36] L. Silverman and J. L. van Leuven, *Phys. Rev.*, **162**, 1175 (1967).

[37] T. S. Nee, R. G. Parr, and R. J. Bartlett, *J. Chem. Phys.*, **64**, 2216 (1976).

[38] P. W. Langhoff, M. Karplus, and R. P. Hurst, *J. Chem. Phys.*, **44**, 505 (1966).

[39] T. C. Caves and M. Karplus, *J. Chem. Phys.*, **50**, 3649 (1969).

[40] A. Szabo and N. Ostlund, *Modern Quantum Chemistry*, MacMillan, New-York (1982).

[41] C. Møller and M. S. Plesset, *Phys*. *Rev*., **46**, 618 (1934).

[42] H. D. Cohen and C. C. J. Roothaan, *J. Chem. Phys.*, **43**, S34 (1965).

[43] For an application of this method and the use of Romberg procedure see Champagne, B.; Kirtman, B. *in Handbook of Advanced Electronic and Photonic Materials and Devices*; Nalwa, H.S., Ed, Academic Press, New York, Vol. 9, Chap. 2, p. 63 (2001).

[44] M. de Wergifosse and B. Champagne, *J. Chem. Phys.*, **134**, 074113 (2011).

[45] H. Sekino and R. J. Bartlett, *Chem. Phys. Lett.*, **234**, 87 (1995).

[46] F. Aiga and R. Itoh, *Chem. Phys. Lett.*, **251**, 372 (1996).

[47] D. Jacquemin, B. Champagne, and C. Hättig, *Chem. Phys. Lett.*, **319**, 327 (2000).

[48] S.J.A. van Gisbergen, P.R.T. Schipper, O.V. Gritsenko, E.J. Baerends, J.G. Snijders, B. Champagne, and B. Kirtman, *Phys. Rev. Lett.*, **83**, 694 (1999).

[49] B. Champagne, E.A. Perpète, D. Jacquemin, S.J.A. van Gisbergen, E.J. Baerends, C. Soubra-Ghaoui, K. Robins, and B. Kirtman, *J. Phys. Chem. A*, **104**, 4755 (2000).

[50] K.Y. Suponitsky, S. Tafur, and A.E. Masunov, *J. Chem. Phys.*, **129**, 044109 (2008).

[51] K. Y. Suponitsky, Y. Liao, and A. E. Masunov, *J. Phys. Chem. A*, **113**, 10994 (2009).

[52] C. Cardoso, P. E. Abreu, B. F. Milne, and F. Nogueira, *J. Phys. Chem. A*, **114**, 10676 (2010).

[53] J. Urdaneta, Y. Bermúdez, F. Arrieta, M. Rosales, N. Cubillán, J. Hernández, O. Castellano, and H. Soscún, *Theor. Chem. Acc.*, **126**, 27 (2010).

[54] S. Miertus, E. Scrocco, and J. Tomasi, *Chem*. *Phys*., **55**, 117 (1981).

[55] E. Cancès, B. Mennucci, and J. Tomasi, *J*. *Chem*. *Phys*., **107**, 8 (1997).

[56] B. Mennucci, E. Cancès, and J. Tomasi, *J*. *Phys*. *Chem*. B, **101**, 10506 (1997).

[57] J. Tomasi, B. Mennucci, and R Cammi, *Chem*. *Rev*., **105**, 2999 (2005).

[58] Gaussian 09 (Revision A.02) M.J. Frisch et al. Gaussian, Inc., Wallingford CT (2009).

Hyper Rayleigh scattering

3. Hyper Rayleigh scattering

3.1. General principles

The hyper Rayleigh scattering [1-3] (HRS) is a nonlinear elastic scattering phenomenon. In the HRS technique, the system is illuminated with photons of frequency ω while scattered photons of frequency 2ω are detected (Figure 3-1). In this case, only non-centrosymmetric systems will give a response. Indeed, no harmonic light scattering can come from a centrosymmetric scatter (Equation (1-8)). By using typical D-π-A dipolar or octupolar molecule [4], this rule is respected.

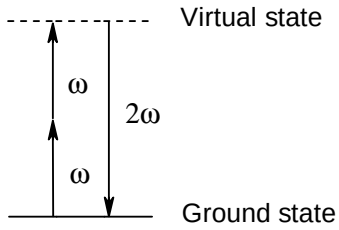

Figure 3-1: Characteristic transition of the hyper Rayleigh phenomenon.

The HRS light intensity, $I_{2\omega}$, is proportional to the square of the incident light, I_{ω}, and to the square of the average over all orientations of the first hyperpolarizability, $\langle\beta^2_{HRS}\rangle$, of molecules by the following expression [5]:

$$I_{2\omega} = \frac{16\pi^5}{c\lambda^4 r^2} N f_{\omega}^4 f_{2\omega}^2 \langle\beta^2_{HRS}\rangle I_{\omega}^2 \qquad (3\text{-}1)$$

where c is the speed of light in vacuum, λ the wavelength of the incident beam, r the distance sample-detector, N the concentration of chromophore, and $f_{\omega}^4 f_{2\omega}^2$ encompasses the local field factors and defines a Lorenz-Lorentz factor, F_L, approximated by:

$$f_{\omega}^4 f_{2\omega}^2 = F_L = \left[\left(\frac{(n_s^{\omega})^2 + 2}{3}\right)^2 \left(\frac{(n_s^{2\omega})^2 + 2}{3}\right)\right] \qquad (3\text{-}2)$$

where n_s^{ω} and $n_s^{2\omega}$ are the refractive indices at optical frequency ω and 2ω, respectively.

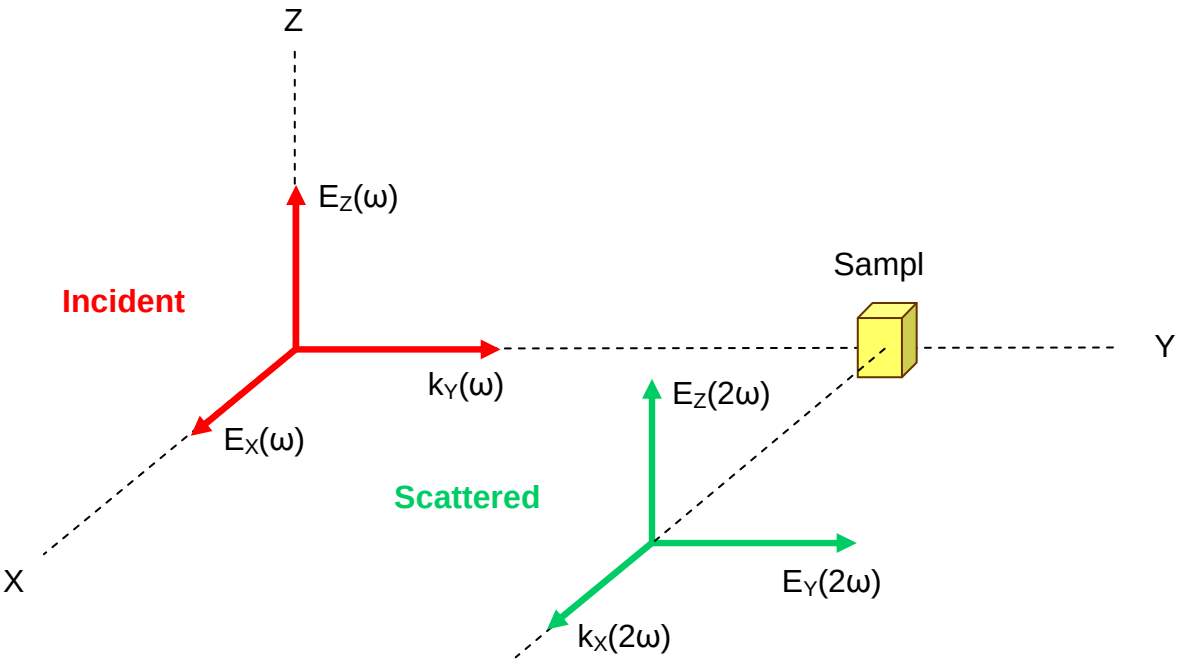

Figure 3-2: Assembly of the 90° scattering HRS geometry in the laboratory referential.

In a classical HRS experiment, the scattered light is analyzed at 90°, if the incident light beam is propagated in the Y-direction (vertically polarized, Z-axis), the scattered light is collected in the X-direction (Figure 3-2). Two configurations are used, HV and VV: HV for a horizontally polarized incident light and vertically polarized scattered light and VV for vertically polarized incident and scattered lights. If the incident light is horizontally polarized, $I_{2\omega}^{HV}$ is proportional to $\left\langle \beta_{ZXX}^2 \right\rangle$ whereas in the other case, the vertically polarized incident light, $I_{2\omega}^{VV}$, is proportional to $\left\langle \beta_{ZZZ}^2 \right\rangle$. Note that the laboratory coordinate system is represented by X, Y, and Z while the molecular coordinate system by the x, y, and z symbols. To switch from the laboratory frame to the molecular referential [6], the $\left\langle \beta_{ZZZ}^2 \right\rangle$ and $\left\langle \beta_{ZXX}^2 \right\rangle$ averages are expressed as a function of the first hyperpolarizability tensor components [10]:

$$\left\langle \beta_{ZZZ}^2 \right\rangle = \frac{1}{7}\sum_{i}^{x,y,z}\beta_{iii}^2 + \frac{4}{35}\sum_{i\neq j}^{x,y,z}\beta_{iij}^2 + \frac{2}{35}\sum_{i\neq j}^{x,y,z}\beta_{iii}\beta_{ijj} + \frac{4}{35}\sum_{i\neq j}^{x,y,z}\beta_{jii}\beta_{iij} + \frac{4}{35}\sum_{i\neq j}^{x,y,z}\beta_{iii}\beta_{jii} + \frac{1}{35}\sum_{i\neq j}^{x,y,z}\beta_{jii}^2 + \frac{4}{105}\sum_{i\neq j\neq k}^{x,y,z}\beta_{iij}\beta_{jkk} + \frac{1}{105}\sum_{i\neq j\neq k}^{x,y,z}\beta_{jii}\beta_{jkk} + \frac{4}{105}\sum_{i\neq j\neq k}^{x,y,z}\beta_{iij}\beta_{kkj} + \frac{2}{105}\sum_{i\neq j\neq k}^{x,y,z}\beta_{ijk}^2 + \frac{4}{105}\sum_{i\neq j\neq k}^{x,y,z}\beta_{ijk}\beta_{jik} \quad (3\text{-}3)$$

$$\left\langle \beta_{XZZ}^2 \right\rangle = \frac{1}{35}\sum_{i}^{x,y,z}\beta_{iii}^2 + \frac{4}{105}\sum_{i\neq j}^{x,y,z}\beta_{iii}\beta_{ijj} - \frac{2}{35}\sum_{i\neq j}^{x,y,z}\beta_{iii}\beta_{jji} + \frac{8}{105}\sum_{i\neq j}^{x,y,z}\beta_{iij}^2 + \frac{3}{35}\sum_{i\neq j}^{x,y,z}\beta_{ijj}^2 - \frac{2}{35}\sum_{i\neq j}^{x,y,z}\beta_{iij}\beta_{jii} + \frac{1}{35}\sum_{i\neq j\neq k}^{x,y,z}\beta_{ijj}\beta_{ikk} - \frac{2}{105}\sum_{i\neq j\neq k}^{x,y,z}\beta_{iik}\beta_{jjk} - \frac{2}{105}\sum_{i\neq j\neq k}^{x,y,z}\beta_{iij}\beta_{jkk} + \frac{2}{35}\sum_{i\neq j\neq k}^{x,y,z}\beta_{ijk}^2 - \frac{2}{105}\sum_{i\neq j\neq k}^{x,y,z}\beta_{ijk}\beta_{jik} \quad (3\text{-}4)$$

where i, j, and k refer to the molecular coordinates system.

In the case of plane-polarized incident light and observation made perpendicular to the propagation plane without polarization analysis of the scattered beam, the second-order NLO response that can be extracted from HRS data reads [7]:

$$\beta^2_{HRS} = \sqrt{\langle \beta^2_{ZZZ} \rangle (1 + 1/DR)} \tag{3-5}$$

where DR, the depolarization ratio (DR), is the ratio between Equations (3-3) and (3-4):

$$DR = \frac{\langle \beta^2_{ZZZ} \rangle}{\langle \beta^2_{ZXX} \rangle} \tag{3-6}$$

The DR value gives information on the geometry of the NLOphore, *i.e.* the part of the molecule responsible for the NLO response. For an ideal D-π-A 1D system, the major tensor component is β_{iii} with I the longitudinal molecular axis, and the depolarization ratio is equal to :

$$DR = \frac{1/7 \ \beta^2_{iii}}{1/35 \ \beta^2_{iii}} = 5 \tag{3-7}$$

whereas for an octupolar molecule the dominant component is β_{ijk}, so that:

$$DR = \frac{3 \times 4/35 \ \beta^2_{ijk}}{3 \times 8/105 \ \beta^2_{ijk}} = 1.5 \tag{3-8}$$

Several research groups have demonstrated the advantages of the hyper Rayleigh scattering in order to determine the molecular second-order nonlinear optical response [1-3,8-10]. Another technique that is frequently used to determine the first hyperpolarizability is the electric field induced second-harmonic generation [11] (EFISHG) technique. The EFISHG measurements require the application of an external electric field to orient the molecules in solution in order to create the non-centrosymmetry. EFISHG enables the characterization of neutral dipolar compounds *via* the projection of the first hyperpolarizability vector onto the dipole moment vector:

$$\beta_{//}(-2\omega;\omega,\omega) = \beta_{//} = \frac{1}{5}\sum_{i}^{x,y,z} \frac{\mu_i}{||\mu||} \sum_{j}^{x,y,z} (\beta_{ijj} + \beta_{iji} + \beta_{jji}) = \frac{1}{5}\sum_{i}^{x,y,z} \frac{\mu_i \beta_i}{||\mu||} \tag{3-9}$$

where $||\mu||$ is the norm of the dipole moment and μ_i and β_i the components of the μ and β vectors. This technique allows therefore the evaluation of the $\beta_{//}$ values but not of the individual β-tensor components. On the other hand, with HRS, a few dominant components of the β tensor can be deduced from the $\langle \beta^2_{ZZZ} \rangle$ and $\langle \beta^2_{XZZ} \rangle$ measurements. The other advantage of the HRS technique is that it allows

characterizing ionic or non polar molecules, which are out of the reach of EFISHG. The use of HRS has thus increased in the recent years, due to its many advantages, including ionic species [12-14], dipolar [15] or octupolar molecules [16,17],…

3.2. Experimental setup

The classical 90° angle HRS geometry is schematized in Figure 3-3. The pulsed laser used is a Neodymium YAG [18] laser emitting in the near-infrared domain (λ = 1064 nm). The block power (P) is constituted of a half-wave plate and a polarizer, which provide linear vertical polarization. This configuration allows the modulation of the incident power of the light beam, measured by an optical fiber (F) that collects the scattered light intensity by a half-wave plate to a photodiode (D). The fundamental relative intensity is precisely measured by using an oscilloscope. The incident polarization of the beam is obtained by a half-wave plate and a rotatable quarter-wave plate. This configuration allows changing the polarization of the beam from vertically linear polarization to horizontally linear polarization *via* left and right circular polarization (±45°) and elliptic polarization. When the polarization state is selected, the laser beam is focused *via* a focal lens (L) on a small volume of the sample contained in a liquid cell Raman-Fluorescence-type (four transparent sides) of 1cm. The scattered light is collected at 90° by a photographic lens placed on a translating system XYZ allowing the focus of the scattered beam to the spectrograph. By using a CCD detector, which is cooled down by liquid nitrogen, the energy of the scattered light is analyzed and the data collections are computer controlled [19].

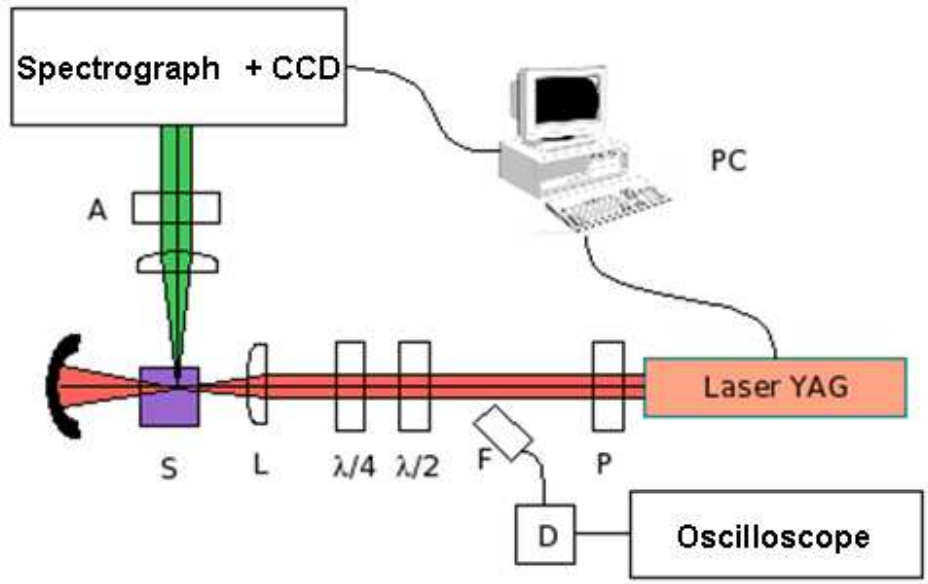

Figure 3-3: Experimental assembly of the 90° angle hyper Rayleigh scattering.

3.3. Determination of the first hyperpolarizability

The hyper Rayleigh experiment is performed by considering a binary system: the solvent and the chromophore at concentration ranging between 10^{-2} and 10^{-6} M, a dilution range in which the linear dependency of absorbance is observed. For all investigated chromophores, the pseudo symmetry C_{2v} has been assumed where the molecules lay in a mean xz-plane, with z the twofold symmetry axis. Finally, the Kleinman's conditions [20] are assumed *i.e.* $\beta_{ZXX} = \beta_{XXZ}$. Accordingly, the nonzero β tensor terms are β_{zzz} and β_{zxx}.

For a two-component system (solvent and chromophore), Equation (3-1) can be generalized and the linearly polarized scattered light in the VV geometry, $I_{2\omega}^{VV}$, is given by:

$$I_{2\omega}^{VV} = GF_L^2\left[\left\langle c_{VV}^{solv}\left(\beta_{ZZZ}^{solv}\right)^2\right\rangle C_{solv} + \left\langle c_{VV}^{chr}\left(\beta_{ZZZ}^{chr}\right)^2\right\rangle C_{chr}\right] I_\omega^2 10^{-A(2\omega)C_{chr}} \qquad (3\text{-}10)$$

where G is a constant containing geometrical, optical, and electrical factors of the experimental setup, c_{VV} is the isotropic average for VV polarization, C_{solv} and C_{chr} are the concentrations of the solvent and chromophore respectively, and A is the absorbance of chromophore at the pulsation 2ω.

Considering an incident light with a state of polarization determined by the ψ angle, circularly polarized light is described by $\psi = \pi/4$ while linearly polarized light is described by $\psi = 0$ (horizontal, H) or $\psi = \pi/2$ (vertical, V). As demonstrated by Kaatz and Shelton [15] and generalized to the pseudo C_{2v} symmetry, the scattered intensity is a function of the polarization angle and is given by:

$$I_{2\omega}^{\psi V} \propto \frac{1}{105}\beta_{zzz}^2\left[\left(15+18R+27R^2\right)-\left(24+68R+4R^2\right)\cos^2\psi+\left(12+48R-12R^2\right)\cos^4\psi\right] \qquad (3\text{-}11)$$

with $R = \beta_{zxx}/\beta_{zzz}$.

The hyper Rayleigh measurement of β involves two steps: a concentration study and a polarization study.

- *Concentration study*

The first experiment consists in determining the $c_{VV}^{chr}\left(\beta_{ZZZ}^{chr}\right)^2$ term in Equation (3-10) by removing the solvent contribution. Both the chromophore concentration and the incident light intensity at 1064 nm are varied. The linear dependence with respect to C_{chr}, as well as the quadratic dependence with respect to the incident intensity, I_ω, are verified (Figure 3-4). The zero-concentration corresponds to solvent alone.

The first step is the HRS measurements of the pure solvent (internal reference), leading to the determination of the $c_{VV}^{solv}\left(\beta_{ZZZ}^{solv}\right)^2$ term. By fitting the surface, the parameters of Equation (3-10) are evaluated and the $c_{VV}^{chr}\left(\beta_{ZZZ}^{chr}\right)^2$ term is determined.

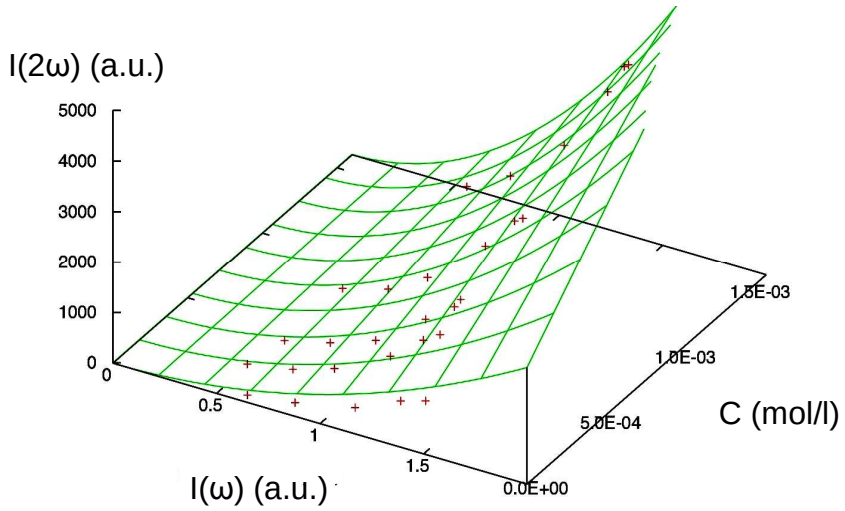

Figure 3-4: 3D-evolution of the HRS signal of a merocyanine in acetonitrile solution as a function of the incident light and of the concentration, experimental points (crosses) and best fitted curve.

➢ *Polarization study*

The second step consists in determining β_{zzz}, β_{zxx}, β_{HRS} and DR. The chromophore concentration and the incident intensity are fixed while the polarization angle ψ is varied and the intensity of the scattered light is measured. Thus, one obtains a representation of the polarization angle as a function of the intensity of the scattered light (Figure 3-5) given by Equation (3-11). The maxima of the curve (90 and 270°) correspond to the VV configuration while the minima (0 and 180°) correspond to the HV configuration.

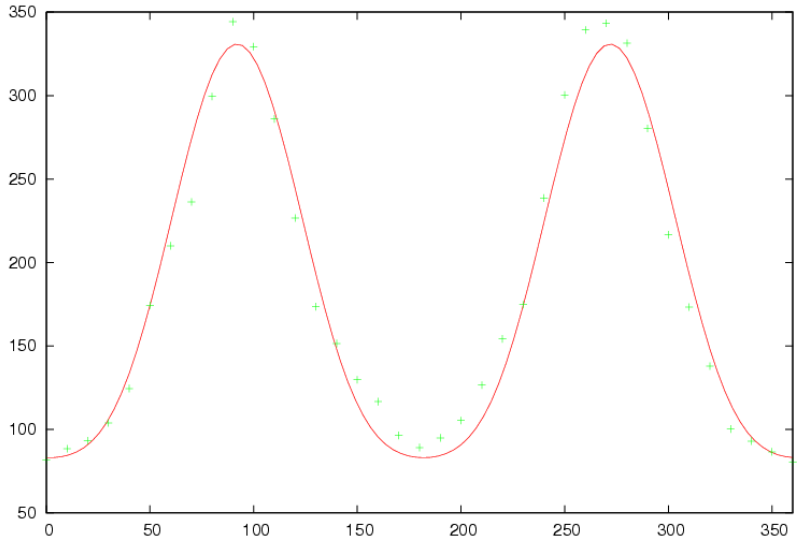

Figure 3-5: Intensity of the scattered light of a merocyanine in acetonitrile solution with respect to the polarization angle.

In the HV and VV cases, Equation (3-11) is reduced to:

$$I_{2\omega}^{VV} \propto c_{VV}\beta_{zzz}^2 = \frac{1}{105}\left(15 + 18R + 27R^2\right)\beta_{zzz}^2 \qquad (3\text{-}12)$$

$$I_{2\omega}^{HV} \propto c_{HV}\beta_{zzz}^2 = \frac{1}{105}\left(3 - 2R + 11R^2\right)\beta_{zzz}^2 \qquad (3\text{-}13)$$

By fitting the curve (Figure 3-5), the R coefficient is determined allowing the evaluation of the c_{VV} and c_{HV} coefficients, leading to the determination of β_{zzz} and β_{zxx} and therefore the β_{HRS} value, while the ratio between c_{VV} and c_{HV} provides the DR.

3.4. References

[1] K. Clays and A. Persoons, *Phys. Rev. Lett.*, **66**, 2980 (1991).

[2] E. Hendrickx, K. Clays, and A. Persoons, *Acc. Chem. Res.*, **31**, 675 (1998).

[3] T. Verbiest, K. Clays, and V. Rodriguez, *Second-order nonlinear optical characterizations techniques: an introduction*, CRC Press, New York (2009).

[4] R. W. Terhune, P. D. Maker, and C. M. Savage, *Phys. Rev. Lett.*, **14**, 681 (1965).

[5] K. Clays, A. Persoons, and L. D. Maeyer, *Adv. Chem. Phys.*, **85**, 455 (1994).

[6] S. J. Cyvin, J. E. Rauch, and J. Decius, *J. Chem. Phys.*, **43**, 4083 (1965).

[7] R. Bersohn, Y. H. Pao, and H. L. Frisch, *J. Chem. Phys.*, **45**, 3184 (1966).

[8] J. Zyss and I. Ledoux, *Chem. Rev.*, **94**, 77 (1994).

[9] G. J. T. Heesiink, A. G. T. Ruiter, N. F. Van Hulst, and B. Bölger, *Phys. Rev. Lett.*, **71**, 999 (1993).

[10] O. Quinet, B. Champagne, and V. Rodriguez, *J. Chem. Phys.*, **121**, 4705 (2004).

[11] M. H. Wu, K. Clays, and A. Persoons, *Rev. Sci. Instrum.*, **67**, 3005 (1996).

[12] T. Verbiest, K. Clays, and A. Persoons, *Opt. Lett.*, **18**, 525 (1993).

[13] E. Chauchard, C. Combellas, E. Hendrickx, G. Mathey, C Suba, A. Persoons, and A. Thiebaud, *Chem. Phys. Lett.*, **238**, 47 (1995).

[14] H. Umezawa, S. Okada, H. Oikawa, H. Matsuda, and H. Nakanishi, *J. Phys. Org. Chem.*, **18**, 468 (2005).

[15] P. Kaatz and D. P. Shelton, J. Chem. Phys., **105**, 3918 (1996).

[16] J. Zyss, T. C. Van, C. Dhenaut, and I. Ledoux, *Chem. Phys.*, **177**, 281 (1993).

[17] T. Verbiest, K. Clays, C. Samyn, J. Wolff, D. Reinhoudt, and A. Persoons, *J. Am. Chem. Soc.*, **116**, 9320 (1994).

[18] K. Clays and A. Persoons, *Rev. Sci. Instrum.*, **63**, 3285 (1992).

[19] V. Rodriguez, J. Grondin, F. Adamietz, and Y. Danten, *J. Phys. Chem. B*, **114**, 15057 (2010).

[20] D.A. Kleinman, *Phys. Rev.*, **126**, 1977 (1962).

In silico optimization of spiropyran-merocyanine compounds as second-order nonlinear optical molecular switches

A. Plaquet, M. Guillaume, B. Champagne, F. Castet, L. Ducasse, J.-L. Pozzo, and V. Rodriguez, *Phys. Chem. Chem. Phys.*, **10**, 6223 (2008).

4. *In silico* optimization of spiropyran-merocyanine compounds as second-order nonlinear optical molecular switches

4.1. Introduction

The design of spiropyran-merocyanine (S-M) switches (Figure 4-1) and particularly their contrast of β have been investigated as a function of the nature, positioning, and number of substituents. Their switching mechanism consists in the light-induced cleavage of the C-O bond in the spiropyran ring.

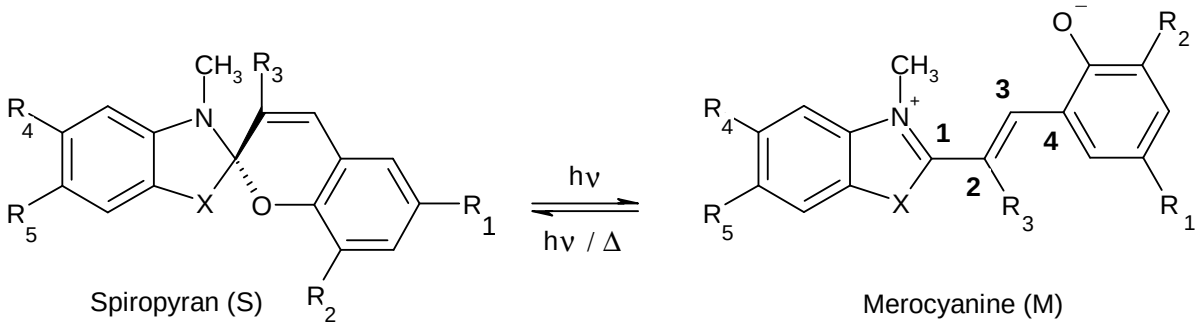

Figure 4-1: Labelling of the spiropyran-merocyanine systems and their substituents.

The advantage of these systems stems from the fact that families of M-S compounds have been synthesized since the fifties owing to their thermochromic and photochromic properties [1-4]. Moreover, structure modifications have been carried out in order to optimize the photochromism of different states of aggregation (small aggregates for multifrequency reversible optical cell, quasi liquid crystals and liquid crystals to obtain a material responding to electric field and irradiation) [5]. In particular, donor/acceptor substituents play an important role on the photochemistry of the M-S couple. For instance, Sheng *et. al.* [6] have investigated the effects of donor/acceptor pairs on the geometrical parameters, particularly the bond length alternation (BLA) of the conjugated bridge, in order to rationalize the activation energy of the switching mechanism. They noted that when R_1 is an acceptor group (NO_2), the BLA decreases, demonstrating a better electron delocalization. Donor/acceptor substitutions are therefore also expected to tune the second-order NLO properties as well as to modulate the contrast of first hyperpolarizability between the two forms, because the zwitterionic merocyanine form presents a charge-transfer character mediated by electron delocalization whereas in the spiropyran species the electron conjugation is interrupted by the spiro junction [7-9].

In this chapter, using quantum chemical approaches, we rationalize the effects on β of different donor/acceptor substitution patterns: on the 6-membered ring

(R_1 and R_2), on the ethylenic bridge (R_3), and on the benzothiazolinic moiety (R_4 and R_5 as well as X). The list of compounds is given in Table 4-1.

	R_1	R_2	R_3	X	R_4	R_5
1	H	H	Me	S	H	H
2	H	OMe	Me	S	H	H
3	OMe	OMe	Me	S	H	H
4	NO_2	H	Me	S	H	H
5	OMe	H	Me	S	H	H
6	H	NO_2	Me	S	H	H
7	CN	H	Me	S	H	H
8	CHO	H	Me	S	H	H
9 #	NO_2	OMe	Me	S	H	H
10	OMe	NO_2	Me	S	H	H
11	NO_2	NMe_2	Me	S	H	H
12	NMe_2	NO_2	Me	S	H	H
13	CN	NMe_2	Me	S	H	H
14	CHO	NMe_2	Me	S	H	H
15	NO_2	OMe	H	S	H	H
16	NO_2	OMe	CN	S	H	H
17	NO_2	OMe	OMe	S	H	H
18	NO_2	OMe	NH_2	S	H	H
19	NO_2	OMe	Me	CMe_2	H	H
20	NO_2	OMe	Me	NMe	H	H
21	NO_2	OMe	H	CMe_2	H	H
22	NO_2	OMe	H	NMe	H	H
23	NO_2	NMe_2	NH_2	NMe	H	H
24	NO_2	OMe	Me	S	NO_2	H
25	NO_2	OMe	Me	S	NMe_2	H
26	NO_2	OMe	Me	S	H	NO_2
27	NO_2	OMe	Me	S	H	NMe_2
28	NO_2	NMe_2	NH_2	NMe	NO_2	H
29	NO_2	NMe_2	NH_2	NMe	NMe_2	H
30	NO_2	NMe_2	NH_2	NMe	H	NO_2
31	NO_2	NMe_2	NH_2	NMe	H	NMe_2

Table 4-1: List of substituents investigated on the spiropyran-merocyanine equlibrium. Atom labels refer to Figure 4-1. # Compound **9** has been characterized by Nakatani *et al.* [10]

4.2. Computational aspects and preliminary study of basis set effects

β was evaluated by using the TDHF (λ = ∞ and 1064 nm) and FF/MP2 methods. Frequency dependent MP2 values were also calculated using the multiplicative scheme (Equation (2-46)). In a preliminary step the choice of atomic orbital basis set for determining β of the spiropyran-merocyanine switches was addressed by considering compound **4**. A collection of basis sets was employed: 6-31G, 6-31G*, 6-31G**, 6-31+G, 6-31+G*, 6-311G, 6-311G*, 6-311G**, 6-311+G, 6-311+G*, cc-pVDZ, aug-cc-pVDZ, and cc-pVTZ, with the aim of substantiating our choice of finding a good compromise between accuracy and computational needs. The results presented in Table 4-2 show that: i) *d*-polarization functions tend to decrease the β_{HRS} magnitude for both forms whereas the *p*-polarization functions have negligible impact, ii) on a relative basis, the effect of the *d*-polarization functions is larger for the spiropyran form, especially for small basis sets, iii) going from a double- to a triple-ζ Pople basis set yields a decrease of β_{HRS}(S) by less than 5 % and an increase of β_{HRS}(M) by less than 16 %, iv) this double- to a triple-ζ effect is reduced when the basis set contains diffuse functions, v) adding diffuse functions can lead to an increase of β_{HRS} by more than 20%, especially for the M form. Summarizing these observations, it appears that diffuse and *d*-polarization functions have generally opposite and overestimated impact when considered separately. Since larger basis sets like the aug-cc-pVTZ are beyond our computational resources, the results obtained using the aug-cc-pVDZ and cc-pVTZ basis sets are the closest to the HF limit and are taken as reference. The smaller 6-311+G* basis set provides a good approximation to these more extended basis sets, and constitutes the best compromise between accuracy and computational costs. The 6-311G* and 6-31+G* basis sets are certainly acceptable alternatives, whereas the 6-311G basis set is less balanced and therefore provides β_{HRS} contrast of lesser quality. In the case of the depolarization ratios, the basis sets, which provide values close to the reference aug-cc-pVDZ and cc-pVTZ results are in general of a triple-ζ character and contain *d*-polarization functions. Moreover, the β_{HRS} contrast is underestimated in absence of *d*-polarization functions and/or for double-ζ basis sets (except using the 6-31+G* basis set). Recently, our group has demonstrated the accuracy of valence triple-ζ + polarization basis sets with one set of diffuse functions [11,12] to reproduce within about 5% the first hyperpolarizability values of push-pull π-conjugated systems by comparing with more extended basis sets like aug-cc-pVDZ, aug-cc-pVTZ, or 6-311++G(2df,p). They have highlighted the good accuracy of 6-31+G* basis set and the importance of diffuse functions on the evaluation of β, in particular for correlated methods like MP2, MP4 or CCSD(T).

Basis set	# Basis Functions	Spiropyran		Merocyanine		Contrast
		β_{HRS}	DR	β_{HRS}	DR	
6-31G	239	417	2.81	2269	2.69	5.44
6-31G*	377	348	2.65	2145	3.00	6.16
6-31G**	419	348	2.63	2171	3.03	6.24
6-31+G	331	444	2.55	2911	2.79	6.56
6-31+G*	469	370	2.31	2756	3.13	7.45
6-311G	349	392	2.60	2595	2.94	6.62
6-311G*	464	337	2.42	2469	3.24	7.33
6-311G**	506	335	2.40	2505	3.26	7.48
6-311+G	441	438	2.54	2957	2.82	6.75
6-311+G*	556	382	2.40	2790	3.12	7.30
cc-pVDZ	396	315	2.31	2330	3.22	7.40
cc-pVTZ	890	343	2.38	2722	3.39	7.94
aug-cc-pVDZ	659	381	2.49	2952	3.31	7.75

Table 4-2: Basis set effects on the TDHF (λ = 1064 nm) second-order NLO responses of the spiropyran-merocyanine couple **4**: β_{HRS}, depolarization ratio (DR), and β_{HRS}(M)/ β_{HRS}(S) contrast. The β values are given in a. u..

4.3. β_{HRS} responses of spiropyran-merocyanine systems

Table 4-4 reports the TDHF/6-311+G* first hyperpolarizabilities for the molecules **1**-**31** in their S and M forms, the β_{HRS}(M)/ β_{HRS}(S) contrasts, as well as the depolarization ratios. The bond length alternations (BLA) on the ethylenic bridge in the M conformers, defined as BLA = $(d_{12}+d_{34}-2d_{23})/2$ (see Figure 4-1 for atom labeling), are also reported as representative indicators of the strength of electronic conjugation along the molecule. Two molecules are taken as reference compounds: molecule **1**, which does not contain any donor/acceptor group on its extremities and presents a β_{HRS}(M)/β_{HRS}(S) contrast of 9.66 and small β_{HRS} values, and molecule **9**, which was initially investigated in Ref. 8. The β_{HRS}(M)/β_{HRS}(S) ratios of compounds **1** and **9** are similar but the β_{HRS} values are more than twice larger in **9**.

For most of the merocyanine forms, rotation around the C_1C_2 and C_3C_4 bonds leads to four different stable conformers (if X = NMe, there are only two conformations, Figure 4-2). In the case of reference compound **9**, their β_{HRS} and DR values were calculated and related to the relative conformer energy (Table 4-3). Starting from conformer I, rotation around the C_3C_4 bond provides conformer III where the R_3 substituent presents strong steric interactions with the oxygen atom, as evidenced by departure from π of the $\theta_{C1C2C3C4}$ and $\theta_{C2C3C4C5}$ torsion angles. Similar repulsive interactions exist in conformer IV, which translates into very small Maxwell-Boltzmann distribution weights whereas the β_{HRS} increases by about 30% with

respect to conformer I. Finally, rotation around the C_1C_2 bond gives conformer II presenting a larger energy. In this case, the difference of β_{HRS} is smaller than 3%. DR of conformers I and II are similar, like these of conformers III and IV, the difference between the two sets being of the order of 20%. Since these steric interactions will be little modified when considering the other merocyanine species of Table 4-1, the coming data are reported only for the most stable conformation I.

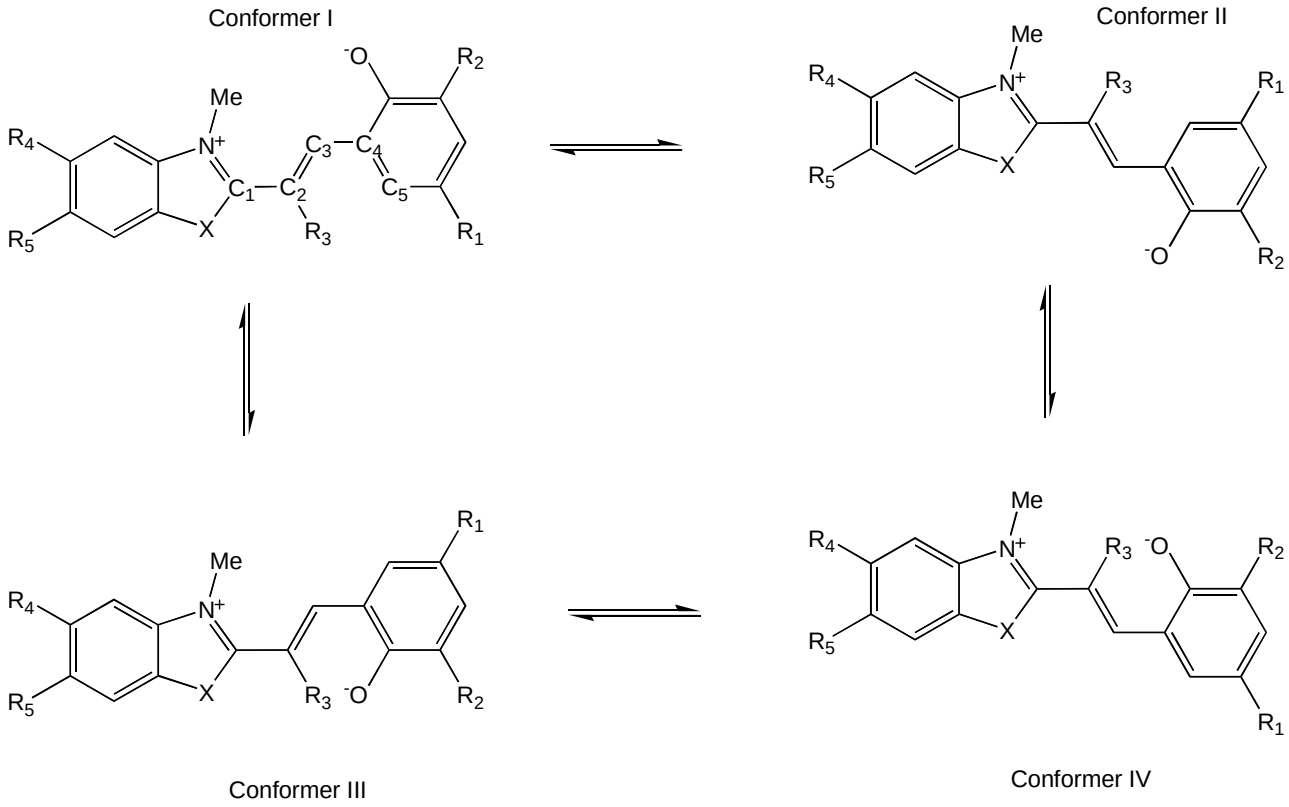

Figure 4-2: Sketch of the four possible conformers obtained by rotation around the C_1C_2 and C_3C_4 bonds.

Conformer	$\theta_{NC1C2C3}$	$\theta_{C1C2C3C4}$	$\theta_{C2C3C4C5}$	β_{HRS} (DR)	ΔE (Weight)
I	-22.3	179.3	-5.3	3342 (3.37)	0.0 (97.6)
II	-160.9	178.6	-5.1	3433 (3.55)	9.6 (2.0)
III	-167.1	170.5	162.5	4294 (2.85)	20.5 (0.1)
IV	23.5	-167.7	-160.0	4293 (2.82)	14.2 (0.3)

Table 4-3: Torsion angles (°), TDHF/6-311+G* β_{HRS} and DR values (a.u.) for the four conformers of the merocyanine form of compound **9** as well as their relative energies (kJ/mol) and Maxwell-Boltzmann distribution weights (%) as estimated at 298.15 K from the electronic energy.

We then investigated the effects of donor/acceptor substituents in R_1 and R_2 (compounds **2**-**14**). Adding to **1** a methoxy group in R_2 (molecule **2**) provokes a slight increase of $\beta_{HRS}(S)$ but decreases $\beta_{HRS}(M)$ by 35%, which reduces the β contrast by almost a factor of 2. With respect to compound **9**, compound **2** highlights the importance of the NO_2 acceptor group in R_1. Replacing the NO_2 acceptor group in R_1 by a OMe donor group is also detrimental to $\beta_{HRS}(M)$ and to the contrast, as found by comparing compounds **3** and **9**. On the other hand, placing the OMe group in R_1 (compound **5**) increases $\beta_{HRS}(M)$ but decreases the contrast with respect to **1** since $\beta_{HRS}(S)$ increases by as much as 100%. Similarly, the NO_2 acceptor group enhances the first hyperpolarizability of both forms when in R_1 position and reduces $\beta_{HRS}(M)$ when in R_2 position, demonstrating cooperative rather than simple additive effects among the substituents. Nevertheless, these effects are stronger for the NO_2 acceptor than for the OMe donor groups.

The impact of an acceptor group in R_1 was further addressed by comparing compound **1** with compounds **4**, **7**, and **8** (R_2 = H). $\beta_{HRS}(M)$ increases in the order H $\rightarrow$ CHO $\rightarrow$ CN $\rightarrow$ NO_2, *i.e.* with the strength of the acceptor group. This increase in $\beta_{HRS}(M)$ is accompanied by an increase of the BLA, which goes from –0.031 Å in **1** to about zero in **4**. On the other hand, the variations in $\beta_{HRS}(S)$ do not follow the same pattern, so that the largest contrast is obtained for R_1 = CN.

Interchanging the position of the OMe/NO_2 donor/acceptor pair, going from **9** to **10**, decreases $\beta_{HRS}(S)$ by 50% but $\beta_{HRS}(M)$ by less than 5%, which is accompanied by a larger contrast. The larger β_{HRS} values for **9** substantiate the stronger impact of the NO_2 group as discussed above. When a stronger donor group is considered (NMe_2), the $\beta_{HRS}(M)$ values of the two position isomers (**11** and **12**) become much different, demonstrating that the preferential positions for a D/A pair is R_2/R_1. Comparing compounds **4**, **9**, and **11** further helps assessing the impact of donor group in R_2. When increasing the strength of the donor group, $\beta_{HRS}(M)$ increases substantially, $\beta_{HRS}(S)$ decreases slightly so that the contrast attains 16 in compound **11**. Note that the BLA of the ethylene bridge is little affected by the strength of the donor group in R_2.

Then, the impact of an acceptor group in R_1 was substantiated by considering this time R_2 = NMe_2 (compounds **11**, **13**, and **14**). Again, $\beta_{HRS}(M)$ increases in the order CHO $\rightarrow$ CN $\rightarrow$ NO_2, which is accompanied by an increase in the BLA, the R_1 = CN compound presents the smallest $\beta_{HRS}(S)$ and therefore the largest $\beta_{HRS}(M)/\beta_{HRS}(S)$ contrast. Nevertheless, the contrast for the R_1/R_2 = NO_2/NMe_2 pair is rather similar while the first hyperpolarizability of the merocyanine form is substantially larger (about 70%). Concluding this investigation on the impact of the R_1/R_2 substituents, compound **11** exhibits not only a larger $\beta_{HRS}(M)/\beta_{HRS}(S)$ contrast than compounds **1** and **9** but also a larger $\beta_{HRS}(M)$ value. There is no clear

tendency in what concerns the depolarization ratios of the merocyanine and spiropyran forms as a function of R_1 and R_2.

The substituent R_3 on the ethylenic bridge was then varied from Me in compound **9** to H, CN, OMe, and NH_2 in compounds **15**-**18**. $\beta_{HRS}(M)$ increases with the donor strength of R_3, in the order CN $\rightarrow$ H $\rightarrow$ Me $\rightarrow$ OMe$\rightarrow$ NH_2 together with the DR and with the bridge BLA, which gets more and more positive (or less and less negative). For the same R_3 substituents, $\beta_{HRS}(S)$ hardly changes but its DR increases with the donor strength.

The nature of X was then investigated for $R_1/R_2 = NO_2/NMe_2$ and for R_3 = H or Me. Substituting the sulfur atom in X by a *gem*-dimethyl group (from **9** to **19** and from **15** to **21**) leads to a decrease of $\beta_{HRS}(M)$ and an increase of $\beta_{HRS}(S)$, so that the $\beta_{HRS}(M)/\beta_{HRS}(S)$ contrast is strongly reduced. On the contrary, replacing X = S by X = NMe (from **9** to **20** and from **15** to **22**) increases $\beta_{HRS}(M)$ by 40-50% while $\beta_{HRS}(S)$ is enhanced to a weaker extent, which therefore leads to an exaltation of the contrast. Note again that the larger the $\beta_{HRS}(M)$ values the more positive the BLA is. This $\beta_{HRS}(X = NMe) > \beta_{HRS}(X = S) > \beta_{HRS}(X = CMe_2)$ ordering for the merocyanine form differs from the $\beta_{HRS}(X = S) > \beta_{HRS}(X = CMe_2) > \beta_{HRS}(X = NMe)$ ordering found at the same level of approximation by our research group for the open forms of the indolino-oxazolidine, benzothiazolo-oxazolidine, and benzimidazolo-oxazolidine [13], though the compounds present many similarities. This difference finds its origin in the substitution pattern of the aryl moiety of the benzazolo-oxazolidines having a donor group in *para* of the ethylenic linker and the associated cooperative effects on that ring.

As an intermediate conclusion, increased efficiencies in the NLO responses of the two forms as well as in the NLO contrast upon switching can be achieved: i) by using the strong NO_2/NMe_2 D/A pair in R_1/R_2, ii) by inserting a donor group in R_3 on the ethylenic bridge, as well as iii) by replacing the X = S of the parent compound by X = NMe. Combining these structural features leads to the optimized compound **23**, having a substantial $\beta_{HRS}(M)$ value (387% larger than in compound **1** and 126% larger than in compound **9**) and a large $\beta_{HRS}(M)/\beta_{HRS}(S)$ contrast, which correspond to a BLA value as large as 0.033 Å.

Then, the impact of donor/acceptor substituents in R_4 and R_5 was analyzed by considering compounds **24-27** in comparison with compound **9**. To enhance $\beta_{HRS}(M)$, R_4 should be a donor group but this is detrimental to the contrast. On the other hand, placing a donor or an acceptor in R_5 leads to both a reduced impact on $\beta_{HRS}(M)$ and a decrease of the contrast. Donor and acceptor groups in R_4 and R_5 were then considered on the basis of the optimized **23** compound. In that case the largest $\beta_{HRS}(M)$ and $\beta_{HRS}(M)/\beta_{HRS}(S)$ values are obtained when R_4 or R_5 is a nitro group. In fact, adding the NMe_2 donor group to either R_4 or R_5 positions reduces

β_{HRS}(M) by about 10% with respect to compound **23** while the contrast further decreases. In compound **28** and **30**, larger β_{HRS}(M) values are associated with smaller BLA, demonstrating a different structure/property relationship. Thus, with respect to compound **1**, an enhancement of β_{HRS}(M) by about one order of magnitude has been achieved whereas the contrast has been increased by about 50%. Consequently, in addition to compound **23**, compounds **28** and **30** were selected as potentially interesting systems and compounds **23** and **30** were subjected to further analysis reported in paragraph 4.4.

Based on the previous discussions on the link between the BLA of the ethylenic bridge and β_{HRS}(M), the two sets of quantities have been plotted in Figure 4-3, leading to a noticeable linear relationship. The larger β_{HRS}(M) values and more positive BLA are associated with a more aromatic structure whereas the opposite trend corresponds to a quinoid ring structure. Nevertheless, since they are associated with different effects, compounds **28** and **30** were excluded from the linear regression.

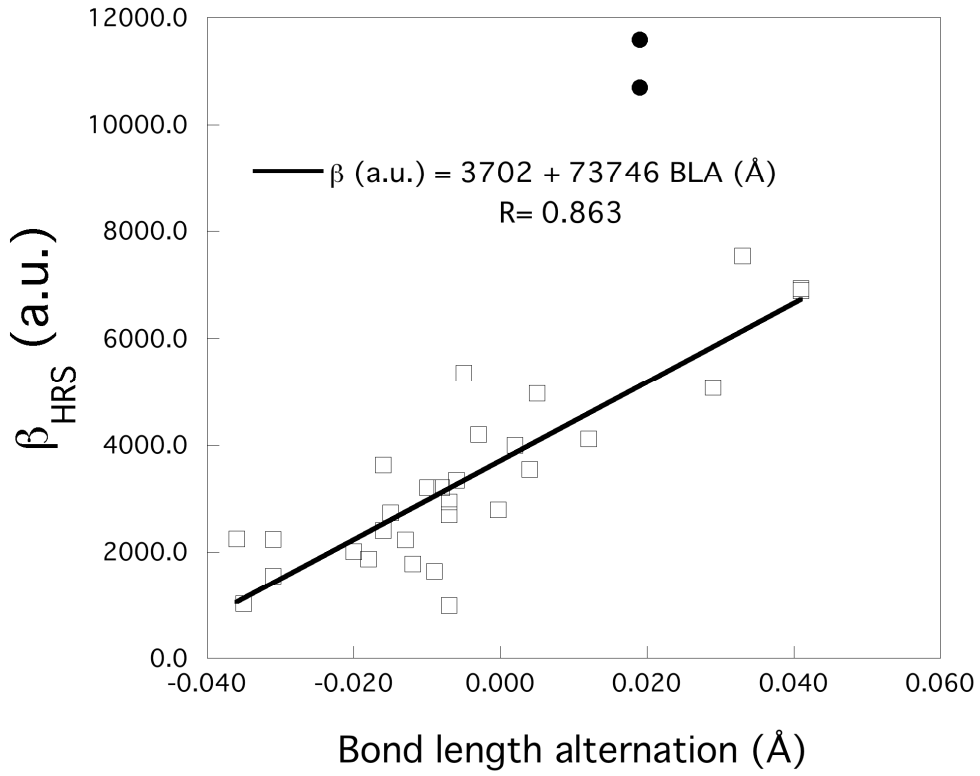

Figure 4-3: Relationship between the bond length alternation (Å) and β_{HRS} (empty squares, TDHF/6-311+G*, in a.u.). Data pertaining to compounds **28** and **30** (filled circles) have not been included in the least-squares linear regression set.

Molecule	Spiropyran (S)		Merocyanine (M)		β_{HRS}(M)/ β_{HRS}(S) Contrast	BLA
	β_{HRS}	DR	β_{HRS}	DR		
1	160	4.34	1546	4.17	9.66	-0.031
2	186	4.74	1020	2.99	5.48	-0.035
3	345	4.58	2248	2.20	6.52	-0.036
4	382	2.40	2790	3.12	7.30	-0.0003
5	321	6.42	2241	2.81	6.98	-0.031
6	185	3.48	986	2.26	5.33	-0.007
7	193	2.70	2699	4.06	13.98	-0.007
8	249	2.19	1775	3.22	7.13	-0.012
9	371	2.72	3342	3.37	9.01	-0.006
10	240	4.88	3206	2.85	13.36	-0.010
11	335	2.80	5363	4.22	16.01	-0.005
12	343	6.66	1643	2.80	4.79	-0.009
13	161	3.76	3200	4.36	19.88	-0.008
14	238	3.60	2230	3.72	9.37	-0.013
15	381	2.53	2936	2.95	7.71	-0.007
16	374	2.11	1873	3.66	5.01	-0.018
17	386	3.23	4199	3.63	10.89	-0.003
18	389	4.49	4967	3.72	12.77	+0.005
19	458	2.95	2736	2.80	5.97	-0.015
20	450	2.84	5087	3.89	11.30	+0.029
21	450	3.42	2405	2.60	5.34	-0.016
22	463	2.61	4119	3.53	8.90	+0.012
23	415	4.69	7538	4.27	18.16	+0.033
24	392	2.29	2008	3.61	5.12	-0.020
25	660	3.69	3991	3.20	6.05	+0.002
26	695	2.48	3632	3.59	5.23	-0.016
27	517	4.48	3547	3.02	6.86	+0.004
28	761	2.64	10697	4.85	14.06	+0.019
29	556	6.71	6897	3.92	12.40	+0.041
30	760	2.64	11589	4.59	15.25	+0.019
31	478	6.19	6932	4.03	14.50	+0.041

Table 4-4: TDHF/6-311+G* first hyperpolarizability (β_{HRS}) and depolarization ratio (DR) in a.u. for the spiropyran and merocyanine forms (λ = 1064 nm). Last column : Bond Length Alternation (Å) in the merocyanine forms.

4.4. Further analysis on three selected systems

The dispersion effects on the β_{HRS} responses, as well as on the β contrasts were estimated from the $\beta_{TDHF}/\beta_{CPHF}$ ratios, as reported in Table 4-5. These dispersion effects are stronger for the merocyanine form than for the spiropyran form but remain rather similar among the three compounds, with slightly larger values for compound **30**. Therefore, the contrasts, which are smaller than 10 at the CPHF/ 6-311+G* level increase by 100% or more when accounting for frequency dispersion effects at a wavelength of 1064 nm.

The large β_{HRS}(M) and β_{HRS}(M)/β_{HRS}(S) values of compounds **23** and **30** with respect to compound **9** were then confirmed from FF/MP2/6-31G* calculations reported in Table 4-6. Electron correlation effects, as estimated from the β_{MP2}/β_{CPHF} ratios, lead to an increase of the HRS first hyperpolarizabilities by 64-98%, except for **9**(M) where the increase attains 200%. This results in the confirmation of β_{HRS}(M)/β_{HRS}(S) ratios larger than 15 for both targeted compounds, though the gain, in contrast to **9**, is reduced at the MP2 level of approximation.

Molecule	Spiropyran		Merocyanine		$\frac{\beta_{CPHF}(M)}{\beta_{CPHF}(S)}$	$\frac{\beta_{TDHF}(M)}{\beta_{TDHF}(S)}$
	β_{CPHF}	$\beta_{TDHF}/\beta_{CPHF}$	β_{CPHF}	$\beta_{TDHF}/\beta_{CPHF}$		
9	275	1.35	1239	2.70	4.51	9.01
23	305	1.36	2702	2.79	8.86	18.16
30	544	1.40	3793	3.06	6.97	15.25

Table 4-5: For selected spiropyran-merocyanine pairs, static HRS first hyperpolarizabilities (β_{CPHF}), $\beta_{TDHF}/\beta_{CPHF}$ ratios, and HRS β contrasts. All β values are given in a.u. and were obtained using the 6-311+G* basis set.

Molecule	Spiropyran			Merocyanine			$\frac{\beta^{SHG}_{MP2}(M)}{\beta^{SHG}_{MP2}(S)}$
	β_{MP2}	β_{MP2}/β_{CPHF}	β^{SHG}_{MP2}	β_{MP2}	β_{MP2}/β_{CPHF}	β^{SHG}_{MP2}	
9	509	1.95	723	3091	3.08	10293	14.24
23	736	2.29	950	5134	1.96	14774	15.55
30	823	1.64	1246	6196	1.69	19585	15.72

Table 4-6: For selected spiropyran-merocyanine pairs, static FF/MP2/6-31G* HRS first hyperpolarizabilities (β_{MP2}), β_{MP2}/β_{CPHF} ratios, dynamic HRS first hyperpolarizability (β^{SHG}_{MP2}) as estimated from Equation (2-46), and HRS β contrasts. All β values are given in a.u..

For these three compounds and their two forms, Table 4-7 lists the norm of the dipole moment and first hyperpolarizability vectors, the angle they form as well as the $\beta_{//}$ and β_{HRS} responses for both TDHF and MP2 levels of approximation. These vectors are then sketched in Figure 4-4. The spiropyran forms are characterized by quasi parallel μ and β vectors whereas for the merocyanine forms, they tend to be antiparallel. Except for **9**(M), these conclusions do not depend on the level (TDHF or MP2) of approximation. As a consequence, all the $\beta_{//}$ values for the M (S) forms are negative (positive). For the M form, going from **9** to **23** and **30** does not lead to changes of the relative orientation of the dipole moment with respect to the molecule but the amplitude changes: it increases between **9** and **23** as a results of stronger X = NMe acceptor group whereas it decreases between **23** and **30** owing to the strong NO_2 acceptor group on the benzimidazolic moiety. On the other hand, the first step is accompanied by a reversal of the β orientation and the second by an increase of the β amplitude. In the case of the spiropyran form, a similar effect is observed, though of smaller amplitude, as could have been figured out from breaking of conjugation at the level of the spiro junction.

At the TDHF/6-311+G* level of approximation, the β contrasts are similar for both HRS and EFISHG responses with a substantial increase when going from compound **9** to compounds **23** and **30**. At the MP2/6-31G* level, there are no such differences and the β contrasts for both responses range from 6 to 8, indicating again that the contrast is substantially enhanced by the frequency dispersion effects.

TDHF/6-311+G* **(λ = 1064 nm)**	$\lvert\vec{\mu}\rvert$	$\lvert\vec{\beta}\rvert$	**θ**	$\beta_{//}$	β_{HRS}
9(S)	5.65	662	9.4	392	371
9(M)	11.40	6595	138.2	-2952	3342
Contrasts				7.53	9.01
23(S)	6.73	972	32.2	493	415
23(M)	14.32	16957	158.7	-9479	7538
Contrasts				19.22	18.16
30(S)	5.51	1328	24.3	726	760
30(M)	7.20	26830	146.8	-13462	11589
Contrasts				18.54	15.25
MP2/6-31G* **(λ = ∞)**	$\lvert\vec{\mu}\rvert$	$\lvert\vec{\beta}\rvert$	**θ**	$\beta_{//}$	β_{HRS}
9(S)	4.67	1110	19.73	627	509
9(M)	9.44	7860	7.59	4675	3091
Contrasts				7.45	6.07
23(S)	5.79	1804	14.9	1046	736
23(M)	13.38	11331	158.3	-6317	5134
Contrasts				6.04	6.97
30(S)	4.56	1560	6.2	930	823
30(M)	6.82	14065	148.3	-7179	6196
Contrasts				7.72	7.53

Table 4-7: Norms of the μ and β vectors, angle (θ, in degrees) between them, $\beta_{//}$ and β_{HRS} values, as well as corresponding contrasts for the spiropyran and merocyanine forms of representative compounds as determined at the TDHF and MP2 levels of approximation. All μ and β values are given in a.u..

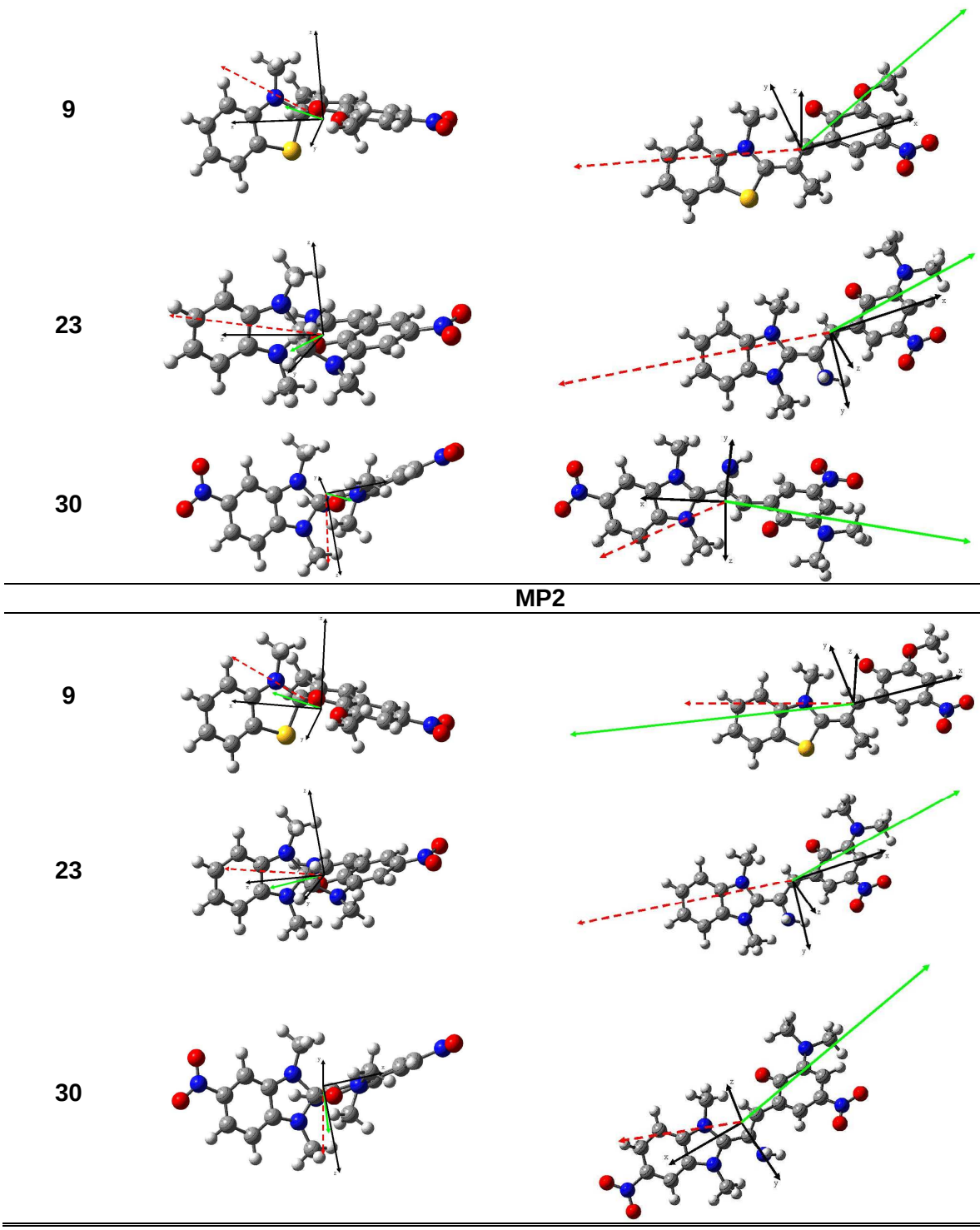

Figure 4-4: Sketch of the dipole moment (red dotted line) and first hyperpolarizability (green full line) vectors for the spiropyran and merocyanine forms as determined at the TDHF (λ = 1064 nm) and MP2 (λ = ∞) levels of approximation. The lengths of μ and β vectors are proportional to their norms and are consistent between the different compounds and methods, if scaling information are not provided (for instance, "β/4" means that, with respect to the other pictures, the length of the β vector has been divided by 4).

4.5. Conclusions

Efficient NLO switching spiropyran-merocyanine systems have been proposed by calculating the first hyperpolarizability of a large variety of spiropyran-merocyanine couples differing by the nature, number, and positioning of the substituents. The substituent effects appear cooperative and therefore difficult to rationalize easily. In particular, different pairs of R_1/R_2 substituents on the phenolate ring can enhance the first hyperpolarizability of the merocyanine form. Nevertheless, when R_1 and R_2 are strong acceptor and donor substituents, respectively, the first hyperpolarizability of the merocyanine form is strongly increased while the β contrast with respect to the spiropyran form is large. Further enhancements of the first hyperpolarizability are achieved by substituting the ethylenic bridge by donor groups, by replacing the indolino (or benzothiazolo) aromatic core by a benzimidazolo ring, as well as by substituting the later ring by a strong acceptor group. When combining the structural patterns together, several performant spiropyran-merocyanine pairs have been designed and characterized. For most of these systems, the amplitude of the β_{HRS} of the merocyanine form has been shown to be directly related to the bond length alternation of the ethylenic bridge, which therefore constitutes a reliable structural parameter to predict the second-order NLO responses of these systems.

Moreover, basis set, frequency dispersion, and electron correlation effects have been addressed for selected systems. On the one hand, this enables to select the 6-311+G* basis set to perform the whole investigation. On the other hand, frequency dispersion has been highlighted as a source of enhancement of the β contrast between the merocyanine and spiropyran forms because frequency dispersion effects are larger for the former than for the later. Moreover, including electron correlation effects at the MP2 level leads to an algebraic increase of the first hyperpolarizability values and could modify the relative importance of the β contrasts.

4.6. References

[1] E. B. Knot, *J. Chem. Soc.*, 3038 (1951).

[2] C. F. Koelsch*, J. Org. Chem.*, **16**, 1362 (1951).

[3] C. F. Koelsch and W. R. Workman, *J. Am. Chem. Soc.*, **74**, 6288 (1952).

[4] E. Fischer and Y. Hirshberg, *J. Chem. Soc.*, 4522 (1952).

[5] G. Berkovic, V. Krongrauz, and V. Weiss, *Chem. Rev.*, **100**, 1741 (2000).

[6] Y. Sheng, J. Leszczynski, A. A. Garcia, R. Rosario, D. Gust, and J. Springer, *J. Phys. Chem. B*, **108**, 16233 (2004).

[7] see for instance Champagne, B.; Kirtman, B. *in Handbook of Advanced Electronic and Photonic Materials and Devices*; Nalwa, H.S., Ed, Academic Press, New York, Vol. 9, Chap. 2, p. 63 (2001) for a discussion on the D/A strengths and their impact on the NLO responses.

[8] J. A. Delaire and K. Nakatani, *Chem. Rev.*, **100**, 1817 (2000).

[9] B.-H. Tan, M. Yoshio, T. Ichikawa, T. Mukai, H. Ohno, and T. Kato, *Chem. Commun.*, 4703 (2006).

[10] K. Nakatani, Y. Atassi, and J. A. Delaire, *Nonlinear Opt.*, **15**, 351 (1996).

[11] M. de Wergifosse and B Champagne, *J. Chem. Phys.*, **134**, 074113 (2011).

[12] S.N. Labidi, M.B. Kanoun, M. de Wergifosse, and B. Champagne, *Int. J. Quantum Chem.*, **111**, 1583 (2011).

[13] F. Mançois, L. Sanguinet, J.-L. Pozzo, M. Guillaume, B. Champagne, V. Rodriguez, F. Adamietz; L. Ducasse, and F. Castet, *J. Phys. Chem. B*, **111**, 9795 (2007).

Investigation on the second-order nonlinear optical responses in the keto–enol equilibrium of anil derivatives

A. Plaquet, M. Guillaume, B. Champagne, L. Rougier, F. Mançois, V. Rodriguez, J.-L. Pozzo, L. Ducasse, and F. Castet, *J. Phys. Chem. C*, **112**, 5638 (2008).

5. Investigation on the second-order nonlinear optical responses in the keto–enol equilibrium of anil derivatives

5.1. Introduction

Among photochromic compounds of interest for advanced functionalized materials, salicylideneanilines and related Schiff bases, usually called anils, have received particular attention due to their ability to photoswitch between two forms, the enol-imine (E) and keto-amine (enaminone) (K) isomers, *via* an intramolecular proton transfer reaction and *cis*-*trans* isomerization to the final *trans*-keto photochromic form that can occur both in solution and in the crystalline state [1,2,3]. In this chapter, we address the NLO responses and contrasts of two anil derivatives: the N-(4-hydroxy)-salicylidene-amino-4-(methylbenzoate) denoted **4A** and the N-(3,5-di-tert-butylsalicylidene)-4-aminopyridine denoted **4P** (Figure 5-1), synthesized by Sliwa *et al.*, and in particular their variations upon switching between the K and E forms via an intramolecular proton-transfer [4,5].

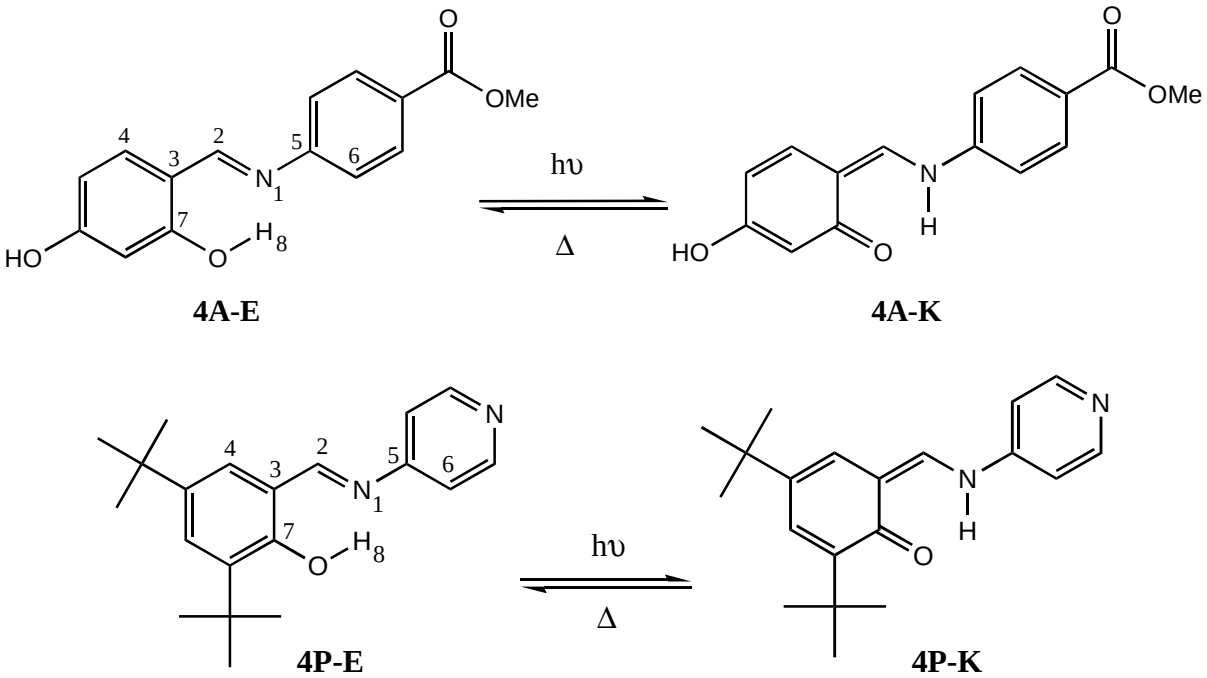

Figure 5-1: Enol (E) and keto (K) tautomeric forms of Schiff bases, **4A** and **4P**, with intramolecular hydrogen bond.

These two molecules exhibit photochromism and nonlinear optical properties in the crystalline state. **4A** involves push-pull substituents (hydroxyl and ester groups) in *para* position at both ends of the reference anil structure, in order to enhance the

molecular second-order NLO responses [3]. In **4P** the introduction of bulky *tert*-butyl groups aims at stabilizing the K isomer. Indeed, the latter compound was found to have the most stable K form among all the anil-type photochromes. Usually the E form of anil derivatives is the most stable while the K form is metastable. Guillaume *et al.* [3] have observed that the K form is stabilized by substituting the salicylidene ring by an acceptor group or the other ring by a donor group. At the molecular level, the NLO properties of **4A** and **4P** have already been characterized by using the electric field induced second-harmonic generation (EFISHG) technique, as well as by means of INDO/S semi-empirical calculations [4]. Following this work, we have performed calculations in order to precisely investigate the thermodynamics and kinetics of the tautomer equilibria, as well as the linear and second-order nonlinear optical responses of the compounds in their two isomeric forms. Moreover, the NLO responses of **4A** and **4P** were also investigated by HRS to provide complementary information on the β tensor with respect to EFISHG [4]. The photochromic form is the *trans*-keto, nevertheless, this form has never been characterized due to the difficulty to define its geometry. Therefore, we have focused our calculation on the enol and *cis*-keto forms.

5.2. Molecular structures and thermodynamics analysis

The representative bond lengths and torsion angles of the equilibrium structures calculated in gas phase at the B3LYP/6-311G* and MP2/6-31G* levels are gathered in Table 5-1 and, for the E forms, compared to X-Ray crystallographic data [4]. At both levels of theory, the two compounds present very similar geometries and the calculated interatomic distances are very close to the crystallographic values. The bond length alternation (BLA) in the bridge between the two rings, estimated as BLA = $(d_{3-2} + d_{1-5} - 2\, d_{2-1})/2$, is about 0.13 Å in the E forms and strongly reduced (0.05-0.06 Å) in the K forms, which is typical of salicylideneaniline derivatives [3]. Moreover, the BLA is identical in the **4A** and **4P** compounds within 0.001 Å. Besides, the length of the N···H hydrogen bond in the E form, which is similar within the two levels of calculations, is slightly longer for **4A** than for **4P**, contrary to experimental findings. This slight difference might be related to the intermolecular interactions or to anharmonicity effects. On the other hand, the typical structural distortion of photochromic anils is well reproduced, the two six-membered rings making an angle of about 40° in the E forms. Note that MP2 calculations predict a larger distortion compared to DFT, particularly appreciable in the K isomer, for which DFT calculations lead to perfectly planar structures.

	4A-E		4A-K		4P-E		4P-K	
	B3LYP	**MP2**	**B3LYP**	**MP2**	**B3LYP**	**MP2**	**B3LYP**	**MP2**
C_5-N_1	1.402	1.412	1.398	1.403	1.402	1.410	1.396	1.400
(Exp)	(1.410)		-		(1.420)		-	
N_1-C_2	1.292	1.300	1.339	1.337	1.290	1.300	1.340	1.337
(Exp)	(1.290)		-		(1.281)		-	
C_2–C_3	1.441	1.446	1.386	1.390	1.446	1.449	1.387	1.394
(Exp)	(1.439)		-		(1.448)		-	
C_7-O	1.337	1.351	1.254	1.270	1.344	1.356	1.257	1.275
(Exp)	(1.350)		-		(1.354)		-	
N_1…H_8	1.765	1.774	-	-	1.735	1.733	-	-
(Exp)	(1.680)		-		(1.770)		-	
O…H_8	-	-	1.752	1.695	-	-	1.750	1.674
BLA	0.130	0.129	0.053	0.060	0.134	0.130	0.051	0.060
C_4-C_3-C_2-N_1	179.1	179.4	180.0	178.9	179.4	179.6	180.0	179.2
(Exp)	(176.3)		-		(178.1)		-	
C_3-C_2-N_1-C_5	177.0	177.6	180.0	178.7	177.3	177.8	180.0	179.0
(Exp)	(173.1)		-		(175.9)		-	
C_2–N_1–C_5–C_6	143.9	137.7	180.0	155.6	143.2	135.9	179.6	159.7
(Exp)	(144.7)		-		(140.1)		-	

Table 5-1: Selected distances (Å) and torsion angles (°) for **4A** and **4P** in their E and K form, as calculated at the B3LYP/6-311G* and MP2/6-31G* levels. Atom labelling is shown in Figure 5-1. Experimental data are given between parentheses.

The sums of the MP2/6-31G* Mulliken atomic charges in different fragments (S_i) for the two compounds are collected in Table 5-2. For both forms, the central moiety (S_3) bears a negative charge. This excess of electron is related to positive S_2 and S_4 fragments, the K forms being characterized by larger positive charges on S_2 and S_4 than the E forms. This indicates that, even in the case of **4A** bearing donor/acceptor groups, there is no real charge transfer between the two extremities of the molecules, the charge transfer mainly occurring from the extremities to the central conjugated bridge.

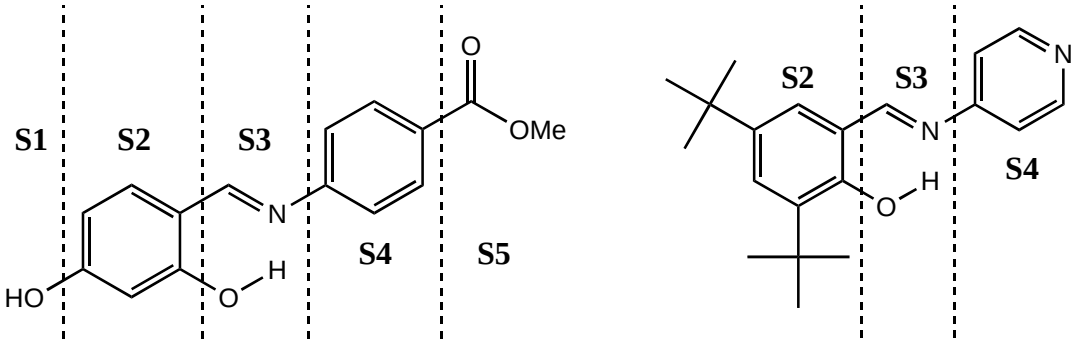

	4A – E	4A – K	4P – E	4P – K
S_1	-0.293	-0.290	-	-
S_2	0.627	0.644	0.357	0.382
S_3	-0.562	-0.682	-0.581	-0.700
S_4	0.249	0.341	0.224	0.318
S_5	-0.020	-0.013	-	-

Table 5-2: MP2/6-31G* Mulliken charge distributions (|e|) for selected moieties of **4A** and **4P**.

Table 5-3 summarizes the main thermodynamic and kinetic data for the tautomeric equilibrium of the two compounds. Gas phase calculations performed at both levels of theory lead to the same conclusion that the K form is metastable at room temperature, in agreement with experiment. However, the Gibbs energies and activation energies for the E→K reaction determined at the MP2/6-31G* level are significantly larger than at the B3LYP/6-311G* level, leading to larger differences in the relative stability of the two forms. The exacerbated instability of the K-isomer predicted at the MP2 level might be, in part, related to the fact that the length of its O···H bond is significantly shorter than within DFT calculations. The transition states of the two compounds are described by large and similar imaginary frequencies indicating a weak effect of the chemical structure on the potential energy surface.

Besides, it is noteworthy that using MP2, the activation Gibbs energy for the reverse reaction (K→E) is negative when solvent effects are omitted. Negative enthalpies of activation have also been reported in previous investigations of hydroxynaphthaldehyde anils and substituted salicylideneanilines [3,6]. This peculiar ordering of the transition state and K form energies finds its origin in the fact that the stationary/transition states on the potential energy surface are determined by considering stationary points on the energy U_0 surface whereas thermodynamics is based on G_{298}, with $G_{298} = U_0 + ZPVE +$ thermal corrections including the entropy term. At the MP2 level, the $\Delta U_0^{\#}$(reverse) values are 1.86 and 1.48 kcal mol^{-1} for **4A** and **4P**, respectively. In the same order, the corrections to $\Delta U_0^{\#}$(reverse) to get

$\Delta G_{298}^{\#}$(reverse) are negative and amount to –2.22 and –2.07 kcal mol^{-1} and thus dominate over the $\Delta U_0^{\#}$ term, leading to a negative activation barrier. Using DFT, the $\Delta U_0^{\#}$(reverse) values are, in kcal mol^{-1}, 4.62 (**4A**) and 4.71 (**4P**), while $\Delta G_{298}^{\#} - \Delta U_0^{\#}$ amount to –2.33 (**4A**) and –2.65 (**4P**).

Compound	B3LYP/6-311G*		MP2/6-31G*	
	In gas phase			
	ΔG_{298}	$\Delta G_{298}^{\#}$ ($\nu^{\#}$)	ΔG_{298}	$\Delta G_{298}^{\#}$ ($\nu^{\#}$)
4A	1.04	3.33 (1396*i*)	6.69	6.33 (1173*i*)
4P	0.69	2.76 (1401*i*)	6.65	6.06 (1098*i*)
	In CCl_4 [a]			
	ΔG_{298}	$\Delta G_{298}^{\#}$	ΔG_{298}	$\Delta G_{298}^{\#}$
4A	0.07	2.88	6.13	8.12
4P	0.07	2.44	6.49	8.09
	In CH_3CN [a]			
	ΔG_{298}	$\Delta G_{298}^{\#}$	ΔG_{298}	$\Delta G_{298}^{\#}$
4A	-1.35	2.16	4.88	4.92
4P	-1.01	1.90	5.26	5.04

Table 5-3: Gibbs energies (kcal mol^{-1}) of reaction [ΔG_{298}] and of activation [$\Delta G_{298}^{\#}$] for the E ⇆ K reaction of compounds **4A** and **4P**. The imaginary frequency (cm^{-1}) of the transition states is given between parentheses.
[a] Using thermal corrections to Gibbs energy calculated on gas phase geometries.

At the two levels of approximation, including solvent effects, leads to a decrease of ΔG_{298} with respect to the gas phase values, the effects being larger in acetonitrile (CH_3CN: ε_0 = 36.64, ε_∞ = 1.806) than in carbontetrachloride (CCl_4: ε_0 = 2.228, ε_∞ = 2.129), whose dielectric constant is smaller. In CCl_4, DFT calculations predict that the E and K forms should exist in similar proportion at room temperature, while in acetonitrile the K form is found to be the most stable. The MP2 level of theory shows a similar reduction of ΔG_{298}.

Overall, these calculations do not reveal significant differences in the thermodynamic properties of **4A** and **4P**, contrary to that observed in the solid state, in which **4P** is almost bi-stable [4]. Except at the IEF-PCM/MP2 level, ΔG_{298} is larger for **4A** than for **4P**, but the difference remains smaller than 1 kcal mol^{-1}. Similarly, $\Delta G_{298}^{\#}$ for **4A** is always slightly larger than for **4P**, except at the IEF-PCM/MP2 level in acetonitrile.

5.3. Linear optical properties

Figure 5-2 displays the low-energy part of the absorption spectra of **4A** and **4P** in their E form, as measured in acetonitrile. Both spectra reveal two distinct absorption bands. For **4A**, the maximum absorption wavelength is found at 344 nm (3.60eV, 29110 cm–1), while a second peak of lower intensity is present at 298 nm (4.16eV, 33600 cm–1). In the case of **4P**, the maximum absorption corresponds to a band located at 288 nm (4.31eV, 34770 cm–1), and the less absorbing state arising at 356 nm (3.48eV, 28130 cm–1) corresponds to the lowest energy band. The molar extinction coefficient of **4A** at 344 nm is 79734 $L.cm^{-1}.mol^{-1}$, and for **4P** it amounts to 83515 $L.cm^{-1}.mol^{-1}$ at λ = 288 nm and to 37164 $L.cm^{-1}.mol^{-1}$ at λ = 356 nm.

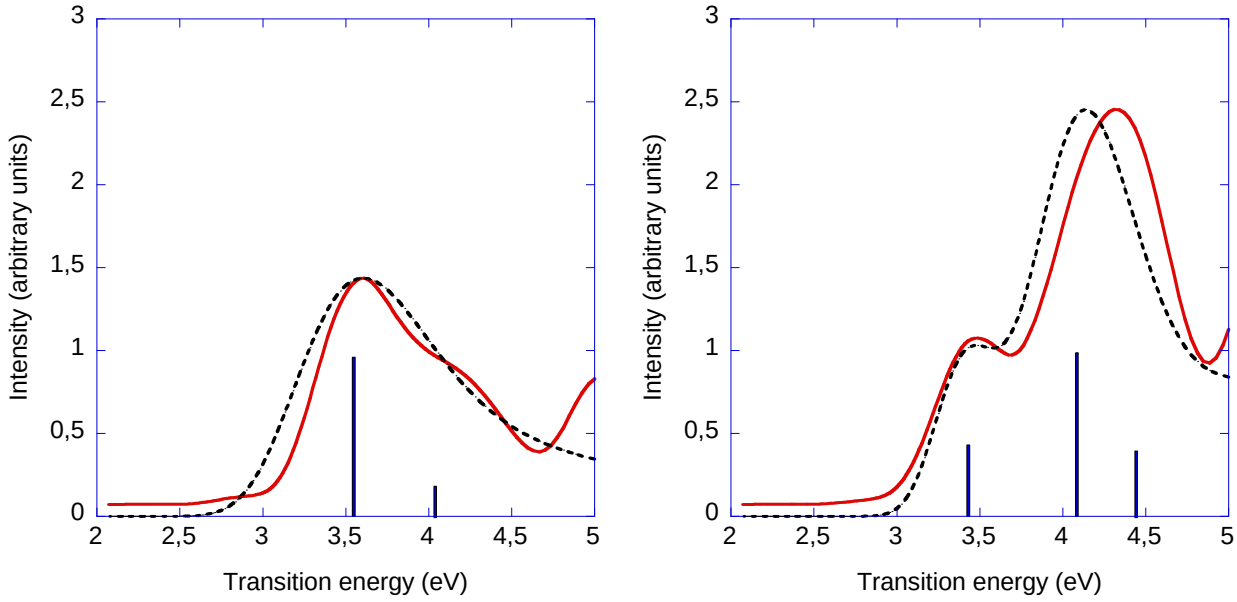

Figure 5-2: Absorption spectra of the E form of **4A** (left) and **4P** (right) measured in acetonitrile (plain line). The bars report the oscillator strengths calculated at the IEF-PCM/TDDFT/B3LYP/6-311+G* level using the B3LYP/6-311G* geometry. The simulated spectrum has been obtained by enlarging each transition using a Gaussian function having a full width at half maximum (FWHM) of 90 nm (**4A**) and 50 nm (**4P**). The intensities at the absorption maxima have been adjusted to coincide in the experimental and simulated spectra.

The bars in Figure 5-2 provide the corresponding simulated absorption spectra for excitation energies in the same 2-5 eV region, as calculated at the IEF-PCM/TDDFT/B3LYP/6-311+G* level using the DFT gas phase molecular geometry. The numerical values of the transition energies, wavelengths and oscillator strengths calculated at various theoretical levels are gathered in Table 5-4.

Excited state	ΔE_{ge}	λ_{ge}	f_{ge}
		4A-E, in gas phase	
1	3.626 (3.670)	342 (338)	0.753 (0.700)
2	4.003 (4.078)	310 (304)	0.201 (0.183)
		4A-E, in CH_3CN	
1	3.548 (3.611)	349 (343)	0.962 (0.892)
2	4.017 (4.077)	309 (304)	0.191 (0.198)
		4P-E, in gas phase	
1	3.437 (3.464)	361 (358)	0.173 (0.147)
2	4.102 (4.155)	302 (298)	0.395 (0.406)
3	4.437 (4.493)	279 (276)	0.161 (0.125)
		4P-E, in CH_3CN	
1	3.427 (3.461)	362 (358)	0.219 (0.185)
2	4.088 (4.147)	303 (299)	0.554 (0.581)
3	4.382 (4.453)	283 (278)	0.144 (0.101)

Table 5-4: Transition energies (ΔE_{ge}, eV), wavelengths (λ_{ge}, nm) and oscillator strengths (*f*) of the E forms of 4**A** and **4P**, as calculated at the TDDFT/B3LYP/ 6-311+G* level using the B3LYP/6-311G* geometries. The values between parentheses are obtained using the MP2/6-31G* geometries.

Without accounting for the vibronic structure, the calculated spectra are in overall good agreement with the measured ones. In particular, the method for geometry optimization, DFT or MP2, does not significantly affect the transition energies. Moreover, the solvent does not have a large impact on the absorption properties, as previously observed by Sliwa *et al.* [4]. For both compounds, the lowest energy charge-transfer excited state (state 1 in Table 5-4) is dominated by a $\pi \rightarrow \pi^*$ transition between the highest occupied molecular orbital (HOMO, H) and the lowest unoccupied molecular orbital (LUMO, L), while the second state is dominated by a [H–1→L] single excitation. The H–1, H and L orbitals are drawn in Figure 5-3.

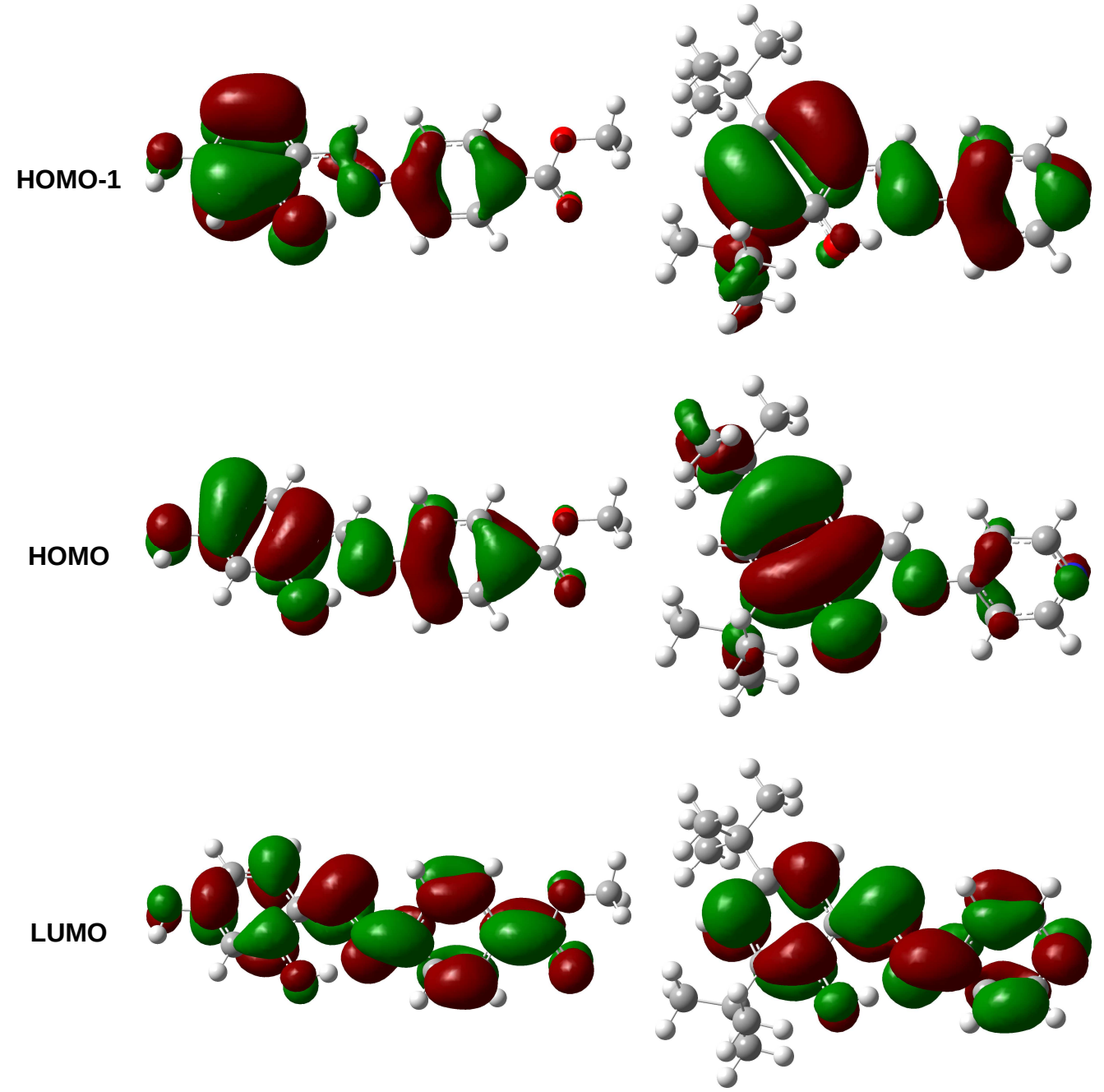

Figure 5-3: Frontier orbitals of **4A-E** and **4P-E** calculated at the B3LYP/6-311+G* level.

5.4. Nonlinear optical properties

Table 5-5 reports the longitudinal (β_{zzz}), transverse (β_{zxx}), and hyper Rayleigh (β_{HRS}) hyperpolarizabilities as well as the depolarization ratios for **4A** and **4P** issued from HRS measurements. The projection of the hyperpolarizability on the dipole moment direction ($\beta_{//}$), measured by EFISHG [4] is also displayed. The calculated

static and dynamic β_{HRS}, DR and $\beta_{//}$ are given in Table 5-6 by considering two solvents with large difference in their dielectric constant: acetonitrile (CH_3CN, $\varepsilon_0 = 36.64$, $\varepsilon_\infty = 1.806$) and carbontetrachloride (CCl_4: $\varepsilon_0 = 2.228$, $\varepsilon_\infty = 2.129$).

	β_{zzz}	β_{zxx}	β_{HRS}	DR	$\beta_{//}$
4A-E	15309	–1904	6086	3.85	1412
4P-E	9496	–942	3798	4.08	787

Table 5-5: Dynamic longitudinal (β_{zzz}), transverse (β_{zxx}), and HRS (β_{HRS}) hyperpolarizabilities (a.u.), as well as depolarization ratios DR measured in acetonitrile at λ = 1064 nm. Last column: hyperpolarizabilities obtained from EFISHG measurements in dioxane at λ = 1907 nm (taken from Ref. 4).

At the CPHF/6-31G* level, the contrast in the HRS first hyperpolarizability between the two forms, $\beta_{HRS}(E)/\beta_{HRS}(K)$, is equal to 1.18 and 0.91 for **4A** and **4P**, respectively. Accounting for electron correlation at the MP2 level has a different impact according to whether the E or K forms are considered. For the E forms, it leads to an increase of the hyperpolarizability values by roughly a factor 2 with respect to the CPHF values, while for the K forms, β_{HRS} significantly decreases in the case of **4P** (–46%) and remains almost unchanged (–0.1%) in the case of **4A**. This results in the enhancement of the $\beta_{HRS}(E)/\beta_{HRS}(K)$ contrast to 2.46 for **4A**, and, in the case of **4P**, inverts the conclusions about the relative magnitude of the first hyperpolarizabilities of the two tautomer forms, with $\beta_{HRS}(E)/\beta_{HRS}(K) = 3.25$. Except for **4P-K**, the behavior of $\beta_{//}$ and $\beta_{//}(E)/\beta_{//}(K)$ with respect to electron correlation is quite similar to β_{HRS}. Including electron correlation at the MP2 level leads to a large increase of the depolarization ratio for the E forms (22% and 48% for **4A-E** and **4P-E**, respectively) and a small variation for the K forms (+3% in the case of **4A-K** and -5% for **4P-K**).

The frequency dispersion effects induced by an incident beam at λ = 1907 nm lead, for the E form of the two compounds, to an increase of β_{HRS} by 8% compared to the static values, while for the K forms, the increase is different for **4A** (+7%) and **4P** (+10%). Similarly, the dynamic $\beta_{//}$ are larger than the static ones, except for **4P-K** whose absolute value $\beta_{//}$ is almost the same while DR increases by a few percents (from 2 to 5%) for the four compounds. Using an incident wavelength of 1064 nm, closer to the resonance, induces a more pronounced enhancement of β_{HRS} and $\beta_{//}$, except again for **4P-K**. With the exception of **4A-K**, the depolarization ratios also increase substantially when accounting for frequency dispersion, figuring out β tensors dominated by a few components.

Accounting for interactions with the solvent leads to a similar enhancement of the static β_{HRS} responses of the K forms of the two compounds (by about 50% in CCl_4 and 85-105% in CH_3CN), while the enhancement factors for **4A-E** and **4P-E** are different (of about 35-45% in CCl_4 and 145% in acetonitrile). The depolarization ratio decreases in all the cases except for the **4P-K** form. Following the same trend, the $\beta_{//}$ responses are significantly exalted in the presence of acetonitrile, especially for the two forms of **4A**, while CCl_4 has a smaller influence. The solvent-induced enhancement of both $\beta_{//}$ and β_{HRS} is reduced in acetonitrile when going from ($\lambda = \infty$) to (λ = 1907 nm) and to (λ = 1064 nm), since the dynamic dielectric constant is smaller than the static one due to the vanishing orientation term. This decrease is not observed in CCl_4, whose dielectric constant remains almost unchanged within the wavelength range because it is nonpolar.

Finally, considering the dynamic (λ = 1064 nm) HRS first hyperpolarizabilies and accounting for both electron correlation and solvent effects (acetonitrile), we obtain a contrast $\beta_{HRS}(E)/\beta_{HRS}(K)$ of 2.36 and 2.49 for **4A** and **4P**, respectively. The ratio between the β_{HRS} responses of the two E forms is equal to 2.40, which is larger but in good qualitative agreement with the measured ratio of 1.60. For both E and K forms, the depolarization ratio of the **4A** compound is larger than in **4P**. Moreover, the E form (of **4A** or **4P**) presents larger DR values than the corresponding K forms. The calculated DR value is in good agreement with experiment for **4A** but not for **4P** where it is underestimated.

At the TDHF level in CCl_4, the $\beta_{//}$(**4A-E**)/$\beta_{//}$(**4P-E**) ratio is equal to 2.30 at λ = 1907 nm, in rather good agreement with the ratio of 1.79 measured in dioxane by Nakatani *et al.* [5]. However, accounting for electron correlation *via* the multiplicative scheme leads to a reversed $\beta_{//}$(**4A-E**)/$\beta_{//}$(**4P-E**) ratio of 0.80. Considering the $\mu\beta_{//}$ product rather than the $\beta_{//}$ quantity for the comparison between theory and experiment, which removes the imprecision associated with the determination of the dipole moment, no improvement is found. Indeed, the experimental $\mu\beta_{//}$(**4A-E**)/$\mu\beta_{//}$(**4P-E**) ratio amounts to 2.02 whereas the theoretical estimate including solvent and electron correlation effects is equal to 0.67 because the relative value of the dipole moment is not reproduced.

	4A-E	4A-K	4P-E	4P-K		4A-E	4A-K	4P-E	4P-K
In gas phase, $\lambda = \infty$									
CPHF					**MP2**				
β_{HRS}	913	777 (1.18)	433	476 (0.91)	β_{HRS}	1747	709 (2.46)	833	256 (3.25)
DR	3.91	3.54	2.91	2.49	**DR**	4.76	3.63	4.30	2.38
$\beta_{//}$	429	-300 (-1.43)	225	-56 (-4.02)	$\beta_{//}$	508	-230 (-2.21)	765	-138 (-5.54)
KS/B3LYP									
β_{HRS}	1713	1383 (1.24)	643	502 (1.28)					
DR	4.52	4.25	3.71	2.90					
$\beta_{//}$	1312	-155 (-8.92)	539	78 (6.91)					
In gas phase, λ = 1907 nm									
TDHF					**MP2**[b]				
β_{HRS}	991	829 (1.20)	469	524 (0.90)	β_{HRS}	1896	756 (2.51)	902	282 (3.20)
DR	3.97	3.63	3.02	2.62	$\beta_{//}$	560	-250 (-2.24)	867	-136 (-6.38)
$\beta_{//}$	473	-326 (-1.45)	255	-55 (-4.64)					
In gas phase, λ = 1064 nm									
TDHF					**MP2**[b]				
β_{HRS}	1214	979 (1.24)	572	702 (0.81)	β_{HRS}	2323	893 (2.60)	1100	378 (2.91)
DR	4.11	3.86	3.30	3.03	$\beta_{//}$	708	-314 (-2.25)	1166	-111 (-10.50)
$\beta_{//}$	598	-410 (-1.46)	343	-45 (-7.62)					

	4A-E	4A-K	4P-E	4P-K		4A-E	4A-K	4P-E	4P-K
In CH_3CN, $\lambda = \infty$									
CPHF					**KS/B3LYP**				
β_{HRS}	1875	1896 (0.99)	797	1161 (0.69)	β_{HRS}	4325	3412 (1.27)	1527	1369 (1.12)
DR	3.64	3.40	2.70	2.62	**DR**	4.43	4.08	3.80	2.97
$\beta_{//}$	963	-647 (-1.49)	279	-210 (-1.33)	$\beta_{//}$	3353	-550 (-6.10)	1269	119 (11.33)
In CH_3CN, λ = 1907 nm									
TDHF					**MP2[c]**				
β_{HRS}	1412	1274 (1.11)	598	770 (0.78)	β_{HRS}	2702	1163 (2.32)	1150	414 (2.78)
DR	3.98	3.67	2.97	2.72	$\beta_{//}$	975	-278 (-3.51)	1020	-209 (-4.88)
$\beta_{//}$	823	-362 (-2.27)	300	-85 (-3.53)					
In CH_3CN, λ = 1064 nm									
TDHF					**MP2[c]**				
β_{HRS}	1764	1569 (1.12)	733	1053 (0.70)	β_{HRS}	3375	1432 (2.36)	1410	566 (2.49)
DR	4.13	3.91	3.24	3.15	$\beta_{//}$	1255	-354 (-3.55)	1384	-207 (-6.69)
$\beta_{//}$	1060	-462 (-2.29)	407	-84 (-4.85)					
In CCl_4, $\lambda = \infty$									
CPHF					**KS/B3LYP**				
β_{HRS}	1303	1185 (1.10)	586	722 (0.81)	β_{HRS}	2692	2126 (1.27)	987	812 (1.22)
DR	3.83	3.51	2.87	2.58	**DR**	4.50	4.20	3.79	2.97
$\beta_{//}$	678	-415 (-1.63)	287	-89 (-3.22)	$\beta_{//}$	2111	-263 (-8.03)	849	122 (6.96)

	4A-E	4A-K	4P-E	4P-K		4A-E	4A-K	4P-E	4P-K
					In CCl_4, λ = 1907 nm				
TDHF					**MP2[c]**				
β_{HRS}	1407	1262 (1.11)	628	792 (0.79)	β_{HRS}	2692	1152 (2.34)	1208	426 (2.84)
DR	3.90	3.61	2.98	2.71	$\beta_{//}$	883	-342 (-2.58)	1105	-209 (-5.29)
$\beta_{//}$	746	-446 (-1.67)	325	-85 (-3.82)					
					In CCl_4, λ = 1064 nm				
TDHF					**MP2[c]**				
β_{HRS}	1761	1556 (1.13)	776	1106 (0.70)	β_{HRS}	3370	1420 (2.37)	1493	595 (2.51)
DR	4.07	3.87	3.26	3.17	$\beta_{//}$	1146	-443 (-2.59)	1516	-182 (-8.33)
$\beta_{//}$	968	-578 (-1.67)	446	-74 (-6.03)					

Table 5-6: First hyperpolarizabilities and depolarization ratios of **4A** and **4P** in their E and K forms, evaluated at different levels of approximation using the 6-31G* basis set.
[a] All values are given in a. u.. The β(E)/β(K) ratios are given in parentheses.
[b] Using Equation (2-46) with β_{TDHF} and β_{CPHF} calculated in gas phase. [c] using Equation (2-46) with β_{TDHF} calculated in solvent.

The μ and β vectors were sketched in the molecular frame (Figure 5-4) in order to analyze the impact of the anil structure as well as the electron correlation and solvent effects. In addition, the angle (θ) formed by the μ and β vectors are listed in Table 5-7. For compound **4A**, the β vector is always directed towards the hydroxyl group with little differences between the E and K forms as well as when taking into account the solvent or electron correlation effects. However, the relative orientation of the dipole moment changes when switching from the E to K forms: in **4A-E**, $\theta < \pi/2$ so that $\beta_{//}$ is positive whereas for **4A-K**, $\theta > \pi/2$ so that $\beta_{//}$ is negative. When going from the HF to MP2 treatment, the amplitude of β increases, as can be estimated from the HRS response, for the enol form but θ gets closer to π/2 so that the enhancement is rather small. For the K form, these MP2-HF effects are smaller. In the case of **4P**, at the TDHF level, the absence of donor/acceptor groups in *para* position on the salicylidene ring yields a different orientation of the β vector with respect to the molecular backbone. Nevertheless, the θ angles remain similar to the parent **4A** compound so that $\beta_{//}$(**4P-E**) is positive while $\beta_{//}$(**4P-K**) is negative and of smaller amplitude. The same conclusions are drawn for the static (CPHF) and dynamic (TDHF) treatments as well as with or without accounting for the solvent effects. Thus, at the TDHF level of approximation, the larger $\beta_{//}$ of **4A-E** is due to the larger β amplitude. The situation is different when considering the MP2 results. Indeed, the β vector of **4P-K** is now oriented towards the pyridine ring and presents a reduced amplitude. Moreover, in the case of **4P-E**, the θ angle is now close to π/4 so that the projection of β on μ gets larger than for **4A-E**. For both **4A** and **4P** compounds, including electron correlation effects at the MP2 level leads to an increase of the $\beta_{//}(E)/\beta_{//}(K)$ ratios, mostly driven by the β amplitude whereas the change of θ angle compensates partially this effect. This analysis also enables to point out that compound **4A** presents similarities with 4'-amino-N-salicylideneaniline (compound **4** of Ref.3), a compound having a stronger donor group in R' position but no acceptor in R. After taking into account the difference of β conventions (T *versus* B), it appears that **4A**, in both E and K forms, displays smaller β responses than compound **4** of Ref.3, and thus than compounds with strong D/A groups. From comparing the θ angles, compound **4P** appears as a new class of anils, where θ(K) – θ(E) is larger than 100°. Again, the β responses are small with respect to other systems with D/A. In addition, on the basis of this analysis, the difference between the measured and the calculated relative $\beta_{//}$ values of **4A-E** and **4P-E** could be associated with difficulties in determining the dipole moment orientation and the effect of the solvent on it.

In view of providing an enlarged comparison of the performance of the different theoretical schemes, DFT calculations of the static first hyperpolarizabilities were carried out and the results are also presented in Table 5-6. It appears that this scheme employing the B3LYP exchange-correlation functional provides β values

sometimes in good agreement with the MP2 results, sometimes close to the CPHF values, and also sometimes far away from both CPHF and MP2 results. Thus, although the corresponding scheme for simulating the absorption spectra is performing well, these DFT β results confirm earlier investigations [9]. This is further substantiated by the angles listed in Table 5-7.

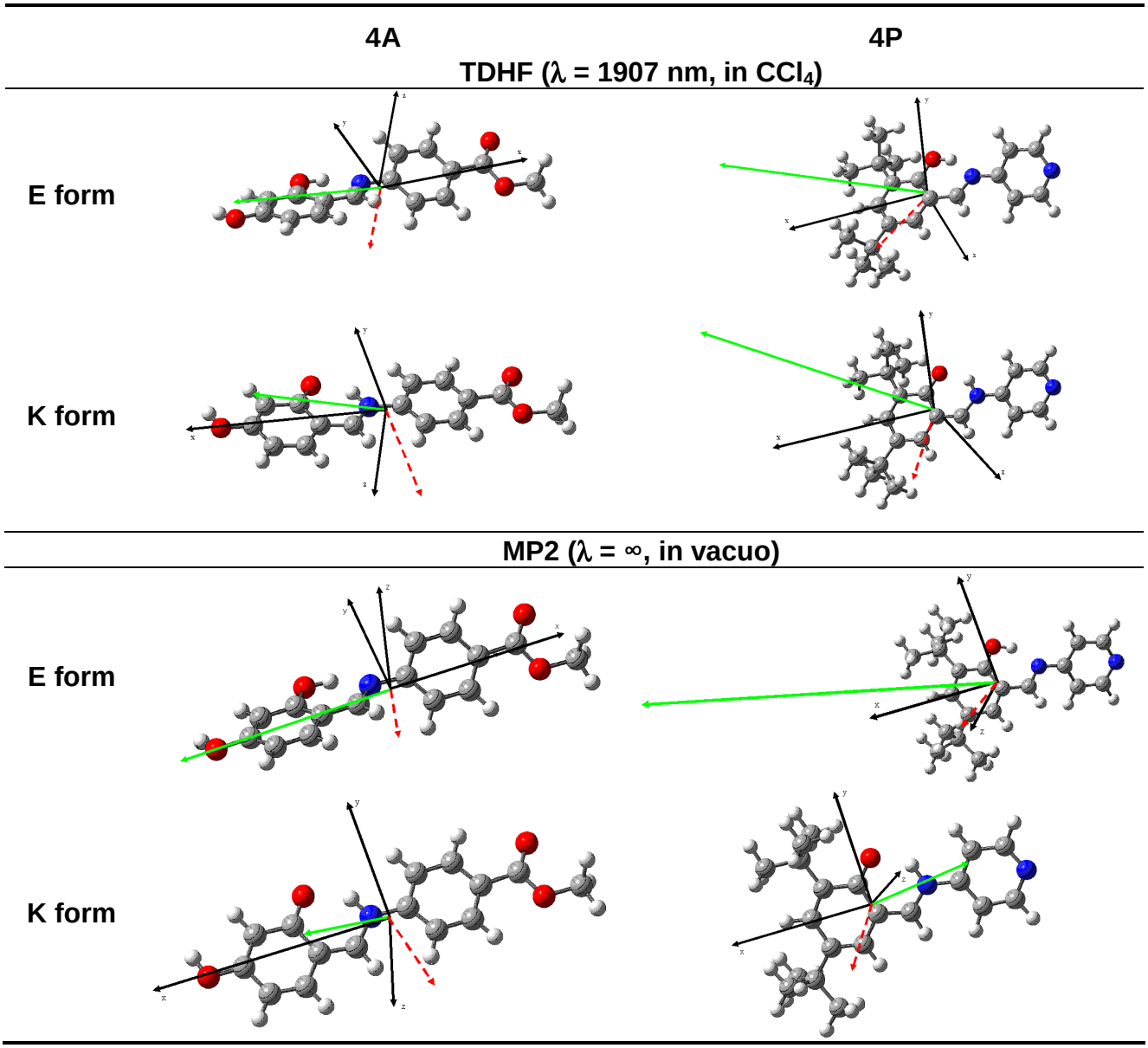

Figure 5-4: Sketch of the dipole moment (red dotted line) and first hyperpolarizability (green full line) vectors for E and K forms of compounds **4A** and **4P** as determined at the TDHF (λ = 1907 nm, CCl_4) and MP2 (λ = ∞ nm, in vacuo) levels of approximation. The lengths of μ and β vectors are proportional to their norms. Note however that for better visualization, the β vectors of the **4A** species have been drawn using a scale five times larger than for the **4P** species.

θ	4A-E	4A-K	4P-E	4P-K
MP2 (in vacuo, λ = ∞ nm)	78.2	104.6	48.2	155.9
KS/B3LYP (in vacuo, λ = ∞ nm)	56.9	94.7	49.9	82.2
CPHF (in vacuo, λ = ∞ nm)	69.3	107.7	62.8	96.7
TDHF (in vacuo, λ = 1064 nm)	68.5	108.8	60.4	93.3
TDHF (in CCl_4, 1907 nm)	66.4	106.1	63.3	95.7

Table 5-7: θ angles (in degrees) formed by the μ and β vectors for the different forms of **4A** and **4P** as a function of the method of calculation.

5.5. Conclusions

This chapter has addressed the second-order NLO responses of two anil derivatives, and more particularly the contrast upon switching between the enol-imine and keto-amine forms within the tautomerization equilibrium. These two compounds are investigated here by means of HRS measurements as well as *ab initio* calculations accounting for both electron correlation and solvent effects. The structural characteristics and molecular optical properties are well reproduced by quantum chemical calculations. In addition, the contrast between the first hyperpolarizability of the E forms of the two compounds, which is consistent with the linear optical properties, is in fair agreement with HRS and EFISHG experiments, in particular, at the TDHF level of approximation. Some reduction of agreement at the MP2 level has been attributed to difficulties in predicting the dipole moment orientation. For both **4A** and **4P**, the E/K first hyperpolarizability ratios are larger than 2, demonstrating that the enol forms present the largest responses. Although the switching is associated with a relatively small β contrast compared to what is observed in other organic photochromes, anils have the advantage to act as NLO switches in the solid state, which is of crucial interest in view of practical applications. Thus, this work constitutes a prerequisite step for future developments that will encompass the theoretical evaluation of the solid state effects on the optical properties, using supermolecule approaches such as those described in Ref.9. Macroscopic properties (linear and nonlinear susceptibilities) of **4A** and **4P** in the crystalline state have been calculated [10] and compared to experimental ones [4] and theoretical calculations reproduce well qualitatively the experimental values. In conclusion, **4A** and **4P** compounds seem to be very interesting candidates for NLO applications in spite of their small β contrasts.

5.6. References

[1] K. Nakatani and J. A. Delaire, *Chem. Mater.*, **9**, 2682 (1997).

[2] L. Lucas, J. De Jong, J. Van Esch, R. M. Kellogg, and B. L. Feringa, *Eur. J. Org. Chem.*, **1**, 155 (2003).

[3] M. Guillaume, B. Champagne, N. Markova, V. Enchev, and F. Castet, *J. Phys. Chem. A*, **111**, 9914 (2007).

[4] M. Sliwa, S. Létard, I. Malfant, M. Nierlich, P. G. Lacroix, T. Asahi, H. Masuhara, P. Yu, and K. Nakatani, *Chem. Mater.*, **17**, 4727 (2005).

[5] M. Sliwa, K. Nakatani, T. Asahi, P. G. Lacroix, R. B. Pansu, and H. Masuhara, *Chem. Phys. Lett.*, **437**, 212 (2007).

[6] W. M. F. Fabian, L. Antonov, D. Nedeltcheva, F. S. Kamounah, and P. J. Taylor, *J. Phys. Chem. A*, **108**, 7603 (2004).

[7] M. Miura, Y. Aoki, and B. Champagne, *J. Chem. Phys.*, **127**, 084103 (2007).

[8] B. Champagne, E. A. Perpète, D. Jacquemin, S. J. A. van Gisbergen, E. J. Baerends, C. Soubra-Ghaoui, K. Robins, and B. Kirtman*, J. Phys. Chem. A*, **104**, 4755 (2000).

[9] M. Guillaume, E. Botek, B. Champagne, F. Castet, and L. Ducasse, *J. Chem. Phys.*, **121**, 7390 (2004).

[10] A. Ségerie *et al.*, in preparation.

Solvent effects on the second-order nonlinear optical responses in the keto – enol equilibrium of a 2-hydroxy-1-naphtaldehyde derivative

E. Bogdan, A. Plaquet, L. Antonov, V. Rodriguez, L. Ducasse, B. Champagne, and F. Castet, *J. Phys. Chem. C*, **114**, 12760 (2010).

6. Solvent effects on the second-order nonlinear optical responses in the keto – enol equilibrium of a 2-hydroxy-1-naphtaldehyde derivative

6.1. Introduction

The modifications of the intrinsic molecular responses have been the topic of many investigations, either experimentally [1-3] or theoretically [4,5], that have shown that the surroundings constitute one of the tunable parameters to optimize the NLO responses. Solvent effects on the NLO responses have initially been investigated for push-pull systems in conjunction with their solvatochromism [6,7]. Indeed, the relative stability of their two resonant forms [valence bond (VB) and charge transfer (CT)] varies as a function of the solvent polarity. As reviewed by Bishop [4], the surrounding presents a double effect: it modulates the field amplitudes, which are experienced by the solute and modifies the geometry and electronic structure of the solute from what they are in the gas phase. Theoretically, studies dealing with the description of the effects of the solvent appeared more than 15 years ago [8-13], and challenges have encompassed i) the development of polarizable continuum models (PCMs) including different contributions to the solute-solvent interactions (See paragraph 2-4 for more details), ii) the related description of the solute cavity, iii) the elaboration of techniques including specific solvent molecules as in QM/MM treatments [14-16], and iv) the description of the local field effects [17-20], in addition to the fact that these methods have been worked out at different levels of approximation ranging from semi-empirical and *ab initio* Hartree-Fock methods to MO-based and density-based correlated schemes [21-23].

In this chapter, we have investigated the solvent effects on the second-order NLO response of the N-(2-hydroxynaphtylidene)-aniline derivative, a compound from the anils family, which displays tautomerism between an enol and a keto form (Figure 6-1) [24]. In addition to the double effect pointed out in the review by Bishop [4], the solvent has here a third role since it can shift the equilibrium between the different forms. For this system, the equilibrium displacement is induced by using different binary mixtures of cyclohexane (C_6H_{12}) and ethanol (EtOH).

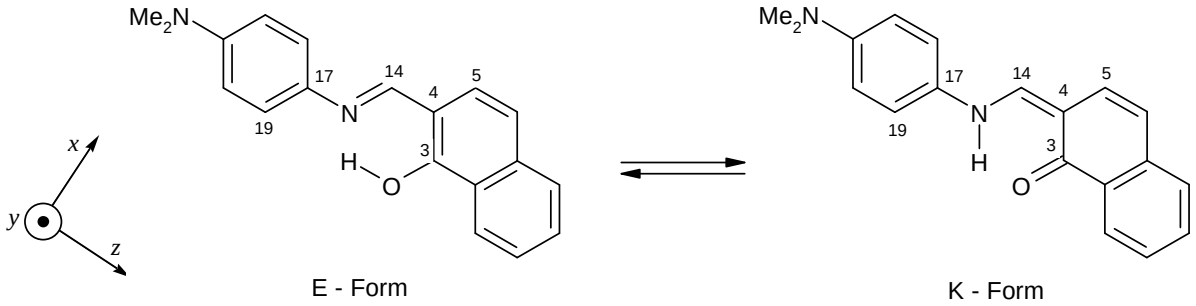

Figure 6-1: Tautomeric equilibrium of the N-(2-hydroxynaphtylidene)-aniline derivative, where the atom labels used in the calculations are reported.

6.2. Experimental aspects

HRS experiments were performed in pure ethanol and cyclohexane solvents as well as in ethanol/cyclohexane mixtures in 30/70 and 70/30 volume ratios. In the context of a solvent mixture, it has been necessary to recalculate the n_{ω}^{S}, $n_{2\omega}^{S}$ and f_L^2 values as a function of the ratio of ethanol in solvent mixtures (Table 6-1). The solvent contribution in Equation (3-10) was previously obtained from HRS measurements on the pure ethanol solution (cyclohexane has no HRS response) using acetonitrile as an external reference. The determination of the second-order nonlinear optical response of the anil derivative has been accomplished with respect to the response of ethanol, taken now as an internal reference. For the sake of homogeneity of the measurements, the acetonitrile response has also been used as an external reference for the solute in pure cyclohexane solutions.

% EtOH	n_{ω}	$n_{2\omega}$	f_L^2
0	1.420	1.426	5.803
30	1.399	1.406	5.320
70	1.371	1.381	4.744
100	1.350	1.361	4.346

Table 6-1: Refractive indices at optical frequencies ω and 2ω and local field correction as a function of the ethanol proportion.

6.3. Molecular structures and thermodynamic analysis

In addition to the most stable *cis* isomer, both the E and K forms can adopt a *trans* structure, which is obtained by rotating the naphtyl unit with respect to the dimethylaminophenyl group by about 180°. However, as a result of breaking the intramolecular H-bond, their energies, as determined at the B3LYP/6-311G* level, are larger, leading therefore to a negligible statistical weight. Therefore, only the *cis*-conformers, which correspond to the direct reactant and product of the tautomeric

reaction, are considered hereafter. This is consistent with recent work on similar compounds [25].

Table 6-2 reports the relative Gibbs free energies (ΔG) and the activation barriers ($\Delta G^{\#}$) calculated for a temperature of 298.15 K for the E ⇆ K equilibrium, as well as the values of the imaginary frequencies associated with the transition states. Both in the gas phase and in solution, the small energy differences and activation barriers indicate the coexistence of the E and K forms at room temperature. Single-point IEF-PCM/MP2/6-311G* calculations using the geometry calculated at the IEF-PCM/B3LYP/6-311G* level predict that the E-tautomer should be the most stable both in the gas phase and in solution. Moreover, when the solvent is changed from cyclohexane to ethanol, the reaction energy decreases together with the activation barrier, indicating that the tautomeric equilibrium is shifted towards the K form. These results are consistent with other studies on the tautomerism of (hydroxylnaphthalidene)-anilines, which have shown that more polar solvents favor the proton transfer [24,26]. Besides, the application of the Maxwell-Boltzmann distribution scheme using the IEF-PCM/MP2/6-311G* relative free energies leads to relative E/K populations of 91/9 in cyclohexane and 64/36 in ethanol.

	ΔG	**$\Delta G^{\#}$ ($\nu^{\#}$)**
	In the gas phase	
B3LYP/6-311G*	-1.80	1.85 (1424i)
MP2/6-311G* [a]	1.96	4.49
	In C_6H_{12}	
IEF-PCM/B3LYP/6-311G*	-2.68	1.48 (1416i)
IEF-PCM/MP2/6-311G* [a]	1.37	4.08
	In EtOH	
IEF-PCM/B3LYP/6-311G*	-4.04	0.73 (1394i)
IEF-PCM/MP2/6-311G* [a]	0.35	3.31

Table 6-2: Relative Gibbs free energies and activation barriers ($\Delta G = G_K - G_E$ and $\Delta G^{\#} = G_{TS} - G_E$, kcal/mol) of the E⇆K reaction, and imaginary frequencies of the transition state ($\nu^{\#}$, in cm^{-1}).
[a] Single-point calculations using the geometry calculated at the IEF-PCM/B3LYP/ 6-311G* level.

The main geometrical features (distances and dihedral angles) of the two tautomeric forms and transition state, as optimized in the gas phase and in solvent at the B3LYP/6-311G*, are listed in Table 6-3. Theoretical values are compared to

X-Ray data of the N(2-hydroxynaphthalidene)-aniline compound, in which the NMe_2 group has been replaced by an H atom [27]. The last line of Table 6-3 reports the bond length alternation, defined as $(d_{14\text{-}4} + d_{N\text{-}17} - 2d_{N\text{-}14})/2$. In both forms, the central conjugated bridge is in the same plane as the naphtyl ring, as indicated by the values of the C_5-C_4-C_{14}-N and C_4-C_{14}-N-C_{17} dihedral angles very close to 180°. The C_{19}-C_{17}-C_4-C_3 dihedral angle between the mean planes of the naphtyl and phenyl rings is reduced by about 10° along the E→K reaction, leading to a stronger electron delocalization in the K form and to a reduction of the BLA by a factor of 2.

	X-Ray [a]	In the gas phase			In EtOH			In C_6H_{12}		
		E	TS	K	E	TS	K	E	TS	K
C_{14}–N	1.314	1.291	1.308	1.334	1.292	1.306	1.327	1.291	1.307	1.331
N–O	2.603	2.621	2.418	2.629	2.610	2.424	2.654	2.615	2.420	2.637
C_{14}–C_4	1.404	1.448	1.423	1.392	1.451	1.432	1.401	1.449	1.427	1.396
C_4–C_3	1.439	1.405	1.427	1.462	1.404	1.421	1.453	1.404	1.425	1.458
C_3–O	1.266	1.337	1.298	1.251	1.343	1.311	1.261	1.339	1.303	1.255
N···H	0.917	1.727	1.272	1.029	1.708	1.293	1.026	1.717	1.279	1.027
O···H	0.998	0.996	1.215	1.785	1.000	1.197	1.821	0.998	1.209	1.796
C_3–O–H	104.5	107.7	104.3	104.2	107.3	104.0	103.7	107.5	104.2	103.9
C_{14}–N–H	116.4	99.2	104.0	112.5	99.5	103.8	113.1	99.3	103.9	112.6
C_4–C_3–O	122.8	122.0	120.7	122.3	121.6	120.5	122.3	121.8	120.6	122.3
C_{14}–C_4–C_3	120.2	121.3	118.1	120.3	121.5	118.6	120.9	121.3	118.3	120.5
N–C_{14}–C_4	123.1	122.6	120.0	124.2	122.1	119.6	124.3	122.4	119.9	124.2
C_{17}–N–C_{14}	126.5	122.3	125.8	127.8	122.6	126.0	128.0	122.5	125.8	128.1
C_{19}-C_{17}-N-C_{14}	179.0	152.9	157.3	162.3	156.4	161.9	164.5	154.1	158.1	164.4
BLA		0.27	0.21	0.13	0.27	0.23	0.16	0.27	0.22	0.14

Table 6-3: Representative structural parameters of the E and K forms, as well as of the transition structure, calculated at the B3LYP/6-311G* level in the gas phase and in solvent using the IEF-PCM scheme. The distances are given in Angströms and the angles in degrees.
[a] From Ref. 28.

Finally, Table 6-4 reports the total dipole moments and solvation energies of the two tautomeric forms, as calculated at the IEF-PCM/B3LYP/6-311G* and IEF-PCM/MP2/6-311G*//IEF-PCM/B3LYP/6-311G* levels. It is noteworthy that the dipole moment of the compound significantly increases along the E→K transformation and, as expected from simple electrostatics, with the polarity of the solvent. At both

theoretical levels, the solvation energies calculated in ethanol are 3.2 times larger than those calculated in cyclohexane.

	IEF-PCM/B3LYP/6-311G*		IEF-PCM/MP2/6-311G* [a]	
	E	**K**	**E**	**K**
		In the gas phase		
Dipole moment	4.17	6.04	3.21	5.27
		In cyclohexane		
Dipole moment	4.68	6.96	3.67	6.01
Solute-solvent energy	-3.61	-4.61	-4.28	-5.50
		In ethanol		
Dipole moment	5.43	8.41	4.32	7.26
Solute-solvent energy	-11.69	-15.01	-13.92	-17.96

Table 6-4: Total dipole moments (in Debye) and solute-solvent energies (kcal/mol) of the two tautomeric forms.
[a] Single-point calculations using the geometry optimized at the IEF-PCM/B3LYP/ 6-311G* level.

6.4. Linear optical properties

6.4.1. Experimental absorption spectra and relative E/K populations

The UV-Visible spectra of the compound were measured in pure ethanol and cyclohexane solvents, as well as in two ethanol/cyclohexane mixtures at 30/70 and 70/30 volume ratios (Figure 6-2). In pure cyclohexane, most of the molecules are present in their E form, as shown by the small relative intensity of the long-wavelength band (~ 480 nm, 2.58 eV) associated to the $\pi \rightarrow \pi^*$ transition of the K-tautomer compared to the short-wavelength band (~ 410 nm, 3.02 eV) associated to the $\pi \rightarrow \pi^*$ transition of the E tautomer [24]. When the ethanol proportion is increased, the intensity of the K-band progressively increases, which confirms that the polarity of the medium moves the tautomeric equilibrium toward the K-tautomer, as already shown in previous studies [28]. The relative populations of E and K forms have been evaluated in every solvent mixture from the UV-Visible spectra using the procedure described in Ref.29 and 30, by decomposing the long-wavelength E- and K-bands using five and four sub-bands, respectively (Figure 6-3). The absorption spectra of the individual tautomers were also obtained, and the total oscillator strengths of the E and K forms are equal to 0.460 and 0.433, respectively. In ethanol/cyclohexane solvents with 0/100, 30/70, 70/30 and 100/0 ratios, the obtained relative E/K

populations are 90/10, 54/46, 43/57 and 34/66, respectively (Figure 6-4). These populations are in good qualitative agreement with the theoretical values. Indeed, at the MP2 level, the E/K population ratios amount to 91/9 and 64/36 in 0/100 and 100/0 ethanol/cyclohexane solvents, respectively.

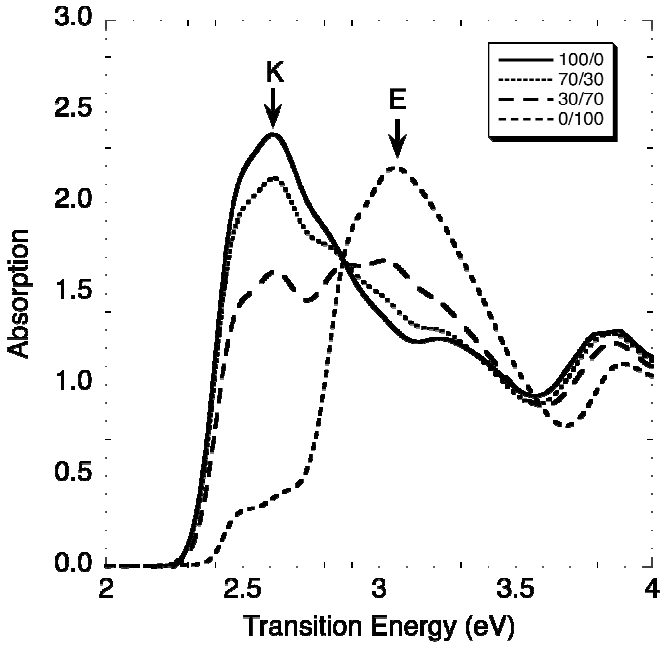

Figure 6-2: Absorption spectra measured in ethanol/cyclohexane mixtures in various proportions.

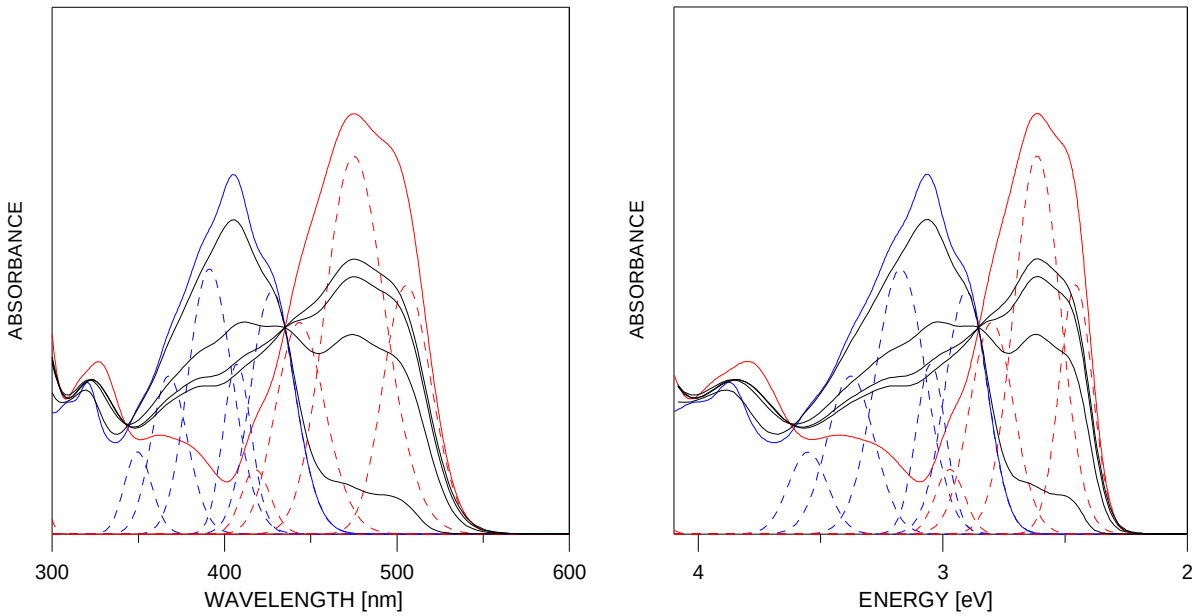

Figure 6-3: Absorption spectra of the investigated compound in ethanol/cyclohexane binary solvent mixtures (solid black lines). Individual spectra of the tautomers (solid lines in blue for the E form and in red for the K form) and the sub-bands composing the long-wavelength tautomer bands (in dashes).

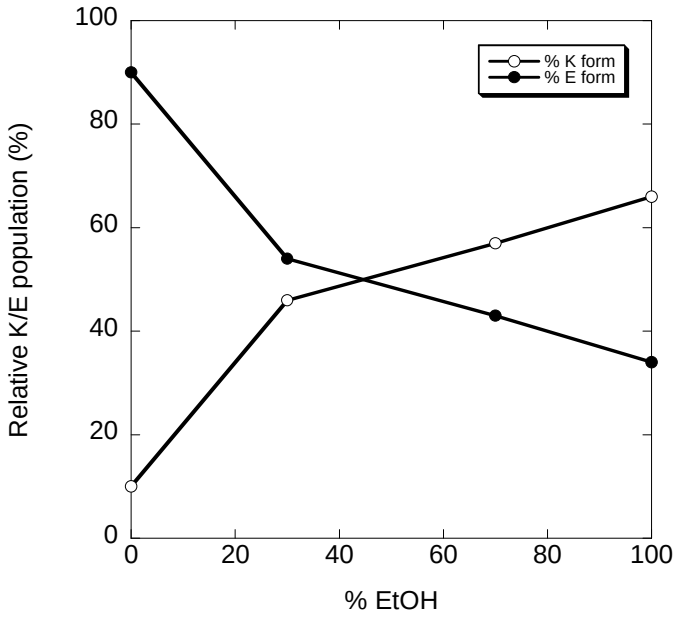

Figure 6-4: Relative population of K- and E- tautomers with respect to the ethanol ratio in the solvent.

6.4.2. Simulated absorption spectra

Table 6-5 gathers the transition energies, wavelengths, and oscillator strengths associated with the main low-energy optical transitions calculated in the gas phase as well as in cyclohexane and ethanol solutions for both the K and E forms. The nature of the MOs involved in these transitions is also given. The main absorption band of both the K- and E-tautomers is associated to a $\pi \rightarrow \pi^*$ transition between the highest occupied (HOMO, H) and the lowest unoccupied (LUMO, L) MOs (Figure 6-5). Consistent with experiments, although of smaller amplitude, DFT calculations predict that the E→K transformation is accompanied by a bathochromic shift of 0.19 eV, which is almost independent of the nature of the solvent. The exchange-correlation functional is responsible for the underestimation of the bathochromic shift, as shown by additional TDDFT/LC-BLYP/6-311G* calculations where the shift attains 0.40 eV, in comparison with the experimental value of 0.37 eV. The less intense absorption band observed around 330 nm is also well reproduced by the B3LYP calculations, and corresponds to the [H→L+1] transition.

The oscillator strength associated with the E-band (λ_{ge} = 428 nm at the B3LYP/6-311G* level) decreases when going from cyclohexane to ethanol (from 0.903 to 0.858), while the reverse is true for the K-band (λ_{ge} = 459 nm), whose oscillator strength slightly increases. Note that, although the oscillator strengths are overestimated by a factor 2, the relative intensities of the K- and E-bands are well reproduced by the DFT calculations. Indeed, the calculated f_K/f_E ratio amounts to 0.98 while the experimental value is equal to 0.94. These results demonstrate that IEF-PCM provides reliable trends regarding the displacement of the tautomeric

equilibrium with respect to the solvent polarity. Finally, the total absorption spectra of the anil compound in both solvents have been simulated by weighting the spectra of the E and K forms calculated at the IEF-PCM/TDDFT/B3LYP/6-311G* level by their relative populations deduced from experiments (Figure 6-6), highlighting again that the displacement of the maximum absorption band toward the low energies when the solvent polarity is increased is well accounted for by the TDDFT calculations.

	λ_{ge}	ΔE_{ge}	f_{ge}
		In the gas phase	
K	434	2.838	0.704 (H→L)
E	409	3.034	0.759 (H→L)
	322	3.847	0.131 (H→L+1)
		In cyclohexane	
K	459	2.702	0.882 (H→L)
	328	3.778	0.139 (H→L+1)
E	428	2.898	0.903 (H→L)
	328	3.776	0.155 (H→L+1)
		In ethanol	
K	466	2.662	0.885 (H→L)
	336	3.690	0.132 (H→L+1)
E	435	2.851	0.858 (H→L)
	333	3.720	0.133 (H→L+1)

Table 6-5: Wavelengths (λ_{ge}, nm), Transition Energies (ΔE_{ge}, eV), Oscillator Strengths (f_{ge}) and main electronic transitions of the E and K forms of the compound as calculated at the IEF-PCM/B3LYP/6-311G* level.

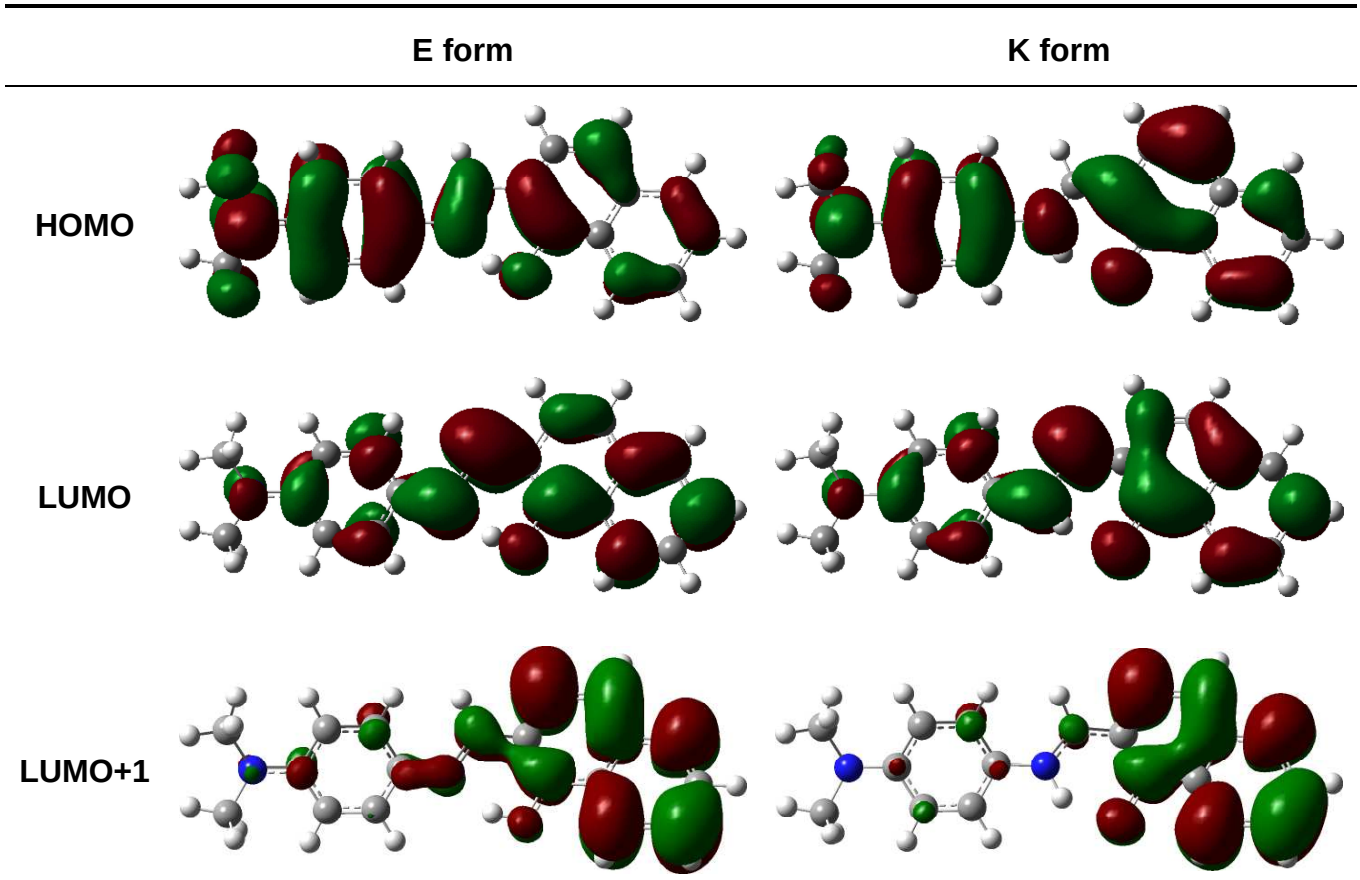

Figure 6-5: Frontier orbitals of the E and K forms, calculated at the IEF-PCM/B3LYP/ 6-311G* level in ethanol.

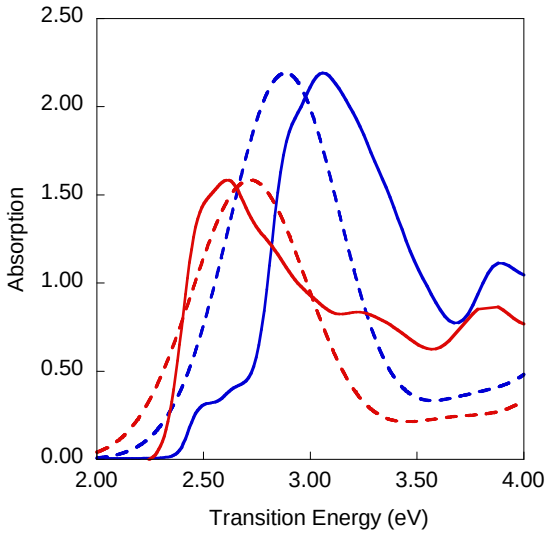

Figure 6-6: Experimental (solid lines) and theoretical absorption spectra (dotted lines) in cyclohexane (blue) and ethanol (red) accounting for the relative populations of the K and E forms deduced from UV-Visible experiments. The calculations have been carried out at the IEF-PCM/TDDFT/B3LYP/6-311G* level and each transition has been enlarged using a Gaussian function having a full width at half-maximum (FWHM) of 0.6 eV. The intensities at the absorption maxima have been adjusted to coincide in the experimental and simulated spectra.

6.5. Second-order nonlinear optical properties

6.5.1. Polarized HRS experiments

The macroscopic β responses were first obtained. The solvent and solute contributions to the second-harmonic intensity, as well as the estimated macroscopic $\langle \beta_{ZZZ}^2 \rangle$ responses due to the solute, are reported in Table 6-6. In pure cyclohexane, the $\langle \beta_{ZZZ}^2 \rangle$ values are significantly smaller than in solvents containing ethanol. In cyclohexane/ethanol mixtures, the $\langle \beta_{ZZZ}^2 \rangle$ contribution of the solute increases with the ethanol proportion.

%EtOH	$Gf_L^2 \langle (\beta_{ZZZ}^{solv})^2 \rangle$	$Gf_L^2 \langle (\beta_{ZZZ}^{chr})^2 \rangle 10^{-6}$	$\langle (\beta_{ZZZ}^{chr})^2 \rangle 10^{-6}$
0	0	0.198 ± 0.003	10.71 ± 0.17
30	3.69 ± 0.56	1.086 ± 0.008	52.60 ± 0.40
70	7.85 ± 0.82	1.358 ± 0.012	72.12 ± 0.64
100	10.03 ± 1.52	1.372 ± 0.028	80.67 ± 1.65

Table 6-6: Solvent and solute contributions to the scattered light intensity, and macroscopic first hyperpolarizability of the solute measured from HRS experiments. All values are in a.u.[2].

By procedure detailed in paragraph 3.3, the molecular components of the β tensor were then estimated. The parameter R defined as $R = \beta_{zxx}/\beta_{zzz}$ Is evaluated for every solvent mixture (Table 6-7). The major (β_{zzz}) and minor (β_{zxx}) components of the solute were further deduced and are given in Table 6-7. In every solvent, the β_{zzz} components are 1 order of magnitude larger than the β_{xzz} component, with an opposite sign. These results warrant the validity of our previous assumption of the so-called Kleinman condition that states that $\beta_{zxx} = \beta_{xxz}$ since off-diagonal components are indeed weak with respect to the longitudinal one, which is actually enhanced by pre-resonance effects. In addition, note that these experimental values do not correspond to the properties of individual molecules, in either the E or K form. Indeed, since the two forms of the compound are present in every solution, these values represent molecular properties weighted by their compositions.

Finally, depolarization ratios, as well as HRS responses, are also reported in Table 6-7 (see also Figure 6-7). As shown by the large changes in the DR values, solvent effects have a significant impact on the symmetry of the NLO-phore. In particular, it is noteworthy that DR is smaller in solvent mixtures than in pure cyclohexane or ethanol solvents. Note however that the DR value measured in cyclohexane must be considered with caution, since the HRS intensity detected in this solvent is very weak compared to what is observed in the other solvents. Hence,

the experimental error is likely larger than the value reported in Table 6-7, which only includes the errors due to the fitting procedures.

% EtOH	R	β_{zzz}	β_{zxx}	β_{HRS}	DR
0	- 0.065 ± 0.012	13683 ± 476	-888 ± 145	5526 ± 37	4.39 ± 0.11
30	- 0.161 ± 0.016	29804 ± 1439	-4790 ± 564	11764 ± 63	3.55 ± 0.13
70	- 0.152 ± 0.009	34787 ± 996	-5298 ± 370	13775 ± 64	3.62 ± 0.07
100	- 0.083 ± 0.009	35688 ± 1112	-2959 ± 316	14334 ± 121	4.22 ± 0.08

Table 6-7: Longitudinal (β_{zzz}) and transverse (β_{zxx}) molecular first hyperpolarizability components (a.u.) of the solute measured from HRS experiments. Since the two forms of solute are present in solution, these values represent an average over the solute composition.

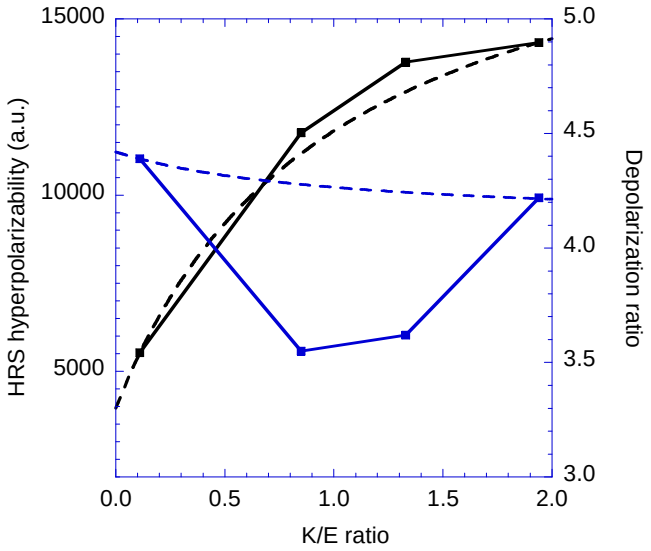

Figure 6-7: Depolarization ratio (blue plain line) and HRS hyperpolarizability (black plain line) measured for solutions with various K/E ratios. Dotted lines are obtained assuming that the HRS hyperpolarizability and DR of the individual tautomers do not depend on solvent.

6.5.2. Theoretical results

The static and dynamic (λ = 1064 nm) values of $\langle\beta^2_{ZZZ}\rangle^{1/2}$, $\langle\beta^2_{ZXX}\rangle^{1/2}$, and β_{HRS} as well as the depolarization ratios of the K and E forms were calculated for the isolated molecules and for the two solvents (Table 6-8), at both the HF/6-311+G* and MP2/6-31G* levels. The major (β_{zzz}) and minor (β_{zxx}) molecular components are reported in Table 6-9. At the CPHF/6-311+G* level in the gas phase, β_{HRS}(E) is larger than β_{HRS}(K), with a β_{HRS}(K)/β_{HRS}(E) ratio of 0.83. Both frequency dispersion

and solvent effects significantly enhance the HRS hyperpolarizabilities of the two forms but these effects have a weak impact on the β contrast, which remains close to 0.9.

When electron correlation at the MP2 level is accounted for, the static hyperpolarizability of both the E and K forms increases compared to the HF values, but the enhancement is larger for K than for E, leading to an inversion of the relative magnitude of the hyperpolarizability of the two forms. Such an inversion in the $\beta_{HRS}(K)/\beta_{HRS}(E)$ ratios between HF and MP2 has already been observed for other anil derivatives [32] (See Table 5-6 in chapter 5). Thus, both in the gas phase and in solvent, the $\beta_{HRS}(K)/\beta_{HRS}(E)$ contrast calculated at that MP2 level turns out to be close to 2. Accounting for frequency dispersion effects via multiplicative scheme increases further the $\beta_{HRS}(K)$ and $\beta_{HRS}(E)$ values without changing significantly the $\beta_{HRS}(K)/\beta_{HRS}(E)$ contrast.

	E form				**K form**				$\frac{\beta^K_{HRS}}{\beta^E_{HRS}}$
	$\langle\beta^2_{ZZZ}\rangle^{1/2}$	$\langle\beta^2_{ZXX}\rangle^{1/2}$	β_{HRS}	DR	$\langle\beta^2_{ZZZ}\rangle^{1/2}$	$\langle\beta^2_{ZXX}\rangle^{1/2}$	β_{HRS}	DR	
				HF/6-311+G*					
λ = ∞ / vacuo	774	342	847	5.13	643	277	700	5.39	0.83
λ = 1064nm / vacuo	1337	601	1466	4.95	1144	514	1254	4.95	0.86
λ = ∞ / C_6H_{12}	1066	472	1166	5.10	899	393	982	5.23	0.84
λ =1064nm / C_6H_{12}	1902	857	2087	4.93	1660	757	1824	4.81	0.87
λ = ∞ / EtOH	1497	669	1639	5.01	1272	588	1401	4.67	0.85
λ =1064nm / EtOH	1987	894	2179	4.93	1885	841	2064	5.03	0.95
				MP2/6-31G*					
λ = ∞ / vacuo	971	455	1072	4.56	1997	866	2177	5.32	2.02
λ = ∞ / C_6H_{12}	1448	675	1598	4.60	2881	1243	3137	5.37	1.96
λ = ∞ / EtOH	2205	1028	2433	4.60	4171	1784	4536	5.47	1.86
				From multiplicative scheme					
λ =1064nm / vacuo	1677	800	1855	4.40	3553	1607	3900	4.89	2.10
λ =1064nm / C_6H_{12}	1155	530	2860	4.74	2264	950	5827	5.67	2.04
λ =1064nm / EtOH	3934	1867	3235	4.45	7702	3436	6683	5.00	2.07

Table 6-8: Macroscopic β-responses, as well as first HRS hyperpolarizabilities , and depolarization ratios for the E and K forms of the compound calculated using various theoretical approximations, in vacuo and in solvent, in the static limit (λ = ∞) and for an incident wavelength of 1064 nm. All β values are given in atomic units.

	E form		K form	
	β_{zzz}	β_{zxx}	β_{zzz}	β_{zxx}
			HF/6-311+G*	
$\lambda = \infty$ / vacuo	-1938	-325	-1384	-459
λ = 1064nm / vacuo	-3427	-434	-2673	-560
$\lambda = \infty$ / C_6H_{12}	-2656	-474	-1885	-688
λ =1064nm / C_6H_{12}	-4863	-638	-3825	-859
$\lambda = \infty$ / EtOH	-3665	-788	-2386	-1188
λ =1064nm / EtOH	-5112	-597	-4485	-760
			MP2/6-31G*	
$\lambda = \infty$ / vacuo	-2552	-360	-5134	-280
$\lambda = \infty$ / C_6H_{12}	-3802	-530	-7364	-466
$\lambda = \infty$ / EtOH	-5758	-877	-10500	-935

Table 6-9: Longitudinal (β_{zzz}) and transverse (β_{zxx}) components (a. u.) of the first hyperpolarizability for the E and K forms of the compound, calculated using various theoretical levels, in vacuo and in solvent, in the static limit ($\lambda = \infty$) and for an incident wavelength of 1064 nm.

6.5.3. Discussion

To account for the equilibrium between the E and K forms in solution, we had to generalize Equation (3-10) as follows:

$$I_{VV}^{2\omega} \propto \left[\left\langle\beta_{ZZZ}^2(\text{solv})\right\rangle C_{solv} + \left\{\left\langle\beta_{ZZZ}^2(\text{E})\right\rangle \times x + \left\langle\beta_{ZZZ}^2(\text{K})\right\rangle \times (1-x)\right\} C_{chr}\right]_{\omega}^2 10^{-\left[xA_{2\omega}^{E} + (1-x)A_{2\omega}^{K}\right]C_{chr}} \qquad (6\text{-}1)$$

where $\left\langle\beta_{ZZZ}^2(\text{E})\right\rangle$ and $\left\langle\beta_{ZZZ}^2(\text{K})\right\rangle$ are the macroscopic averages of the β tensors of the E and K forms, respectively, and x is the proportion of E form in solution. However, it is not possible to extract from the HRS experiments the individual contributions of the tautomeric forms to $I_{VV}^{2\omega}$, since they do not only depend on the K/E ratio, but also on the nature of the solvent. Indeed, as already mentioned, the solvent has multiple effects on the NLO responses of the solute. It impacts the geometry and electronic properties of the solute through intermolecular interactions, it modulates the electrical field that is felt by the solute molecules, and it dictates the relative K/E proportion in the solution.

One way to disentangle these various effects consists in assuming that the individual HRS hyperpolarizabilities of the tautomeric forms are only impacted by the equilibrium displacement, and not by the nature of the solvent. In this case, the solvent-independent β_{HRS}(E) and β_{HRS}(K) values can be extracted from the experiments performed in pure solvents, by considering that the measured HRS

response is the sum of the individual responses of the two forms, weighted by their populations: it gives β_{HRS}(E) = 3952 a.u. and β_{HRS}(K) = 19688 a.u.. The evolution of the HRS response of the solution, estimated using the solvent-independent β_{HRS}(E) and β_{HRS}(K) values, is reported in Figure 6-7 with respect to the K/E ratio. It is noticeable that deviations from the experimental points do not exceed 6%, which indicates that the variation of the HRS hyperpolarizability of the solution is mainly driven by the equilibrium displacement. The same conclusion may be reached in light of the theoretical calculations.

The theoretical β_{HRS} responses of the solute in pure solvents can be estimated by weighting the calculated β_{HRS} values of the tautomeric forms by their relative populations deduced from UV-Visible measurements. The so-obtained values are 3157 a.u. and 5511 a.u. in cyclohexane and ethanol, respectively. This corresponds to a solvent-induced enhancement of 1.75, which, although underestimated, is in good agreement with the measured value of 2.8. The solvent-induced equilibrium displacement toward the K-tautomer is thus the main origin of the exaltation of the HRS response when going from cyclohexane to ethanol. This enhancement might also be partly related to the formation of J-aggregates, which are expected to present smaller β responses. Indeed, the formation of these aggregates might be favored in cyclohexane with respect to ethanol, where stronger solute-solvent interactions facilitate dissolution. Although no evidence for aggregation has been observed at room temperature in these systems [33], this assumption is supported by i) the very weak HRS intensity detected in cyclohexane and ii) the relative amplitudes of the dipole-dipole interactions and of the solute-solvent energies (Table 6-4). The stabilization energy due to dipolar interactions was estimated as $E = -2\mu^2/R^3$ where μ is the dipole moment of the chromophores and R the distance between their centers of mass. Considering an intermolecular distance of 4 Å typical of a π-stacking, and the dipole moment values calculated at the B3LYP level (Table 6-4), the dipole-dipole interaction energy for a pair of molecules in their E form is equal to –9.87 kcal/mol, while the total IEF-PCM/B3LYP/6-311G* solute-solvent energy is equal to –7.22 kcal/mol, so that J-aggregation would be favored in cyclohexane. The analogous calculations for the ethanol solution lead to –13.28 kcal/mol for dipole-dipole interactions and to –23.38 kcal/mol for the total solute-solvent energy. In this latter case, the solvation of the individual chromophores would be favored. Nevertheless, it is worth stressing that the variation of the harmonic light intensity with the polarization of the incident light measured in cyclohexane remains characteristic of a dipolar solute, which is in contradiction with the aggregation hypothesis.

Finally, using the same approach for DR, the solvent-independent DR(E) and DR(K) values extracted from experimental data obtained in pure solvents are equal to 4.39 and 4.22, respectively. Contrary to β_{HRS}, the evolution of the DR of the

solution estimated using the assumption that the DR values of the two tautomers are not impacted by the nature of the solvent widely differs from the experimental measurements (see Figure 6-7). Varying the cyclohexane/ethanol ratio in the solvent mixture has thus a strong impact on the DR values of the tautomeric forms, while their HRS hyperpolarizabilities are less directly affected by the nature of the solvent. The reason why the DR values are smaller in solvent mixtures than in pure solvent remains an open question. Using the theoretical results and weighting the calculated depolarization ratios of the tautomeric forms by their relative populations leads to DR values of 4.83 and 4.81 in cyclohexane and ethanol, respectively. This last result is consistent with the experiments carried out in pure solvents, which provide similar DR values for the two solutions.

Theoretical results are thus in good agreement with experiments carried out in pure solvents, as they qualitatively reproduce the enhancement of the HRS hyperpolarizability and the consistency of the DR when going from cyclohexane to ethanol. The remaining discrepancies between calculations and measurements likely originate from the fact that the solute/solvent interactions are approximated within the continuum solvation model, where weak intermolecular bonds are not treated explicitly. Moreover, as previously reported by Wortmann and Bishop [34], the macroscopic electrical field applied to the medium is different from the local field felt by the solute molecule in the solution. Thus, though the interactions between the solute and solvent are incorporated in the calculations, the discrepancies between the experimental and theoretical results might also originate from the approximate local field factors. Another source of discrepancy might originate from the conformational flexibility of the anil derivatives and in particular from the rotational freedom of the (dimethylamino)-phenyl group. However, as shown in Table 6-10, the amplitudes of the β_{HRS} variations upon rotations by +10° and -10° are sma ll and cancel each other since the two directions of rotation have the same probability.

	E		**K**	
	$\lambda = \infty$	**λ = 1064 nm**	**$\lambda = \infty$**	**λ = 1064 nm**
θ	847	1466	700	1254
$\theta + 10°$	976 (+15.2%)	1703 (+16.2%)	761 (+8.7%)	1404 (+12.0%)
$\theta - 10°$	802 (-5.3%)	1172 (-20.0%)	708 (+1.1%)	1035 (-17.5%)

Table 6-10: First HRS hyperpolarizability (a.u.) for the E and K forms of the compound when varying the dihedral angle $\theta = C_{19}\text{-}C_{17}\text{-}N\text{-}C_{14}$ by ± 10° with respect to its optimized value (the optimized values for θ calculated at the B3LYP/ 6-311G* level are equal to 152.9° and 164.5° for the E and K forms, respectively. For the E (K) form, the changes of energy, as estimated at the B3LYP/6-311G* level, amount to 0.19 and 0.22 kcal/mol (0.13 and 0.10 kcal/mol) for negative and positive rotations), as calculated at the HF/6-311+G* level in vacuo, in the static limit ($\lambda = \infty$) and for an incident wavelength of 1064 nm.

6.6. Conclusions

In this chapter, HRS experiments and *ab initio* calculations have been combined to investigate the solvent effects on the second-order NLO responses of a N-(2-hydroxynaphtylidene)-aniline derivative, that commutes between an enol and a keto form. Therefore, in addition to changing the properties of the E and K forms, the solvent modifies the keto-enol equilibrium, resulting in a more complex dependence of the global NLO response with respect to the solvent. In this investigation, the solvent effects were triggered by using different binary mixtures of ethanol and cyclohexane. We show that increasing the polarity of the solvent, by increasing progressively the ethanol ratio in cyclohexane/ethanol mixtures, leads to the displacement of the tautomeric equilibrium toward the K form, which gives rise to a bathochromic shift and large enhancement of the HRS hyperpolarizability. Quantum chemical calculations, performed in pure solvents using the IEF-PCM, fairly reproduce the bathochromic shift of the main absorption band, as well as the exaltation of the first hyperpolarizability along the E⇆K reaction. This also demonstrates that pure solvent effects on the E and K forms properties are not negligible and add to the effects from the displaced equilibrium. Indeed, when switching from cyclohexane to ethanol solutions, at the MP2 level, β_{HRS} of the E and K forms increase by 52% and 45%, respectively. This chapter also highlights the difficulties in conciliating HRS experiments performed in solvents exhibiting specific interactions with the solute, possibly favoring in some cases J-aggregates, with computational results.

6.7. References

[1] M. Stähelin, D. M. Burland, and J. E. Rice, *Chem. Phys. Lett.*, **191**, 245 (1992).

[2] P. Kaatz, E. A. Donley, and D. P. Shelton, *J. Chem. Phys.*, **108**, 849 (1998).

[3] D. P. Shelton, *J. Chem. Phys.*, **130**, 114501 (2009).

[4] D. M. Bishop, *Int. Rev. Phys. Chem.*, **13**, 21 (1994).

[5] B. Champagne and D. M. Bishop, *Adv. Chem. Phys.*, **126**, 41 (2003).

[6] E. Buncel and S. Rajagopal, *Acc. Chem. Res.*, **23**, 226 (1990).

[7] C. Reichardt, *Solvent and Solvent Effects in Organic Chemistry*, VCH, Weinheim (1990).

[8] J. Yu and M. C. Zerner, *J. Chem. Phys.*, **100**, 7487 (1994).

[9] K. V. Mikkelsen, Y. Luo, H. Ågren, and P. Jørgensen, *J. Chem. Phys.*, **100**, 8240 (1994).

[10] S. Di Bella, T. J. Marks, and M. A. Ratner, *J. Am. Chem. Soc.*, **116**, 4440 (1994).

[11] G. Chen, D. Lu, and W. A. Goddard, *J. Chem. Phys.*, **101**, 5860 (1994).

[12] W. Bartkowiak, R. Zalesny, W. Niewodniczanski, and J. Leszcynski, *J. Phys. Chem. A*, **105**, 10702 (2001).

[13] P. C. Ray and J. Leszcynski, *Chem. Phys. Lett.*, **399**, 162 (2004).

[14] J. Kongsted, A. Anders, K. V. Mikkelsen, and O. Christiansen, *J. Chem. Phys.*, **120**, 3787 (2004).

[15] L. Jensen and P. T. van Duijnen, *J. Chem. Phys.*, **123**, 074307 (2005).

[16] C. B. Nielsen, O. Christiansen, K. V. Mikkelsen, and J. Kongsted, *J. Chem. Phys.*, **126**, 154112 (2007).

[17] P. Macak, P. Norman, Y. Luo, and H. Ågren, *J. Chem. Phys.*, **112**, 1868 (2000).

[18] R. W. Munn, Y. Luo, P. Macak, and H. Ågren, *J. Chem. Phys.*, **114**, 3105 (2001).

[19] H. Reis, A. Grzybowski, and M. G. Papadopoulos, *J. Phys. Chem. A*, **109**, 10106 (2005).

[20] H. Reis, M. G. Papadopoulos, and A. Grzybowski, *J. Phys. Chem. B*, **110**, 18537 (2006).

[21] H. Ågren, O. Vahtras, H. Koch, P. Jørgensen, and T. Helgaker, *J. Chem. Phys.*, **98**, 6417 (1993).

[22] L. Frediani, H. Ågren, L. Ferrighi, and K. Ruud, *J. Chem. Phys.*, **123**, 144117 (2005).

[23] L. Ferrighi, L. Frediani, C. Cappelli, P. Salek, H. Ågren, T. Helgaker, and K. Ruud, *Chem. Phys. Lett.*, **425**, 267 (**2006**).

[24] L. Antonov, W. M. F. Fabian, D. Nedeltcheva, and F. S. Kamounah, *J. Chem. Soc., Perkin Trans.*, **2**, 1173 (2000).

[25] D. Nedeltcheva and L. Antonov, *J. Phys. Org. Chem.*, **22**, 274 (2008).

[26] W. M. F. Fabian, L. Antonov, D. Nedeltcheva, F. S. Kamounah, and P. J. Taylor, *J. Phys. Chem. A*, **108**, 7603 (2004).

[27] D. Nedeltcheva, F. S. Kamounah, L. Mirolo, K. L. Fromm, and L. Antonov, *Dyes Pigm.*, **83**, 121 (2009).

[28] M. Ziólek, J. Kubicki, A. Maciejewski, R. Naskręcki, and A. Grabowska, *J. Chem. Phys*., **124**, 124518 (2006).

[29] L. Antonov and D. Nedeltcheva, *Chem. Soc. Rev.*, **29**, 217 (2000).

[30] L. Antonov and V. Petrov, *Anal. Bioanal. Chem.*, **374**, 1312 (2002).

[31] T. Verbiest, K. Clays, and V. Rodriguez, *Second-order nonlinear optical characterizations techniques: an introduction*, CRC Press, New York, (2009).

[32] M. Guillaume, B. Champagne, N. Markova, V. Enchev, and F. Castet, *J. Phys. Chem. A*, **111**, 9914 (2007).

[33] D. Nedeltcheva, L. Antonov, A. Lycka, B. Damyanova, and S. Popov, *Curr. Org. Chem.*, **13**, 217 (2009).

[34] R. Wortmann and D. M. Bishop, *J. Chem. Phys*., **108**, 1001 (1998).

Theoretical investigation of the dynamic first hyperpolarizability of DHA–VHF molecular switches

A. Plaquet, B. Champagne, F. Castet, L. Ducasse, E. Bogdan, V. Rodriguez, and J.-L. Pozzo, *New J. Chem.*, **33**, 1349 (2009).

7. Theoretical investigation of the dynamic first hyperpolarizability of DHA–VHF molecular switches

7.1. Introduction

We have investigated the dihydroazulene (DHA)-vinylheptafulvene (VHF) equilibrium whose synthesis and some experimental characterizations have been reported a few years ago by Daub and co-workers [1-6] and presents an interesting potential to display efficient NLO switching properties. In fact, the DHA-VHF system can commute between three forms: the DHA species that can undergo a photo-opening of the five-membered ring to form the VHF form in *cis* configuration, which can further be thermally converted into the VHF-*trans* form (Figure 7-1). When going in the opposite direction, all transformations are thermally induced. It has been noticed that the DHA to VHF transformation is usually accompanied by a change or appearance of color depending on the substituent.

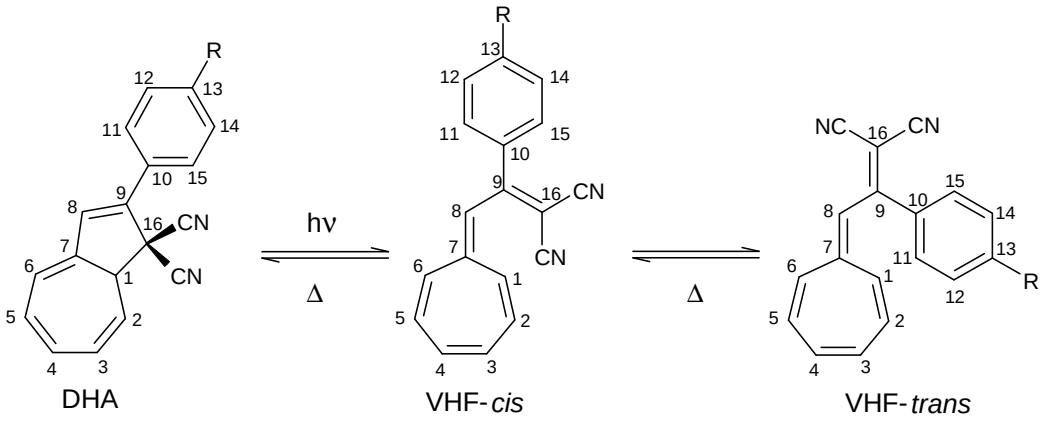

Figure 7-1: Photo and thermochromic equilibrium for the DHA-VHF system.

In general, the DHA compounds are thermally stable, exhibit a photochromic behaviour at room temperature, display absorption bands in the UV domain, and show fluorescence in the visible region. The reaction from the DHA to the VHF forms, having at room temperature a rather high quantum yield with values between 0.1 and 0.6, is accompanied by a large shift of the absorption band. Then, the VHF open form is metastable, non fluorescent, and shows a high solvent dependency of the S_0-S_1 absorption transition, compared to DHA [1]. The activation barrier for the back reaction ranges between 75 and 88 kJ mol^{-1} [1], as a function of the substituent as well as of the polarity of the solvent: the more polar the solvent is, the faster the rearrangement is. The high quantum yield for the photochromic in DHA $\rightarrow$ VHF reaction, as well as the lack of fluorescence or photochemical back-reaction from

VHF has been rationalized by Boggio-Pasqua *et al.* by means of complete active space-self consistent field calculations [7].

During the photochemical ring opening of the DHA form, the electronic structure of the π-system changes considerably. Indeed, unlike in the DHA form, the cyano groups of the VHF form are conjugated with the π-system. Since this rearrangement is accompanied with a lowering of the transition energies, one can expect that it will also be accompanied by substantial modifications of the first hyperpolarizability. It is also expected that the substituent R on the phenyl ring will play an important role on the first hyperpolarizability and on its contrast. In this chapter, we have described and rationalized these effects for substituents R = H, CH_3, NH_2, and NO_2 by means of quantum chemical calculations.

7.2. Molecular structures

A selection of remarkable geometrical parameters of the DHA, VHF-*cis*, and VHF-*trans* forms calculated at the IEF-PCM/B3LYP/6-311G* level of approximation (solvent = acetonitrile) are listed in Table 7-1. The charges on the different fragments of the three forms obtained within Mulliken population analysis are reported in Table 7-2. As expected from the chemical formulas, going from DHA to VHF-*cis* is accompanied by a reversal of the single and double CC bonds of the seven-membered ring whereas the changes in the phenyl ring are equal or smaller than 0.01 Å. The BLA in the central part of the molecule, defined as $BLA_1 = (d_{C7-C8}+d_{C9-C16}-2d_{C8-C9})/2$ and $BLA_2 = (d_{C7-C8}+d_{C9-C10}-2d_{C8-C9})/2$, decreases substantially (from 0.14 Å to -0.018/0.004 Å for BLA_1 and from 0.097/0.085 Å to 0.024/0.058 Å for BLA_2), indicating that the electron delocalization is better in VHF-*cis* than in DHA. Going from the *cis* to the *trans* form, the bond length values change little, though BLA_2 decreases by 0.002 to 0.015 Å. The largest variations are attributed to the C_9-C_{10} bond, which decreases by about 0.01 Å. This shortening of the C_9-C_{10} bond is accompanied by a lengthening of the C_9-C_{16} bond and by an increased charge transfer between the substituent R and the $C(CN)_2$ acceptor groups, in particular when R = NH_2. Moreover, the optimized DHA geometry is essentially planar with the C_7-C_8-C_9-C_{16} and C_7-C_8-C_9-C_{10} torsion angles close to 0° and 180° while the C_8-C_9-C_{10}-C_{11} torsion angle determining the position of the phenyl ring amounts to approximately 15°. Upon transition to the VHF-*cis* form, planarity is partially lost with departure from planarity of 30° (C_7-C_8-C_9-C_{16} and C_7-C_8-C_9-C_{10},) and 60° (C_8-C_9-C_{10}-C_{11}). In such a conformation, the phenyl ring is weakly conjugated with the rest of the system. Finally, the *cis-trans* isomerization restores a part of planarity. In particular, in the R = NH_2 case, the smaller C_8-C_9-C_{10}-C_{11} torsion angle is consistent with a partial equalization of the C_9-C_{10} and C_9-C_{16} bond lengths describing a better electron delocalization from the donor to the acceptor groups.

Changing the R substituent from the NH_2 donor to the NO_2 acceptor groups has a limited impact on the geometrical parameters of the DHA form. The situation is different for the VHF forms for which one can notice variations of the C_7-C_8, C_8-C_9, and C_9-C_{10} bond lengths by 0.01-0.02 Å, leading to a (slightly) negative BLA for R = NH_2. These differences evolve monotonically with the donor or acceptor strength of the R group. Note that, changing the substituent also leads to variations of the bond lengths in the phenyl ring, though small, which describe an increased quinoid character for strong donor and acceptor groups.

	R = H	**R = CH_3**	**R = NH_2**	**R = NO_2**
			DHA	
C_7-C_8	1.436	1.435	1.433	1.434
C_8-C_9	1.354	1.354	1.359	1.357
C_9-C_{16}	1.553	1.554	1.554	1.550
C_9-C_{10}	1.465	1.464	1.455	1.461
C_8-C_9-C_{16}	108.4	108.6	108.1	108.5
C_7-C_8-C_9-C_{16}	-5.8	-5.0	-5.7	-6.0
C_7-C_8-C_9-C_{10}	177.5	177.3	178.0	178.4
C_8-C_9-C_{10}-C_{11}	-13.8	-11.2	-11.0	-17.0
BLA_1	0.141	0.141	0.135	0.135
BLA_2	0.097	0.096	0.085	0.091
			VHF-*cis*	
C_7-C_8	1.406	1.406	1.401	1.413
C_8-C_9	1.413	1.412	1.421	1.405
C_9-C_{16}	1.405	1.406	1.407	1.405
C_9-C_{10}	1.498	1.497	1.488	1.503
C_8-C_9-C_{16}	126.7	126.7	125.3	128.3
C_7-C_8-C_9-C_{16}	-29.4	-28.7	-31.8	-25.9
C_7-C_8-C_9-C_{10}	154.4	155.2	151.6	158.7
C_8-C_9-C_{10}-C_{11}	62.4	63.4	51.1	87.5
BLA_1	-0.008	-0.006	-0.018	0.004
BLA_2	0.039	0.039	0.024	0.058
			VHF-*trans*	
C_7-C_8	1.407	1.406	1.401	1.409
C_8-C_9	1.412	1.413	1.422	1.408
C_9-C_{16}	1.408	1.409	1.412	1.408
C_9-C_{10}	1.491	1.488	1.473	1.493
C_8-C_9-C_{16}	120.1	119.9	119.0	120.7
C_7-C_8-C_9-C_{16}	-167.3	-165.2	-158.8	-168.9
C_7-C_8-C_9-C_{10}	17.0	19.2	25.3	16.4
C_8-C_9-C_{10}-C_{11}	57.8	54.9	44.5	58.8
BLA_1	-0.005	-0.005	-0.016	0.001
BLA_2	0.037	0.034	0.015	0.043

Table 7-1: Selection of distances (Å) and angles (°) for the DHA, VHF-cis, and VHF-trans forms, as calculated at the IEF-PCM/B3LYP/6-311G* level of approximation. $BLA_1 = (d_{C7-C8}+d_{C9-C16}-2d_{C8-C9})/2$ and $BLA_2 = (d_{C7-C8}+d_{C9-C10}-2d_{C8-C9})/2$. Atom labels refer to Figure 7-1.

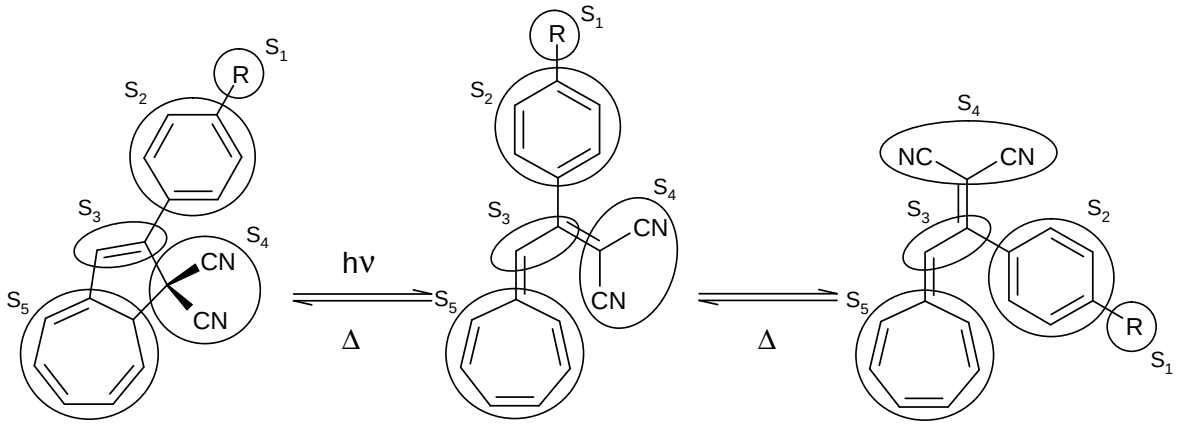

		R = H	R = CH_3	R = NH_2	R = NO_2
DHA	**S_1**	+0.234	+0.011	-0.105	-0.446
	S_2	-0.106	+0.134	+0.321	+0.492
	S_3	+0.108	+0.099	+0.081	+0.126
	S_4	-0.401	-0.398	-0.409	-0.393
	S_5	+0.165	+0.152	+0.112	+0.221
VHF-*cis*	**S_1**	+0.231	+0.005	-0.114	-0.429
	S_2	-0.206	+0.026	+0.212	+0.385
	S_3	+0.030	+0.028	+0.031	+0.046
	S_4	-0.516	-0.522	-0.543	-0.514
	S_5	+0.462	+0.464	+0.414	+0.512
VHF-*trans*	**S_1**	+0.234	+0.010	-0.102	-0.424
	S_2	-0.250	-0.009	+0.191	+0.349
	S_3	+0.062	+0.065	+0.081	+0.072
	S_4	-0.527	-0.537	-0.590	-0.503
	S_5	+0.482	+0.472	+0.418	+0.507

Table 7-2: Mulliken population analysis for the remarkable fragments (S_1-S_5) of the DHA, VHF-*cis*, and VHF-*trans* forms as determined at the IEF-PCM/B3LYP/6-311G* level of approximation.

Mulliken population analysis (Table 7-2) also shows i) the systematic decrease of the electronic density on the seven-membered ring when going from DHA to VHF, associated with π-electron delocalization in the ring and aromaticity, ii) the transfer of most of this charge on the $C(CN)_2$ and phenyl moieties, and iii) the mesomer D/A effects of the NH_2/NO_2 groups on the seven-membered ring of DHA and VHF forms when compared to R = H and R = CH_3.

Table 7-3 lists the relative energies as well as the dipole moments of the different forms as a function of the nature of the R substituent. The energy of the VHF-*cis* form is 31-33 kJ mol^{-1} higher than in DHA and it depends little on the nature of the substituent. When switching from the *cis* to the *trans* configuration, the VHF form is stabilized so that, in average, it is 13-14 kJ mol^{-1} higher in energy than the reference DHA form. However, the nature of the substituent has an impact on the energy difference, which goes down to 9 kJ mol^{-1} in the case of R = NH_2 whereas it attains 19 kJ mol^{-1} for R = NO_2. These variations of E(VHF-*trans*) – E(DHA) with the nature of R results from several effects including the increase of planarity from R = NO_2 to R = NH_2 and the reduction in BLA_2. Note that similar reasons could be raised for the variations of E(VHF-*cis*) – E(DHA) with the nature of R but that in that case, the larger dipole moment of the R = NO_2 compound has a supplementary stabilizing effect. If the solvent effects are not taken into account, the relative energies of the VHF forms are much larger, by about 16 kJ mol^{-1}, and this difference can partly be taken into account by the increase in dipole moment between the DHA and VHF forms.

	R = H	**R = CH_3**	**R = NH_2**	**R = NO_2**
E(VHF-*cis*) – E(DHA)	33.1 (48.1)	33.1 (48.3)	33.1 (49.1)	30.9 (48.3)
E(VHF-*trans*) – E(DHA)	13.1 (30.0)	12.8 (29.6)	9.3 (27.1)	18.6 (33.1)
μ(DHA)	6.0	5.9	6.4	9.6
μ(VHF-*cis*)	11.6	11.7	10.2	14.8
μ(VHF-*trans*)	15.7	15.6	15.7	15.4

Table 7-3: Relative energies (kJ.mol^{-1}) between the three forms and dipole moments (Debye) as determined at the MP2/6-31G* level of approximation taking into account the effects of the solvent with the IEF-PCM scheme (solvent = acetonitrile). The values in parentheses were obtained without accounting for the effects of the solvent in both geometry optimization and energy calculation.

7.3. Nonlinear optical properties

Table 7-4 reports the first hyperpolarizabilities and the depolarization ratios evaluated at different levels of approximation *i.e.* TDHF/6-311+G* in *vacuo* and in acetonitrile, MP2/6-31G* in acetonitrile, and dynamic MP2 values estimated using the multiplicative scheme.

It is interesting to consider first the values calculated at the highest level of approximation, *i.e.* the $\beta_{MP2}^{CH_3CN}(-2\omega;\omega,\omega)$ values. In the case of the DHA form, $\beta_{MP2}^{CH_3CN}(-2\omega;\omega,\omega)$ increases by a factor of 5 when going from R = H to R = Me. This

enhancement is accompanied by a rotation of the β vector, which aligns itself along the *para* substitution axis of the phenyl ring, as shown in Figure 7-2 in the case of the corresponding static values. $\beta_{MP2}^{CH_3CN}(-2\omega;\omega,\omega)$ is further enhanced when R = NH_2 and R = NO_2, with ratios of 47 and 54 with respect to the R = H case, respectively. Moreover, in both cases, the β vector remains aligned with respect to the *para* axis, though for R = NO_2, it points in the other direction, owing to its acceptor character. The substitution effects on the dipole moment amplitude and orientation are much smaller (Table 7-3), which can be attributed to the dominant role played by the two cyano groups. Thus, the angle between the μ and β vectors remain close to 80° for R = H, Me, and NH_2 whereas for R = NO_2, the angle gets much smaller and the μ amplitude increases by about 50%.

The VHF-*cis* form presents a $\beta_{MP2}^{CH_3CN}(-2\omega;\omega,\omega)$ value for R = H, which is about 40 times larger than in the DHA form. On the other hand, changing the R group has a much more limited impact: with respect to R = H, $\beta_{MP2}^{CH_3CN}(-2\omega;\omega,\omega)$ decreases by 9% and 50% for R = Me and NO_2, respectively whereas it increases by 75% in the case of R = NH_2. This attributes some acceptor character to the seven-membered ring and explains the enhancement of β when it is conjugated to the amino group. Moreover, the nature of the substituent has a limited impact on the θ angle and on the orientation of the β vector with respect to the molecular frame. The situation presents some similarities for the VHF-*trans* form. Indeed, going from R = H to R = Me, NH_2, and NO_2, $\beta_{MP2}^{CH_3CN}(-2\omega;\omega,\omega)$ changes by +14%, +104%, and –8%, respectively, whereas the θ angle remains close to 30-40°, except for R = NO_2. This change in θ is attributed to the rotation of both μ and β vectors with respect to the molecular frame. Qualitatively, these changes of orientations for μ and β are consistent with a donor character for the seven-membered ring, an acceptor character for the $C(CN)_2$ group, and a varying D/A character for –Ph-R as a function of the nature of R.

		DHA		VHF-*cis*		VHF-*trans*	
		β_{HRS}	DR	β_{HRS}	DR	β_{HRS}	DR
R = H	$\beta_{TDHF}^{vacuo}(-2\omega;\omega,\omega)$	258	5.42	1417	2.84	1623	2.39
	$\beta_{TDHF}^{CH3CN}(-2\omega;\omega,\omega)$	229	5.11	1567	1.85	5390	3.50
	$\beta_{MP2}^{CH_3CN}(0;0,0)$	212	3.32	5973	4.55	4393	3.37
	$\beta_{MP2}^{CH_3CN}(-2\omega;\omega,\omega)$	138	-	5160	-	3466	-
R = CH_3	$\beta_{TDHF}^{vacuo}(-2\omega;\omega,\omega)$	743	5.25	1346	2.45	1702	2.13
	$\beta_{TDHF}^{CH3CN}(-2\omega;\omega,\omega)$	869	5.28	1679	1.94	4916	3.08
	$\beta_{MP2}^{CH_3CN}(0;0,0)$	775	4.32	5693	4.34	5087	3.43
	$\beta_{MP2}^{CH_3CN}(-2\omega;\omega,\omega)$	704	-	4706	-	3945	-
R = NH_2	$\beta_{TDHF}^{vacuo}(-2\omega;\omega,\omega)$	2528	4.91	2231	2.17	2093	1.63
	$\beta_{TDHF}^{CH3CN}(-2\omega;\omega,\omega)$	4334	4.92	4091	2.22	4176	1.57
	$\beta_{MP2}^{CH_3CN}(0;0,0)$	6320	4.93	8198	3.12	8292	3.01
	$\beta_{MP2}^{CH_3CN}(-2\omega;\omega,\omega)$	6434	-	9013	-	7055	-
R = NO_2	$\beta_{TDHF}^{vacuo}(-2\omega;\omega,\omega)$	2036	4.34	576	2.27	1920	2.90
	$\beta_{TDHF}^{CH3CN}(-2\omega;\omega,\omega)$	5038	4.59	3331	4.49	7307	3.98
	$\beta_{MP2}^{CH_3CN}(0;0,0)$	5796	5.16	2075	5.09	3625	2.89
	$\beta_{MP2}^{CH_3CN}(-2\omega;\omega,\omega)$	7396	-	2583	-	3190	-

Table 7-4: Hyper Rayleigh scattering quantities (β_{HRS} and DR) of DHA, VHF-*cis*, and VHF-*trans* evaluated at different levels of approximation. Dynamic MP2 values were estimated using multiplicative scheme. All values are given in atomic units.

To address the NLO switching properties of these systems, the β_{HRS}(VHF-*cis*)/β_{HRS}(DHA) and β_{HRS}(VHF-*trans*)/β_{HRS}(DHA) ratios were calculated. For R = H, they amount to 37.4 and 25.1, respectively, as a consequence of the very small first hyperpolarizability of the DHA form. These large contrasts do not originate from resonance effects since similar values are obtained at the static MP2 level of approximation. On the other hand, they account for the increase of π-conjugation upon going from the DHA to either of the two VHF forms, leading to an exaltation of β. When R = Me, the ratios, given in the same order, are 6.7 and 5.6. Then, for the strong donor or acceptor substituents, the ratios get much smaller, owing to the substantial increase of β_{HRS}(DHA): for R = NH_2, β_{HRS}(VHF-*cis*)/β_{HRS}(DHA) = 1.40 and β_{HRS}(VHF-*trans*)/β_{HRS}(DHA) = 1.10 while, for R = NO_2, β_{HRS}(VHF-*cis*)/β_{HRS}(DHA) = 0.35 and β_{HRS}(VHF-*trans*)/β_{HRS}(DHA) = 0.43. On the other hand, the contrast

between the *cis* and *trans* forms amounts to 1.49, 1.19, 1.28, and 0.81 for R = H, Me, NH_2, and NO_2, respectively. As a conclusion, with the exception of R = NH_2 where the ratios are close to 1.0, the three other systems present contrasts of β at least larger than 2.3 between the DHA form and the VHF forms, demonstrating their NLO switching abilities.

The depolarization ratios also evidence modifications upon commuting between the different forms. The VHF-*trans* forms show a DR value around 3.0, quite far from the 1D reference value of 5.0. This demonstrates the non-dipolar character of this form. The DHA forms with the strong D or A groups present a DR value close to 5.0, which is in agreement with a 1D dipolar character. On the other hand, for the VHF-*cis* form, R = NO_2 is associated with a DR close to 5.0 whereas it is close to 3.0 for R = NH_2. The DR value for R = NH_2 is consistent with the three-branch shape of the molecule and the D/A characters of the branches whereas for R = NO_2, the strong acceptor character of the nitro group might overcome these of the seven-membered ring, as suggested by the orientation of the β vector in Figure 7-2.

	DHA	VHF-*cis*	VHF-*trans*
R = H	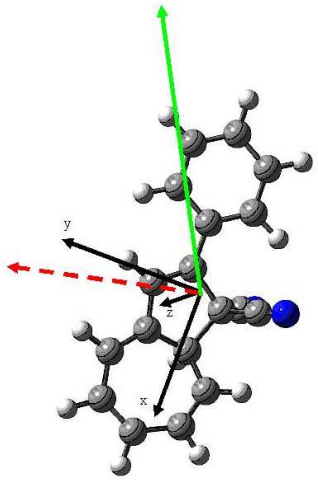	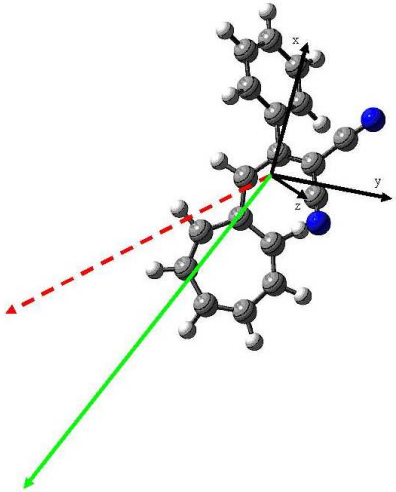	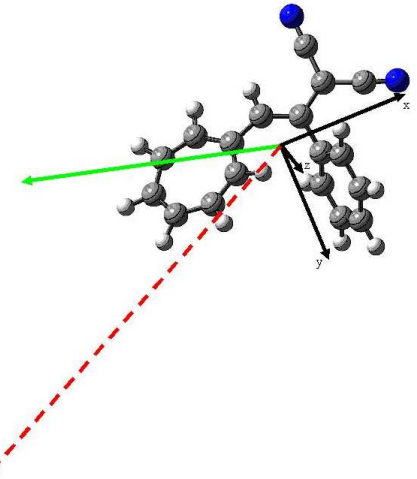
	β/50 θ = 73.5°	β/1000 θ = 30.1°	β/1000 θ = 41.4°
R = CH_3	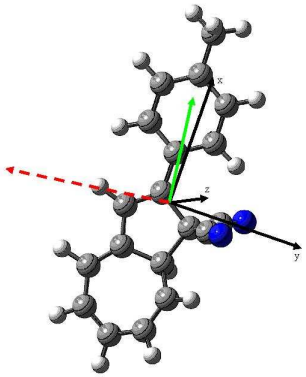	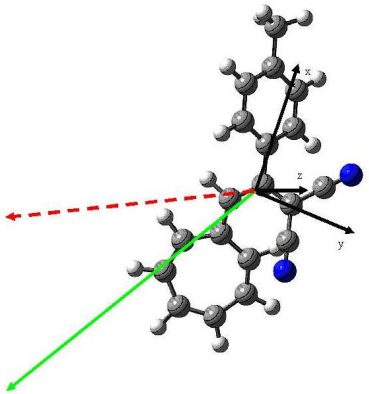	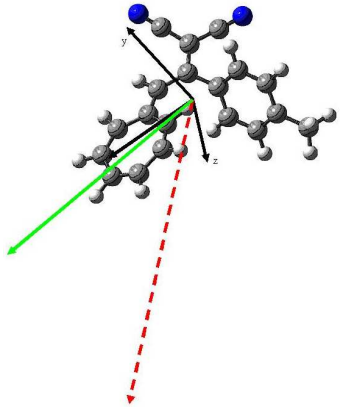
	β/500 θ = 95.6°	β/1000 θ = 30.1°	β/1000 θ = 37.3°

R = NH_2	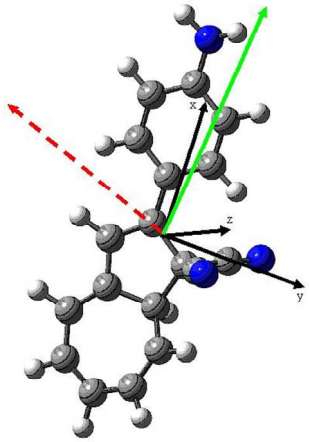	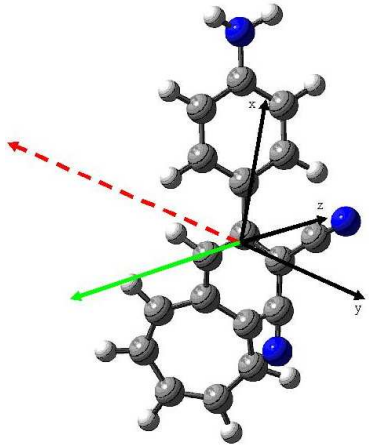	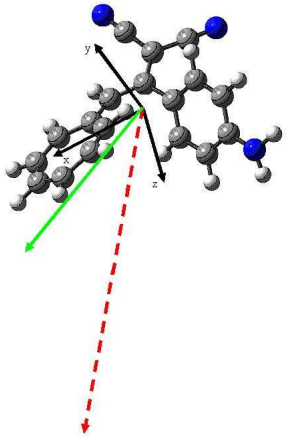
	β/500 θ = 71.1°	β/2000 θ = 26.9°	β/2000 θ = 26.8°
R = NO_2	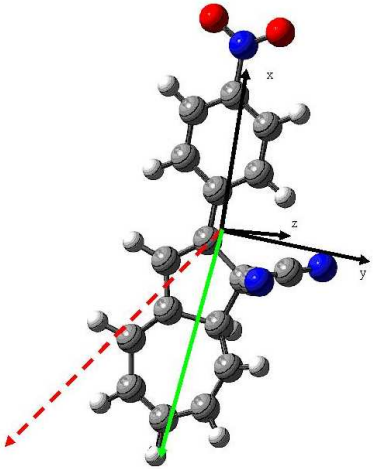	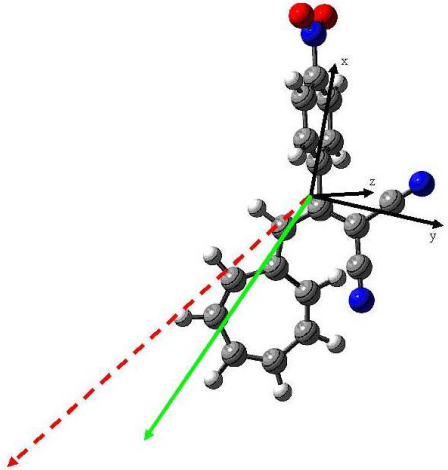	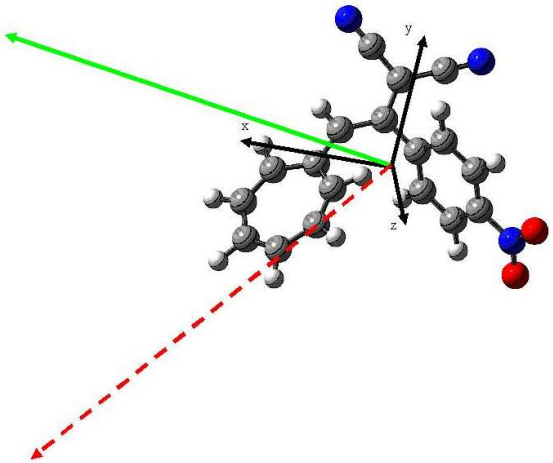
	β/2000 θ = 32.5°	β/500 θ = 23.2°	β/500 θ = 63.3°

Figure 7-2: Sketch of the dipole moment μ (dotted line) and first hyperpolarizability β (plain line) vectors for DHA, VHF-*cis*, and VHF-*trans* determined at the MP2/6-31G* (λ = ∞) level of approximation. θ is the angle (in degrees) between the μ and β vectors.

The data reported in Tables 7-5 and 7-6 enable to assess the effects of frequency dispersion and electron correlation on the HRS first hyperpolarizabilities. In acetonitrile ($\varepsilon_\omega < \varepsilon_0$), the dynamic/static ratios are close to 1.0 and, in several cases, even smaller than 1.0. In fact, these dynamic/static ratios obey the following relationships: H < Me < NH_2 < NO_2 for DHA, H ~ Me < NH_2 < NO_2 for VHF-*cis*, and H ~ Me < NH_2 ~ NO_2 for VHF-*trans*. The impact of electron correlation, as estimated from the MP2/HF ratios, is less systematic within the four substituents and within the three forms. Indeed, its effect ranges from a decrease by a factor of 2.2 to an increase by a factor of 3.3. Such a broad spectrum of MP2/HF ratios should probably draw our attention on the reliability of the multiplicative scheme, which implies similar MP2 and HF values, or rather, since we are comparing systems, similar MP2/HF ratios within a family of compounds.

R	DHA	VHF-*cis*	VHF-*trans*
H	0.65	0.86	0.79
CH_3	0.91	0.83	0.78
NH_2	1.02	1.10	0.85
NO_2	1.28	1.24	0.88

Table 7-5: Effect of the frequency dispersion estimated from the $\beta_{TDHF}^{CH3CN}(-2\omega;\omega,\omega)/\beta_{CPHF}^{CH3CN}(0;0,0)$ ratio for the DHA, VHF-*cis*, and VHF-*trans* forms.

R	DHA	VHF-*cis*	VHF-*trans*
H	0.60	3.29	0.64
CH_3	0.81	2.80	0.80
NH_2	1.48	2.20	1.69
NO_2	1.47	0.78	0.44

Table 7-6: Effect of electron correlation estimated from the $\beta_{MP2}^{CH_3CN}(0;0,0)/\beta_{CPHF}^{CH_3CN}(0;0,0)$ ratio for the DHA, VHF-*cis*, and VHF-*trans* forms.

In the next step, the $\beta_{//}$ values were analyzed (Table 7-7 and Figure 7-2). Owing to the modulating effect of the θ angle, some of the ordering relationships observed for the HRS responses are not reproduced for the EFISHG quantities. Thus, for the DHA form, the EFISHG $\beta_{MP2}^{CH_3CN}(-2\omega;\omega,\omega)$ values are in the ratio 0.01, -0.01, 0.33, 1.00 for R = H, Me, NH_2, and NO_2 whereas, in the same order, for

the VHF-*cis* form they amount to –2.48, 0.09, 4.28, 1.00 and to 2.00, 2.33, 1.85, 1.00 for the VHF-*trans* form. Again, the NLO contrasts are large: for R = H, Me, and NO_2, the three forms can be distinguished whereas for R = NH_2, the VHF-*cis* form displays β values roughly 5 times larger than the two other forms. Though the three forms of the R = Me compound present large ratios between the first hyperpolarizabilities, the β values of the DHA and VHF-*cis* forms are small so that the practical contrast might only be visible between, on the one hand, the VHF-*trans* form and, on the other hand, the two other forms that display almost negligible β values.

		DHA	**VHF-*cis***	**VHF-*trans***
R = H	$\beta_{TDHF}^{vacuo}(-2\omega;\omega,\omega)$	-133	1218	-447
	$\beta_{TDHF}^{CH3CN}(-2\omega;\omega,\omega)$	-171	474	-6418
	$\beta_{MP2}^{CH_3CN}(0;0,0)$	74	7269	4093
	$\beta_{MP2}^{CH_3CN}(-2\omega;\omega,\omega)$	51	-9044	3082
R = CH_3	$\beta_{TDHF}^{vacuo}(-2\omega;\omega,\omega)$	-101	1069	-329
	$\beta_{TDHF}^{CH3CN}(-2\omega;\omega,\omega)$	-322	-33	-5431
	$\beta_{MP2}^{CH_3CN}(0;0,0)$	-103	6813	5069
	$\beta_{MP2}^{CH_3CN}(-2\omega;\omega,\omega)$	-89	329	3584
R = NH_2	$\beta_{TDHF}^{vacuo}(-2\omega;\omega,\omega)$	1276	1862	275
	$\beta_{TDHF}^{CH3CN}(-2\omega;\omega,\omega)$	1526	3350	-1214
	$\beta_{MP2}^{CH_3CN}(0;0,0)$	2963	8697	8623
	$\beta_{MP2}^{CH_3CN}(-2\omega;\omega,\omega)$	3158	15541	2829
R = NO_2	$\beta_{TDHF}^{vacuo}(-2\omega;\omega,\omega)$	2355	-185	130
	$\beta_{TDHF}^{CH3CN}(-2\omega;\omega,\omega)$	5851	-4630	-7690
	$\beta_{MP2}^{CH_3CN}(0;0,0)$	7147	2779	1849
	$\beta_{MP2}^{CH_3CN}(-2\omega;\omega,\omega)$	9497	3627	1534

Table 7-7: EFISHG quantities ($\beta_{//}$) of DHA, VHF-*cis*, and VHF-*trans* evaluated at different levels of approximation. The TDHF calculations (λ = 1064 nm) were performed using the 6-311+G* basis set while the 6-31G* was used for the FF/MP2 calculations. Dynamic MP2 values were estimated using the multiplicative scheme by Equation (2-46). All values are given in atomic units.

7.4. Further discussions, conclusion, and outlooks

The contrast of second-order nonlinear optical response in the DHA-VHF equilibrium has been investigated as a function of the nature of the substituent (R) on the phenyl ring. By considering the hyper Rayleigh scattering response, the contrast for R = H and R = CH_3 between the DHA and VHF forms is larger than 5 while the contrast between the *cis* and *trans* VHF forms is close to 1. Adding the NH_2 donor group in *para* position of the phenyl leads to a substantial increase of the HRS first hyperpolarizability of the three forms, which is detrimental to the contrast. Then, for the NO_2 acceptor group, a contrast is recovered because the HRS first hyperpolarizability of the DHA form is about 2-3 times larger than for both VHF forms. The large first hyperpolarizability values of the R = H and R = CH_3 VHF forms has been attributed to the acceptor character of the seven-membered ring. For R = NO_2, the larger first hyperpolarizability value of the DHA form is due to the NO_2 attractor group, which is conjugated to the double bonds of the non-aromatic seven-membered ring whereas it decreases in the VHF-*cis* and VHF-*trans* forms as a result of the competing acceptor character of the aromatic seven-membered ring, $C(CN)_2$, and NO_2 groups. In the case of the electric field-induced second-harmonic generation (EFISHG) response, contrasts of first hyperpolarizability are observed for the four substituents but they differ from the HRS contrasts because of the double impact of the substituent on the amplitudes and orientations of both β and μ.

As a second step towards high NLO contrast DHA/VHF-based molecular switches, we carried out a preliminary study on the changes of first hyperpolarizability in a family of four tetraethynylethene-substituted DHA/VHF switches, which constitute a three-way chromophoric molecular switch controlled by pH, light, and heat (Figure 7-3) [8].

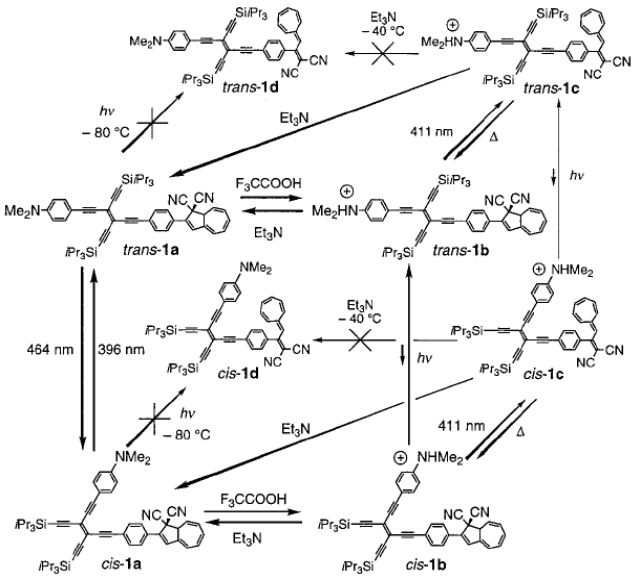

Figure 7-3: Three-way molecular switch based on DHA-VHF compounds [8].

The first hyperpolarizability of these compounds, which display large variations in their absorption and emission spectra, were theoretically characterized. The β_{HRS} values for the DHA, VHF-*cis*, and VHF-*trans* forms with the four different substituents as well as their ratios evaluated at IEF-PCM/MP2/6-31G* with the multiplicative scheme (Equation (2-46)) are listed in Table 7-8:

$\beta_{MP2}^{CH_3CN}(-2\omega;\omega,\omega)$	DHA	VHF-*cis*	VHF-*trans*	$\frac{\beta_{VHF-c}}{\beta_{DHA}}$	$\frac{\beta_{VHF-t}}{\beta_{DHA}}$	$\frac{\beta_{VHF-t}}{\beta_{VHF-c}}$
Substituent **1** R = 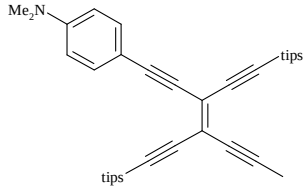	19194	27170	34724	1.4	1.8	1.3
Substituent **2** R = 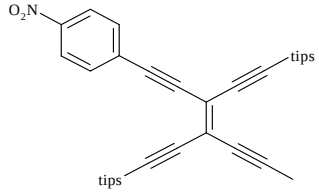	6038	26362	20231	4.4	3.4	0.8
Substituent **3** R = 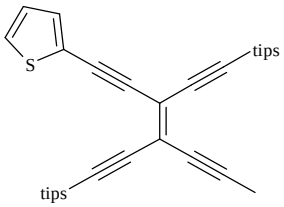	680	15333	18613	22.5	27.4	1.2
Substituent **4** R = 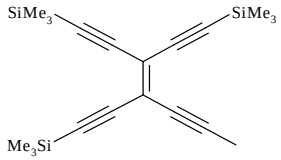	8263	20415	16410	2.5	2.0	0.8

Table 7-8: HRS first hyperpolarizabilties (a.u.) of DHA, VHF-*cis*, and VHF-*trans* with different substituents as weel as $\beta_{VHF\text{-}cis}/\beta_{DHA}$, $\beta_{VHF\text{-}trans}/\beta_{DHA}$, and $\beta_{VHF\text{-}trans}/\beta_{VHF\text{-}cis}$ ratios calculated using the multiplicative scheme (Equation (2-46)) (λ = 1064nm) with the IEF-PCM scheme (solvent = acetonitrile).

Compared to values obtained with H atom in R position (Table 7-4), these four substituents largely enhance the β_{HRS} values. The most exalted ones are obtained for substituent **1**, where β_{HRS} are multiplied by 139, 5, and 10 for the DHA, VHF-*cis*, and VHF-*trans* forms, respectively. With respect to donor R = NH_2, substituent **1**, with NMe_2 donor group, leads to the multiplication of β values by 3 for the DHA and VHF-*cis* forms, and by 5 for the VHF-*trans* form. Similarly, by comparing acceptor

R = NO_2 with acceptor substituent **2**, β value decreases by 18% for the DHA form while, for VHF-*cis* and *trans* forms, the β value is multiplied by 10 and 6, respectively, leading to contrast larger than one whereas, the contrast obtained with R = NO_2 are smaller or close to one. As showed previously, replacing the NH_2 donor group by NO_2 acceptor group enhances β values by 15% for the DHA form and decreases by 71% and 55% for the VHF-*cis* and *trans* forms respectively, while converting the donor substituent **1** by the acceptor substituent **2** leads to a decrease by 69%, 3%, and 42% for the DHA, VHF-*cis*, and VHF-*trans* forms, respectively. This demonstrates the impact of the length of the π-conjugated bridge on the conjugation and on the β values. Finally, the largest contrasts are obtained with the substituent **3** due to a large enhancement of the first hyperpolarizability values for the two VHF forms. As preliminary conclusion, these systems seem to have a high potential as three-way molecular switches, therefore, the next step in this study will be their experimental characterization.

7.5. References

[1] H. Görner, C. Fischer, S. Gierisch, and J. Daub, *J. Phys. Chem.*, **97**, 4110 (1993).

[2] H. Görner, C. Fischer, and J. Daub, *J. Photochem. Photobiol. A: Chem.*, **85**, 217 (1995).

[3] T. Mrozek, H. Görner, and J. Daub, *Chem. Commun.*, 1487 (1999).

[4] J. Ern, M. Petermann, T. Mrozek, J. Daub, K. Kuldová, and C. Kryschi, *Chem. Phys.*, **259**, 331 (2000).

[5] V. De Waele, U. Schmidhammer, T. Mrozek, J. Daub, and E. Riedle, *J. Am. Chem. Soc.*, **124**, 2438 (2002).

[6] V. De Waele, M. Beutter, U. Schmidhammer, E. Riedle, and J. Daub, *Chem. Phys. Lett.*, **390**, 328 (2004).

[7] M. Boggio-Pasqua, M. J. Bearpark, P. A. Hunt, and M. Robb, *J. Am. Chem. Soc.*, **124**, 1456 (2002).

[8] L. Gobbi, P. Seiler, and F. Diederich, *Angew. Chem., Int. Ed.*, **38**, 674 (1999).

Effects of the nature and length of the π-conjugated bridge on the second-order nonlinear responses of push–pull molecules including 4,5-dicyanoimidazole and their protonated forms

8. Effects of the nature and length of the π-conjugated bridge on the second-order nonlinear responses of push–pull molecules including 4,5-dicyanoimidazole and their protonated forms

8.1. Introduction

Push-pull molecules including the highly electron-withdrawing 4,5-dicyanoimidazole moiety are expected to provide large first hyperpolarizabilities. The first synthesis of the 4,5-dicyanoimidazole was reported by Woodward in 1950 [1] while in 1988, Rapoport *et al.* [2] have shown an efficient way to synthesize and functionalize 4,5-dicyanoimidazole. Since that, this moiety has widely been used in different branches of material sciences due to its accessibility, solubility, and acceptor character. For instance, 4,5-dicyanoimidazole has proved its efficiency in organic electronics components [3-7], and recently, photoinduced absorption and birefringence of 4,5-dicyanoimidazole-derived chromophores embedded into poly(methyl-methacrylate) films were studied [8]. In addition, 2-bromo-1-methylimidazole-4,5-dicarbonitrile precursor can easily be substituted by donors with systematically extended π-conjugated path [9], which is a key element to exalt the first hyperpolarizability.

We have investigated a series of six push-pull molecules containing the 4,5-dicyanoimidazole acceptor unit, *N*,*N*-dimethylamino donor group, and systematically enlarged π-conjugated system (Figure 8-1). In particular, we focus on the impact of the π-conjugated path on β. The conjugated segments include double (**3**, **5**) and triple (**6**) bonds as well as one (**2**, **3**) or two (**4**, **5**, and **6**) 1,4-phenylene rings. Moreover, we studied how the protonation of these neutral compounds affects their first hyperpolarizabilty and their applicability as pH-triggered NLO switches. In contrast to other molecular switches, the aforementioned 4,5-dicyanoimidazole derivatives are stable in both neutral/protonated forms.

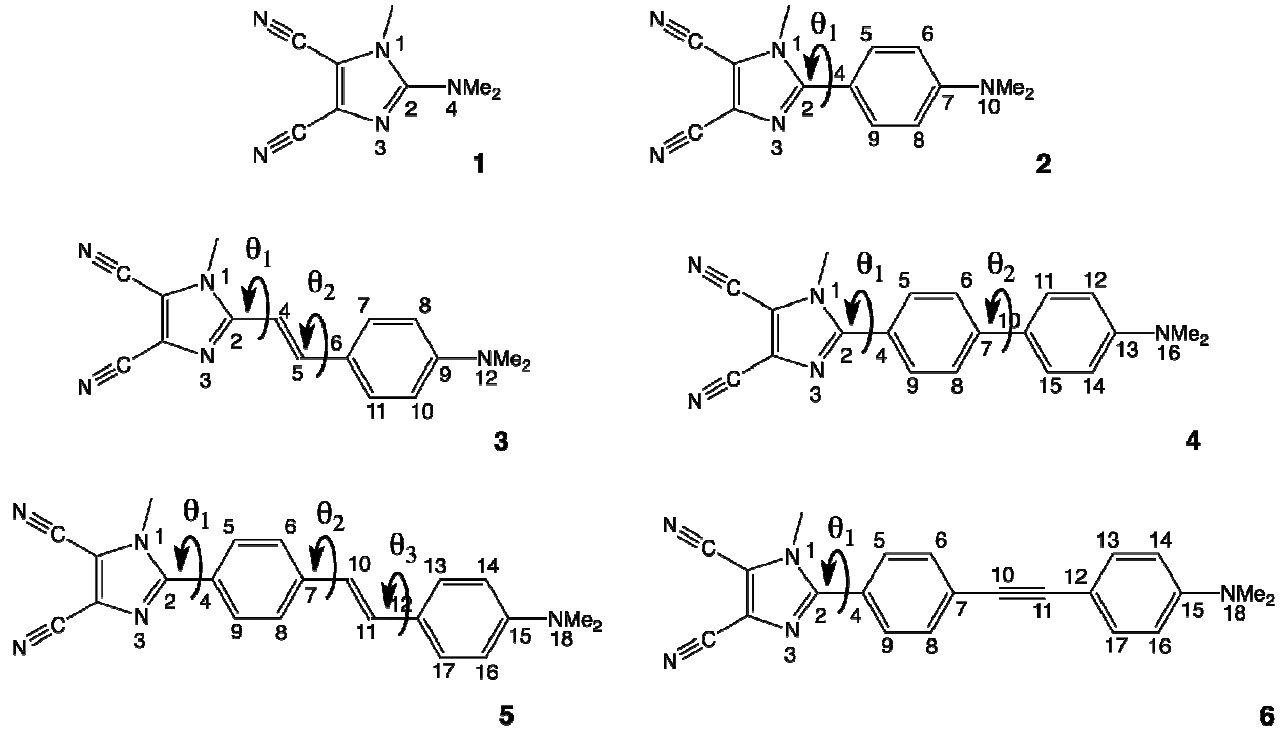

Figure 8-1: Compounds **1**-**6** bearing the 4,5-dicyanoimidazole moiety. The z axis goes from left to right.

8.2. Linear absorption and HRS experimental results

The β_{zzz}, β_{zxx} and β_{HRS} values, as well as the depolarization ratios issued from HRS measurements are listed in Table 8-1. Only the HRS responses of the non protonated forms were reported, those of protonated forms being under the experimental detection limit. The same difficulty arose for compound **1** in its neutral form. Note that to obtain the protonated forms, trifluoroacetic acid in excess was used. Inserting a double bond between the imidazole ring and the 1,4-phenylene ring (from compound **2** to compound **3**) increases β_{HRS} by 110% while adding a second 1,4-phenylene ring (from compound **2** to compound **4**) increases β_{HRS} by 55%. Starting from compound **4**, the inclusion of a double bond or a triple bond between the two 1,4-phenylene moieties leads to an increase of β_{HRS} by 30% and 70%, respectively. Due to the electron delocalization along the π-conjugated path, all DR values are close to 5. Moreover, the $|R| = |\beta_{zxx}/\beta_{zzz}|$ values do not exceed 0.15 (and decrease as the size of the compound increases), which further confirms the 1D character of the compounds.

Molecule	β_{zzz}	β_{zxx}	β_{HRS}	DR
1	-	-	-	-
2	9710	-1186	3860	3.94
3	19708	-3010	8100	4.84
4	14480	-1362	5956	4.13
5	18660	-410	7648	4.79
6	24674	-998	10038	4.61

Table 8-1: Longitudinal (β_{zzz}) and transverse (β_{zxx}) molecular first hyperpolarizabilities components (a.u.) deduced from HRS experiments for the non protonated forms.

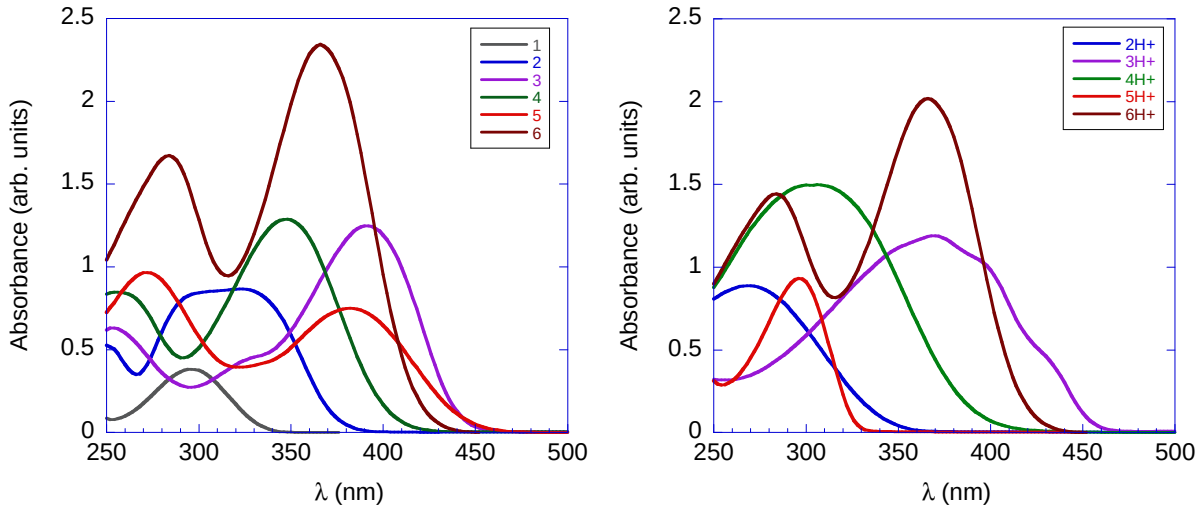

Figure 8-2: Absorption spectra recorded in CH_2Cl_2 for the non protonated forms (left) and the protonated forms (right) of compounds **1**-**6**. The absorption band of $\mathbf{1H^+}$ is located below 250 nm. The concentration of all solutions is 10^{-4} M.

The absorption spectra of the protonated and deprotonated forms are given in Figure 8-2 whereas the characteristics of the main lowest-energy transitions are provided in Table 8-2. In CH_2Cl_2, the maximum absorption wavelength ordering is **1** < **2** < **4** < **6** < **3** ~ **5** for the neutral species while for the acid forms, it becomes **1** < **2** < **4** < **3** ~ **5** ~ **6**. Upon protonation the absorption maximum of all compounds shifts towards higher energy. For **2**, **3**, and **4**, the increase of ΔE amounts to 0.8-0.95 eV whereas it is slightly smaller (0.66-0.74 eV) for the longer chromophores.

Molecules	λ_{ge}	ΔE_{ge} (f_{ge})	λ_{max}	ΔE_{max}
		Non protonated		
1	271	4.58 (0.283) $_{0.697}$H→L	296	4.19
2	305	4.06 (0.366) $_{0.681}$H→L	322	3.85
3	365	3.40 (1.449) $_{0.632}$H→L, $_{-0.295}$H→L+1	388	3.20
4	314	3.95 (0.858) $_{0.569}$H→L, $_{0.374}$H→L+1	348	3.56
5	358	3.46 (1.618) $_{-0.517}$H→L, $_{0.450}$H→L+1	382	3.25
6	351	3.53 (1.764) $_{0.558}$H→L, $_{0.386}$H→L+1	366	3.39
		Protonated		
$1H^+$ (H1)	237	5.24 (0.344) $_{0.675}$H→L	-	-
$1H^+$ (H2)	274	4.52 (0.254) $_{0.700}$H→L	-	-
$2H^+$	260	4.78 (0.603) $_{0.691}$H→L	259	4.79
$3H^+$	314	3.95 (1.352) $_{0.696}$H→L	310	4.00
$4H^+$	273	4.55 (1.117) $_{0.664}$H→L	278	4.46
$5H^+$	323	3.83 (1.767) $_{0.685}$H→L	311	3.99
$6H^+$	318	3.90 (1.801) $_{0.679}$H→L	306	4.05

Table 8-2: IEF-PCM/MPW1K/6-311G* transition energies (ΔE_{ge}, eV), and associated transition wavelengths (λ_{ge}, nm) and oscillator strengths (f_{ge}) for the dominant low energy charge-transfer excitations. The molecular orbitals involved in the main electronic transitions (numbers in index are CI coefficients) are also reported. The last two columns report the experimental absorption maxima results, λ_{max} (nm) and ΔE_{max} (eV).

8.3. Theoretical results

8.3.1. Molecular structures

Three sites of protonation have been envisaged and the corresponding protonation energies were calculated at the IEF-PCM/MP2/6-311G* level of approximation (Table 8-3). For compounds **2**-**6**, the most favorable protonation site is the *N*,*N*-dimethylamino function (H1). Indeed, $\Delta\Delta U = \Delta U(H1) - \Delta U(H2)$ is at least larger than 12 kcal/mol, which corresponds at room temperature to Maxwell-Boltzmann populations in the 0.1:99.9 ratio or higher. Therefore, in the forthcoming analyses of the optical properties we have focused on the species protonated on the NMe_2 group. For compound **1**, in addition to (H1), the protonation on the imidazole N3-position (H2) is also possible, $\Delta\Delta U$ being of the order of 1 kcal/mol.

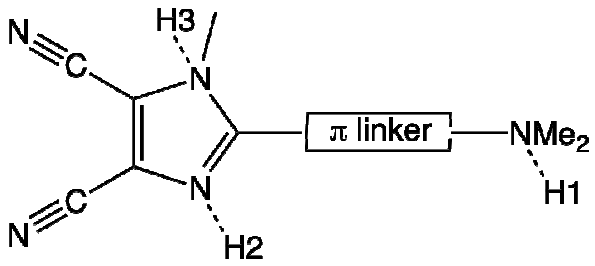

ΔU	1	2	3	4	5	6
H1	-260	-275	-277	-279	-279	-277
H2	-266	-267	-272	-264	-264	-263
H3	-230	-227	-233	-220	-220	-218

Table 8-3: IEF-PCM/MP2/6-311G* protonation energies (ΔU) as a function of the sites of protonation (kcal/mol).

A selection of significant geometrical parameters of compounds **1**-**6** and **1H$^+$**-**6H$^+$** as well as the bond length alternations define as: $BLA_1 = (d_{C2-C4}+d_{C5-C6}-2d_{C4-C5})/2$ and $BLA_2 = (d_{C7-C10}+d_{C11-C12}-2d_{C10-11})/2$ are listed in Table 8-4. Besides the **1**/**1H$^+$** pair for which the changes of geometries are larger, protonation leads to rather small variations of the backbone bond lengths, except for the increase of the C-NMe_2 bond length by 0.08-0.11 Å. Typically, the variations are of the order of a few pm and decrease with the size of the π-conjugated linker. The increase of the C-NMe_2 bond length upon protonation and its identical value (1.476 Å) for compounds **2H$^+$**-**6H$^+$** is a signature of the vanishing donor character of the dimethylamino group. Moreover, there is a systematic decrease of electron conjugation upon protonation, consistent with the increase of ΔE_{ge}. This is characterized by an increase of BLA in the polyene (**3** and **5**) and polyyne (**6**) segments or by an increase of the inter-phenyl bond length (**2** and **4**). Compounds **2**, **4**, and **6** do not display significant change of planarity upon protonation, while significant variations in the dihedral angle θ_2 are observed in compound **3** and **5** (-22° and +8°, respectively).

	1	**2**	**3**	**4**	**5**	**6**
N_1-C_2	1.373	1.375	1.374	1.374	1.374	1.374
N_3-C_2	1.334	1.339	1.340	1.338	1.338	1.338
C_2-C_4	-	1.462	1.450	1.465	1.464	1.465
C_4-C_5	-	-	1.356	-	-	-
C_5-C_6	-	-	1.456	-	-	-
C_7-C_{10}	-	-	-	1.475	1.465	1.423
C_{10}-C_{11}	-	-	-	-	1.357	1.230
C_{11}-C_{12}	-	-	-	-	1.462	1.423
C-NMe_2	1.388	1.387	1.369	1.394	1.393	1.389
θ_1	-	-137.1	180.0	-136.4	-135.9	-137.3
θ_2	-	-	180.0	138.5	156.6	-
θ_3	-	-	-	-	161.0	-
BLA_1	-	-	0.097	-	-	-
BLA_2	-	-	-	-	0.107	0.193
	$1H^+$	**$2H^+$**	**$3H^+$**	**$4H^+$**	**$5H^+$**	**$6H^+$**
N_1-C_2	1.357 (1.359)	1.372	1.373	1.373	1.373	1.373
N_3-C_2	1.316 (1.357)	1.337	1.339	1.337	1.338	1.338
C_2-C_4	-	1.466	1.452	1.466	1.465	1.465
C_4-C_5	-	-	1.353	-	-	-
C_5-C_6	-	-	1.464	-	-	-
C_7-C_{10}	-	-	-	1.478	1.465	1.424
C_{10}-C_{11}	-	-	-	-	1.355	1.229
C_{11}-C_{12}	-	-	-	-	1.466	1.424
C-N^+HMe_2	1.451 (1.338)	1.476	1.476	1.476	1.476	1.476
θ_1	-	-139.0	176.3	-136.9	-135.6	-137.3
θ_2	-	-	158.0	134.9	164.2	-
θ_3	-	-	-	-	157.8	-
BLA_1	-	-	0.105	-	-	-
BLA_2	-	-	-	-	0.111	0.195

Table 8-4: Selected distances (Å) and angles (°) of the **1**-**6** and **$1H^+$**-**$6H^+$** compounds as obtained from IEF-PCM/B3LYP/6-311+G* geometry optimizations. Atoms labels refer to Figure 8-1. For compound **$1H^+$**, values in parentheses correspond to protonation on the imidazole N_3-position (H2).

8.3.2. Linear and nonlinear optical properties

For compounds **2**-**6**, the TDDFT excitation energies shown in Table 8-2 exhibit an increase upon protonation ranging from 0.37 eV (**5** and **6**) to 0.72 eV (**2**), while the protonation-induced shift in compound **1** varies from -0.06 to 0.66 eV with

respect to the protonation site (H1) or (H2). The excited states of the protonated forms are all dominated by HOMO-LUMO singly-excited configurations, whereas significant contributions from the LUMO+1 orbitals arise in the non protonated forms. For all forms, the main absorption transitions display increasing oscillator strengths when enlarging the π-conjugated bridge. The frontiers orbitals of all compounds are sketched in Figure 8-3. When the system gets large enough (**4**, **5** and **6**), the HOMO of the neutral species is located on the NMe_2 group and the adjacent π-conjugated moieties, and not over the 4,5-dicyanoimidazole moiety. The opposite situation characterizes the LUMO (or LUMO+1) orbitals, which are mainly delocalized over the 4,5-dicyanoimidazole moiety and the adjacent π-conjugated bridge, but not or little over the NMe_2 group. Upon protonation of the NMe_2 group, the HOMO keeps its shape but does not extend anymore on the *N*,*N*-dimethylamino group while it spans the 4,5-dicyanoimidazole moiety even for the largest species. The lack of HOMO density on the *N*,*N*-dimethylamino group can also be related to the fact that upon protonation this group no longer participates to the delocalization pattern. In turn, the LUMO of the protonated species moves from the 4,5-dicyanoimidazole moiety to the ring close to the NMe_2 group. In summary, for the largest non protonated compounds, where the pattern differences are the most pronounced, the LUMO and HOMO of the neutral species tend to localize respectively on the 4,5-dicyanoimidazole and *N*,*N*-dimethylamino groups [10], whereas they are more centered in the protonated species. Protonation stabilizes the HOMO and LUMO but the stabilization is larger for the HOMO, which is consistent with the increase of ΔE.

The MP2 first hyperpolarizabilities and the MP2 depolarization ratios (Equations (2-46) and (2-47)) of compounds **1**-**6** and **1H$^+$**-**6H$^+$** are listed in Table 8-5. Taking compound **1** as reference, we observe that adding one (**2**) or two (**4**) 1,4-phenylene rings in the π-conjugated path increases β_{HRS} by 410% and 760%, respectively. Further elongation of the π-conjugated bridge by a double bond between the 4,5-dicyanoimidazole ring and the 1,4-phenylene ring (going from compound **2** to **3)** or between the two 1,4-phenylene rings (going from compound **4** to **5**), β_{HRS} increases by 440% and 160%, respectively. In comparison to adding a double bond (compound **5**), inserting a triple bond between the pair of 1,4-phenylene rings (compound **6**) leads to a slightly smaller increase: 152% with respect to compound **4**. As shown in Table 8-6, the β_{HRS} responses are dominated by the β_{zzz} diagonal tensor components, which is a signature of the one-dimensional character of the compounds. Moreover, the β_{zzz} values of **1**-**6** are in the 0.04 : 0.30 : 1.35 : 0.45 : 1.00 : 1.02 ratio, similar to the 0.04 : 0.23 : 1.24 : 0.38 : 1.00 : 0.97 ratio for the β_{HRS} responses of the compounds given in the same order.

Compound 1

1 – HOMO
(-11.15 eV)

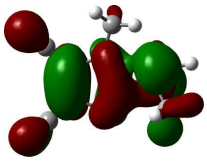

1H$^+$ (H1) – HOMO
(-9.43 eV)

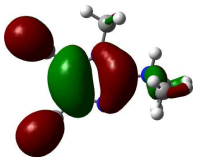

1H$^+$ (H2) – HOMO
(-10 .57 eV)

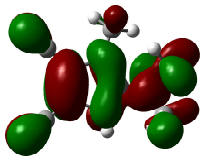

1 – LUMO
(-0.62 eV)

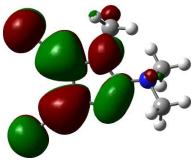

1H$^+$ (H1) – LUMO
(0.16 eV)

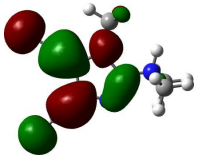

1H$^+$ (H2) – LUMO
(-1.09 eV)

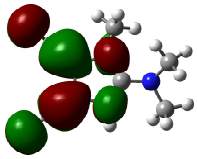

Compound 2

2 – HOMO (-8.38 eV)

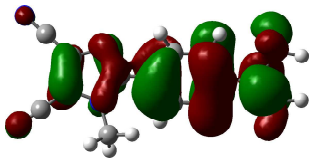

2H$^+$ – HOMO (-10.12 eV)

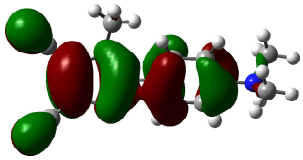

2 – LUMO (0.14 eV)

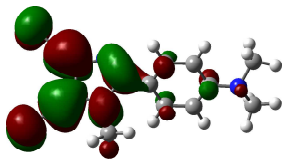

2H$^+$ – LUMO (-0.36 eV)

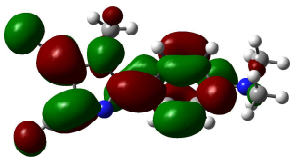

Compound 3

3 – HOMO (-7.77 eV)

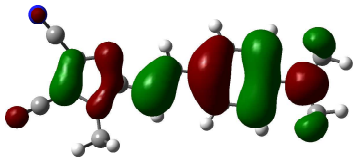

3H+ – HOMO (-9.39 eV)

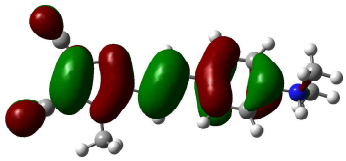

3 – LUMO (0.02 eV)

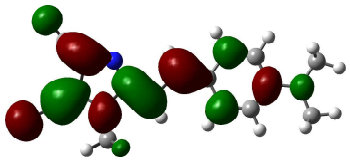

3H+ – LUMO (-0.65 eV)

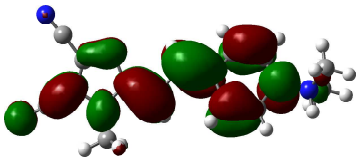

3 – LUMO+1 (0.55 eV)

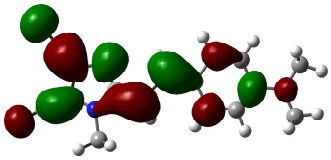

Compound 4

4 – HOMO (-8.12 eV)

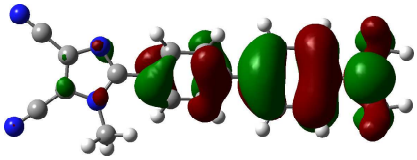

4H+ – HOMO (-9 .62 eV)

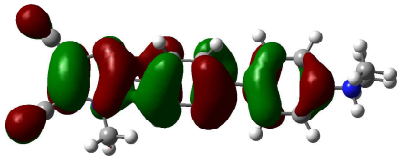

4 – LUMO (0.05 eV)

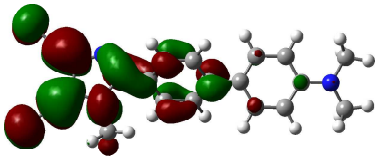

4H+ – LUMO (-0.24 eV)

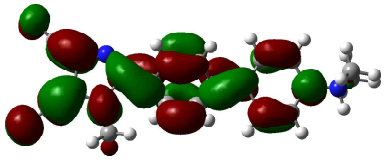

4 – LUMO+1 (0.73 eV)

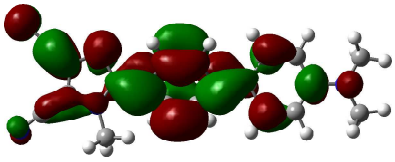

Compound 5

5 – HOMO (-7.84 eV)

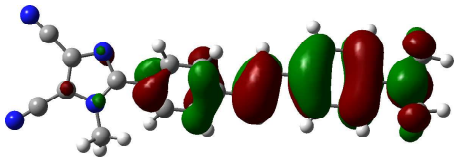

5H+ – HOMO (-9.08 eV)

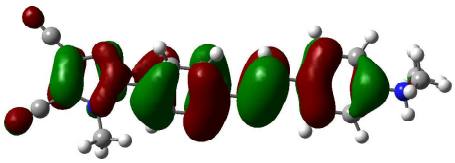

5 – LUMO (-0.04 eV)

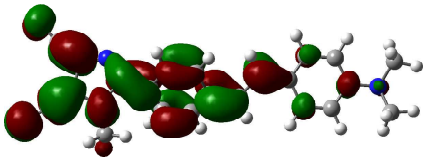

5H+ – LUMO (-0.52 eV)

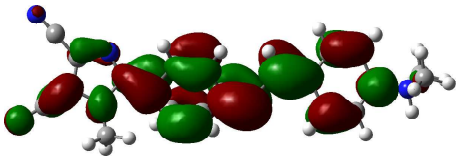

5 – LUMO+1 (0.37 eV)

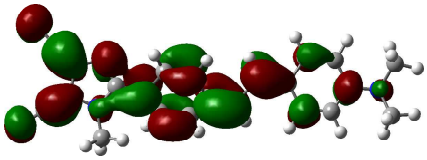

Compound 6

6 - HOMO (-7.97 eV)

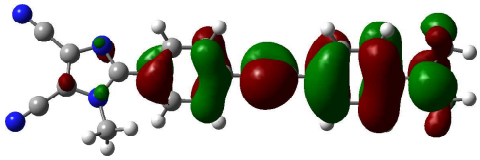

6H+ - HOMO (-9.26 eV)

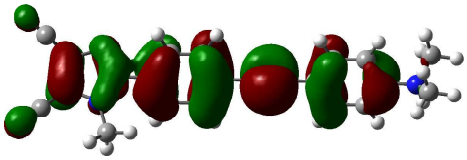

6 - LUMO (-0.13 eV)

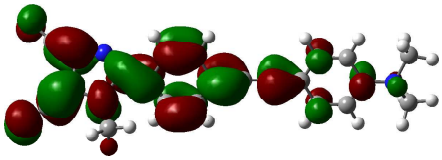

6H+ - LUMO (-0.64 eV)

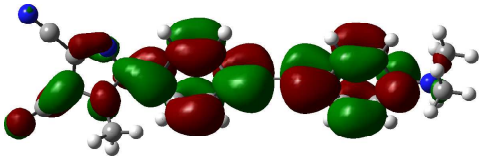

6 - LUMO+1 (0.32 eV)

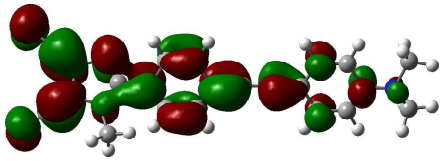

Figure 8-3: Frontier orbitals of compounds **1**-**6**/**1H**$^+$-**6H**$^+$ as well as their energies calculated at the IEF-PCM/MPW1K/6-311G* level of approximation.

All the DR values for the non protonated forms are close to 5, which demonstrates the one-dimensional character of the molecules, while for the protonated forms the DR values get smaller than 2.5. This is attributed to the break of the charge-transfer exaltation of β and particularly to the reduction of its β_{zzz} longitudinal component (Table 8-6). This is consistent with i) the blue shift of the absorption spectra and with ii) the β_{HRS}(deprotonated)/β_{HRS}(protonated) contrasts, which, with the exception of the small compound **1**, are always of at least 7. From a theoretical perspective, Table 8-7 lists the β_{HRS}(MP2)/β_{HRS}(HF) ratios for both the protonated and non protonated species. For the latter, including electron correlation leads to an increase of β_{HRS} by 75 to 119 % whereas for the former β_{HRS} decreases by 14 to 28%. The only exception in these trends is compound **6H$^+$** where β_{HRS} increases by 21%. This demonstrates the need to include electron correlation effects, because it is more than simply scaling the β_{HRS} values of all compounds by the same factor.

Molecule	**Non protonated form**		**Protonated form**		**Ratio**
	$\beta_{MP2}(-2\omega;\omega;\omega)$	DR	$\beta_{MP2}(-2\omega;\omega;\omega)$	DR	
1	379	4.87	114	1.78	3.32
2	1938	5.48	256	1.65	7.57
3	10485	5.11	541	1.87	19.38
4	3264	5.40	290	2.28	11.26
5	8485	5.15	361	1.78	23.50
6	8236	5.15	639	2.44	12.89

Table 8-5: HRS first hyperpolarizabilties (a.u.) and depolarization ratios (DR) of compounds **1**-**6**/**1H$^+$**-**6H$^+$** calculated using the multiplicative scheme (Equation (2-46)) (λ = 1064nm) with the IEF-PCM scheme (solvent = CH_2Cl_2). The β(non protonated)/β(protonated) ratios are listed in the last column.

Molecule	Non protonated form			Protonated form		
	β_{zzz}	β_{zxx}	$R=\lvert\beta_{zxx}/\beta_{zzz}\rvert$	β_{zzz}	β_{zxx}	$R=\lvert\beta_{zxx}/\beta_{zzz}\rvert$
1	590	-173	0.29	-46	-47	1.02
2	4385	-392	0.09	-416	-123	0.30
3	19777	-1308	0.07	-342	-690	2.02
4	6643	-271	0.04	-40	-273	6.83
5	14632	-719	0.05	-661	-310	0.47
6	14864	-257	0.02	-1347	-312	0.23

Table 8-6: Longitudinal (β_{zzz}) and off-diagonal (β_{zxx}) components (a. u.) of the first hyperpolarizability tensor for the non protonated and protonated forms of **1**-**6** compounds calculated using IEF-PCM/MP2/6-31G* scheme (solvent = CH_2Cl_2) in the static limit ($\lambda = \infty$).

	1	**2**	**3**	**4**	**5**	**6**
Non protonated	1.23	1.38	2.19	1.75	1.84	1.75
Protonated	0.72	0.78	0.86	0.78	0.83	1.21

Table 8-7: Effects of electron correlation estimated from the MP2/HF ratios of β_{HRS}.

8.4. Discussion

4,5-Dicyanoimidazole-based compounds **1**-**6** bear a terminal *N*,*N*-dimethylamino group that can be protonated leading to substantial modifications of their linear and nonlinear optical properties. Both theory and experiment show that protonation leads to a hypsochromic shift of the lowest-energy UV-visible absorption band. This shift has been measured to range between 0.66 and 0.94 eV whereas the TDDFT calculations predict slightly smaller shifts. This substantiates that the protonation occurs on the *N*,*N*-dimethylamino group, at least for compounds **2**-**6** as predicted from protonation energies. Another proof of the protonation on the *N*,*N*-dimethylamino group is provided by the calculated first excitation energies of compound **3** protonated on the two other sites. Indeed, TDDFT calculations performed with the same parameters predict ΔE_{ge} values of 3.06 and 2.40 eV for protonation in H2 and H3, in comparison with ΔE_{ge} of 3.40 and 3.95 eV for the neutral and H1-protonated compounds, respectively. Only the protonation on the *N*,*N*-dimethylamino group leads to a hypsochromic shift.

Protonation also leads to a decrease of the HRS first hyperpolarizabilities by about one order of magnitude for **2**-**6** as well as of the depolarization ratios. So, the protonation changes the $N(CH_3)_2$ donor into a $NH(CH_3)_2^+$ acceptor and the compound switches between a A-π-D pattern having a large β to a A-π-A' pattern, having much smaller β. Further analysis of the β_{HRS} contrasts is however hampered by the very low β_{HRS} values of the protonated species, which do not enable their measurements. Experimentally, β_{HRS} increases in the order **2** < **4** < **5** < **3** < **6** while theoretically, this order becomes: **1** < **2** < **4** < **5** ~ **6** < **3**. The two series differ by the position of compound **6**, which corresponds to an underestimation of β_{HRS} for the species containing a triple bond linker. A similar situation has been encountered in a previous work on benzimidazolo[2,3-b]oxazolidines [11] where the HRS experiments conclude that the open form with a triple CC bond linker between the donor and acceptor moieties displays a larger first hyperpolarizability than the corresponding system with a double CC bond linker whereas the opposite is predicted from *ab initio* calculations. It was then argued that the discrepancy could come from the lack of solvent effects in the simulation. This argument can, however, not be employed here, at least as far as the PCM scheme is satisfactory and specific solute-solvent interactions are not capital. An interpretation for this inversion between compounds **5** and **6** could be the existence of a mixture of *cis* and *trans* forms for compound **5** because the first hyperpolarizability of the *cis* form is expected to be smaller. However, the calculated energy difference between the two forms is too large – in favor of the *trans* form – and amounts to 5.85 kcal/mol.

All the DR values, calculated and measured, are close to 5 (Table 8-5), which supports a 1D-like or rod-like NLO-phore and results from the presence of a main charge-transfer axis, between the donor and acceptor groups.

The relative electron-acceptor strength of the 4,5-dicyanoimidazole moiety has been assessed by comparing the first hyperpolarizability of compound **5** to the one of its analog where the later group is replaced by a nitro group, so as to obtain *N*,*N*'-dimethylaminonitrostilbene (DANS). Using the multiplicative scheme (Equation (2-46)), the β_{HRS} response of DANS amounts to 25460 a.u. (DR = 5.22), *i.e.* 67% larger than in compound **5**, demonstrating that the electron accepting ability of 4,5-dicyanoimidazole moiety is less than that of NO_2 group.

8.5. Conclusion

In this chapter, using theoretical and experimental methods of characterization we have investigated a series of six push-pull molecules containing the 4,5-dicyanoimidazole acceptor unit, the *N*,*N*-dimethylamino donor group, and systematically enlarged π-conjugated linkers in view of assessing their first hyperpolarizabilities as well as their variations upon protonation. The results

demonstrate that the protonation occurs at the *N*,*N*-dimethylamino functionality, which leads to break the electronic charge-transfer delocalization: the A-π-D pattern of the neutral species having large β is transformed to a A-π-A' pattern, which displays much smaller β. This feature makes these systems potentially applicable as pH-triggered NLO switches. In particular, protonation leads to a decrease of the HRS first hyperpolarizabilities by at least one order of magnitude as well as to a decrease of the depolarization ratio, which goes from about 5 for the neutral species, which also supports the 1D-like NLO-phore nature, to about 2 for the protonated ones. Moreover, switching between the A-π-D and A-π-A' patterns corresponds to some extent to the commutation between one-photon allowed low energy transitions and two-photon-like ones, opening the field to new switching properties.

8.6. References

[1] D.W. Woodward, *US Patent*, 2534331 (1950).

[2] J. F. O'Connell, J. Parquette, W. E. Yelle, W. Wang, and H. Rapoport, *Synthesis*, 767 (1988).

[3] P. G. Apen and P. G. Rasmussen, *J. Am. Chem. Soc.*, **113**, 6178 (1991).

[4] A. Carella, R. Centore, A. Fort, A. Peluso, A. Sirigu, and A. Tuzi, *Eur. J. Org. Chem.*, 2620 (2004).

[5] A. Carella, R. Centore, A. Sirigu, A. Tuzi, A. Quatela, S. Schutzmann, and M. Casalboni, *Macromol. Chem. Phys.*, **205**, 1948 (2004).

[6] R. Y. C. Shin, P. Sonar, P. S. Siew, Z.-K. Chen, and A. Sellinger, *J. Org. Chem.*, **74**, 3293 (2009).

[7] F. Bureš, J. Kulhánek, T. Mikysek , J. Ludvík, and J. Lokaj, *Tetrahedron Lett.*, **51**, 2055 (2010).

[8] J. Kulhánek, F. Bureš, A. Wojciechowski, M. Makowska-Janusik, E. Gondek, and I. V. Kityk, *J. Phys. Chem. A*, **114**, 9440 (2010).

[9] J. Kulhánek, F. Bureš, O. Pytela, T. Mikysek, J. Ludvík, and A. Růžička, *Dyes and Pigments*, **85**, 57 (2010).

[10] D. Shi, Y. Cao, N. Pootrakulchote, Z. Yi, M. Xu, S.M. Zakeeruddin, M. Grätzel, and P. Wang, *J. Phys. Chem. C*, **112**, 174 (2008).

[11] L. Sanguinet, J.-L. Pozzo, M. Guillaume, B. Champagne, F. Castet, L. Ducasse, E. Maury, J. Soulié, F. Mançois, F. Adamietz, and V. Rodriguez, *J. Phys. Chem. B*, **110**, 10672 (2006).

Symmetrical and nonsymmetrical chromophores with Tröger's base skeleton: chiroptical, linear, and quadratic nonlinear optical properties – A joint theoretical and experimental study

S. Sergeyev, D. Didier, V. Boitsov, A. Teshome, I. Asselberghs, K. Clays, C. M. L. Vande Velde, A. Plaquet, and B. Champagne, *Chem. Eur. J.*, **16**, 8181 (2010).

9. Symmetrical and nonsymmetrical chromophores with Tröger's base skeleton: chiroptical, linear, and quadratic nonlinear optical properties – A joint theoretical and experimental study

9.1. Introduction

Tröger's base (2,8-dimethyl-6*H*,12*H*-5,11-methanodibenzo[*b*,*f*][1,5]diazocine, compound **1** (Figure 9-1), is a chiral diamine with two stereogenic bridgehead nitrogen atoms. The unique set of structural features (C_2-symmetry and a rigid V-shape geometry with the two aromatic rings nearly perpendicular to each other) makes derivatives of Tröger's base very attractive as nanometer-sized molecular scaffolds for supramolecular chemistry and molecular recognition. The chemistry of Tröger's base analogues has been extensively reviewed [1-8]. Most applications of these compounds reported to date have exploited the folded geometry and, in some instances, the chirality of Tröger's base. Another interesting structural feature, namely, the two tertiary amine functionalities, has hardly been used until now. Due to the presence of two nitrogen atoms, Tröger's base can be viewed as a structural analogue of N,N-dialkylanilines, which have found extensive application in the design of chromophores with NLO properties [9]. Recently, the use of Tröger's base in the design of V-shaped push pull-chromophores comprising pyridinium acceptors which have proven to be highly efficient in linear chromophores [10,11], was pioneered. Interesting solid-state fluorescence properties of these V-shaped chromophores were reported, but no information on their NLO properties was disclosed [12,13].

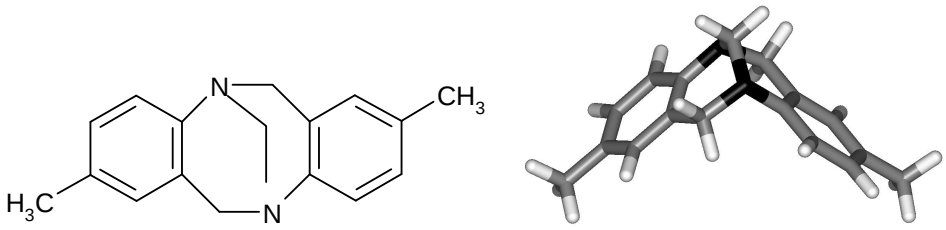

Figure 9-1: Tröger's base (compound **1**).

In the course of our study on chromophores with potential NLO activities, we decided to explore the chiral, V-shaped scaffold of 6H,12H-5,11-methanodibenzo [b,f]-[1,5]diazocine, which provides the possibility to incorporate two chromophoric units within one molecule, in addition to their dipole moments being nonantiparallel to

one another. The introduction of chiral elements within the conjugated system might prove beneficial in obtaining noncentrosymmetrical crystals. Examples of V-shaped push-pull chromophores are known. For instance, axially chiral C_2-symmetrical binaphthyl derivatives have exhibited high first hyperpolarizabilities [14-16]. Other V-shaped systems have been suggested as NLO-chromophores [17,18], as exemplified by various derivatives of the (dicyanomethylene)pyran [19] in which strong electronic interactions between the two chromophores occur, since they share the same acceptor group. This leads to specific relationships between the opening angle, donor/acceptor strengths, and first hyperpolarizability of these compounds. In the case of Tröger's base derivatives, these interactions are expected to be small because the two chromophores have distinct nitrogen donor atoms, though they are close to one another.

In this chapter, we report on the joint theoretical and experimental studies of the quadratic NLO properties of compounds **2** to **5** in comparison with the benchmark chromophores **6** and **7**, which feature dimethylamino group as a donor (Figure 9-2). Compounds **2** and **3** are derived from 6H,12H-5,11-methanodibenzo[b,f][1,5] diazocine and feature two identical acceptors, while compounds **4** and **5** are unsymmetrical chromophores featuring only one acceptor. The synthesis of these compounds has been reported [20-22] but is not detailed in this framework.

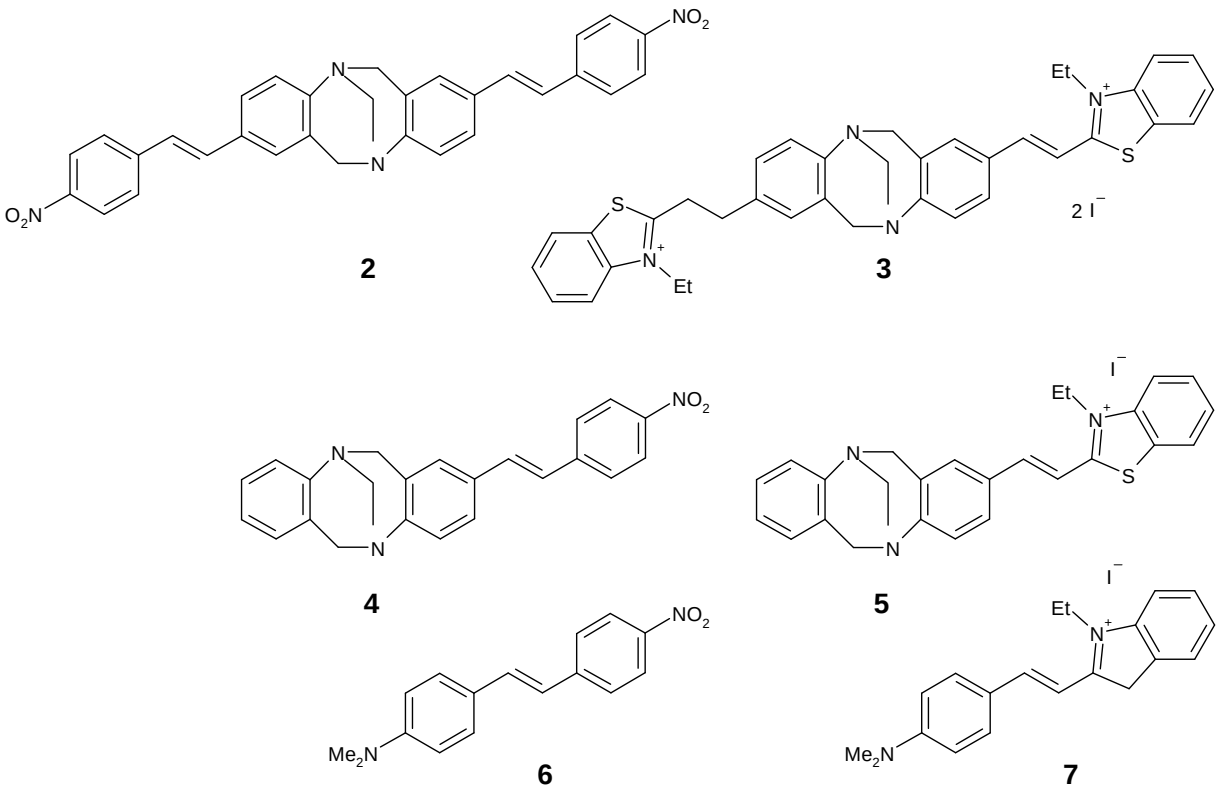

Figure 9-2: Structures of compounds **2** to **5** derived from the Tröger's base and compounds **6** and **7** featuring dimethylamino group as a donor.

9.2. Linear and second-order nonlinear optical properties

The linear and second-order NLO properties for compounds **2**-**7** are reported in Table 9-1. The static first hyperpolarizability values $\beta_{HRS,0}$ listed in this table are the experimentally obtained dynamic values $\beta_{HRS,800}$, corrected for different degrees of resonance enhancement. The first observation is the longer wavelength of maximal absorption (λ_{max}) for all the benzothiazolium acceptor-based chromophores (**3**, **5**, and **7**) compared with the corresponding analogues that have the nitro group as an acceptor (**2**, **4**, and **6**). This is in agreement with other studies that compare the electron-accepting strength of the benzothiazolium moiety with that of more conventional acceptors, such as the nitro group [23]. Congruent with this observation in linear optics are the experimental results in second-order nonlinear optics.

Compound	λ_{max}	ε_{max}	$\beta_{HRS,800}$	$\beta_{HRS,0}$,	DR	θ
2	391	50800	41199 ± 2777	1435 ± 231	3.0 ± 0.4	76 ± 5
3	436	56200	24766 ± 1389	3240 ± 231	2.5 ± 0.2	77 ± 5
4	389	24000	42125 ± 3472	1713 ± 231	3.8 ± 0.2	–
5	433	20500	25460 ± 2315	3240 ± 231	4.2 ± 0.3	–
6	443	30200	40273 ± 2777	6249 ± 463	3.7 ± 0.2	–
7	525	59000	27775 ± 926	11341 ± 463	3.7 ± 0.2	–

Table 9-1: Wavelengths (λ_{max}, nm), extinction coefficient at $\lambda_{max,\ abs}$ (ε_{max},L mol^{-1} cm^{-1}), dynamic (λ = 800 nm) HRS ($\beta_{HRS,800}$) and static (derived with the two-state approximation) HRS ($\beta_{HRS,0}$) hyperpolarizabilities (a.u.), depolarization ratios, as well as derived opening angle between two arms of Tröger's base bis-chromophoric derivatives (θ), measured in DMF

The static first hyperpolarizability values $\beta_{HRS,0}$ are all approximately two times larger for the benzothiazolium-derived compounds (**3**, **5**, and **7**) than for the corresponding 4-nitrophenyl analogues (**2**, **4**, and **6**). This is a confirmation of the relative acceptor strengths and is not related to the use of Tröger's base as an alternative electron-donor moiety. Note that the dynamic hyperpolarizability values $\beta_{HRS,800}$ are larger for all the chromophores based on the nitrophenyl acceptor, but this is only due to this resonance enhancement when using a fundamental laser wavelength of 800 nm, for which the second-harmonic wavelength of 400 nm is very close to the electronic resonance.

A second observation is the blue-shift of the absorption spectra upon replacing the dimethylaminophenyl donor moiety by the Tröger's base skeleton. In compounds derived from both the nitrophenyl and benzothiazolium acceptors, a substantial blue shift is observed. For the bis-chromophoric compounds **2** and **3** this

has been observed before [22]. This experimental observation was rationalized by theoretical calculations in terms of reduced conjugation between the lone pair on the nitrogen atom and the aromatic ring in the Tröger's base skeleton, compared with N,N-dimethylaniline. This is due to the geometric constraints imposed by the bridgehead nitrogen atom in Tröger's base. Nevertheless, it has been suggested that conjugation between the lone pair of the nitrogen atom and the aromatic ring is not negligible.

This part of the work shows the impact on the second-order NLO properties of this "partial conjugation" due to geometric constraint. The static first hyperpolarizability values $\beta_{HRS,0}$ are all substantially smaller for the Tröger's base derivatives (**2** - **5**) than for analogues with the dimethylaminophenyl donor (**6**, **7**). This is in agreement with the expectations based on the observation of the blueshifts in linear absorption spectra. Less conjugation with the nitrogen-derived donor moiety in Tröger's base will also mean that it is a less efficient donor.

Availability of both the mono- and the bis-chromophoric systems allowed a more detailed comparative study towards the effectiveness of the Tröger's base molecular scaffold for nonlinear optics. It had been conjectured that the mono-chromophoric derivative **4** could be a good monomeric reference chromophore with respect to the bis-chromophoric derivative **2** based on the very small splitting calculated between the two highest occupied and the two lowest unoccupied molecular orbital energy levels [22]. Here, the theoretical conjecture was experimentally confirmed, as the electronic spectral properties for both the mono- and the bis-chromophoric structures (**2** *vs.* **4** and **3** *vs.* **5**) are essentially identical, whereas the oscillator strength for the bis-chromophoric compounds is roughly twice the value for the mono-chromophoric reference compounds (see Table 9-1). Figure 9-3 compares the linear optical properties (UV-Vis absorption spectra) of the nitrophenyl acceptor-based benchmark **6**, the mono-chromophoric compound **4**, and the bis-chromophoric compound **2**. These observations confirm that the electronic coupling between the two separate arms of the bis-chromophoric compound is small. There is rather a conservation of the original confinement of the conjugation in the two separate arms of the bis-chromophoric compound.

This negligible coupling then allows for a simple structural analysis of the second-order NLO properties for both the mono- and the bis-chromophoric compounds in terms of the opening angle between the two chromophores [24]. If the mono-chromophoric compound can be used as the "monomer" model (as supported by the absorption properties) for the bis-chromophoric compound, (the "dimer"), the vector addition model results in a relation between the first hyperpolarizability of the dimer, β_{dimer} and the first hyperpolarizability of the monomer, β_{mono}, and the opening angle θ between the two "monomers" can be estimated as

β_{zzz}(dimer) = 2β_{zzz}(monomer) [cos(θ/2)]^3, in which the diagonal tensor components are obtained using $\beta_{zzz} = ((35/6)^{1/2})\beta_{HRS}$.

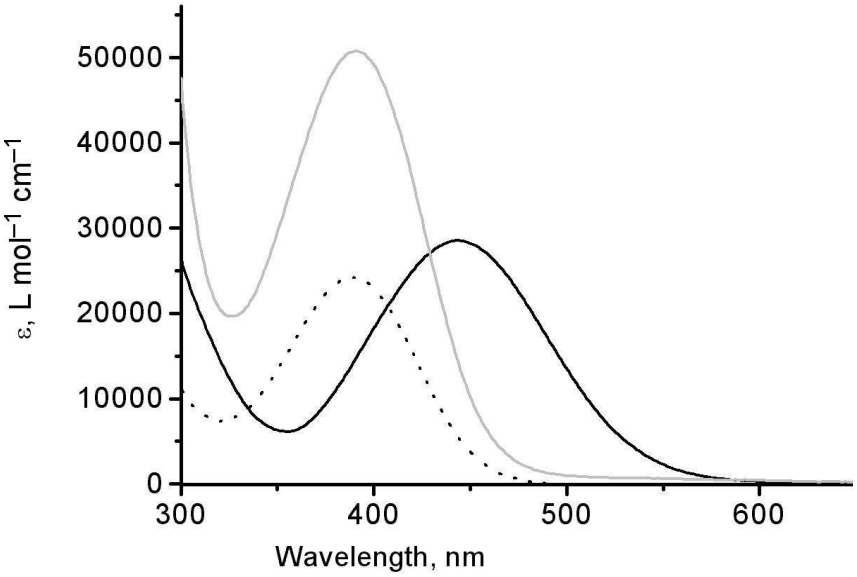

Figure 9-3: UV-Vis absorption spectra of **2** (grey line), **4** (black dashed line), and **6** (black solid line) in DMF.

When applying this relationship to the dynamic hyperpolarizability values, $\beta_{zzz,800}$, the values for the opening angles reported in Table 9-1 result. These data suggest that the opening angles between the two chromophoric moieties for Tröger's base analogues **2** and **3** would be 76 ± 5° and 77 ± 5°, respectively. From the XRD studies it is known that the angles between the planes of aromatic rings of Tröger's base analogues featuring the methanodiazocine moiety fused with various (hetero)aromatic rings typically fall within 85°–105° range [3], although "extreme" values as small as 80.2° [25] or as large as 113.9° [26] have been encountered. This spread is largely due to crystal packing effects: semi-empirical geometry optimization predicts an approximately 100° angle between the planes of the aromatic rings for 6H,12H-5,11-methanodibenzo[b,f][1,5]diazocine derivatives [27]. The values obtained from DFT geometry optimization are 103° and 108° for **2** and **3**, respectively. Since the angle between the planes of the aromatic rings and the opening angle between the dipole moment vectors of the two chromophores do not exactly coincide, the estimation obtained from the analysis of dynamic hyperpolarizability values is quite reasonable. Further limitations of the model are: i) the assumption that β_{HRS} value of the dimeric chromophore is dominated by β_{zzz}, which leads to an underestimation of θ because β_{zzz} is overestimated and the β_{zxx} component is underestimated and ii) the neglect of cross-polarization interactions between the chromophore units, which usually decreases the global response. Note that when the same relationship is

applied to the static hyperpolarizability values, $\beta_{zzz,0}$, essentially the same values result, since the degree of resonance enhancement is also essentially identical, this is due to the similar value for $\lambda_{max,\ abs}$ for both the "monomer" and the "dimer".

Additional experiments in the form of the measurement of the depolarization ratio for the nonlinear scattering confirm that the monomeric chromophores **4** and **5** are good "monomeric" model compounds. A good monomeric model compound should have a $\beta_{zzz,}$, along the molecular dipolar *z*-axis. This then justifies relating the experimental result, β_{HRS}, to just one tensor component by using $\beta_{zzz} = \beta_{HRS}\ (35/6)^{1/2}$. A single major hyperpolarizability tensor component β_{zzz} along the dipolar molecular z-axis shows up experimentally as a relatively large depolarization ratio. The experimental observation that the depolarization ratio is relatively large for both the Tröger's base mono-chromophoric analogues **4** and **5** and also for our benchmarks compounds **6** and **7** indicates that the second-order NLO response of these chromophores is dominated by the single major hyperpolarizability tensor component, β_{zzz}. The lower values observed for the depolarization ratio of the bis-chromophoric compounds **2** and **3** is completely in line with our model.

9.3. Theoretical analysis of NLO data

Hyper Rayleigh scattering data (β_{HRS} and DR) of compounds **2** to **7** calculated at the IEF-PCM/MP2/6-31G* level of approximation are listed in Table 9-2. They show that the dipolar character of the compounds decreases when going from **4** and **6** to **2** (or from **5** and **7** to **3**). This is evidenced by the depolarization ratios, which change from the almost ideal dipolar value (DR = 5) to 3.72 and 2.88, respectively. This is further confirmed by the approximate β_{HRS} and DR values that can be calculated by using either only one dominant β tensor component for the dipolar molecules **4** – **7**, or two dominant β tensor components for V-shaped molecules **2** and **3**, and which closely match the full values. Thus, the β_{HRS} values of **4** – **7** are fully determined by one tensor component, whereas two are necessary to obtain the values for **2** and **3**. Note that, when using compound **2** as the example, only the $\beta_{zzz,0}$ value cannot reproduce the β_{HRS} value (12 *vs.* 42 for the full $\beta_{HRS,0}$ value).

It is comforting to observe that these theoretical predictions for the depolarization ratio are in good agreement with the experimental observations, taking into account the above mentioned practical considerations. For the mono-chromophoric Tröger's base derivatives **4** and **5** and for the benchmark chromophores **6** and **7**, the calculated values are identical to or almost equal to the limiting value of five, but for the V-shaped bis-chromophoric "dimers" **2** and **3**, these values are substantially lower. Within these two lower values, we can further differentiate between the nitro-acceptor based compound **2** (intermediate value) and

the benzothiazolium-acceptor based compound **3** (the lowest value for the calculated depolarization ratio). The observation that the experimental values for these depolarization ratios also reflect this differentiation beyond the estimated statistical uncertainty, strengthens our assumption for the analysis of the solution-phase structure of the bis-chromophoric Tröger's bases **2** and **3**.

Compound	$\beta_{zzz,o}$	$\beta_{zxx,0}$	$\beta_{HRS,0}$	DR	$\beta_{HRS,0}$ (full)	DR (full)	θ
2	6944	13887	9490	3.73	9721	3.72	100
3	6944	22451	14813	3.18	14582	2.88	104
4	17591	-	7175	5.00	7638	4.90	-
5	37496	-	15507	5.00	15739	4.75	-
6	39579	-	16433	5.00	16433	4.89	-
7	77769	-	32172	5.00	31941	4.96	-

Table 9-2: IEF-PCM/MP2/6-31G* $\beta_{zzz,0}$, $\beta_{xxz,0}$, β_{HRS}, depolarization ratio (DR) (a.u.), and opening angle between the two arms of Tröger's base derivatives (θ in degrees determined from B3LYP/6-311G* geometry optimizations). The full $\beta_{HRS,0}$ and DR values are given as well as approximates, which were calculated from only one or two dominant tensor components in order to address the dimensionality of the NLO-phore.

To further compare the experimental and theoretical β values, a pre-treatment of the experimental data was necessary. Indeed, the experimental data are impacted by resonance conditions since the measurements are carried out at a frequency within the absorption band, slightly above or below the maximum, whereas this effect is absent in the calculations. Evaluating the magnitude of this effect is however difficult [28]. The simplest way to estimate the impact of frequency dispersion in pseudo-dipolar chromophores is to consider the two-state approximation [29], which assumes that only one excited state contributes to the second-order NLO response. Considering a homogeneous damping γ and neglecting the non-resonant terms [30-34], the frequency-dispersion factor for any of the diagonal components of the first hyperpolarizability tensor, $F(\omega,\omega_{ge},\gamma)$ is as shown in Equation (9-1):

$$F(\omega,\omega_{ge},\gamma)=\frac{\beta_{zzz}(-2\omega;\omega,\omega)}{\beta_{zzz}(0;0,0)}=\frac{\omega_{ge}^2\left(\omega_{ge}-i\gamma\right)^2}{\left(\left[\omega_{ge}-i\gamma\right]^2-4\omega^2\right)\left(\left[\omega_{ge}-i\gamma\right]^2-\omega^2\right)} \qquad (9\text{-}1)$$

in which g and e are the two electronic, ground and excited, states contributing to the β value, and ω_{ge} is the corresponding excitation energy. Assuming that the same treatment can be applied to the off-diagonal β_{zxx} component, which is a good approximation because the splitting of the excitation energies is small, the extrapolated static β values obtained by setting γ to zero as well as by choosing γ

values matching the half width at half maximum (HWHM) of the corresponding absorption spectra (*i.e.* $\gamma \approx 1.2$ HWHM of the $e^{-[(\omega-\omega_{ge})/\gamma]^2}$ Gaussian function) are shown in Table 9-3. These estimates of the dispersion factors have then been improved by incorporating an inhomogeneous broadening based on the absorption spectrum, which implicitly contains information on the distribution of the transition frequencies as well as taking into account the vibronic structure of the excited states. According to Campo *et al.* [28], for an incoherent process like HRS, the dispersion factor reads:

$$\left|\frac{\beta^{HRS}(-2\omega;\omega,\omega)}{\beta^{HRS}(0;0,0)}\right| = \left\{\int N(\omega'_{ge})\left|F(\omega,\omega'_{ge},\gamma)\right|^2 d\omega'_{ge}\right\}^{1/2} \qquad (9\text{-}2)$$

in which the $N(\omega'_{ge})$ value, the normalized distribution of the transition frequencies, is approximated by a Gaussian function reproducing the experimental HWHM of the corresponding main absorption band. Moreover, the distribution of the transition frequencies can further be improved by considering the single-mode vibronic model and replacing $N(\omega'_{ge})$ by:

$$N(\omega'_{ge}) = \sum_{n}^{vib.levels}\left[\frac{S^n e^{-S}}{n!}\right] e^{-[(\omega'_{ge}-\omega_n)/\gamma_{vib}]^2} \qquad (9\text{-}3)$$

where $\omega_n = \omega_{ge} + n\,\omega_{vib}$ corresponds to the transition from the ground state to the n^{th} vibrational level of the excited state. S are the Huang-Rhys factors which were chosen to reproduce the shape of the absorption band. The ω_{vib} and γ_{vib} values were also chosen to best reproduce the absorption spectra. The parameters for compounds **2** – **7** are listed in Table 9-4.

Good qualitative agreement for chromophores **2** – **7** is obtained between theory and experiment. Therefore, by employing the values extrapolated using Equation (9-1) ($\gamma = 0$), the change from one chromophore branch to two in the Tröger's base derivatives almost does not change the first hyperpolarizabilities. The β value then increases by a factor between three and four when going from chromophore **4** to **6** or from chromophore **5** to **7** as a result of planarity of the nitrogen and therefore of better conjugation. These relationships are confirmed when using the other extrapolated data, although the increase of β value due to planarity is somehow reduced. Together with the calculated MP2 values, the extrapolated data obtained using Equation (9-1) ($\gamma = 0$) also demonstrate the stronger acceptor character of the benzothiazolium units and the associated larger β values. The relative magnitude of the static β values is, however, not reproduced when using Equation (9-1) ($\gamma \neq 0$), whereas using Equations (9-2) and (9-3), the relative magnitude is only reproduced for **6** *vs.* **7**. These differences should be associated with the limitation of the models of extrapolation.

Compound	Extrapolated from Equation (9-1), $\gamma = 0$	Extrapolated from Equation (9-1), $\gamma \neq 0$	Extrapolated from Equations (9-2 and 9-3)	Calculated (MP2/IEF-PCM)
2	1435	9258	112546	9721
3	3240	6712	2106	14582
4	1713	7869	2315	7638
5	3240	6712	2106	15739
6	6249	11804	3703	16433
7	11341	12730	9027	31941

Table 9-3: Comparison between calculated (MP2/IEF-PCM), and extrapolated by different methods values of the first hyperpolarizabilities $\beta_{HRS,\,0}$ (a.u.).

Compound	$\hbar\omega_{ge}$ (eV) λ_{eg} (nm)	$\gamma_{homogeneous}$ (eV)	$\gamma_{inhomogeneous}$ (cm^{-1})	S	ω_{vib} (cm^{-1})	γ_{vib} (cm^{-1})
2	3.17; 391	0.458	480	0.0	-	-
3	2.84; 436	0.418	480	0.5	1600	1600
4	3.19; 389	0.375	480	0.0	-	-
5	2.86; 433	0.427	480	0.5	1600	1600
6	2.80; 443	0.444	480	0.0	-	-
7	2.36; 525	0.266	480	0.5	1600	1600

Table 9-4: Best parameters fitting the UV/vis absorption spectra

9.4. Conclusion

We have investigated the NLO properties of novel chiral push-pull chromophores derived from the V-shaped skeleton of 6H,12H-5,11-methanodibenzo [b,f][1,5]diazocine, a parent heterocyclic system of Tröger's base. Detailed analysis of the data led to the conclusion that molecules possessing one or two chromophoric "arms" show approximately equal HRS second-order NLO properties. This observation is very useful for the future studies, since the structure of the future chromophores can be chosen to be C_2 symmetrical or asymmetric ones, based on considerations such as solubility and synthetic feasibility, without compromising their NLO properties. Between the two families of molecules studied, the systems featuring a cationic benzothiazolium acceptor have proven to be the most efficient. It was, however, demonstrated that the molecular first hyperpolarizabilities of the two families of chromophores are three to four times lower than those of analogues with a "classical" dimethylamino donor group. Notwithstanding, 6H,12H-5,11-methanodibenzo[b,f][1,5]diazocine holds considerable promise as a scaffold for NLO

chromophores. Chromophores with a chiral element constituting a part of the conjugated system appear to be promising for materials with bulk NLO activity, since the introduction of chirality is an effective approach towards bulk noncentrosymmetric crystals. Such crystals have a higher number density than amorphous thin films or chromophores dispersed in a polymer matrix, a common approach that requires additional poling to orient the chromophores. Furthermore, the lower depolarization ratio and large off-diagonal tensor component for the bis-chromophoric V-shaped derivatives will translate into lower polarization sensitivity for NLO application [35]. Lower molecular hyperpolarizabilities can be increased by the extension of the π-system and/or the incorporation of “auxiliary donors”, for example, electron-rich heterocycles such as thiophene. The efficiency of this general approach was demonstrated by many previous examples [36-43]. We can also imagine grafting molecular switch at the end of one or two chromophoric “arms”. This idea could pave the way towards chiral molecular switches with all advantages mentioned previously.

9.5. References

[1] S. Sergeyev, *Helv. Chim. Acta*, **92**, 415 (2009).

[2] M. Valík, R. M. Strongin, and V. Král, *Supramol. Chem.*, **17**, 347 (2005).

[3] B. Dolenský, J. Elguero, V. Král, C. Pardo, and M. Valík, *Adv. Heterocycl. Chem.*, **93**, 1 (2007).

[4] F. R. Fischer, P. A. Wood, F. H. Allen, and F. Diederich, *Proc. Natl. Acad. Sci. U. S. A.*, **105**, 17290 (2008).

[5] Y.-M. Jeon, G. S. Armatas, D. Kim, M. G. Kanatzidis, and C. A. Mirkin, *Small*, **5**, 46 (2009).

[6] P. R. Brotherhood, I. J. Luck, and M. J. Crossley, *Magn. Reson. Chem.*, **47**, 257 (2009).

[7] C. Michon, M.-H. Goncalves-Farbos, and J. Lacour, *Chirality*, **21**, 809 (2009).

[8] E. B. Veale, D. O. Frimannsson, M. Lawler, and T. Gunnlaugsson, *Org. Lett.*, **11**, 4040 (2009).

[9] S. R. Marder, *Chem. Commun.*, 131 (2006).

[10] B. J. Coe, D. Beljonne, H. Vogel, J. Garin, and J. Orduna, *J. Phys. Chem. A*, **109**, 10052 (2005).

[11] C. Lambert, W. Gaschler, G. Noll, M. Weber, E. Schmalzlin, C. Brauchle, and K. Meerholz, *J. Chem. Soc. Perkin Trans. 2*, 964 (2001).

[12] C.-X. Yuan, X.-T. Tao, L. Wang, J.-X. Yang, and M.-H. Jiang, *J. Phys. Chem. C*, **113**, 6809 (2009).

[13] C.-X. Yuan, X.-T. Tao, Y. Ren, Y. Li, J.-X. Yang, W.-T. Yu, L. Wang, and M.-H. Jiang, *J. Phys. Chem. C*, **111**, 12811 (2007).

[14] H.-J. Deussen, C. Boutton, N. Thorup, T. Geisler, E. Hendrickx, K. Bechgaard, A. Persoons, and T. Bjornholm, *Chem. Eur. J.*, **4**, 240 (1998).

[15] S. V. Elshocht, T. Verbiest, M. Kauranen, L. Ma, H. Cheng, K. Y. Musick, L. Pu, and A. Persoons, *Chem. Phys. Lett.*, **309**, 315 (1999).

[16] E. Hendrickx, C. Boutton, K. Clays, A. Persoons, S. van Es, T. Biemans, and B. Meijer, *Chem. Phys. Lett.*, **270**, 241 (1997).

[17] M. Yang and B. Champagne, *J. Phys. Chem. A*, **107**, 3942 (2003).

[18] V. Ostroverkhov, R. G. Petschek, K. D. Singer, and R. J. Twieg, *Chem. Phys. Lett.*, **340**, 109 (2001).

[19] C. R. Moylan, S. Ermer, S. M. Lovejoy, I. H. McComb, D. S. Leung, R. Wortmann, P. Krdmer, and R. J. Twieg, *J. Am. Chem. Soc.*, **118**, 12950 (1996).

[20] J. Jensen, J. Tejler, and K. Wärnmark, *J. Org. Chem.*, **67**, 6008 (2002).

[21] S. Sergeyev, M. Schär, P. Seiler, O. Lukoyanova, L. Echegoyen, and F. Diederich, *Chem. Eur. J.*, **11**, 2284 (2005).

[22] V. Lemaur, J. Cornil, D. Didier, A. Mujawase, and S. Sergeyev, *Helv. Chim. Acta*, **90**, 2087 (2007).

[23] B. J. Coe, J. A. Harris, J. J. Hall, B. S. Brunschwig, S.-T. Hung, W. Libaers, K. Clays, S. J. Coles, P. N. Horton, M. E. Light, M. B. Hursthouse, J. Garin, and J. Orduna, *Chem. Mater.*, **18**, 5907 (2006).

[24] G. Hennrich, M. T. Murillo, P. Prados, H. Al-Saraierh, A. El-Dali, D. W. Thompson, J. Collins, P. E. Georghiou, A. Teshome, I. Asselberghs, and K. Clays, *Chem. Eur. J.*, **13**, 7753 (2007).

[25] M. J. Crossley, T. W. Hambley, L. G. Mackay, A. C. Try, and R. Walton, *J. Chem. Soc., Chem. Commun.*, 1077 (1995).

[26] F. Hof, D. M. Scofield, W. B. Schweizer, and F. Diederich, *Angew. Chem., Int. Ed.*, **43**, 5056 (2004).

[27] Y. Ishida, H. Ito, D. Mori, and K. Saigo, *Tetrahedron Lett.*, **46**, 109 (2005).

[28] J. Campo, W. Wenseleers, E. Goovaerts, M. Szablewski, and G. H. Cross, *J. Phys. Chem. C*, **112**, 287 (2008).

[29] J. L. Oudar and D. S. Chemla, *J. Chem. Phys.*, **66**, 2664 (1977).

[30] C. H. Wang, *J. Chem. Phys.*, **112**, 1917 (2000).

[31] G. Berkovic, G. Meshulam, and Z. Kotler, *J. Chem. Phys.*, **112**, 3997 (2000).

[32] J. N. Woodford, C. H. Wang, A. E. Asato, and R. S. H. Liu, *J. Chem. Phys.*, **111**, 4621 (1999).

[33] M. A. Pauley and C. H. Wang, *Chem. Phys. Lett.*, **280**, 544 (1997).

[34] P. Kaatz and D. P. Shelton, *J. Chem. Phys.*, **105**, 3918 (1996).

[35] I. C. Pintre, N. Gimeno, J. L. Serrano, M. B. Ros, I. Alonso, C. L. Folcia, J. Ortega, and J. Etxebarria, *J. Mater. Chem.*, **17**, 2219 (2007).

[36] Y.-K. Wang, C.-F. Shu, E. M. Breitung, and R. J. McMahon, *J. Mater. Chem.*, **9**, 1449 (1999).

[37] X. Ma, R. Liang, F. Yang, Z. Zhao, A. Zhang, N. Song, Q. Zhou, and J. Zhang, *J. Mater. Chem.*, **18**, 1756 (2008).

[38] A. K. Y. Jen, V. P. Rao, K. Y. Wong, and K. J. Drost, *J. Chem. Soc., Chem. Commun.*, 90 (1993).

[39] S.-S. P. Chou, D.-J. Sun, J.-Y. Huang, P.-K. Yang, and H.-C. Lin, *Tetrahedron Lett.*, **37**, 7279 (1996).

[40] H. Meier, *Angew. Chem., Int. Ed.*, **44**, 2482 (2005).

[41] F. Wuerthner, F. Effenberger, R. Wortmann, and P. Kraemer, *Chem. Phys.*, **173**, 305 (1993).

[42] R. M. F. Batista, S. P. G. Costa, M. Belsley, and M. M. M. Raposo, *Tetrahedron*, **63**, 9842 (2007).

[43] F. Quist, C. M. L. Vande Velde, D. Didier, A. Teshome, I. Asselberghs, K. Clays, and S. Sergeyev, *Dyes and Pigments*, **81**, 203 (2009).

Conclusions and outlooks

10. Conclusions and outlooks

This work has aimed at characterizing and optimizing molecular switches presenting large contrasts of their second-order nonlinear optical properties in view of providing promising multifunctional molecular switches. Known switching species have been investigated by varying their structure or changing the conjugated path and/or substituents in a pluridisciplinary approach that combines the synthesis of the compounds (by our collaborators) as well as their linear and nonlinear optical characterizations, experimentally (by UV-Visible spectroscopy and hyper Rayleigh scattering) and theoretically (*ab initio* calculations), to predict and interpret their properties. We were particularly interested in the NLO responses of photochromic, acidochromic, and thermochromic compounds, *i.e.* compounds changing their colour by irradiation, pH modification, or temperature variations.

Several families of compounds have been investigated, of which the spiropyran derivatives that commute between an open and a closed form where the electronic conjugation between the electron-acceptor and electron-donor group decreases. We have calculated the first hyperpolarizabilities of such merocyanine-spiropyran compounds differing by the nature, number, and positioning of the substituents. The substituent effects appear cooperative and therefore often difficult to rationalize easily. Calculations have predicted promising NLO contrasts (of the order of 9) for the original system. By selecting the best combination of substituents, we have increased the β value and maximized the contrast (until 18):

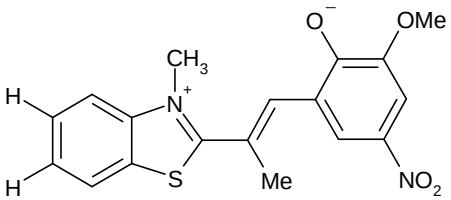

β_{mero} = 3342 a.u. $\qquad \frac{\beta_{mero}}{\beta_{spiro}} = 9.01$

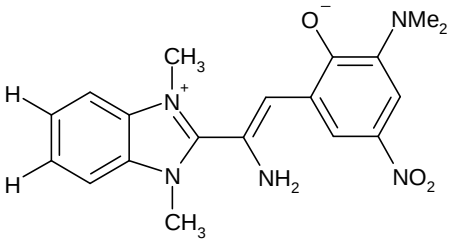

β_{mero} = 7538 a.u. $\qquad \frac{\beta_{mero}}{\beta_{spiro}} = 18.16$

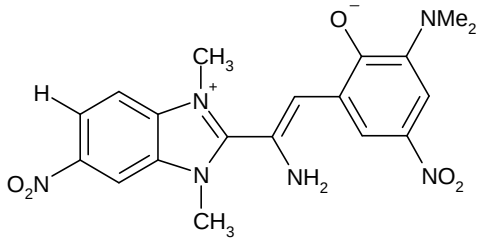

β_{mero} = 11589 a.u. $\qquad \frac{\beta_{mero}}{\beta_{spiro}} = 15.25$

These optimized compounds have not yet been synthesized to confirm our theoretical predictions. Moreover within that investigation, basis set effects have been addressed and enable to select the 6-311+G* basis set to perform the whole investigation.

The second part was the determination of the linear and nonlinear optical properties of anil derivatives, which vary upon switching between a keto and an enol forms. We have demonstrated the difficulty to elaborate NLO molecular switches based on keto-enol equilibrium because the highest contrasts are related to small β values while in other cases, the contrast is close to 1. First, two anil derivatives were investigated by means of hyper Rayleigh scattering measurements and *ab initio* calculations, demonstrating a good agreement for the evaluation of the structural characteristics and the molecular properties. These values were also compared to those obtained with EFISHG method. To rationalize the impact of the anil structure the μ and β vectors were sketched. As shown in Figure 10-1 for **4A**, the relative orientation of the dipole moment changes when switching from the E to K form allowing to explain the negative value of $\beta_{//}$ of the latter. At the MP2 level of approximation, some differences between the measured and calculated $\beta_{//}$ values for the E form were explained by the difficulty to determine the dipole moment orientation.

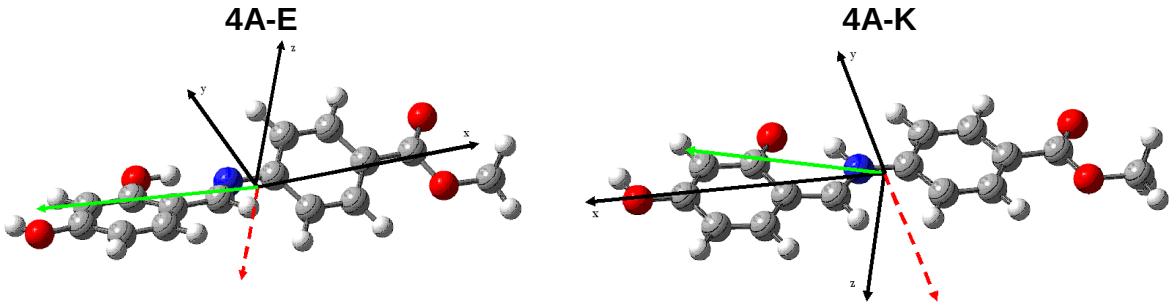

Figure 10-1: Sketch of the dipole moment (red dotted line) and first hyperpolarizability (green full line) vectors for E and K forms of compounds **4A**.

Secondly, hyper Rayleigh scattering experiments and *ab initio* calculations were combined to investigate the effects of different binary mixtures of solvents (ethanol/ cyclohexane) on the keto-enol equilibrium and on their second-order NLO responses. We have demonstrated that by increasing the solvent polarity, the tautomeric equilibrium is displaced toward the K form leading to a bathochromic shift and a large enhancement of the first hyperpolarizability. This effect was fairly reproduced by theoretical calculations using IEF-PCM model, also demonstrating the pure solvent effects on E and K forms properties. We have highlighted the difficulty to conciliate

HRS experiments in different solvent due to the possibility of the formation of J-aggregates.

The third family of compounds was the dihydroazulene-vinylheptafulvene equilibrium. The contrasts of second-order NLO properties of this system have been investigated theoretically as a function of the substituent R on the phenyl ring. First, we have compared systems with R = H, CH_3, NH_2, and NO_2. The substitution with R = H and R = CH_3 leads to contrast between the DHA and VHF forms larger than 5 while between the *cis* and *trans* VHF forms the contrast is close to 1. The NH_2 donor group increases the first hyperpolarizability for the three forms, which is detrimental to the contrast. Finally, the NO_2 acceptor group leads to a large increase of the first hyperpolarizability of the DHA form and to a contrast of about 0.4. In a preliminary theoretical study, we have demonstrated the remarkable changes of first hyperpolarizability for DHA-VHF compounds proposed by Diederich *et al.* [1], which contain large substituents composed of triple bonds and aryl group substituted with donor or acceptor groups (Figure 10-2) and grafted in R position. They are of particular interest due to their possibility to commute in a three-way chromophoric molecular switch controlled by pH, light, and heat. Large first hyperpolarizability contrasts are also expected (up to 25) experimentally for these compounds.

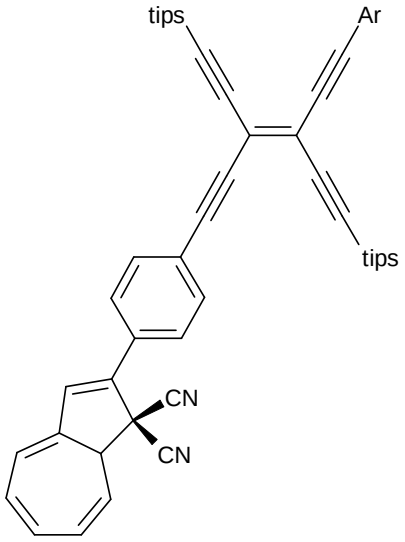

Figure 10-2: DHA-VHF equilibrium proposed by Diederich to act as a three-way molecular switch.

The impact of the length and the nature of the π-conjugated bridge on the first hyperpolarizability has been demonstrated on molecules containing the dicyanoimidazole moiety as electron-acceptor and the *N,N*-dimethylamino group as electron-donor anchored on enlarged π-conjugated bridge (Figure 10-3) as well as their variation upon protonation. The protonation leads to a reduction of the donor

character and of the electronic delocalization along the π-conjugated bridge, to a decrease of the β value by more than one order of magnitude, and therefore to interesting contrasts of first hyperpolarizability (up to 36). This decrease was confirmed by hyper Rayleigh scattering: the protonated forms could not be characterized due to the weakness of the signal.

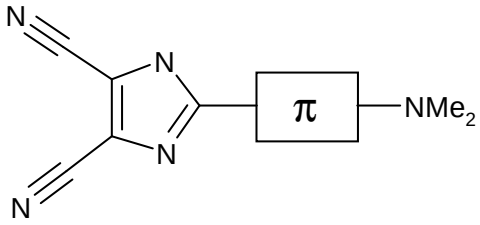

Figure 10-3: Push-pull molecules containing 4,5-dicyanoimidazole and NMe_2 moieties anchored on systematically enlarged π-conjugated system.

Finally, we have investigated the chiroptical properties of push-pull molecules based on the Tröger's bases containing symmetrical chromophore featuring two identical acceptors (R = R') as well as unsymmetrical chromophore featuring only one acceptor (R ≠ R' = H):

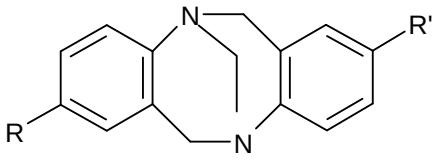

Figure 10-4: Tröger's base derivatives.

The joint theoretical and experimental studies have provided insight into the relationship between the structure of the new chromophores and their NLO properties. We have showed how molecular interactions can modify the linear and nonlinear optical responses leading to the possibility of elaborating chiral molecular switches with large contrast of their first hyperpolarizability. Molecules possessing one or two acceptor groups show approximately equal second-order NLO properties, which is very useful for the development of devices since the structure of the chromophores can be chosen to be C_2 symmetrical or asymmetric ones, based on considerations such as solubility or easier synthesis without compromising their NLO properties.

So, we have proposed strategies in order to obtain large first hyperpolarizability values and large contrasts. We have also proved that the

evaluation and the interpretation of the linear and nonlinear optical properties have to take into account several parameters: i) the environment effects, ii) the impact of the electron correlation to evaluate molecular properties; in particular we have demonstrated that DFT methods with conventional exchange-correlation functionals is not yet appropriate to reproduce the β contrasts while it is generally an efficient method to describe the linear properties, and iii) the impact of the frequency dispersion on the nonlinear responses and the efficiency of a vibronic model to extract the static or off-resonant values from experimental data.

However, these studies call for further investigations, including i) the synthesis of the designed merocyanine-spiropyran compounds and their experimental characterization, ii) the characterization of the macroscopic properties (linear and nonlinear susceptibilities) of anil derivatives in the crystalline state , iii) the experimental characterization of DHA-VHF compounds with large substituents [1], and iv) the study of the impact of substitution by donor or acceptor groups on the seven-membered ring of the DHA-VHF equilibrium on the first hyperpolarizability whose synthesis has recently been reported by Nielsen *et al.* [2]:

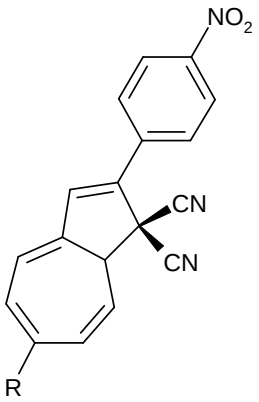

Figure 10-5: Seven-membered ring functionalized DHA.

Furthermore, by following the working strategy developed during this thesis, many other compounds could be characterized. In particular, we are now interested in nonlinear optical sensors, *i.e.* multifunctional compounds that are able to selectively detect analytes while changing their NLO properties, as example, the detection of alcaline and alcalino-earth cations as well as heavy and transition metals. For instance, Zakharova *et al.* [3] have recently investigated the spiropyran-merocyanine equilibrium to act as metal complexing photochromic molecules. They have demonstrated that the addition of cations such as Co_2^+, Ni_2^+, or Zn_2^+ in an acetonitrile solution of benzothiazole benzopyrane leads to the complexation

between the metal cation and the merocyanine. One can therefore anticipate that they will display large β contrasts.

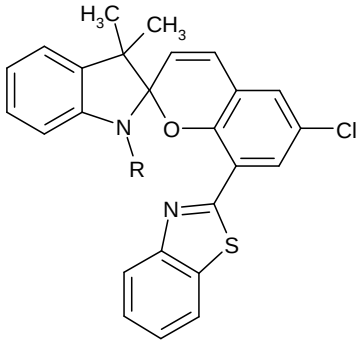

Figure 10-6: Benzothiazole benzopyrane. R = CH_3, C_3H_7, or $CH_2CH(CH_3)_2$.

These photochromic and metallochromic molecules are expected to lead to the design of sensors with remarkable properties and new performances because they will combine a NLO contrast with cation-triggered switching [4], providing a very interesting ecological potential to act, for instance, as selective sensors for metallic pollutants.

References

[1] L. Gobbi, P. Seiler, and F. Diederich, *Angew. Chem. Int. Ed.*, **38**, 674 (1999).

[2] S. L. Broman, M. A. Petersen, C. G. Tortzen, A. Kadziola, K. Kilså, and M. B. Nielsen, *J. Am. Chem. Soc.*, **132**, 9165 (2010).

[3] M.I. Zakharova, C. Coudret, V. Pimienta, J.C. Micheau, S. Delbaere, G. Vermeersch, A.V. Metelitsa, N. Voloshin, and V.I. Minkin, *Photochem. Photobiol. Sci.* **9**, 199 (2011).

[4] A. Datta, *J. Phys. Chem. C*, **113**, 3339 (2009).